DIAGNOSIS AND ANALYSIS OF ARTERIOSCLEROSIS IN THE LOWER LIMBS FROM THE ARTERIAL PRESSURE PULSE

by

JEFFREY KENT RAINES

B.S.M.E., Clemson University
(1965)

M.M.E., University of Florida
(1967)

SUBMITTED IN PARTIAL FULFILLMENT
OF THE REQUIREMENTS FOR THE DEGREE OF
DOCTOR OF PHILOSOPHY
at the
MASSACHUSETTS INSTITUTE OF TECHNOLOGY
September, 1972

Signature of Author_____
Department of Mechanical Engineering
August, 1972

Certified by_____
Thesis Supervisor

Accepted by_____
Chairman, Departmental Committee
on Graduate Students

Archives
MASS. INST. TECH.
OCT 16 1972
LIBRARIES

DIAGNOSIS AND ANALYSIS OF ARTERIOSCLEROSIS IN THE LOWER LIMBS FROM THE ARTERIAL PRESSURE PULSE

by

Jeffrey Kent Raines

Submitted to the Department of Mechanical Engineering
on August 7, 1972 in partial fulfillment of
the requirement for the degree of Doctor of Philosophy

ABSTRACT

An electronic instrument is described which permits a reasonably accurate non-invasive recording of the arterial pressure pulse in the extremities. These recordings are calibrated by independent measurements of systolic and diastolic pressure, and compare favorably with direct intra-arterial measurements. The instrument has been used clinically to study peripheral arterial dynamics in both healthy and diseased arterial systems. In these studies it was found that the pressure pulse is grossly affected by arterial disease. A computer simulation of the arterial dynamics of the lower extremity was developed to aid in the interpretation of our clinical observations; dog experiments were also performed. Results indicate changes in the pressure pulse contour distal to an obstruction are due to the dynamics of the obstruction itself and also to an impedance mismatch between the larger arteries and the peripheral resistance. The fluid mechanics of intermittent claudication are also discussed.

Thesis Supervisor: Michel Y. Jaffrin

Title: Associate Professor
Department of
Mechanical Engineering

ACKNOWLEDGEMENTS

Individuals too numerous to mention both at the Massachusetts Institute of Technology and the Massachusetts General Hospital deserve credit for their part in this research.

Special thanks are extended to Professor M.Y. Jaffrin for his encouragement, hard work, and guidance. Professor R. Clement Darling and his staff provided the energy, faith, and medical environment that enabled results of this work to be useful in clinical practice. Professors A.H. Shapiro and R.S. Lees were very close to this project and provided suggestions and interpretations of great value.

Mr. Steve Holford and Mr. Karsten Sorensen spent endless hours in the design of the complex electronic circuits required to make this project possible.

Mrs. Dianna Evans and Mrs. Sandy Williams transformed my sometimes illegible handwriting into this accurately typed manuscript. This effort is sincerely appreciated.

My wife Sonja has worked and successfully maintained a home without a husband while I have pursued my education. She has made many sacrifices and I have often wondered if the wife should receive a degree for understanding.

This work was supported in part by NIH Grant HL 14-209 and in a form of a predoctoral NIH Fellowship to the author.

TABLE OF CONTENTS

		Page No.
I.	INTRODUCTION	1
II.	PRESSURE PULSE RECORDER - DEVELOPMENT AND DESCRIPTION	6
	2.1 Current Non-Invasive Devices	6
	2.2 The Pressure Pulse Recorder	7
	2.3 Description and Operating Procedures	8
	2.4 Measurement of Systolic and Diastolic Pressure in the Lower Limbs	10
	2.5 Dynamics of the Air in the Cuff	12
	2.6 Comparisons with Intra-Arterial Measurements	16
	2.7 Frequency Response	18
III.	CLINICAL STUDIES AND OBSERVATIONS	20
	3.1 Case Studies	21
	3.2 Pressure Pulse Contours	26
IV.	MATHEMATICAL MODEL OF ARTERIAL FLOW	29
	4.1 Governing System of Equations	31
	4.2 Linearized Equations	33
	4.3 Boundary Conditions	34
	Proximal Boundary Condition	34
	Distal Boundary Condition	35
	Conditions at Branching	37
	4.4 Friction Term	37
	4.5 Leakage Term	38
V.	NUMERICAL SOLUTION BY FINITE DIFFERENCE METHOD	39
	5.1 Proximal Pressure Prescribed	40

		Page No.
5.2	Proximal Flow Prescribed	40
5.3	Stability Criterion	43
VI.	PHYSIOLOGICAL MODEL	45
6.1	Geometric Properties	45
6.2	Elastic Properties	47
6.3	Flow Distribution	51
6.4	Branches and Termination	53
6.5	Control Case	54
VII.	DYNAMICS OF CONTROL CASE	56
7.1	Pressure and Flow Pulses	56
7.2	Effect of Convective Acceleration	57
7.3	Effect of Blood Viscosity	57
VIII.	ARTERIAL DYNAMICS IN HEALTH AND DISEASE	59
8.1	Branching	59
8.2	Effect of Taper	60
8.3	Effect of Arterial Compliance	60
8.4	Effect of Distal Reflections	62
8.5	Effect of Arterial Obstruction	65
	Computer Simulation of Arterial Obstruction	65
	Experimental Arterial Obstruction in Dog	67
	Discussion and Comparison of Data	68
IX.	CONCLUSIONS	71
	CAPTIONS FOR FIGURES	73
	FIGURES (1-60)	78
	APPENDIX A - Computer Listing (A1-A17)	79
	APPENDIX B - % Area Reduction as a Function of Clamp Opening	167
	APPENDIX C - Electrical Drawings and Specifications	170

	Page No.
MEDICAL GLOSSARY	172
REFERENCES	178
BIOGRAPHY	185

NOMENCLATURE

A	cross-sectional area
A_o	local area at reference pressure
BP	brachial artery blood pressure (systolic/diastolic)
BPM	beats per minute (HR)
c	pulse-wave velocity (wave speed)
C	segment volumetric compliance
CC	control case
C_a	compliance of arterial section surrounded by monitoring cuff ($\delta V_a/\delta p_a$)
C_u	vessel compliance per unit length ($\partial A/\partial P$)
C_T	volume compliance of tibial termination
D	diameter
D_c	clamp gap
D_{co}	clamp gap (no obstruction)
f	wall friction force per unit mass of blood
F	approximate viscous coefficient in momentum equation
GAIN	PPR electrical gain
HR	heartrate (BPM)
Hz	hertz (cycles per second)
i	time notation for finite difference method
j	$\sqrt{-1}$
k_e	entrance loss coefficient
K	reflection coefficient (magnitude)

KHz	1000 hertz
L	length of obstruction
Ln(X)	the natural log of X
L_u	inertance per unit length (ρ/A_o)
N	spatial notation for finite difference method
p	pressure
$\bar{p}$	mean pressure
p_{ATM}	atmospheric pressure
p_a	arterial pressure
p_c	absolute cuff pressure
P_{CUFF}	cuff gage pressure (P_c)
p_o	reference pressure
PPR	pressure pulse recorder
p_v	venous pressure
p_s	systolic pressure
Q	volume rate of flow
$\bar{Q}$	mean flow
Q_L	leakage term in continuity equation
R	leg peripheral resistance
R_1	primary termination or branch resistance
R_2	secondary termination or branch resistance
R_H	hypogastric resistance
R_p	profunda resistance
R_{PR}	real peripheral resistance
R_T	tibial resistance also ($R_1 + R_2$) for general representation
t	time

u	mean fluid velocity (1 - D)
V_c	volume of air in cuff monitoring circuit of PPR
V_I	injected volume
V_1	tube volume from an internal shut-off valve in the PPR to the monitoring cuff
V_2	tube volume from the shut-off valve in the PPR to the syringe
x	longitudinal distance
X_N^i	denotes the value of X at the i^{th} time step and the N^{th} spatial step
Z_o	characteristic impedance
Z_T	termination or load impedance
α	percent arterial area change per 50 mm-Hg at 100 mm-Hg
β	proportionality constant relating p to C_u
δp_c	cuff pressure change
δV	volume change applied to cuff
δV_a	arterial volume change
δV_c	cuff volume change
δV_x	volume change due to the expansion of the bladder over a monitoring cycle
Δ	relative amplitude of PPR traces
ΔP	pressure drop across obstruction
ΔP_{BL}	pressure loss due to developing boundary layer in obstruction model
ΔP_c	pressure loss due to contraction in obstruction model
ΔP_u	pressure loss due to unsteady flow
ΔP_x	expansion pressure loss

Δt	time step for finite difference method
Δx	spatial element for finite difference method
η	Womersley Frequency Parameter
γ	ratio of specific heats
ϕ	phase of reflection coefficient
μ	dynamic viscosity
ν	kinematic viscosity
ω	pulsatile or circular frequency
ρ	fluid density
ψ	symbol used in the finite difference method
θ	symbol used in the finite difference method

I. INTRODUCTION

Arteriosclerosis is a term applied to a number of pathological conditions in which there is thickening, hardening, and loss of elasticity of the arterial wall. Atherosclerosis is a form of arteriosclerosis in which there are localized inflammatory lesions (atheromas) within or beneath the intimal surface of the arterial wall. This condition is thought to be due to general arterial wear and metabolic defect involving lipids and lipoproteins (1,2) and is one of the common causes of arterial narrowing and occlusion.

Arteriosclerosis is present to some extent in almost all adults and can involve almost any artery, thus producing a variety of symptoms and consequences. The most common examples of acute conditions include:

i) myocardial infarction - a portion of the heart muscle becomes damaged because of interruption of its blood supply by atherosclerotic occlusion, acute thrombosis, or coronary artery embolism.

ii) stroke - the blood supply to portions of the brain is suddenly reduced by cerebral arterial occlusion or embolus.

iii) gangrene - the blood supply to a peripheral tissue mass is reduced due to arterial occlusion and the tissue dies.

More chronic conditions include angina, transient cerebral ischemia, and intermittent claudication.

In the last ten years options open to physicians for the treatment of arteriosclerosis have increased at a rapid pace (3). Surgical revas-

cularization is now possible in an increasing number of anatomical areas ranging from the myocardium to the arteries of the lower limbs (4,5,6,7). This has been possible through the development of prosthetic grafts, techniques involving the removal of atheroma, and the use of vein segments for arterial bypass (8). Drug and dietary treatment for high blood levels of cholesterol and triglyceride, as well as hypertension have also been expanded with success (9).

As these new procedures have become more common the need for early and accurate evaluation of arteriosclerosis has become more acute, both for the clinician and the research scientist.

Arteriography is the primary invasive technique for the diagnosis of arteriosclerosis in man. It is performed by injecting radio-opaque dye into an artery in the region of interest and taking roentgenograms of the area. Figure 1 is an example of an arteriogram taken in a patient with aorto-iliac disease. The procedure consists of inserting 18 gauge needles in the common femoral arteries at the level of the inguinal ligament and injecting 35cc of Renograffin-60^{R} into each artery just prior to X-ray. While this technique often provides the vascular surgeon with an arterial "roadmap" there are a number of drawbacks:

i) The technique is expensive. It requires hospitalization and is performed either in the operating room or in an elaborate radiology suite. Typically two physicians, a nurse, and an X-ray technician are required for an hour with an aggregate cost, including hospitalization, of approximately $500.

ii) The procedure is uncomfortable for the patient, producing varying degrees of pain during and immediately following the dye injection. Many patients describe arteriography as more of an ordeal than the operation for which they are being examined. In addition, the dye may produce nausea and diuresis, and in some cases cannot be used due to allergy.

iii) Hazards of the procedure are not uncommon and include possible intimal damage to the artery at the site of puncture, local artery thrombosis, and hematoma in the region where surgery will be performed.

iv) It is often quite difficult to interpret arteriograms (10). Even when arteriograms have been taken in two orthogonal planes lumen obstruction and hemodynamic significance of the lesions are not clear.

v) The procedure cannot be performed repeatedly.

Since present non-invasive techniques have many shortcomings that will be outlined in a subsequent section of this paper, new non-invasive techniques for preoperative evaluation, monitoring during arterial reconstruction, post-operative monitoring and assessment of arterial condition after and during drug and dietary treatment are needed.

The rationale we have adopted to develop a new non-invasive technique is based on the fact that arteriosclerosis produces pathological

conditions such as increased arterial wall stiffness by calcified deposits (Fig. 2) and decreased lumen area by atheromatous build-up (Fig. 3) which in turn change the pressure and flow characteristics of the arterial pulse. The effects of these pathological changes on the arterial pressure and flow pulses will be discussed with the aid of experimental and theoretical data.

In this investigation the diagnosis and analysis of peripheral vascular disease in the lower limbs were chosen as the focal points. This decision was made because of the prevalence of all forms of arteriosclerosis below the renal arteries (11) and because arteries of the lower limbs are accessible to different forms of diagnostic measurement.

The first task in the research was to develop a device, referred to here as a Pressure Pulse Recorder (PPR), that could be used non-invasively to measure the pressure pulse at specific sites on the lower extremities. The second step was to study the pressure pulse characteristics recorded with the PPR in diseased and healthy arteries. In accomplishing this, patients undergoing vascular reconstruction were studied pre-operatively, intra-operatively, post-operatively, and during office follow-up examinations during an 18-month period. Results provided by the PPR were compared to arteriograms, surgical findings, and clinical information.

To aid in the interpretation of measurements made during the clinical studies a computer simulation of the arteries of the lower extremities extending from the iliac bifurcation to the tibial vessels

was developed. The major requirement of the model was to accurately mimic the pulse propagation along the arteries. Relevant physiological data were obtained and used in the model. When a control case corresponding to a normal healthy individual was defined, the arterial elasticity, reflection coefficients, and other circulatory parameters were varied and their effects analyzed with the model. In addition various degrees of obstruction were introduced in the simulated arteries. Verification of model results were obtained from human data and dog experiments.

In summary, this report describes:

i) the development of an instrument to non-invasively record the pressure pulse on the lower extremities.

ii) the measurement of arterial pressure pulses in diseased and normal arteries.

iii) the interpretation of observations of the arterial pressure pulse by means of computer simulation of arterial dynamics.

II. PRESSURE PULSE RECORDER-DEVELOPMENT AND DESCRIPTION

The development of the PPR was prompted by the fact that no adequate non-invasive instrument was available for the measurement and recording of arterial pressure pulses in the extremities.

2.1 Current Non-Invasive Devices

The examination of a patient for an arterial abnormality generally includes symptomatology, pulse palpation, auscultation by stethoscope (bruit location), as well as observations such as limb pallor, temperature, and capillary filling.

In addition to the stethoscope as previously mentioned there are some other non-invasive instruments currently in use.

The oscillometer (12,13) is the oldest of the devices used specifically to aid in the diagnosis of vascular problems. It consists of two small overlapping blood pressure cuffs and a mechanical pressure transducer. When its sensitivity is adequate, it provides a qualitative indication of limb volume pulse with its output read on an aneroid gage. It is highly qualitative, cannot be standardized, provides no contour information, provides no permanent record, and in most cases is not sensitive enough to distinguish all but the most obvious peripheral vascular abnormalities. It is, however, easy to use and inexpensive.

In recent years the transcutaneous Doppler ultrasonic blood-velocity detector (14,15,16) has gained popularity among vascular surgeons (17,18,19,20,21,22). The Doppler velocity detector can detect

the presence of blood flow in arteries and can be used in conjunction with the cuff occlusion method to accurately measure systolic blood pressure in the lower limbs. With the Doppler velocity detector in its present form it is virtually impossible to obtain transcutaneously any quantitative measurement of blood velocity because the angle between the ultrasonic beam and the vessels is not known accurately and cannot be maintained.

Two other instruments deserve mention. They are the mercury-in-silastic strain gage (23,24) and the impedance segmental plethysmograph (25). The mercury-in-silastic strain gage measures the change in limb or digit circumference. The impedance segmental plethysmograph measures impedance changes in a limb segment secondary to pulsatile blood volume changes. Both of these devices do produce hardcopy readout and contour information, however, they cannot be standardized and produce traces with high noise content. For these reasons they are not of great use in diagnosis or in following the state of the peripheral vascular system.

2.2 The Pressure Pulse Recorder

The following sections describe an instrument that produces a reasonably accurate recording of the arterial pressure pulse at various sites on the extremities. This instrument records the segmental limb volume displacement due to the passage of the arterial pressure pulse. With the aid of some experimental work including *in vivo* simultaneous measurement of intra-arterial pressure and non-invasive pressure pulse

recordings an operating procedure was developed such that the pulsatile volume displacement is approximately proportional to the arterial pressure pulse. The trace can be calibrated by two independent pressure measurements of systolic and diastolic pressure and the instrument constitutes then an arterial pressure pulse recorder (PPR).

For screening purposes the instrument is essentially used to compare the pressure pulse amplitudes recorded at different locations along the two legs (at the thigh, calf and ankle). If the amplitudes are different in the two legs, this is interpreted as the presence of an obstruction proximal to the monitoring site in the leg which has the smallest amplitude. A sharp amplitude drop in the same leg between two sites is also indicative of a block. For monitoring, a comparison of the pulse amplitudes recorded before and after revascularization provides a verification that surgery has improved peripheral circulation.

Although pulse amplitude by itself provides important information, it is logical to assume that additional information can be extracted from the entire pulse contour. For this reason, it is important that the recording represent as accurately as possible the true arterial pressure pulse. The accuracy of this instrument rests on an optimum design of the electronic components permitting a large amplification of the signal and the use of low cuff pressures.

2.3 Description and Operating Procedures

The PPR (Fig. 4) consists of two non-overlapping air-filled cuffs*, one for pressure monitoring and the other for occluding the

---

* manufactured by W.A. Baum, Co., Copiague, New York.

artery for calibration purposes. These cuffs consist of a neoprene bladder (13 cm wide, 23 cm long) covered by a semi-rigid nylon-velcro band. When recordings are made at the thigh a larger cuff (18 cm wide, 35 cm long - bladder size) of the same material is used. The monitoring cuff is connected by stiff latex tubing to a pressure sensitive transistor (Pitran - 0.1 psid series). The Pitran is a silicon NPN planar transistor with its emitter-base junction mechanically coupled to a diaphragm. A differential pressure applied to the diaphragm produces a large, reversible change in the gain of the transistor which has a uniform frequency response up to 150 KH_z. Figure 5 provides additional technical data on the Pitran, while a diagram of the layout is represented on Fig. 6. The instrument is compact and self-contained and can be operated by paramedical personnel after a brief training period.

The other electronic components of the PPR are:

i) A sample-and-hold circuit operating in closed-loop fashion to maintain the proper operating point for the pressure sensor.

ii) Logic circuits to configure the 120 volt AC solenoid valves* according to the mode selected by the operator.

iii) A dual-limit comparator to detect and correct for excessive differential pressure applied to the sensor.

iv) A panel switch to provide DC-coupled or AC-coupled output to the chart recorder with a sensitivity selected by the operator.

---

* Skinner (B-model, subminiature), Skinner, Co., New Britain, Conn.

v) A peak-to-peak detector to provide an indication of relative pulse volume on the panel meter.

Detail electrical drawings and specifications are provided in Appendix C. This appendix was prepared by the Medical Engineering Company, Mansfield, Massachusetts.

Either cuff can be connected to an aneroid pressure gage which serves to measure the mean cuff pressure. A built-in syringe is used to introduce a definite volume of air at atmospheric pressure into the bladder of the cuff (generally 75 ml for the arm, ankle and calf cuff and 200 ml for the thigh cuff). The band around the bladder of the cuff is used to adjust the pressure in the monitoring cuff to a value sufficient to insure close contact with the skin, but well below diastolic pressure. The proximal cuff is open to atmospheric pressure. The passage of the arterial pulse causes the segmental volume of the limb surrounded by the cuff to change. The changes in limb volume are absorbed by the bladder which is contained by the semi-rigid band. The cuff pressure fluctuations caused by the cuff volume changes are transformed into electric signals by the transistor. The output signal is displayed on a convenient recording device (an ECG recorder is adequate).

2.4 Measurement of Systolic and Diastolic Pressure in the Lower Limbs

To permit maximum use of the chart width and provide stable recordings, the instrument is AC-coupled with a time constant of 1 sec. As a result the pressure trace is centered on the chart and the

location of zero pressure is not known. It is therefore necessary to calibrate the pressure scale by measuring independently the systolic and diastolic pressures at the site of the recording. This calibration is made with an occlusion cuff placed proximally. A typical measurement of systolic and diastolic pressure with the PPR for the brachial artery is shown in Fig. 7. The pressure in the occlusion cuff is raised above systolic pressure (no oscillations in the monitoring cuff) then is slowly lowered until the pressure in the monitoring cuff starts to fluctuate. The systolic pressure is read from the aneroid gage at the onset of the pressure fluctuations in the monitoring cuff. As the pressure is lowered in the occluding cuff the oscillations in the monitoring cuff grow in amplitude and generally overshoot the control value obtained when the pressure in the occluding cuff was zero. At the point the oscillations reach a maximum diastolic pressure is read as the pressure in the occluding cuff. Although the cuff pressure at which oscillations reach their maximum amplitude does not rigorously correspond to the diastolic pressure, a study illustrated in Fig. 8 has indicated that it provides a convenient and reasonably criterion for diastolic pressure especially if the venous return is not interrupted for a long period. This figure gives a comparison of systolic and diastolic pressures obtained by the occlusion and auscultatory methods in the brachial arteries of 13 healthy volunteers using standard blood pressure cuffs 13 cm in width. As suggested by Karvonen et al. (26) the diastolic pressures indicated by the auscultatory method have been decreased by

7-8 mm-Hg. This correction generally brings the diastolic pressure in closer agreement with those indicated by the PPR. The systolic pressures determined by the PPR are consistently higher than those obtained by the auscultatory method, but the difference is small. Systolic and diastolic pressures obtained by the PPR have also been compared with pressures measured by cannulation of the radial and common femoral arteries at surgery and during arteriography, respectively. The agreement was very similar to that presented in Fig. 8.

2.5 Dynamics of the Air in the Cuff

To aid in the development of the PPR operating procedure and the interpretation of its recordings it was important to understand how the pressure of the air in the cuff related to the arterial pressure. In order to accomplish this a number of experiments were performed in addition to analysis.

First, consider the constant mass of air in the cuff at an absolute pressure p_c in a volume V_c. Further, if it is assumed that the gas undergoes an isentropic process the following equation may be written

$$p_c V_c^{\gamma} = \text{const} \qquad [1]$$

where γ is the ratio of specific heats (for air, $\gamma = 1.4$).

To test the validity of the isentropic assumption the pressure measuring components of the PPR were connected to a rigid cylinder (50 ml volume). Also included in the pneumatic circuit was a small piston-in-cylinder pump with a 1 ml stroke volume. The pump was used to oscillate the total volume of the system at various frequencies while measuring the pressure changes. It was found that at frequencies from 0.25 Hz to 20 Hz (highest frequency tested) the pressure amplitude remained constant. The

pressure amplitude increased approximately 34% gradually from zero frequency (isothermal) to 0.25 Hz.* This experiment suggests that in the range of frequencies encountered in clinical use (0.50 to 1.5 Hz) the air in the cuff undergoes an isentropic process, changing from isothermal to isentropic between zero and 0.25 Hz. The heat transfer characteristics of the bladder may be different than the rigid cylinder due to geometry and material differences. This is discussed in a later section. Also, it will be shown later that the identification of the process is not critical to the analysis as its effect is to be combined with the elastic expansion of the cuff. Since the volume excursions in the cuff are a small fraction (2% max) of its mean volume, Eq. [1] can be differentiated to give

$$\delta p_c = -\frac{\gamma \bar{p}_c}{\bar{V}_c} \delta V_c \qquad [2]$$

where p_c and V_c have been replaced by their time-mean values $\bar{p}_c$ and $\bar{V}_c$ respectively. The time-mean volume $\bar{V}_c$ is also a function of cuff pressure and the injected air mass. If the initial volume of air injected at atmospheric pressure (p_{ATM}) is V_I, the volume of air in the cuff is defined by Eq. [3]

$$\bar{V}_c = \frac{p_{ATM}}{\bar{p}_c} (V_I + V_1 + V_2) - V_2 \qquad [3]$$

Here V_1 is the tube volume from an internal shut-off valve in the PPR to the monitoring cuff; V_2 represents the tube volume from the shut-off valve to the syringe. In the prototype built V_1 and V_2 are 21 and 22 cc, respectively. The compression of the injected air is assumed to be isothermal since it subsists for a long period of time, much longer than 4 sec (0.25 Hz).

---

*These results are plotted in Fig. 8a.

Combining Eqs. [2] and [3] we find

$$\delta p_c = \frac{-\gamma \delta V_c \bar{P}_c}{(p_{ATM}/\bar{p}_c (V_I + V_1 + V_2) - V_2)} \qquad [4]$$

To investigate the validity of Eq. [4] another experiment was performed. The monitoring cuff was connected to the PPR electronics with a 1.0 ml syringe also in the pneumatic circuit. The syringe was used to change the total air volume in increments of 0.25 ml from 0.25 ml to 1.0 ml at different cuff pressures and initial injected volumes. Cuff gage pressures of 20,40,60,80 and 100 mm-Hg were used with injected volumes of 25,50,75 and 100 ml. The results of this experiment indicated that the bladder constrained by the nylon-velero band is not inextensible, but instead expands with pressure over a monitoring cycle. The edges and corners of the bladder which are not constrained by the cuff may move and make additional volume available. The actual volume change of the air in the bladder δV_c is calculated from the measured pressure change using Eq. [4]. Then the volume δV_x due to the expansion of the cuff is defined by

$$\delta V_x = \delta V - \delta V_c \qquad [5]$$

where δV is the volume change applied to the cuff.

Figure 9 illustrates how the ratio $\delta V_x/\delta V$ varies with mean cuff pressures and injected volumes. It is interesting to note that the extrapolation of the measurements to $p_c \to 0$ leads to $\delta V_x = \delta V$,

and that even at high cuff pressures the expansion is still present, but to a lesser degree as the bladder becomes stiffer. The fact that wrapping an inextensible band around the cuff does not change the results suggests that end effects, not the stretching of the bladder, is the dominant factor. This observation suggests that the sensitivity of the instrument may be considerably improved by designing a cuff which absorbs all the limb volume change. Including the results of the preceding experiment we rewrite Eq. [4] as

$$\delta p_c = \frac{-\gamma \delta V \left(1 - \frac{\delta V_x}{\delta V}\right)}{\left[\frac{(p_{ATM}/\bar{p}_c)(V_I + V_1 + V_2) - V_2}{\bar{p}_c}\right]} \qquad [6]$$

The next step in the analysis is to assume that the volume changes of the limb caused by the passage of the pressure pulse are proportional to the changes in the arterial volume δV_a encompassed by the cuff. We write

$$\delta V = \delta V_a = C_a \, \delta \, p_a \qquad [7]$$

where $C_a = \delta V_a / \delta p_a$ is the compliance of the arterial section surrounded by the cuff and p_a denotes the arterial pressure. Combining Eqs. [6] and [7]

$$\delta p_c = \frac{\gamma C_a \delta p_a \left(1 - \frac{\delta V_x}{\delta V}\right)}{\left[\frac{(p_{ATM}/\bar{p}_c)(V_I + V_1 + V_2) - V_2}{\bar{p}_c}\right]} \qquad [8]$$

Since $\delta V_x/\delta V$ is approximately independent of δV, it follows from Eq. [8] that if C_a remains constant the variations in the cuff pressure are proportional to the variations in arterial pressure and the output of the pressure sensitive transistor will yield a good representation of the arterial pulse contour. The critical experiment to test the accuracy of this analysis is of course the comparison with direct intra-arterial measurements.

2.6 Comparisons with Intra-Arterial Measurements

To verify the accuracy of the pressure pulse contours produced by the PPR, recordings were compared with direct intra-arterial pressure measurements taken at the same location. Five comparisons on different subjects prior to surgery were performed by placing the PPR monitoring cuff around the forearm while simultaneously recording radial artery pressure with a cannula (the radial cannula had been placed for surgical monitoring purposes). The transducer used for all the direct pressure measurements was a Hewlett Packard Model 267 BC. The cannula was an 18 gauge needle connected to a 2 foot length of rigid wall catheter. All comparisons yielded the same degree of agreement, even though patient size, weight, and age were in general different. Figures 10a-10e show comparisons made at the radial artery with recordings taken externally in the same arm with various adjustments of the mean cuff pressure. Only the recordings for 30 (lowest value for good bladder contact) and 100 mm-Hg are shown as the traces corresponding to intermediate values fall between these two limiting curves. Since the

purpose is to compare the contours only, the recordings have been redrawn and scaled to the same amplitude. Five additional comparisons were made during arteriography with the PPR monitoring cuff placed high on the thigh while simultaneously recording common femoral artery pressure via a cannula. In all cases, no arterial block was present in the short distance between the cannula and the cuff. Figures 11a-11e illustrate comparisons taken at the thigh after appropriate scaling. Further studies at the calf were made during arterial reconstruction by introducing a catheter down the popliteal artery. The results showing identical trends as illustrated by Figs. 10 and 11.

The results of our studies indicate that the smaller the cuff pressure, the closer the PPR recording is to the true pressure contour. We postulate, since the presence of the cuff reduces the transmural pressure in the artery beneath it, at high cuff pressure, the nonlinearity of the arterial pressure-volume relationship (27) produces a marked distortion in the recorded pulse contour. The distortion is proportionally larger in the diastolic part of the pulse. Viscoelastic effects present in the tissue and arterial wall also probably distort the PPR traces. However, the cuff pressure must be sufficient to produce adequate contact between the bladder and the skin. A cuff pressure of 30 mm-Hg provides good bladder contact and still gives a reasonably good agreement with intra-arterial measurements.

In another study we changed injected volume while holding cuff pressure constant over a range of 20 ml to 125 ml. The results indicate

that the injected volume in the cuff does not alter significantly the pressure pulse contour [see Fig. 12] and that the injected volume in the cuff may be lowered as low as 20cc if a larger signal is desired without danger of distorting the pulse contour.

2.7 Frequency Response

The frequency response of the complete device (cuff and electronic circuit) was tested by connecting a liquid-filled bladder to a small piston-in-cylinder pump producing a sinusoidal change in volume in the bladder. This bladder was strapped around a rigid plastic cylinder and surrounded by the air-filled monitoring cuff of the device. The action of the pump produced oscillations in the volume, and consequently in the pressure of the monitoring cuff. The amplitude of the air pressure oscillations in the cuff remained constant from 0.25 Hz to 20 Hz (as in the rigid cylinder experiment). The natural frequency of the cuff and electronic system was determined to be approximately 55 Hz by sharply tapping the monitoring cuff and measuring the frequency of the vibration from the trace (28). Two important conclusions may be drawn from these observations. First, the frequency response is sufficient for monitoring the pressure pulse since a frequency response of 20 Hz is considered to be adequate (29). Secondly, we have an experimental confirmation of the assumption that the pressure pulse compresses the cuff isentropically. If the compression was isothermal (or at least non-adiabatic) at the usual heart frequency, it would certainly become adiabatic at higher frequencies (between 0.25 and 20 Hz) when the duration of each cycle is too small for

heat transfer to occur. If this was the case the change in the coefficient γ in Eq. [2] (from 1 for isothermal compression to 1.4 for adiabatic compression) would cause a 40% increase in cuff pressure amplitude over the frequency range.

In summary, it has been established that the readings produced by the PPR are reasonably close to the actual arterial pulse contour if the pressure in the cuff is at 30 mm-Hg or below.

Sample recordings taken at the brachial artery, forearm, thigh, calf, and ankle of both upper and lower extremities in a healthy subject are shown in Fig. 13.

III. CLINICAL STUDIES AND OBSERVATIONS

Two Pressure Pulse Recorders were constructed and tested at the Fluid Mechanics Laboratory at M.I.T. The conceptual design and general construction were performed by the author. The electronic circuits were built by the Medical Engineering Company of Mansfield, Massachusetts. When the units had undergone sufficient laboratory testing they were transferred to the Massachusetts General Hospital. One unit was placed in the office of R. Clement Darling, M.D., for initial patient evaluation and follow-up. The other unit remained in the hospital to be used for in-patient pre-operative, intra-operative, and post-operative studies. The plan included studying as many patients as possible undergoing vascular reconstruction and comparing data obtained with the PPR with results from current methods. In the course of an 18-month period over 200 patients were examined with the PPR.

The clinical PPR examinations include:

i) the measurement of systolic blood pressure at the brachial artery, thigh, calf, and ankle at rest in all extremities.

ii) recordings of thigh, calf, and ankle pressure pulse contours in both legs at rest.

iii) noting the presence or absence of femoral, popliteal, and pedal pulses.

iv) patients were asked to walk at their normal rate until claudication occurred or 200 yards was reached; immediately (generally within 20 sec.)

upon completing walking, recordings were taken at the ankle; the maximum walking time and character of the recordings and pressures after exercise were measured (a treadmill is now being used).

v) other pertinent clinical information was recorded such as absence or presence of rubor and bruits, as well as, limb skin temperature.

A wide spectrum of vascular disease was encountered: aneurysmal and occlusive disease of the aorta and distal vessels, vasospastic disease, and occlusive disease of the upper and lower extremities. The following cases are given to illustrate how the PPR data were used, and how they correlated with the clinical and angiographic findings.

3.1 Case Studies

The first case was a 50 year old female (YW) presented with sudden onset of claudication of the right calf radiating to the thigh. All pulses were palpable in both lower extremities. Figure 14 is a comparison of the angiographic findings and the resting pre-operative PPR examination. On the right side the pulse amplitudes [Δ] were severely reduced despite palpable pulses at rest. A 60 mm-Hg systolic pressure difference (measured with the PPR using the occlusion method) was present between the brachial artery and the right femoral artery. No difference was present on the left side. Her claudication developed

on the right side after walking 150 yards in 1.5 minutes. Figure 15 shows the pulse amplitude at the right ankle became flat and required 2.5 minutes after ceasing exercise before returning to the normal resting level. The pulse amplitude at the left ankle actually increased after exercise and returned to normal after a short period of time. Figure 16 shows that, after insertion of an aortoiliac bifurcation graft, the pulse amplitude in the lower extremities were equal. In addition, no pressure difference in systolic pressure between upper and lower extremities could be demonstrated. Figure 17 shows that, post-operatively, after exercise no diminution in pulse amplitudes at the ankles were present. Actually the pulse amplitudes in the ankles increased twofold with exercise.

The second case [KM] was a 65 year old stockbroker, a heavy smoker, and diabetic for 25 years. He presented a long history of bilateral calf claudication and threatened gangrene of toes on the right foot. Good femoral pulses were the only pulses palpable. Pre-operative findings are presented in Fig. 18. The PPR examination suggested severe ischemia on the right side with a 70 mm-Hg difference in systolic pressure between the brachial artery (left arm) and the superficial femoral arteries in both legs. The patient was not asked to exercise because of the threatened gangrene of the right foot. The diagnosis of bilateral superficial femoral occlusion with tibial vessel involvement was made and confirmed by arteriogram. Figure 19 illustrates the findings of the examination following insertion of a femoro-popliteal saphenous

vein bypass graft in the right leg. No vascular reconstruction was performed in the left leg. The pulse amplitude increase on the right side is evident by examining pre- and post-operative traces (Figs. 18 and 19). In addition, the systolic pressure differences between the brachial artery and the superficial femoral artery on the right side was reduced from 70 mm-Hg to 10 mm-Hg. Figure 20 shows the results after walking the patient 100 yards in 2.5 minutes. Note the left ankle pulse amplitude goes to zero and requires three minutes to return to normal. Following surgery claudication was no longer present at the right calf.

The object of the third case is to emphasize the application of monitoring with the PPR during vascular reconstruction. The patient (TB) was a 62 year old male, ex-smoker presented with a 10 cm abdominal aortic aneurysm, right superficial femoral occlusion, and left iliac obstruction secondary to the aneurysm. Prior to surgical preparation, blood pressure cuffs used with the PPR were placed at the calf level of both legs. At the beginning of surgery, readings were taken at the right and left calves (the device is placed at a convenient location in the operating room and the air hose from the cuffs connected to the electronics). These pre-operative readings along with the remaining readings of this study are given in Fig. 21. With the aneurysm resected and the left anastomosis completed, a recording was taken as the clamp was removed from the left iliac limb. At this point, as illustrated, a 33 mm relative pressure pulse amplitude was recorded at the left calf. When the right anastomosis was completed and the clamp removed, the pulse amplitude remained zero at the calf although the pre-operative recording was 8mm. A good femoral pulse, however, could be felt on the operating table. Due to the

superficial femoral artery occlusion no palpable pulses were expected below the femoral level after surgery. The PPR provided a non-invasive method of immediately evaluating the reconstruction. The common femoral was explored and a thrombus removed at the profunda femoris level. When this was completed the recorded amplitude at the right calf was 10 mm. The remainder of the procedure was uneventful and angiography was notnecessary.

In addition to the frequent vascular conditions previously described the PPR was used in other less common clinical situations. PPR examinations were requested by the Pediatric Service for two infants because of suspected coarctation of the aorta (conventional blood pressure measurements had not proved useful). In the first case a 50 mm-Hg systolic pressure difference between the upper and lower limbs confirmed the diagnosis, and further study was warranted. In the second case no systolic difference was present and the child was discharged. In three cases involving the catheterization of very young children the PPR was used to look for the complication of femoral artery thrombosis. When the examinations proved positive, thrombectomy was performed in all three cases. The device was used for intra-operative monitoring and post-operative follow-up as well. In one case the thrombectomy was not successful and the child was examined at regular intervals over a two week period and released when the device indicated adequate collateral circulation had developed. In two cases the PPR was used for verification of thoracic outlet syndrome. Angiography had not proven decisive in either case. In one case the syndrome was convincingly demonstrated by near

zero PPR amplitudes when the patient extended her neck and arms to the point of pain. In the other case no arterial changes occurred with position, the symptoms later found to be of neurological origin only.

During the clinical evaluation period the PPR was demonstrated to be consistent in the monitoring of arterial pressure as shown by the following examples.

A patient (RS) was examined four times with the PPR over a nine month period. He was followed for general atherosclerotic disease after a carotid endarterectomy was performed. Figure 22 illustrates the PPR traces at the left calf using the same cuff pressures and volumes during the period of study. The consistency of the PPR traces is confirmed by the patient's clinical evaluation regarding the peripheral arterial system of the lower limbs. It is important to note that the PPR traces were not affected by seasonal temperature variations. All recordings were taken in a standard examination room with no special temperature control.

A patient (JA) was examined seven times with the PPR over a twelve month period following insertion of an aorto-femoral bypass graft (Fig. 23). On the fourth visit it was found that the left limb of the graft had occluded. The amount of collateral circulation after occlusion may also be assessed from these traces.

In a series of seven patients in which one extremity (upper or lower) was grossly enlarged while the extremity on the other side remained normal in the absence of arterial disease on either side, it was concluded that, when properly applied the PPR will produce virtually

identical traces on the left and right limbs. An example is patient (BM) who developed lymphedema of the left arm following an automobile accident. The circumference of her left upper arm was twice that of the right arm. Figure 24 shows that recordings taken at the left and right brachial artery at the same cuff pressure and injected volume are almost identical. From this series of patients we concluded that edematous tissue does not appreciatively alter the contour or amplitude of the PPR recordings.

3.2 Pressure Pulse Contours

In addition to pressure pulse amplitude changes, there are distinct alterations in the pressure pulse contour with peripheral vascular disease. Figure 25 shows recordings taken at the right calf of three healthy athletic young men. Note the sharp rise and fall of the pulse during the initial phase followed by a distinct wave in the latter half of the trace. For reasons to be explained later this wave will be referred to as a reflected wave.

Figure 26 presents recordings taken at the right and left ankles of a 50 year old male (WP). This patient had an occlusion of the left superficial femoral artery and complained of claudication at 50 yards. His right leg was asymptomatic and the corresponding ankle recording was relatively normal. At the left ankle the systolic pressure was reduced by 15 mm-Hg, in addition this contour is considerably different. The upstroke was sharp, however, the descending phase of the curve was slow and the reflected wave was absent.

Figure 27 illustrates recordings taken at the right and left calves of a 30 year old female (MM). This patient had a long standing right common femoral artery thrombosis which was caused as a result of a left heart catheterization. The left femoral artery was normal. Right calf claudication was present after walking 100 yards and pain radiated to the thigh with continued exertion. The contour changes seen in this case are similar to the changes observed in the preceding case.

It is beyond the scope of this work to make a detailed analysis of all the parameters and situations that have been dealt with during the clinical studies. However, regarding the contour of the pressure pulse, certain changes deserve attention. In all cases when significant occlusive disease was present a reflected wave was never observed distal to the obstruction. Instead, traces similar to those of the symptomatic side in Figs. 26 and 27 were found. In older persons the reflected wave was often not present, however, in these cases when the vessels were open a rapid rise was noted along with an exponential pressure decay. This is in contrast to the patient with arterial occlusion where the rate of pressure rise distal to occlusion is reduced and the pressure decay slow.

Blood pressure levels and palpable pulses are often normal at rest in patients with significant peripheral vascular disease; in this case the only indication of an abnormality at rest is the shape of the pressure pulse contour. However, if significant occlusive disease is present the muscle mass distal to an obstruction will not be adequately perfused when the patient exercises. This inadequate perfusion causes claudication and

pressure reduction. This pressure reduction (both mean and pulse pressure) results in decreased recordings distal to the muscle mass as demonstrated in Figs. 15 and 20. To determine what happens to the recordings in the normal individual with exercise, healthy athletes were examined before and after running. Typical results are presented in Fig. 28. The recorded amplitude increases with exercise and returns to normal shortly after ceasing exercise. In addition, the reflected wave is no longer present directly after exercise, but returns with time. Post-exercise examination with the PPR is helpful in monitoring the state of the peripheral vascular system under stress.

In summary, the PPR traces provide consistent information with regard to the state of the peripheral vascular system, and can be used to follow patients over extended periods of time. PPR recordings taken after exercise may reveal vascular abnormalities that would not be detected in the resting state. In addition, the device has been most helpful for intra-operative monitoring during vascular reconstruction (30). Finally, arterial occlusions can be detected by contour and amplitude changes in the distal pressure pulse.

IV. MATHEMATICAL MODEL OF ARTERIAL FLOW

Since the pioneering work of Frank (31) in 1899, numerous electrical, mechanical and computer simulations of the arterial system have been attempted, all aimed at a better understanding of cardiovascular dynamics. An extensive survey of mathematical models is given by Noordergraaf (32). Most of these simulations require that some restrictions be placed on the geometric and elastic properties of the arterial system as required by the electrical components themselves or by linearization of the equations of a computational model. This section presents a convenient and economical method of calculation, based on a finite difference technique, for a one-dimensional pulsatile flow in a network of elastic tubes having arbitrary geometric and elastic properties. As more data on the dimensions and the compliance of arteries become available this method makes possible more realistic and more accurate models of the arterial system than can be done with electrical and other linearized models.

Our own observations reported in Chapter 3, as well as those of others (33,34) have shown that a patient afflicted with severe vascular disease has a peripheral pressure pulse markedly different from that of a healthy person. The ultimate goal of the arterial model and method of calculation described in this section is to aid in the diagnosis of peripheral vascular diseases such as thrombosis and atherosclerotic plaque formation, starting from observations of the shape of the pressure pulse contour, such as those taken with the PPR.

In order to be able to make accurate diagnoses from computed pressure pulse contours these contours must be free from artifacts resulting from the model itself or from the computational techniques used. Therefore the choice of the model, its degree of complexity, and the computational scheme of solution, are all crucial to the method. The model cannot reproduce the complete arterial tree, not only because the mathematical complexity and the computation time would be enormous, but also because physiologic data on arteries are still too limited to permit a model of great detail. It is clear that a compromise must be sought and that the different options available for describing the blood flow and the arterial tree must be tried and compared against each other in order to arrive at the simplest model which still describes reliably the shape of the pressure pulse as it propagates into the peripheral arteries.

The arterial models proposed in the past have ranged from electrical analogues made of lumped elements to elaborate mathematical models with continuously distributed properties. The lumped-element models are adequate for studying the relations between cardiac output and peripheral load, but, because of the small number of lumped-elements present, they cannot mimic the high frequency behavior of the cardiovascular system. An important step towards more versatile and more realistic models was the discovery that the linearized one-dimensional equations of a flow in an elastic tube are formally identical to the telegraph equations [Landes (35]; thus the theoretical literature of electrical engineering on transmission lines could be immediately applied to the dynamics of the arterial system.

Although the models based on the transmission line analogy can be made to yield a qualitatively correct behavior of the pressure pulse, they all possess intrinsic limitations due to their linearity. On the contrary, the fluid mechanical equations are nonlinear because of the term for the convective fluid acceleration in the equations of motion, and, even more importantly, because of the dependence of the compliance and cross section on pressure. Solutions to the nonlinear equations for certain physiological states can be drastically different from solutions of the same equations once they are linearized. This has been illustrated by Mickisz (36) and in recent papers by Rockwell (37) and Raines et al. (38).

4.1 Governing System of Equations

In this analysis, the pressure and velocity are assumed to be uniform over the entire arterial cross section. This is an approximation to real arterial flow and means that we are considering spatial average values of the dependent flow variables at each cross section. In making this assumption it is implied that the boundary layers are thin and that the streamlines are almost straight. We must, therefore, exclude small arteries as well as those with bends or rapid changes in cross section. In pulsatile flow the thickness of the boundary layer is related to the Womersley Frequency parameter [η] (39).

$$\eta = \frac{D}{2}\sqrt{\omega/\nu} \qquad [9]$$

where ν is the kinematic viscosity of blood and ω is the pulsatile frequency. The thickness of the boundary layer is of the order D/η .

In the arteries of the lower extremities η is approximately 7. The streamlines are relatively straight in the lower extremities because the area taper is gradual and sharp bends are not present to produce secondary flows. Westerhof et al. (40), Jager (41,42) and Noordergraaf (43) have analyzed the limitations of this assumption and have found it to be in accord with experimental results.

The continuity and momentum equations for a one-dimensional flow in a flexible tube are, respectively,

$$\frac{\partial Q}{\partial x} + \frac{\partial A}{\partial t} = 0 \qquad [10]$$

$$\frac{\partial u}{\partial t} + u \frac{\partial u}{\partial x} = \frac{1}{\rho} \frac{\partial p}{\partial x} + f \qquad [11]$$

Here u denotes the one-dimensional mean fluid velocity, A the tube cross sectional area, ρ the fluid density, p the pressure, and Q [= uA] the volume rate of flow; x is the longitudinal distance along the vessel and t denotes time. The symbol f represents the wall friction force per unit mass of fluid and will be explained later. On multiplying Eq. [10] by u and Eq. [11] by A, and adding the resulting equations, we obtain

$$\frac{\partial Q}{\partial t} + \frac{\partial (Q^2/A)}{\partial x} = -\frac{A}{\rho} \frac{\partial p}{\partial x} + fA \qquad [12]$$

Equation [12] will be used instead of [11] as the momentum equation in this analysis. The system of governing equations is completed by

the "equation of state" of the vessel, which we assume to be represented in the form

$$A = A(p,x) \qquad [13]$$

Note that Eq. [13] allows the vessel to be tapered and distended in an arbitrary way by the transmural pressure, but excludes active muscular contraction of the vessel wall, relaxation effects, wall inertia, and viscoelasticity. Attinger (44) and Westerhof (45) have shown experimentally and theoretically, respectively, that these effects do not play a significant role in arterial dynamics. However, other investigators are currently developing models including these effects (46).

4.2 Linearized Equations

Equation [11] is non-linear in two respects: (i) because of the quadratic term in Q, and (ii) because of the pressure dependence of A. This equation has been linearized by several authors (40,47,48) by assuming that the cross sectional area is a linear function of pressure and also that changes in area are relatively small, that is

$$\left|(p - p_o)\, C_u(x)\right| << A_o(x) \qquad [14]$$

where

$$A(x,p) = A_o(x) + (p - p_o)\, C_u(x)$$

Here $C_u = \partial A/\partial p$ is the vessel compliance per unit length and $A_o(x)$ is the local area at the reference pressure p_o. If, in addition, the

quadratic term in Q is neglected in Eq. [12], Eqs. [10] and [12] may be written in linearized form as

$$\frac{\partial Q}{\partial x} + C_u(x) \frac{\partial p}{\partial t} = 0 \qquad [15]$$

$$\frac{\partial p}{\partial x} + L_u(x) \frac{\partial Q}{\partial t} = f \qquad [16]$$

Here $L_u(x) \equiv \rho/A_o(x)$ is the inertance per unit length of the fluid. Equations [15] and [16] show the well-known analogy with transmission lines with the corresponding quantities being: Q, electric current; p, electric potential; C_u, capacitance per unit length; L_u, inductance per unit length; f, electric resistance per unit length. From the same analogy the local "characteristic impedance" of the vessel is defined as

$$Z_o(x) = \left(\frac{\rho f + jL_u(x)\omega}{jC_u(x)\omega} \right)^{1/2} \qquad [17]$$

where $j \equiv \sqrt{-1}$ and ω is the circular frequency ($\omega = 120\pi/HR$).

In all studies performed in this report non-linear features were retained. However, the electrical analogy, although it is strictly valid only in the linearized case, proves especially useful for obtaining insight into the treatment of boundary conditions.

4.3 Boundary Conditions

Proximal Boundary Condition

The proximal boundary condition (closest to the heart) may be set by giving either the flow or the pressure distribution as a

function of time. Here we consider only a periodic boundary condition, although the calculational method works as well with arbitrary time functions.

Distal Boundary Condition

In order to reduce the complexity, small arteries, arterioles and capillaries are generally not represented in detail in arterial models. Rather, it is customary to truncate the arterial tree at some point and to replace the remaining part by a lumped pure resistance. As seen from the electrical analogy reflected waves will occur at a termination point when the terminal arterial characteristic impedance does not match the local peripheral impedance. If this mismatch is present the steady-state component of the response to a sinusoidal driving function will not be a simple travelling-wave pair of voltage and current (pressure and flow). It will be a more complicated function, which may be resolved mathematically into the sum of two oppositely moving sinusoidal travelling-wave pairs; the incident and the reflected waves. The reflection coefficient is defined as the ratio of magnitudes of the reflected waves and incident waves. Since reflected waves are observed to some extent physiologically (49,50,51), a practical scheme should be developed for arterial models in which the magnitude of the reflection coefficient [K] is a parameter. The electrical analogy gives a clue as to how this may be accomplished. The reflection coefficient at the end of a transmission line is (52)

$$K = \frac{Z_T - Z_0}{Z_T + Z_0} \qquad [18]$$

where Z_0 is the characteristic impedance and Z_T is the load impedance. Many previous investigators (40,48) have set $Z_T = Z_0$ in their arterial models. This produces no reflected waves and therefore is not realistic in the regions where reflected waves are important or when anatomical accuracy is desired.

In this study a distal boundary condition is employed which provides realistic values for the reflection coefficients while retaining the physiological values of characteristic impedance and blood flow. In the small arteries forming transition between the large arteries and the arterioles the resistance to the flow increases progressively as the arterial diameter decreases. At the same time the coupling between vessel compliance and the frictional resistance helps damp out the large reflections as in acoustic mufflers. This is presumably the reason why large high frequency reflections are not observed in the normal human arterial system. Thus it is essential that at least some distensibility of the small vessels and vascular bed past the point of truncation be accounted for in the distal boundary condition. The simplest manner in which this can be done is to terminate the model of the artery at the truncation by a lumped compliance in parallel between <u>two</u> lumped resistances. The equivalent electrical network is represented in Fig. 29a. With this model the complex load impedance is given by

$$Z_T = R_1 + \frac{R_2 \ (1 - jR_2 C_T \omega)}{1 + R_2^2 \ C_T^2 \ \omega^2} \qquad [19]$$

The sum of the resistances is taken to be equal to the terminal resistance which is obtained from the known mean flowrate and mean pressure at the point of termination.

Conditions at Branching

Another set of boundary conditions is given at a bifurcation [see Fig. 29b]. The conservation of volume flow requires that $Q_1 = Q_2 + Q_3$. Since the mean velocities in the three branches are in general different, the pressures will also be different, according to Bernouilli's equation. However, because the dynamic pressure of blood ($\tilde{\sim}$ 2 mm-Hg) in large arteries represents a small fraction of the unsteady pressure amplitude ($\tilde{\sim}$ 50 mm-Hg), the pressures at points 1, 2 and 3 may be considered equal to a good approximation.

4.4 Friction Term

It is convenient to express the friction force per unit mass f in Eq. [12] as

$$f = FQ/\rho A^2 \qquad [20]$$

In the equations that follow the viscous coefficient F depends on the assumptions made for the viscous effects. If they are neglected $F = 0$. For Poiseuille flow, $F = 8\pi\mu$, where μ is the dynamic viscosity of blood. To obtain an approximate expression for the viscous effects in this study the coefficient derived from Poiseuille flow was used. This friction term is not very accurate for pulsatile flow in arteries but, since, the viscous pressure drops represents a small percentage of the mean pressure, accuracy is not felt to be too important.

In addition models employing this assumption have been compared to experimental data obtained by Attinger (44,53,54) in anatomical regions pertinent to this model and found to be in good agreement.

4.5 Leakage Term

It may be in some instances important to account for the outflow of blood in small vessels off the main artery. For this effect a "leakage" term [Q_L] is introduced in the following equations which is equal to the leakage flow per unit length at a given referenced pressure. It can be interpreted as the rate at which the flow decreases along a main vessel due to small branches. In the equations to follow this term is assumed to vary in a linear fashion with local instantaneous pressure. Since all significant branches were included in the model, Q_L was set to zero. It is nevertheless presented for completeness and reference for use in future models.

V. NUMERICAL SOLUTION BY FINITE DIFFERENCE METHOD

The system to be solved is composed of Eqs. [10], [12], and [13]. However since the pressure p and the rate of flow Q are the dependent variables of main interest, Eq. [10] is rewritten incorporating a leakage term and the vessel compliance per unit length as

$$\frac{\partial Q}{\partial x} + C_u \frac{\partial p}{\partial t} = - Q_L p \qquad [21]$$

The method of characteristics may be used to solve the system of equations ([12], [13], and [21]) in this analysis, and has been used by previous investigators for the solution of non-linear partial differential equations (40 , 55 , 56). However, for this analysis we have chosen to use a finite difference method. We have extended the linear method outlined by Fox (57) in order to include the non-linear term, viscous term, leakage term, and variable coefficients present in our system of equations. The finite difference method is easy to program (can be written in one subroutine), economical, and flexible.

In the finite difference method each segment of the arterial tree must be divided into a number of finite length elements. The partial differential equations are then written in finite difference form with Δx representing the length element and Δt the small finite time interval. Arbitrary initial conditions are taken for each spatial node and the dependent variables are determined by solving the finite difference equations at time intervals of Δt until they become periodic; usually about 4 periods are required. Due to the interactive stability require-

ments, different schemes are used according to whether the pressure or the flow is given as the proximal boundary condition.

5.1 Proximal Pressure Prescribed

If the pressure is given, Eqs. [21] and [12] are expressed in finite difference form, respectively, as

$$\frac{Q_N^i - Q_N^i - 1}{\Delta x} + \frac{C_{uN}^i (p_N^{i+1} - p_N^i)}{\Delta t} = - Q_{L_N}^i p_N^{i+1} \qquad [22]$$

$$\frac{Q_N^{i+1} - Q_N^i}{\Delta t} - 2Q_N^{i+1} (C_{uN}^i / A_N^i) \frac{(p_N^{i+1} - p_N^i)}{\Delta t}$$

$$- Q_N^{i+1} (Q_N^i / A_n^{2i}) \frac{(A_{N+1}^i - A_N^i)}{\Delta x} =$$

$$- (A_N^i / \rho) \frac{(p_{N+1}^{i+1} - p_N^{i+1})}{\Delta x} - FQ_N^{i+1} / (\rho A_N^i) \qquad [23]$$

where X_N^i denotes the value of X at the i^{th} time step and at the N^{th} spatial step. N runs from unity at the inlet to N_f at the exit of a particular segment.

Solving the system of Eqs. [22] and [23] for p_N^{i+1} and Q_N^{i+1} we have respectively,

$$p_N^{i+1} = \frac{p_N^i - \frac{\Delta t}{\Delta x\, C_{uN}^i}\,(Q_N^i - Q_{N-1}^i)}{1 + \Delta t\, Q_{L_N}^i / C_{uN}^i}$$

$$\text{for } N = 2, \ldots N_f \qquad [24]$$

$$Q_N^{i+1} = \psi_1/(1 - \psi_2 - \psi_3 - \psi_4) \qquad [25]$$

with

$$\psi_1 = Q_N^i - A_N^i\,(\Delta t/\rho\Delta x)\,(p_{N+1}^{i+1} - p_N^{i+1}) \qquad [26]$$

$$\psi_2 = 2(C_{uN}^i/A_N^i)\,(p_N^{i+1} - p_N^i) + 2(\Delta t/A_N^i)\,Q_{L_N}^i\, p_N^{i+1} \qquad [27]$$

$$\psi_3 = Q_N^i\,(\Delta t/A_N^{2i}\Delta x)\,(A_{N+1}^i - A_N^i) \qquad [28]$$

$$\psi_4 = -F\,\Delta t/\rho A_N^i \qquad [29]$$

$$\text{for } N = 1, \ldots N_f - 1$$

At the final spatial location, $Q_{N_f}^{i+1}$ is found with the help of the terminal boundary conditions.

5.2 Proximal Flow Prescribed

When the flow is given, Eqs. [21] and [12] are expressed in finite difference form, respectively, as

$$\frac{Q_{N+1}^{i} - Q_{N}^{i}}{\Delta x} + \frac{C_{uN}^{i}\,(p_{N}^{i+1} - p_{N}^{i})}{\Delta t} = Q_{L_N}{}^{i}\, p_{N}^{i+1} \qquad [30]$$

$$\frac{Q_{N}^{i+1} - Q_{N}^{i}}{\Delta t} + \frac{2(Q_{N}^{i}/A_{N}^{i})\,(Q_{N}^{i+1} - Q_{N-1}^{i+1})}{\Delta x}$$

$$- Q_{N}^{i+1}\,(Q_{N}^{i}/A_{N}^{2i})\,\frac{(A_{N}^{i} - A_{N-1}^{i})}{\Delta x} =$$

$$- (A_{N}^{i}/\rho)\,\frac{(p_{N}^{i+1} - p_{N-1}^{i+1})}{\Delta x} - F\,Q_{N}^{i+1}/\rho A_{N}^{i}) \qquad [31]$$

Solving the system of Eqs. (30) and (31) for p_N^{i+1} and Q_N^{i+1} we have respectively

$$p_{N}^{i+1} = \frac{p_{N}^{i} - (\Delta t/\Delta x C_{uN}^{i})(Q_{N+1}^{i} - Q_{N}^{i})}{1 + \Delta t\; Q_{L_N}{}^{i}/C_{uN}^{i}} \qquad [32]$$

for $N = 1, \ldots N_f - 1$

$$Q_{N}^{i+1} = (\theta_1 + \theta_{2A})/(1 - \theta_2 - \theta_3 - \theta_4) \qquad [33]$$

with

$$\theta_1 = Q_N^i - A_N^i(\Delta t/\rho\Delta x)\ (p_N^{i+1} - p_{N-1}^{i+1}) \qquad [34]$$

$$\theta_2 = -2\ \Delta t\ Q_N^i/(\Delta x\ A_N^i) \qquad [35]$$

$$\theta_{2A} = 2\ \Delta t Q_N^i\ Q_{N-1}^{i+1}/(\Delta x\ A_N^i) \qquad [36]$$

$$\theta_3 = \Delta t\ (Q_N^i/A_N^{2i}\ \Delta x)\ (A_N^i - A_{N-1}^i) \qquad [37]$$

$$\theta_4 = -F\Delta t/(A_N^i\rho) \qquad [38]$$

$$\text{for}\quad N = 2, \ldots N_f$$

At the final spatial location, p_{N_f} is found with the help of the terminal boundary condition.

5.3 Stability Criterion

Fox (57) and Lax (58) have found that the stability criterion for a system of linear equations of the type represented by Eqs. [15] and [16] with constant coefficients C_u and L_u and f=0 takes the simple form

$$\Delta t \leq \Delta x/c \qquad [39]$$

where $c = (L_u C_u)^{-1/2}$ is the pulse-wave velocity. The inequality [39] states that it is not permissible to cross the characteristics and that a solution only exists within a domain limited by the characteristics (59). To obtain stability when the non-linear, leakage and viscous terms are present and when the coefficients are variable, the value of Δt required for stability is less than that given by Eq. [39]. The amount of reduction required depends upon the parameters of the problem. In our calculations Δx was always taken as 2 cm and c ranged from 500 to 2500 cm/sec. Δt was adjusted by trial and error until a stable solution was obtained. The time step used in the majority of the cases was .001 sec; .0005 sec was used for the cases with pulse-wave velocity greater than 1500 cm/sec.

VI. PHYSIOLOGICAL MODEL

The physiological model represents the human arterial system of a single leg beginning at the iliac bifurcation and ending at the distal end of the popliteal artery. The hypogastric and profunda femoris branches are represented by lumped elements. Geometric and elastic properties, as well as the flow rates, are intended to represent a young healthy adult of normal height and weight.

This case will be referred to as the control case (CC). The following sections describe how these data were obtained.

6.1 Geometric Properties

A survey of current literature indicated that very little quantitative information was available on the geometrical properties of human arteries in the lower limbs. This is in contrast to the abundant literature that is found on the aorta. A number of investigators have performed studies of the common femoral artery and have reported values for the impedance, diameter, and compliance (60,62,63,64,65,68). Two papers were found in which arterial diameters were quoted at a number of sites in the lower limbs (40,72). Since these data were limited, a study was performed with the help of the Radiology Department of the Massachusetts General Hospital. The recent files were searched for patients who had undergone arteriography involving the arteries from the descending aorta to the tibial vessels. Of this group, 24 adult patients were chosen on the basis of age, normal height and weight, quality of arteriograms, and minimum lumen obstruction. The arteriograms of this

group were enlarged photographically on a large screen with a reference scale included; lengths and diameters of the relevant arteries were measured. The magnification factor of the X-ray equipment used was measured and found to be 1.2. This factor was taken into account in the reduction of the data. Figure 30 is a diagram of the physiological model, including the mean arterial lengths determined by this study. Figure 31 illustrates the mean diameters and corresponding cross-sectional areas as a function of distance from the iliac bifurcation. For use in the model the reference pressure [p_o] at which these measurements were obtained was taken to be 100 mm-Hg. This has little effect on the model because the absolute change in arterial area with pressure in these arteries is quite small.

Equations [40] and [41] represent the best fit of the arteriographic data for cross-sectional area with the distance from the iliac bifurcation.

$$A(p_o,x) = .505\, e^{-.1925\sqrt{x}} \qquad 0 \leq x < 13 \qquad [40]$$

$$= .327\, e^{-.0206\, x} \qquad 13 \leq x \leq 60 \qquad [41]$$

where p_o = 100 mm-Hg , x is expressed in cm and A in cm^2 . It is interesting to note that the iliac arteries (common and external) are more tapered than the femoral and popliteal arteries.

The geometrical data determined by this study were compared to values from the available literature (40,72). Table 1 is a comparison

of arterial lengths measured in this study and of the values reported by Westerhof et al. (40).

Table 1

	LENGTH (CM)	
ARTERY	ANGIOGRAPHIC STUDY	WESTERHOF et. al. (40)
Common Iliac	6.0	5.8
External Iliac	7.0	8.3
Common Femoral	7.0	6.1
Superficial Femoral	20.0	25.4
Popliteal	20.0	18.9

Figure 32 shows that the angiographic study gives essentially the same results for diameter as a function of distance from the iliac bifurcation as previously reported in the literature.

6.2 Elastic Properties

To define the "equation of state" of an artery it is necessary to describe how its cross-sectional area changes with transmural pressure. Measurements in arteries suggest that the compliance is inversely proportional to the pressure

$$C_u = \frac{\partial A(p,x)}{\partial p} = \beta/p \qquad [42]$$

The integration of [42] with respect to p gives

$$A(p,x) = A(p_o,x)[1 + \beta/A(p_o,x)\ \mathrm{Ln}(p/p_o)] \qquad [43]$$

where p is expressed in mm-Hg and A in cm^2.

At this point it is convenient to define a variable α as the percentage cross-sectional area change per 50 mm-Hg. This pressure change was taken to be $\pm$ 25 mm-Hg around a reference pressure (p_o) of 100 mm-Hg. With this definition

$$\beta/A_o(p_o,x) = \frac{\alpha}{100\ \mathrm{Ln}\left(\frac{p_o + 25}{p_o - 25}\right)} = \frac{\alpha}{31.1} \qquad [44]$$

The assumption concerning the pressure dependence of the cross-sectional area was compared with experimental data (after appropriate normalization) obtained in human iliac arteries by Boughner and Roach (68) and Learoyd and Taylor (62) for several age groups at various transmural pressures (Fig. 33). The agreement is excellent over the physiological range encountered in this study (pressure and age).

For the control case it was necessary to obtain a value for α that was consistent with physiological experience. From the experiments of many previous investigators (60,63,64,66,68) it was impossible to deduce a consistent value of α. A large spread was found for the iliac and femoral arteries (1.6% --- 13.2%). This is undoubtedly due to the difficulty of the experiment and the large number of variables involved.

Since review of directly obtained compliance data did not reveal a consensus of opinion as to the value of α , an indirect method was used.

The parameter α may be expressed in terms of the pulse-wave velocity (c), for which values may be found in the literature. The wave speed is given by the Moens-Korteweg Equation (67).

$$c = \sqrt{\frac{A}{\rho(\partial A/\partial p)}} \qquad [45]$$

Using Eqs. [42], [43] and [44], Eq. [45] can be rewritten as:

$$c = \sqrt{\frac{1333\ p}{\rho}\ \left[\frac{51.1}{\alpha} + \mathrm{Ln}\ (p/p_o)\right]} \qquad [46]$$

where c is expressed in cm/sec and ρ in grams/cm^3. It should be noted that, due to the assumed form for $A(p,x)$, the wave speed is a function of pressure and α , but not of location. Cachovan et al. (69) measured the foot-to-foot pulse-wave velocity at three different locations along the femoral and popliteal arteries in 40 men with segmental impedance plethysmography. In this study they were unable to detect significant differences in pulse-wave velocity with location when atherosclerotic disease was not present, supporting the validity of Eq. [46] in the region of interest. They also concluded on the basis of post-mortem studies that if c was greater than 1200 cm/sec in normotensive patients significant pathological changes had occurred in the arteries of the lower limbs.

Zangeneh and Nassereslami (70) also measured foot-to-foot pulse-wave velocity in 640 subjects free of significant atherosclerosis over a wide age range between the inguinal ligament and the foot. The results of their study indicate:

i) c changes very little with age in the absence of atherosclerotic disease.

ii) In hypertension, c in the lower limbs may be increased by 100%.

iii) At a mean blood pressure of 100 mm-Hg, c was measured to be 1037 $\pm$ 186 cm/sec.

Figure 34 is plot of c as a function of α (Eq. [46]) at 100 mm-Hg. In order to be in agreement with Zangeneh and Nassereslami α should be approximately 6%. This value is in close agreement with two of the most carefully performed experiments for the direct measurement of arterial compliance (60,68). Mozersky *et al.* (60) found α to be 5.2% in 24 femoral arteries in men free of atherosclerosis under 35 years of age. They used an ultrasonic echo tracking system to perform their measurements transcutaneously and *in vivo*. Boughner and Roach (68) found α *in vitro* to be 5.4% in iliac arteries using a carefully designed plethysmograph. The two studies found in the literature in which α varies significantly from the 6% value are those of Schutz et al. (66) and of Arndt and Kober (63). Schutz *et al.* found α to be 1.6%; if this were true, c would be 2000 cm/sec in the lower extremities. This value is certainly too high. Also, their work involved *in vitro* measurement of whole aorto-iliac bifurcations which probably could not be constrained

properly. Arndt and Kober obtained 13.2% with a technique very similar to the one used by Mozersky et al., and their procedure has been criticized by the latter paper. In this work a value for α of 6% was chosen for the control case. Figure 35 is a plot of c as a function of pressure for α = 6%. This relation is not applicable at low pressures. However, for the pressures encountered in the model (>40 mm-Hg) it is adequate. It can be noted from this curve that the pulse-wave velocity changes significantly over the cardiac cycle.

6.3 Flow Distribution

In order to determine the values of peripheral resistance for the termination and branch boundary conditions it is necessary to know the mean flow rates. Wade and Bishop (61) have estimated the normal resting blood flow [$\bar{Q}$] through the human common iliac artery to be 450 ml/min. Assuming a normal cardiac output of 5000 ml/min, this figure indicates that 9% of the cardiac output is used to perfuse one leg. Attinger et al. (54) found this percentage to be 10% in dogs.

Studies performed during surgery with electromagnetic flowmeters (7,71,65,73,74) suggest that of the total flow through the common iliac artery half of this flow goes into the hypogastric branch and the remaining half continues down the external iliac. It is believed that flow again divides equally at the junction of the profunda branch and superficial femoral artery. Since the mean pressure drop along the main arterial system is small, to a good aproximation the hypogastric resistance (R_H) is half the value of the profunda resistance (R_p) and also of the tibial resistance (R_T). This can be represented in equation form by:

$$2R_H = R_p = R_T \qquad [47]$$

Since the mean input pressure [$\bar{p}$] is known as well as the mean flow (Wade and Bishop) and venous pressure [p_v], the peripheral resistance of the leg [R] may be calculated.

$$R = \frac{\bar{p} - p_v}{\bar{Q}} = 8.0 \text{ mm-Hg sec/ml} \qquad [48]$$

Since

$$\frac{1}{R} = \frac{1}{R_H} + \frac{1}{R_p} + \frac{1}{R_T} \qquad [49]$$

using Eq. [47] one finds:

$$R_H = 16 \text{ mm-Hg sec/ml}$$

$$R_p = 32 \text{ mm-Hg sec/ml}$$

$$R_T = 32 \text{ mm-Hg sec/ml}$$

These values of resistances and pressures lead to the following mean flowrates in the control case:

TABLE 2

Artery	Mean Flow (ml/min)
Common Iliac	450
Hypogastric	225
External Iliac	225
Common Femoral	225
Profunda	112.5
Superficial Femoral	112.5
Popliteal	112.5

6.4 Branches and Termination

It has been estimated that the volume compliance of the entire arterial system is approximately 1.0 ml/mm-Hg (33,75). On combining Eqs. [42] and [44] and taking α equal to 6% and pressure equal to 100 mm-Hg an integration may be performed from the iliac bifurcation to the tibial vessels to obtain the total arterial compliance, excluding the branches. The value obtained is proportional to α and is .035 ml/mm-Hg for α = 6%. It appears reasonable to assume that the arterial volumetric compliance of both legs is approximately 15% of the total arterial compliance. With this assumption the total branch and termination volume compliance in one leg is .04 ml/mm-Hg. It is further assumed that this compliance is divided among the branches and termination in proportion to their flow. The values are given in the following section.

Employing the representation illustrated by Fig. 29a for the hypogastric (branch), profunda (branch), and tibial vessels (termination) the total peripheral resistance for each of these segments must be divided between two resistances. Table 3 defines this division for the control case, as well as the total volumetric compliance of the segment [C], and the magnitude and phase of the distal reflection coefficients, [K] and [ϕ], respectively. These values of K for the branches and the termination are in reasonable agreement with the values suggested by McDonald and Attinger (76). Figure 36 is a plot of K and ϕ at the tibial vessels as a function of R_1/R_T. Comparison of simulation results and published experimental measurements suggest that for this

model R_1 should be approximately 20% of the total peripheral resistance of the branch or termination. It should be noted that if R_1 is zero the Windkessel representation is obtained. If R_1 is set equal to the peripheral resistance, then R_2 is zero and no compliance is included.

TABLE 3

Artery	R_1	R_2	R_T	C	K	ϕ
	$\frac{\text{mm-Hg sec.}}{\text{ml}}$	$\frac{\text{mm-Hg sec.}}{\text{ml}}$	$\frac{\text{mm-Hg sec.}}{\text{ml}}$	ml/mm-Hg	%	o
Hypogastric	3.2	12.8	16.0	0.02	15.3	-154
Profunda	6.4	25.6	32.0	0.01	11.7	-154
Tibial Vessels	6.4	25.6	32.0	0.01	19.1	-39

6.5 Control Case

It is necessary to define a control case to establish a basis of comparison in studying the effects of various parameters. Equations [43] and [42] were used to obtain the geometric and elastic properties of the main arteries in the control case. Table 4 summarizes the values of the parameters used in the control case and in other cases unless otherwise indicated.

TABLE 4

ARTERY	MEAN FLOW ml/min	R_1	R_2 mm-Hg / ml/sec	R_T	C cc / mm-Hg	K %	ϕ o
Common Iliac	450	--	--	--	--	--	--
Hypogastric	225	3.2	12.8	16	0.02	15.3	- 154
External Iliac	225	--	--	--	--	--	--
Common Femoral	225	--	--	--	--	--	--
Profunda	112.5	6.4	25.6	32	0.01	11.7	- 154
Superficial Femoral	112.5	--	--	--	--	--	--
Popliteal	112.5	--	--	--	--	--	--
Tibial Vessels	112.5	6.4	25.6	32	0.01	19.1	- 39

ρ = 1.06 grams/cm^3 or dyne-sec^2/cm^4 α = 6% percent area change/50 mm-Hg

μ = .045 poise or dyne-sec/cm^2 HR = 75 beats/min

p_o = 100 mm-Hg p_v = 20 mm-Hg $\bar{p}$ = 80 mm-Hg

VII. DYNAMICS OF CONTROL CASE

Figure 37 is a plot of the pressure distribution as a function of time used as the proximal boundary condition in the CC. This trace was obtained with the PPR on the thigh of a healthy 27 year old male, and is assumed for the purposes of the model to represent the pressure at the iliac bifurcation. The mean pressure $[\bar{p}]$ is 80 mm-Hg. To check the precision of the computer schemes this pressure distribution was used to obtain the flow distribution at the iliac bifurcation. The obtained flow distribution was used as the proximal boundary condition with all other parameters remaining unchanged to recalculate the pressure distribution. These two pressure distributions were then compared and found to be virtually identical.

7.1 Pressure and Flow Pulses

Figure 38 represents the pressure and flow pulses at four locations for the CC. The pressure pulse amplifies away from the iliac bifurcation; the mean pressure falls slowly due to friction, while the mean flow decreases as a result of branching. Figure 39 illustrates the flow pulses in the hypogastric and profunda femoris branches. Figure 40 is a plot of systolic pressure, diastolic pressure, pulse pressure, mean pressure, peak flow-rate, minimum flow-rate, and mean flow as a function of distance from the iliac bifurcation. The pulse-wave velocity calculated between the iliac bifurcation and the tibial vessels was found to be 1279 cm/sec from peak to peak and 910 cm/sec from foot-to-foot. This difference is due to the relationship between pulse-wave velocity and pressure. As seen from Fig. 35 the wave travels faster at

high pressure. Figure 41 is a plot of the pressure and flow pulses at the iliac bifurcation and illustrates the well documented observation (49) that flow actually leads pressure. In this case, the phase lead is 10°.

The model permits the evaluation of the importance of the non-linear convective acceleration and of the viscous forces. These effects have often been neglected by other investigators.

7.2 Effect of Convective Acceleration

Figure 42 illustrates the effect of neglecting the convective acceleration on distal popliteal pressure in the CC. The effect is small, producing only a 3 mm-Hg decrease in systolic pressure. If an order of magnitude analysis is performed on the continuity and momentum equations it can be shown that the convective acceleration effect increases with the ratio u/c . For the CC at the distal popliteal artery this ratio at peak systole is approximately .07. This study suggests that if $u/c > 0.1$ is anticipated, the convective acceleration term should be included in the formulation. At normal resting conditions u/c will not be greater than 0.1 in the lower extremities. However, when flow is increased (as in exercise) this is no longer the case. During the systolic phase of a normal resting cardiac cycle u/c is generally greater than 0.1 in the aorta, therefore, the convective acceleration should not be neglected in the aorta (38).

7.3 Effect of Blood Viscosity

As previously outlined, blood viscosity is accounted for in an approximate manner through a linear resistance term. For the CC,

assuming a viscosity coefficient $\mu = .045$ poise, the mean pressure is reduced by 5 mm-Hg from the iliac bifurcation to the tibial vessels (Fig. 40). Figure 43 illustrates the effect of neglecting viscosity in the CC on the flow at the iliac bifurcation and the pressure at the distal popliteal. Viscous effects reduce systolic pressure by 18 mm-Hg, and the diastolic pressure by 4 mm-Hg.

Unsteady effects may increase the apparent viscosity used in this calculation by an additional 20 to 50% (39). In our model vessel diameters ranged from approximately 8 mm at the iliac bifurcation to 3.5 mm at the distal popliteal artery. We conclude then that the effect of viscosity is important only in vessels of less than about 5 mm in diameter.

VIII. ARTERIAL DYNAMICS IN HEALTH AND DISEASE

In the preceding sections we have described a general and flexible method for simulating arterial dynamics. We have defined a control case based on average typical data for normal healthy individuals which reproduces the observed characteristics of arterial flow in the lower extremities. However, one must keep in mind that there are variations among healthy individuals and that vascular disease alters the configuration and the elasticity of arteries. Therefore, we proceed now to make a systematic study of the effects of arterial geometry and elasticity on the dynamics of the pressure and flow pulses.

8.1 Branching

Since it is not practical to include all the arteries branching off the main arterial stream it is important to know whether the pressure pulse is affected by branching. Another interesting question is how the flow redistributes when a major branch is occluded by arteriosclerosis. In this study the effects of viscosity, convective acceleration, and reflections at the distal boundary condition were excluded while the pressure pulse was imposed as the proximal boundary condition. Figure 44 shows a comparison of the pressure pulse at the distal popliteal artery in the CC and with the hypogastric and profunda femoris branches occluded. With the branches occluded, the pressure rise during the systolic phase is slightly steeper, however, the pressure levels remain the same. In this case the reflection coefficients at the hypogastric and profunda branches are approximately 15% and 12%, respectively. In our clinical

observations we were not able to detect any changes in pressure pulse contour when branches were occluded; the mathematical analysis is in agreement with this observation.

8.2 Effect of Taper

It has been mentioned earlier that the systolic and pulse pressures increase as the pulse propagates away from the heart. In order to investigate the part played by the elastic and geometric tapers of the arteries in the amplification of the pulse we eliminated the effects of viscosity, convective acceleration, branching, and distal reflections on the CC. Figure 45 shows the comparative results for the distal popliteal artery when the pressure is specified at the iliac bifurcation. With no taper and no reflections for a constant diameter of 5 mm and pulse-wave velocity of 1000 cm/sec the pressure pulse propagates without distortion with merely a phase shift due to the finite propagation speed. Both the area and elastic tapers produce pulse amplification as well as a steepening of the pressure upstroke. The net results amount to a distortion and a "sharpening" of the pulse. The reason is that the taper produces distributed positive reflection sites along the arterial system which in turn amplify and distort the pressure pulse. It will be shown later that the presence of reflections at the distal boundary condition will also change the contour of the pressure pulse in a similar manner.

8.3 Effect of Arterial Compliance

Since arteriosclerosis causes the arterial wall to become less compliant, this effect was studied with the computer model.

In a previous chapter, it was established that the normal value of α is 6%. Mozersky et al. (60) found that this value may be reduced by a factor of 3 in the presence of severe arteriosclerosis. For the purposes of this study, the control case (α = 6%) was compared against results obtained with the compliance divided by a factor of 4 (α = 1.5%). To maintain the proper metabolic balance the amount of blood flow to the leg must remain constant, therefore, for this study the flow pulse was specified as the proximal boundary condition at the iliac bifurcation for both values of the compliance. Figure 46 shows the pressure at the iliac bifurcation and the distal popliteal artery in the two cases. Two interesting remarks can be made. First, the systolic pressure is elevated and the diastolic pressure slightly decreased by the decrease in compliance, especially at the iliac bifurcation. This phenomenon is always observed in patients with calcified arteries. The other important point is that increasing the arterial wall stiffness, even by a factor of 4, does not appreciably change the contour of the distal pressure pulse, while the foot-to-foot pulse-wave velocity is increased by a factor of two.

In addition to changing the strength of the distributed reflections the change in compliance modifies the reflection coefficient at the distal end. Figure 47 shows that, as α decreases below the normal value of 6%, there is a rapid change in the phase of the reflection coefficient, however, its magnitude [K] remains small until α falls below 1%. In the limit $\alpha \to 0$ the reflection coefficient goes to -1. It will be shown later that the abnormal pulse contours observed in

patients with generalized arteriosclerosis can be reproduced by the model if the reflection coefficient is large and negative. On the basis of Fig. 47 it seems unlikely that such reflection coefficients can be caused in the physiological system by arterial hardening alone since it would require very stiff walls. In the next section, another possible mechanism for producing this effect is discussed.

8.4 Effect of Distal Reflections

We have seen before that the distal reflection coefficient is given by

$$K = \frac{Z_T - Z_0}{Z_T + Z_0}$$

where Z_T is the terminal impedance and Z_0 the characteristic impedance at the termination. For simplicity we exclude here the effects of taper, viscosity, and branching, and we consider a cylindrical elastic tube of 60 cm in length with a diameter of 5 mm and a constant pulse-wave velocity of 1000 cm/sec at the reference pressure of 100 mm-Hg. The tube is terminated by a pure resistance R_{PR} (the peripheral resistance) and it follows that in this case the reflection coefficient is real. It is clear that K is positive (phase = 0) if $R_{PR} > Z_0$ and that K is negative (180° phase) if $R_{PR} < Z_0$. In this study the peripheral resistance is varied while the characteristic impedance remains constant; the pressure used in the CC is prescribed at the proximal boundary. Figure 48 illustrates the effect on the distal pressure of increasing the peripheral resistance (vasoconstriction) in such a way as to produce reflection coefficients of 0, + 0.2, and + 0.6. As the reflection

coefficient increases the peaks of the pulse become higher and the valleys deeper. We interpret this result as due to the increased contribution of reflected waves.

To verify this finding an experiment was carried out on human subjects. The PPR monitoring cuff was placed around the calf of the subject and a distal cuff around the ankle. With the monitoring cuff set at a mean pressure of 20 mm-Hg, recordings were taken at the calf with different values of distal cuff pressure. The intent of the experiment was to show that increasing the distal resistance enhances wave reflection. Figure 49 illustrates the results obtained from this experiment.

We were surprised to find that when we first began occluding the arteries at the ankle the reflected wave decreased in amplitude, and when the arteries were occluded the reflected wave then increased as we produced a stiffer reflection site at the ankle. To aid in interpreting the results of this experiment it is helpful to consider a compliant chamber located between two resistances. The first resistance (R_1) corresponds to the occluding cuff and the second (R_2) to the peripheral resistance of the foot. Figure 50 is a plot of the magnitude and phase of the reflection coefficient as a function of R_1, holding all other parameters constant, including the characteristic impedance of the artery just proximal to the distal cuff. As R_1 increases, K initially decreases causing less reflections; as R_1 is increased further, K the increases producing increased reflections. Thus the theoretical results appear to be in agreement with the experimental observations.

Two interesting conclusions can be drawn from these results. First, vasoconstriction indeed increases the relative magnitude of the reflected wave in the pressure pulse contour. This can also be shown by placing the foot in iced water and recording the pressure pulse contour at the calf. Secondly, the results of this experiment indicate that even in regions as distal as the foot, arterial compliance is still important. In addition we have experimental evidence that the model we have chosen for the distal boundary condition is probably appropriate and more realistic than just a pure resistance.

Figure 51 illustrates the effect on the distal pressure of decreasing peripheral resistance (vasodilation) to produce reflection coefficients of -0.2 and -0.4. The character of the pressure pulse produced by vasodilation is similar to that of those observed clinically distal to an obstruction or at exercise.

To verify this result a second experiment was performed on human subjects. A control PPR recording was taken at the calf of a volunteer. The subject's foot was then placed in hot water until the skin temperature reached 95°F, producing vasodilation. A recording was then taken at the calf with the PPR. Results of this experiment are plotted in Fig. 52. The reflected wave disappears after vasodilation, while the mean pressure drops. Both experiments described in this section were repeated on four subjects with identical results.

The foregoing conclusions remain qualitatively valid for the arterial model (Fig. 53) with the difference that the reflection coefficient is complex.

8.5 Effect of Arterial Obstruction

Obstruction of the arterial lumen is another common manifestation of arteriosclerosis. In this section we simulate the effect of an obstruction in the arterial model and compare the results with experiments.

Computer Simulation of Arterial Obstruction

To simulate the effects of atheromatous deposits a mathematical model of an obstruction was used in conjunction with the control case. Figure 54 is a schematic representation of the simulated obstruction. This figure serves as a link between the geometry encountered in arterial obstruction and the idealized mathematical analysis used to simulate its fluid dynamics.

As illustrated the geometry of the obstruction may be divided into three sections:

1. the entrance (1 - 2)
2. the minimum lumen section (2 - 3)
3. the expansion (3 - 4)

To compare this model with systolic and diastolic pressures measured experimentally it is necessary to compute the instantaneous pressure change across the obstruction (1 - 4). This value is given by the following formula.

$$\Delta P = \Delta P_c + \Delta P_{BL} + \Delta P_x + \Delta P_u \qquad [50]$$

Where: ΔP - instantaneous pressure change across the obstruction

ΔP_c - total pressure loss at the entrance

ΔP_{BL} - total pressure loss across the minimum lumen section

ΔP_x - total pressure loss at the expansion

ΔP_u - pressure decrease due to inertial forces in the minimum lumen section

It should be pointed out that individually ΔP_c, ΔP_{BL} and ΔP_x are total pressure losses due to friction and turbulence. However, since the fluid velocities are equal at both ends of the obstruction the sum of these quantities is a pressure change.

a) Entrance loss

The loss of total pressure at the entrance is due to boundary-layer friction and, possibly, to separation if the entrance is not sufficiently gradual. Since the entrance length is short compared to the length of the minimum lumen section, the effect of friction at the entrance is neglected. One would expect the entrance to an arterial obstruction to be reasonably well rounded, producing small losses. The total pressure loss may be represented in the form

$$\Delta P_c = k_e \rho Q^2/2A_2^2 \qquad [51]$$

where A_2 is the cross-sectional area of the minimum lumen section and k_e is the entrance loss coefficient. The latter depends upon the Reynolds Number and upon the entrance geometry (77). The inlet to a partially occluded arterial segment is generally not as abrupt as a square-edge entrance or as gradual as a bell-mouthed inlet, the

geometry being quite variable. For these reasons it was decided to use the value 0.1 for k_e in the model, which represents an inlet with some rounding. This value is felt to be an upper limit. With k_e equal to 0.1 the entrance loss is small compared to the other losses, therefore, further refinement is not necessary for this section.

b) Viscous loss in minimum lumen section

On taking the entrance to this section to be sufficiently gradual to produce no separation, it may further be assumed that the loss in this section is due to the development of a boundary layer. The total pressure loss along a tube of length L for this flow situation is given by Shapiro et al. (78) as

$$\Delta P_{BL} = 3.5\sqrt{\pi\rho L u}\, Q^{3/2}/A_2^2 \qquad [52]$$

For this equation to be applicable three conditions exist: the flow must be laminar; the flow must be quasi-steady; the boundary layer thickness must be small when compared to the tube diameter. The Reynolds Number (Re) with no obstruction in the arterial model based on the mean flowrate is 350(1500 based on the peak flowrate); with 85% obstruction of area the Re based on mean flow-rate is 700 (2000 based on peak flowrate). These numbers indicate the flow is laminar throughout the range of interest in the model. The Womersley frequency parameter

[η] for this section with no obstruction is approximately 4.5, which does not indicate quasi-steady flow. However, as the diameter is reduced to the point where the losses are significant η becomes of the order of unity or less, and the quasi-steady condition is approximately met. There is a direct analogy for this boundary layer growth to the boundary layer growth experienced in laminar flow over a flat plate. For the boundary layer thickness (δ) to be small compared to the tube diameter,

$$\sqrt{L/D} \ll \sqrt{Re_D}$$

With an obstruction length of 2cm at 85% area obstruction $\sqrt{L/D}$ is 2.8 and $\sqrt{Re_D}$ based on the mean flowrate is 26.4. These numbers indicate the boundary layer thickness to be small compared with the tube diameter.

c) Expansion loss

The expansion of the flow downstream of the minimum lumen section is accompanied by separation and turbulent reattachment. With the assumption of a sudden expansion the total pressure loss is given by (79)

$$\Delta P_x = \rho/2 \, (Q/A_2 - Q/A_3)^2 \qquad [53]$$

where A_3 is the cross-sectional area downstream of the obstruction. This assumption is supported by experiments with conical diffusion which indicate that when the divergence angle is greater than 50°, 95% of the total pressure loss expected with a sudden expansion

is present (77). Since Eq. [53] is applicable for a steady flow it is important to check its applicability in our case. The residence time (τ_f) of a fluid particle in the expansion jet is on the scale between D/V and 10D/V, where D is the diameter of the minimum lumen section and V is the mean fluid velocity in that section; we shall take it as of the order 3D/V. With an 85% area obstruction D is 2.5 mm and V is 120 cm/sec, therefore $\tau_f \tilde{=} 0.006$ sec. For Eq. [53] to be valid the residence time should be small compared with the time it takes for a significant percentage change in flow to occur (τ_p). Considering the shape of the flow pulse we assume τ_p to be 5% of a period. With a heart-rate of 75 beats/min the period is 0.8 sec, therefore, $\tau_p = 0.04$ sec. With these values $\tau_f/\tau_p = 0.15$ which further justifies the use of Eq. [53].

d) Inertial effect on pressure

The instantaneous pressure decreases due to the time-dependent inertial forces are maximum in the minimum lumen section. This pressure decrease is

$$\Delta P_u = \rho \, L/A_2 \, \frac{dQ}{dt} \qquad [54]$$

The contribution of this term turned out to be relatively small.

To determine the effect of obstruction in the common iliac artery the obstruction model was placed at 4 cm downstream of the iliac

bifurcation. Various amounts of area reduction were analyzed. The length of the obstruction (L) was 2 cm.

Experimental Arterial Obstruction in Dog

A search of the literature provided three references (80,81,82) in which pressure was measured upstream and downstream of various obstructions as well as the flowrate. The first and second papers (80) and (81) only gave mean pressures and flows and no reference to the instantaneous values. The third paper (82) provided instantaneous values for pressure and flow, but only for one value of the relative area obstruction. Since instantaneous values at various obstructions are required to study the contour of the pressure and flow pulses, we conducted a series of dog experiments in the Department of Anesthesia at the Massachusetts General Hospital.

Three male dogs all weighing 22 kg were given intravenous nembutal injections for anesthesia. The left common iliac artery was exposed through a midline abdominal incision. A small catheter was inserted into the distal aorta through the single hypogastric artery which was occluded around the catheter. A similar catheter was inserted into the left profunda and passed proximally until its tip lay in the terminal common femoral artery. These catheters were connected to Hewlett Packard Type 267 BC pressure transducers. Blood flow in the left iliac artery was measured with a square wave electromagnetic flowmeter and a non-cannulating flow probe of appropriate size for the artery. Pressures and blood flow were traced on a Sanborn 350 Direct-Writing Eight Channel Recorder.

A one-inch micrometer was modified to produce a flat clamp 2 cm in width to provide measured occlusion between the two pressure sites. Appendix B describes how the ratio of clamp opening to non-occluding clamp opening was converted into the percentage of arterial area obstruction.

Discussion and Comparison of Data

To be in accord with the dog experiments performed in the common iliac artery the obstruction model was placed at 4 cm downstream of the iliac bifurcation in the CC. The length of the obstruction was the same as in the dog experiments (2cm). Figure 55 is a comparison of the % pressure reduction (systolic and diastolic) distal to the obstruction as a function of percentage of area reduction obtained from the model and the experiment. Due to the higher flowrates present during systole, systolic pressure begins to fall off earlier than diastolic pressure in the computer model as well as in the dog experiments. Systolic pressure is reduced by 10% at a percentage of obstruction of about 50%, whereas diastolic pressure is not reduced by more than 10% until 80% obstruction is reached. Both pressures fall rapidly when the obstruction exceeds 85% of the initial area. As demonstrated in Fig. 56 the time-mean flowrate also falls off gradually until 85% obstruction is reached, and then falls rapidly thereafter. As indicated by these studies a patient may have a severe stenosis (60% - 70%) and still have a easily palpable pulse with little reduction in flow.

It is of interest to examine the effects of length of obstruction and flow rate on the pressure drop calculated by the obsruction model. Consider an obstruction of length L_1 producing a pressure drop of ΔP_1 at a flowrate of Q_1. Figure 57 shows how the relative pressure drop $\Delta P/\Delta P_1$ increases as a function of L/L_1 for various % obstructions holding flowrate constant. Figure 58 is a plot of $\Delta P/\Delta P_1$ as a function of Q/Q_1 for various % obstructions holding length constant. These curves indicate the effect of flowrate on the pressure drop is far more important than that of length. Also, the significance of the obstruction may be magnified when increased flowrate is required, as in exercise, when the peripheral resistance is lowered. Claudication occurs when blood flow is inadequate to maintain normal metabolic balance. Flowrate through a stenosis is limited to a maximum value due to the available pressure drop. When this maximum flowrate is inadequate claudication occurs.

Figures 59 and 60 represent the pressure pulse upstream and downstream of a 88% obstruction, determined by the simulation and measured in dog respectively. Both indicate that obstruction alters the contour of the pressure pulse. With increased obstruction the initial slope is reduced and the crest becomes more rounded. However, the reflected wave is still present at large area reductions, up to 95%. This observation suggests that the reflected wave is altered more by a mismatch between peripheral resistance and the arterial characteristic impedance than by arterial narrowing alone. It is not unreasonable to postulate that as obstruction increases and the flow reduces, the

peripheral resistance decreases (vasodilation) to maintain the required blood flow.

IX. CONCLUSIONS

This work touched on many problems in the fields of engineering and medical sciences. It raised many questions and provided the ground work for more detailed analysis of vascular dynamics. The major conclusions that can be drawn from this research are:

1) It is possible to make reliable and reproducible non-invasive recordings of the arterial pressure pulse contour on the upper and lower extremities; an instrument has been built for this purpose.

2) The arterial pressure pulse contour is altered by the arteriosclerotic process. The alterations observed clinically are probably due to an impedance mismatch between the larger arteries and the arterioles and capillaries forming the peripheral resistance. With arteriosclerosis the characteristic impedance of the larger arteries is increased by decreased elasticity in the arterial wall, while the peripheral resistance may be lowered by vasodilation.

3) A computer model of the arterial system of the lower extremities confirms that a severe obstruction of the arterial lumen is necessary to cause significant damping of the pressure pulse. When severe obstruction is present the blood flowrate through an obstruction is limited by the obstruction and no longer controlled by vasotone. When this maximum flowrate becomes

insufficient to meet increased demands, as in exercise, there is not enough blood to maintain normal metabolic balance and ischemic pain results.

CAPTIONS FOR FIGURES

Fig. No.

1 Arteriogram of a patient with aorto-iliac atherosclerotic disease. Note complete block of right external iliac at the level of the hypogastric branch.

2 X-ray of a profunda and superficial femoral artery illustrating stiff calcified deposits in the arterial wall.

3 A cross-sectional view of a common iliac artery in which the lumen has been significantly reduced as a result of atheroma build-up.

4 Sketch of the Pressure Pulse Recorder (PPR).

5 (a) (b) Technical data on the Pitran.

6 PPR System Diagram.

7 Typical pressure calibration run at the brachial artery showing comparison with auscultatory method.

8 Comparison of systolic and diastolic pressures obtained by the occlusion and auscultatory methods in the brachial artery of 13 volunteers.

8a Pressure amplitude as a function of frequency in the rigid cylinder experiment.

9 $\delta V_x / \delta V$ as a function of mean cuff pressure and injected volume.

10a-e Comparison of pressure pulse contours obtained with the PPR and direct arterial cannulation at the radial artery.

Fig. No.

11a-e	Comparison of pressure pulse contours obtained with the PPR and direct arterial cannulation at the common femoral artery.
12	Effect of injected volume on the recorded pulse contour at constant cuff pressure.
13	PPR recordings taken at the brachial artery, forearm, thigh, calf, and ankle of both upper and lower extremities in a healthy subject.
14	Pre-operative information on Patient (YW). On the left, angiographic findings are illustrated, including a +0 to +4 grade for palpable pulses. On the right, the PPR recordings are given for the thigh, calf, and ankle of each leg. The units are in mm of deflection.
15	Pre-operative PPR recordings after exercise - Patient (YW).
16	Post-operative PPR recordings at rest - Patient (YW).
17	Post-operative PPR recordings after exercise - Patient (YW).
18	Pre-operative PPR recordings at rest - Patient (KM).
19	Post-operative PPR recordings at rest - Patient (KM).
20	Post-operative PPR recordings after exercise - Patient (KM).
21	Intra-operative PPR recordings - Patient (TR).
22	PPR traces taken at the left calf of Patient (RS) over a nine month period with consistent cuff pressures and volumes.

Fig. No.

23 PPR traces taken at the left calf of Patient (JA) over a twelve month period in which the left limb of an aorto-iliac graft occluded.

24 PPR traces taken at the right and left brachial arteries of Patient (BM) in which the left arm was enlarged due to lymphedema.

25 PPR traces taken at the right calf of three healthy athletic young men.

26 PPR traces taken at the right and left ankles of Patient (WP). The left superficial femoral artery is occluded.

27 PPR traces taken at the right and left calves of Patient (MM). The right common femoral artery is occluded.

28 PPR traces taken at rest and after exercise in a healthy athlete.

29 (a) Electric analog of the distal boundary condition.

(b) Schematic of a bifurcation.

30 The Physiological Model showing the anatomical sketch on the left and a schematic of the simulated arteries on the right.

31 Arterial diameter and cross-sectional area as a function of distance from the iliac bifurcation as determined by the angiographic study. The mean pressure is estimated to be 100 mm-Hg.

32 Comparison of the angiographic study with the data from Westerhof *et al.* and Singer.

33 Comparison of Eq. [43] with measurements taken by Boughner and Roach.

Fig. No.

34 Wave speed in the arterial model as a function of α at 100 mm-Hg.

35 Wave speed in the arterial model as a function of pressure for α = 6%.

36 Magnitude and phase of the reflection coefficient at the tibial vessels as a function of R_1/R_T.

37 Pressure pulse used as the proximal boundary condition in the Control Case.

38 Pressure and flow pulses in the Control Case.

39 Flow pulses in the hypogastric and profunda branches for the Control Case.

40 Systolic pressure, diastolic pressure, pulse pressure, mean pressure, peak flowrate, minimum flowrate, and mean flow as a function of distance from the iliac bifurcation in the Control Case.

41 Pressure and flow pulses at the iliac bifurcation for the Control Case.

42 The effect of convective acceleration on distal popliteal pressure (x = 60 cm) in the Control Case.

43 The effect of blood viscosity on the flow at the iliac bifurcation and the pressure at the distal popliteal in the Control Case.

44 A comparison of the pressure pulse at the distal popliteal artery in the Control Case and with the hypogastric and profunda occluded.

45 Effects of area and compliance taper on the distal popliteal pressure.

46 The effect of arterial wall compliance on the distal popliteal pressure in the Control Case.

47 Magnitude and phase of the reflection coefficient at the tibial vessels in the Control Case as a function of α .

Fig. No.

48 The effect of increased distal resistance on the distal pulse in a uniform cylindrical elastic tube.

49 Effect of a distal cuff on the pressure pulse in the calf.

50 Magnitude and phase of the reflection coefficient as a function of R_1 at the distal boundary condition.

51 The effect of decreased distal resistance on the distal pulse in a uniform cylindrical elastic tube.

52 Effect of vasodilation on the pressure pulse in the calf.

53 Effect of changing the distal reflection coefficient on the distal popliteal pressure in the arterial model.

54 Obstruction Model.

55 Pressure reduction (systolic and diastolic) downstream of a 2 cm long obstruction as a function of area reduction in the common iliac artery (comparison of simulation and experimental results).

56 Mean flow reduction due to a 2 cm long obstruction as a function of area reduction in the common iliac artery (comparison of simulation and experimental results).

57 Effect of obstruction length on the pressure drop at a constant rate of flow.

58 Effect of flowrate on the pressure drop for an obstruction of fixed length.

59 Calculated pressure pulses upstream and downstream of an 88% obstruction of 2 cm long in the common femoral artery.

60 Measured pressure pulses upstream and downstream of an 88% obstruction in the common iliac artery of a dog.

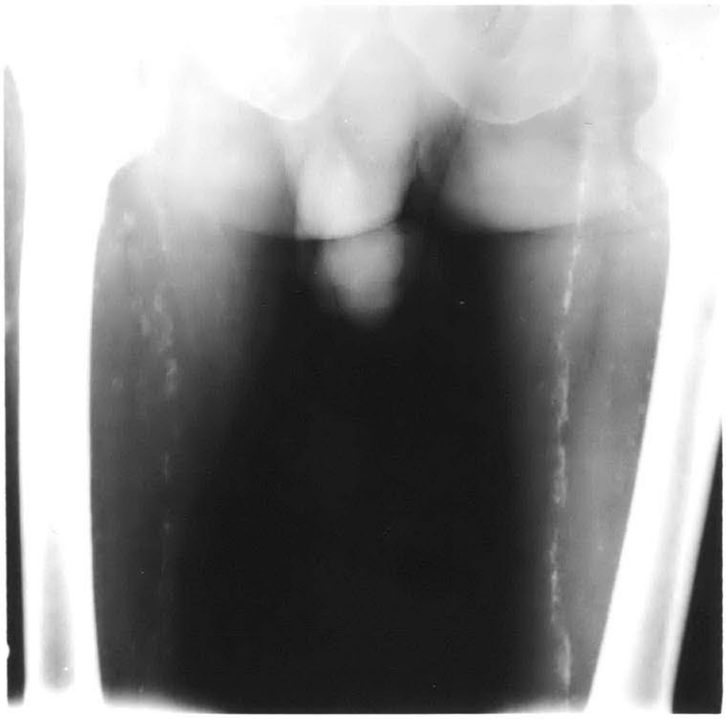
FIGURES

1 --- 60



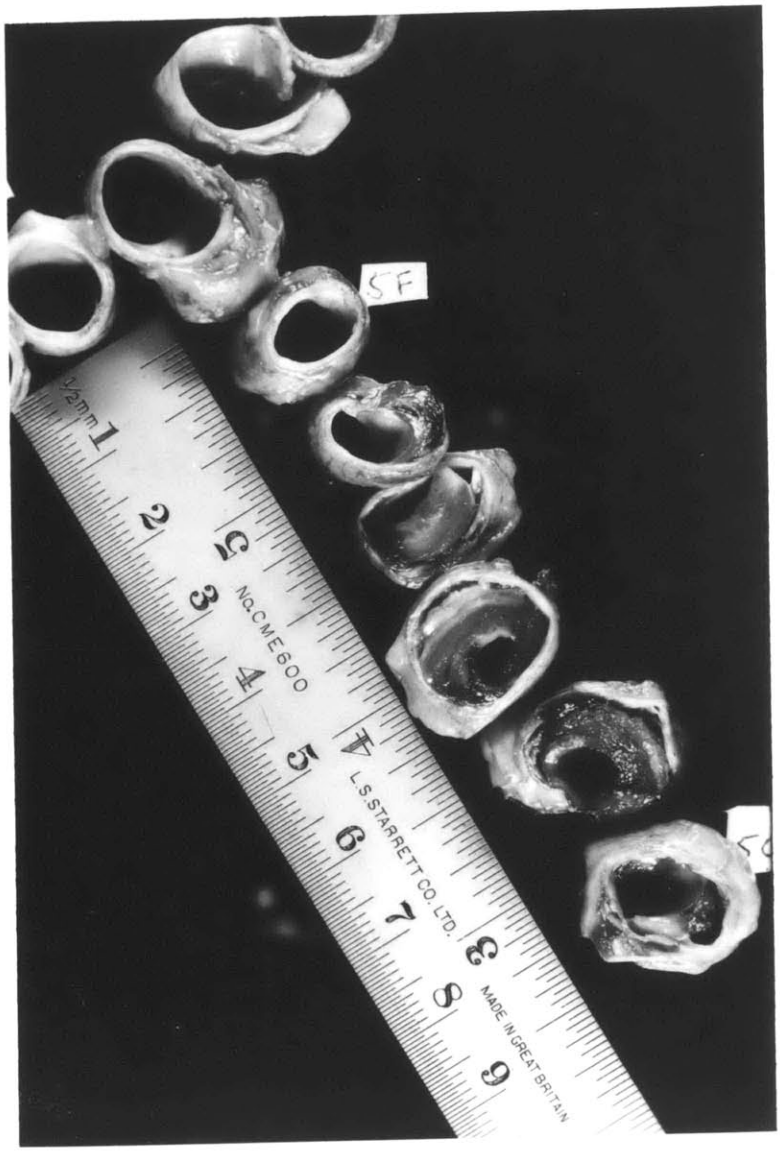
Arteriogram of a patient with aorto-iliac atherosclerotic disease. Note complete block of right external iliac at the level of the hypogastric branch.

Fig. 1



X-ray of a profunda and superficial femoral artery illustrating stiff calcified deposits in the arterial wall.

Fig. 2



A cross-sectional view of a common iliac artery in which the lumen has been significantly reduced as a result of atheroma buildup.

Fig. 3

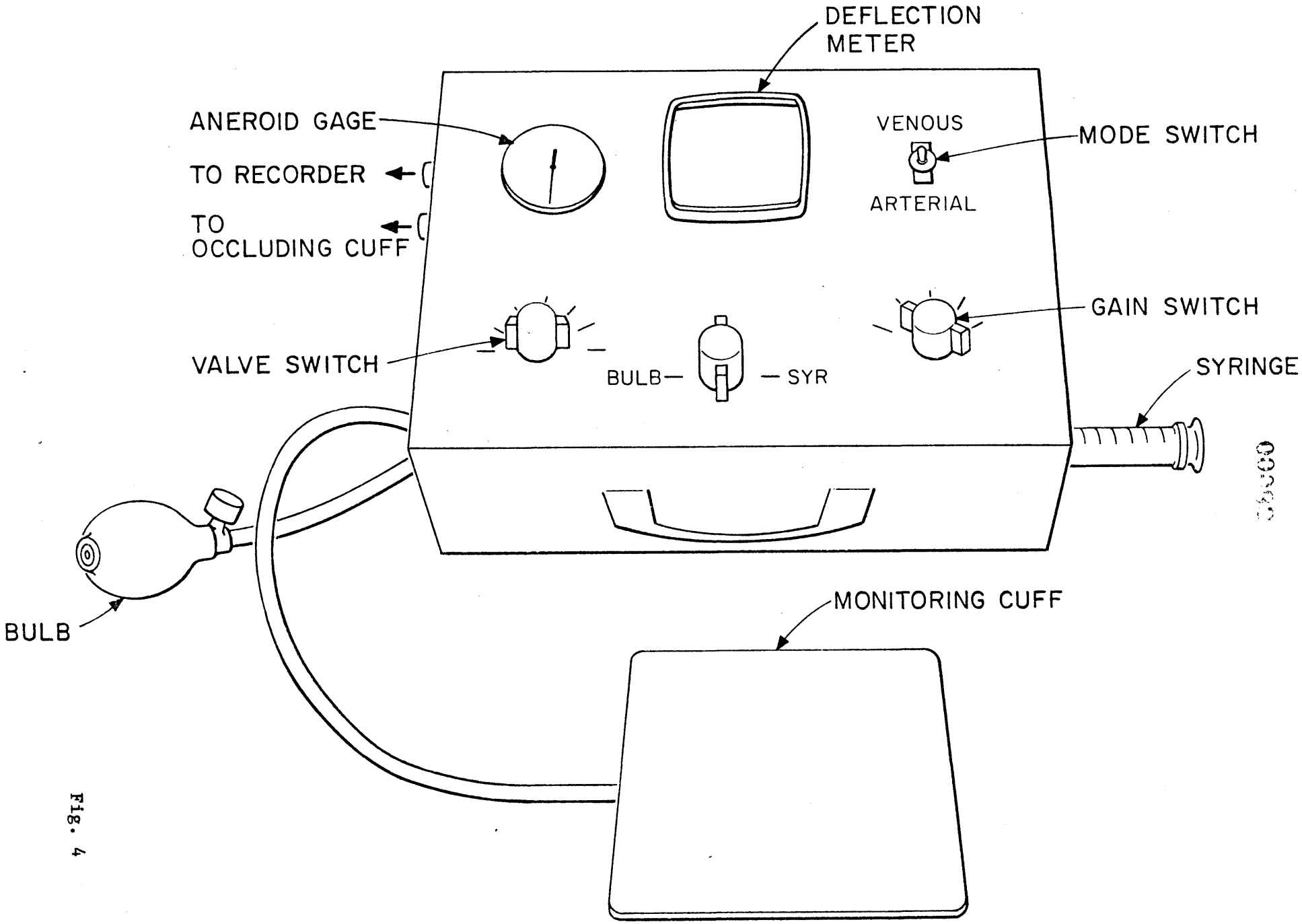

DEFLECTION METER
ANEROID GAGE
TO RECORDER
TO OCCLUDING CUFF
VENOUS
ARTERIAL
MODE SWITCH
GAIN SWITCH
VALVE SWITCH
BULB
SYR
SYRINGE
BULB
MONITORING CUFF

Fig. 4

00083

0.1 psid Series PITRAN®
Pressure Sensitive Transistors

STOLAB

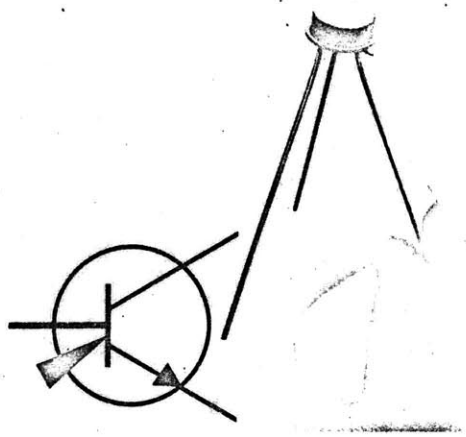


Fig. 5a

The PITRAN is a silicon NPN planar transistor that has its emitter-base junction mechanically coupled to a diaphragm. A differential pressure applied to the diaphragm produces a large, reversible change in the gain of the transistor, i.e., the PITRAN's output is modulated by the mechanical variable.

Model	TEMP. COEF. ZERO SHIFT −mV/°C	
	Typical	Maximum
PT-L2	±200	±400
PT-L3	± 50	±100
PT-L2P	0 to +200	0 to +400
PT-L3P	0 to + 50	0 to +100

LINEAR PRESSURE RANGE EQUIVALENTS

PSID	Inches H_2O	Torr (mm Hg)	dB (re 2 x 10^{-4} dynes/cm²)	Gram/cm²	Millibars
0.07	1.94	3.62	148	4.92	4.90
0.1	2.77	5.17	151	7.03	6.89
0.17	4.71	8.79	155	12.0	11.7

	MINIMUM	TYPICAL	MAXIMUM	
Linear Pressure Range†	0.07	0.1	0.17	psid (see equivalent pressure table above)
Linear Output*‡	20			% of applied voltage
Linearity*		±0.5	±1.0	% deviation from best straight line
Hysteresis*		±0.5	±1.0	%
Overload Pressure Range‡	500	700		% of linear pressure range
Temperature Coefficient*				
Zero Shift	Depends on model. See chart above.			
Sensitivity Change		−0.2	−0.5	%/°C
Noise*		0.3	1	mV
Dynamic Range	65			dB
Rise Time		10		microseconds
Volumetric Displacement		4 x 10^{-8}		in³ for full scale pressure
Diaphragm Displacement				
Full Scale		2		microinches
To Overload		4		microinches
Mechanical Resonance Frequency	100	150		kHz
Life	10			billion cycles
h_{FE}*		10	40	at V_{CE} = 2 V, I_C = 800 μA, Δ P = O
Electrical Frequency Response		100		MHz
I_{CBO}*		0.01	1	μA at V_{CB} = 60 V
BV_{CEO}*	50	120		volts at I_C = 10 μA
Operating Temperature	−40		+75	°C
Acceleration			300	g
Vibration Sensitivity*		1		millivolt/g perpendicular to diaphragm
Weight, Including Leads			1/3	gram

*Measured in the Standard Circuit shown on the reverse side. †See Pressure Characteristics Curve. ‡See Linear Pressure Range Curve at V_{CE} = 2 V.

STOW LABORATORIES INC. KANE INDUSTRIAL DRIVE • HUDSON, MASS. 01749 • PHONE: (617) 562-9347 • TWX: 710-390-0346

00083

0.1 psid Series PITRAN®
Pressure Sensitive Transistors

STOLAB

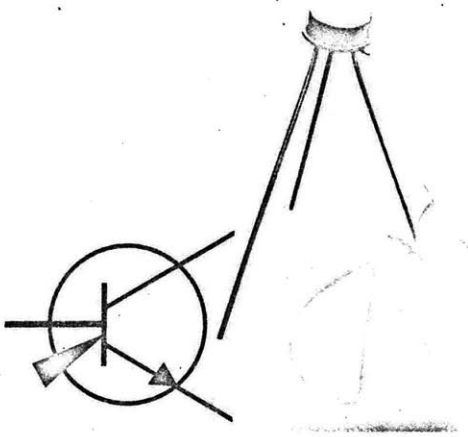


Fig. 5a

DESCRIPTION

The PITRAN is a silicon NPN planar transistor that has its emitter-base junction mechanically coupled to a diaphragm. A differential pressure applied to the diaphragm produces a large, reversible change in the gain of the transistor, i.e., the PITRAN's output is modulated by the mechanical variable.

Model	TEMP. COEF. ZERO SHIFT −mV/°C	
	Typical	Maximum
PT-L2	±200	±400
PT-L3	± 50	±100
PT-L2P	0 to +200	0 to +400
PT-L3P	0 to + 50	0 to +100

LINEAR PRESSURE RANGE EQUIVALENTS

PSID	Inches H_2O	Torr (mm Hg)	dB (re 2 x 10^{-4} dynes/cm²)	Gram/cm²	Millibars
0.07	1.94	3.62	148	4.92	4.90
0.1	2.77	5.17	151	7.03	6.89
0.17	4.71	8.79	155	12.0	11.7

PERFORMANCE

	MINIMUM	TYPICAL	MAXIMUM	
Linear Pressure Range†	0.07	0.1	0.17	psid (see equivalent pressure table above)
Linear Output*‡	20			% of applied voltage
Linearity*		±0.5	±1.0	% deviation from best straight line
Hysteresis*		±0.5	±1.0	%
Overload Pressure Range‡	500	700		% of linear pressure range
Temperature Coefficient*				
Zero Shift	Depends on model. See chart above.			
Sensitivity Change		−0.2	−0.5	%/°C
Noise*		0.3	1	mV
Dynamic Range	65			dB
Rise Time		10		microseconds
Volumetric Displacement		4 x 10^{-8}		in³ for full scale pressure
Diaphragm Displacement				
Full Scale		2		microinches
To Overload		4		microinches
Mechanical Resonance Frequency	100	150		kHz
Life	10			billion cycles
h_{FE}*		10	40	at V_{CE} = 2 V, I_C = 800 μA, Δ P = O
Electrical Frequency Response		100		MHz
I_{CBO}*		0.01	1	μA at V_{CB} = 60 V
BV_{CEO}*	50	120		volts at I_C = 10 μA
Operating Temperature	−40		+75	°C
Acceleration			300	g
Vibration Sensitivity*		1		millivolt/g perpendicular to diaphragm
Weight, Including Leads			1/3	gram

*Measured in the Standard Circuit shown on the reverse side. †See Pressure Characteristics Curve. ‡See Linear Pressure Range Curve at V_{CE} = 2 V.

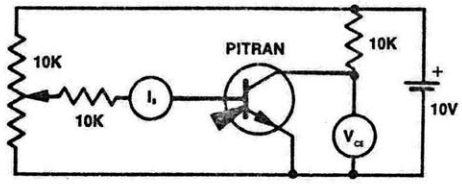
STOW LABORATORIES INC. KANE INDUSTRIAL DRIVE • HUDSON, MASS. 01749 • PHONE: (617) 562-9347 • TWX: 710-390-0346

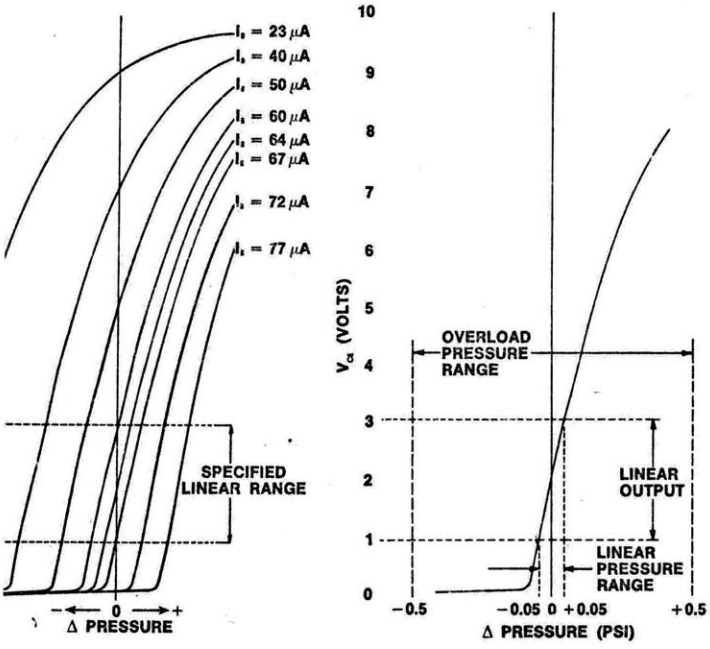
0.1 psid Series PITRAN®
Pressure Sensitive Transistors

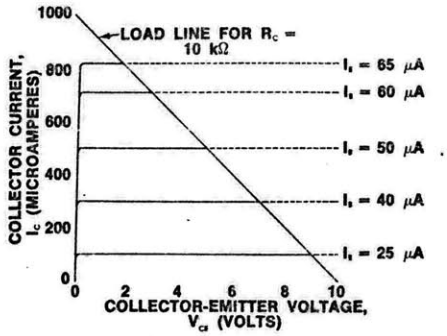
00084

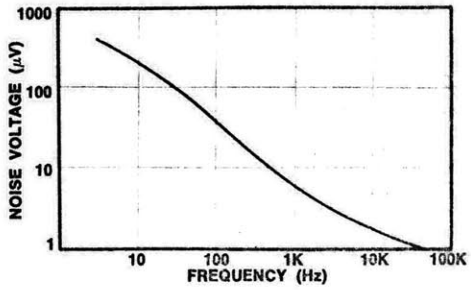
TYPICAL PERFORMANCE

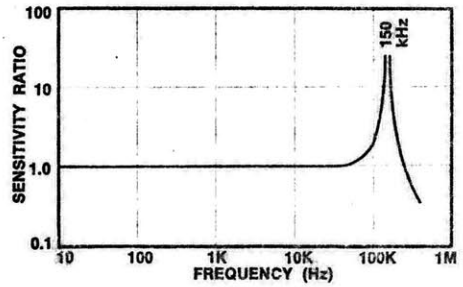
The PITRAN is calibrated in the standard circuit shown below. The simple common-emitter configuration provides a linear dc output of at least 2 volts when rated pressure is applied to the PITRAN'S diaphragm.



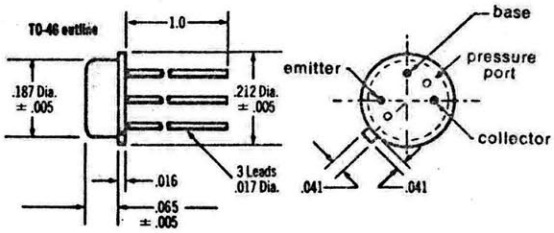








MECHANICAL SPECIFICATIONS



Diaphragm:	Beryllium copper, nickel and gold plated
Case:	Kovar, nickel and gold plated
Leads:	Kovar, gold plated

The gold plated PITRAN diaphragm can measure pressure in almost any fluid. However, the reference side of the PITRAN is in contact with the NPN chip. Therefore, the pressure medium on the reference side must be nonconductive and noncorrosive.

Stow Laboratories reserves the right to make changes in these specifications.

STOLAB STOW LABORATORIES INC.

KANE INDUSTRIAL DRIVE • HUDSON, MASS. 01749 PHONE: (617) 562-9347 • TWX: 710-390-0346

Fig. 5b

Copyright Stow Laboratories Inc. 1970

Printed in USA — 4/70

PPR
SYSTEM DIAGRAM

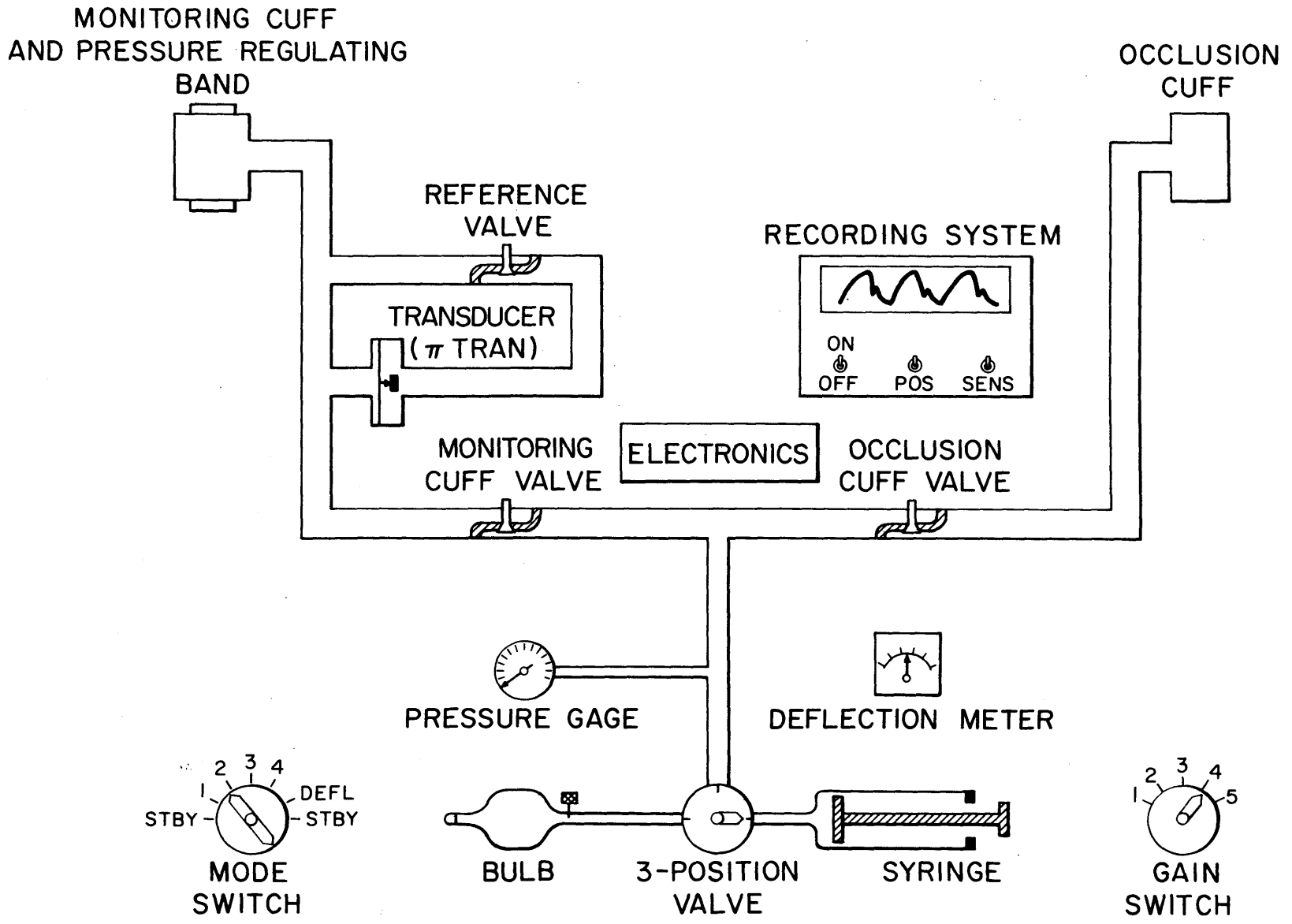


Fig. 6

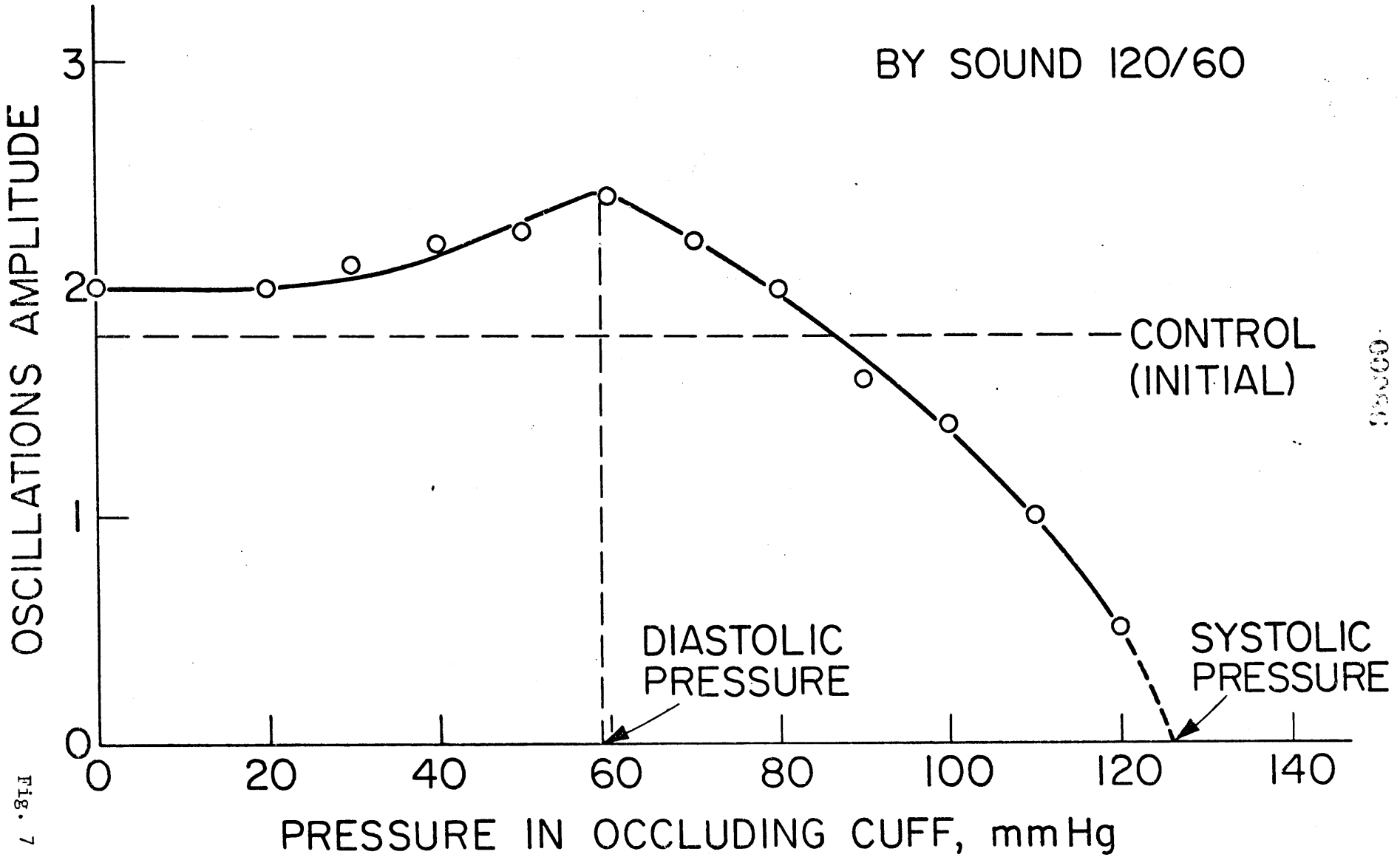

BY SOUND 120/60
OSCILLATIONS AMPLITUDE
3
2
1
0
CONTROL
(INITIAL)
DIASTOLIC
PRESSURE
SYSTOLIC
PRESSURE
0
20
40
60
80
100
120
140
PRESSURE IN OCCLUDING CUFF, mmHg

FIG. 7

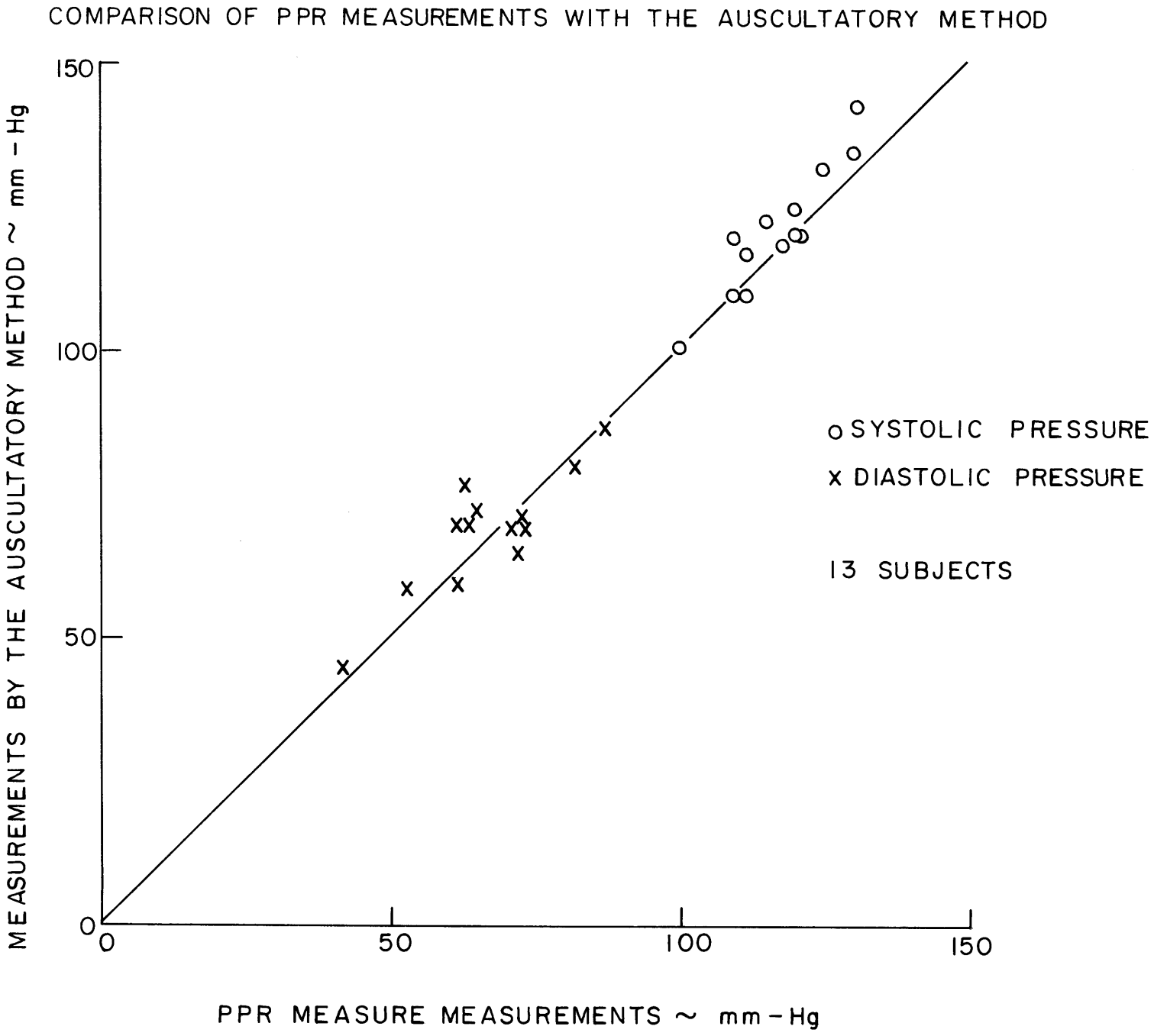

COMPARISON OF PPR MEASUREMENTS WITH THE AUSCULTATORY METHOD
MEASUREMENTS BY THE AUSCULTATORY METHOD ~ mm - Hg
150
100
50
0
0
50
100
150
PPR MEASURE MEASUREMENTS ~ mm - Hg
o SYSTOLIC PRESSURE
x DIASTOLIC PRESSURE
13 SUBJECTS

Fig. 8

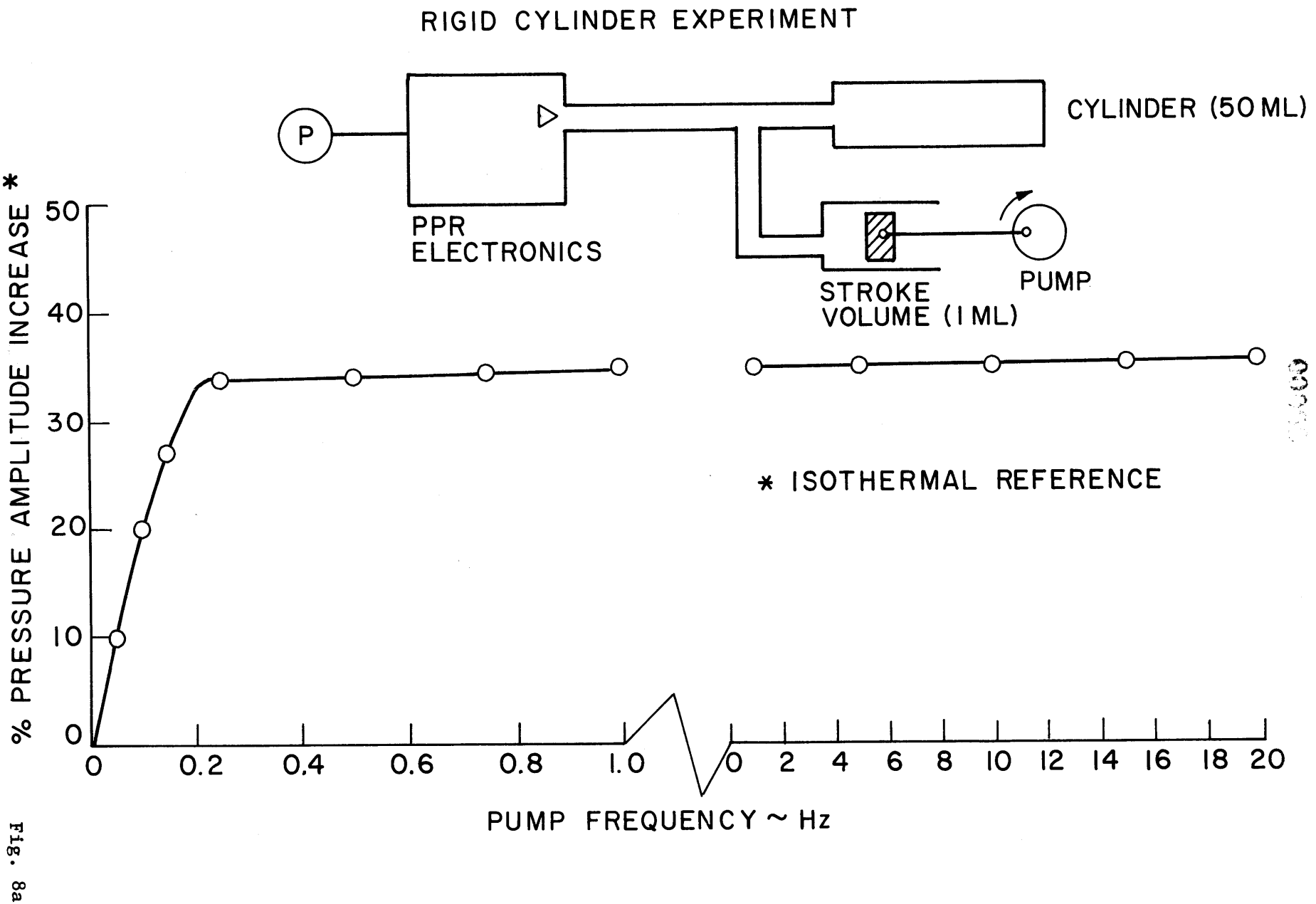

RIGID CYLINDER EXPERIMENT
P
PPR
ELECTRONICS
CYLINDER (50 ML)
STROKE
VOLUME (1 ML)
PUMP
% PRESSURE AMPLITUDE INCREASE *
50
40
30
20
10
0
0
0.2
0.4
0.6
0.8
1.0
0
2
4
6
8
10
12
14
16
18
20
PUMP FREQUENCY ~ Hz
* ISOTHERMAL REFERENCE

Fig. 8a

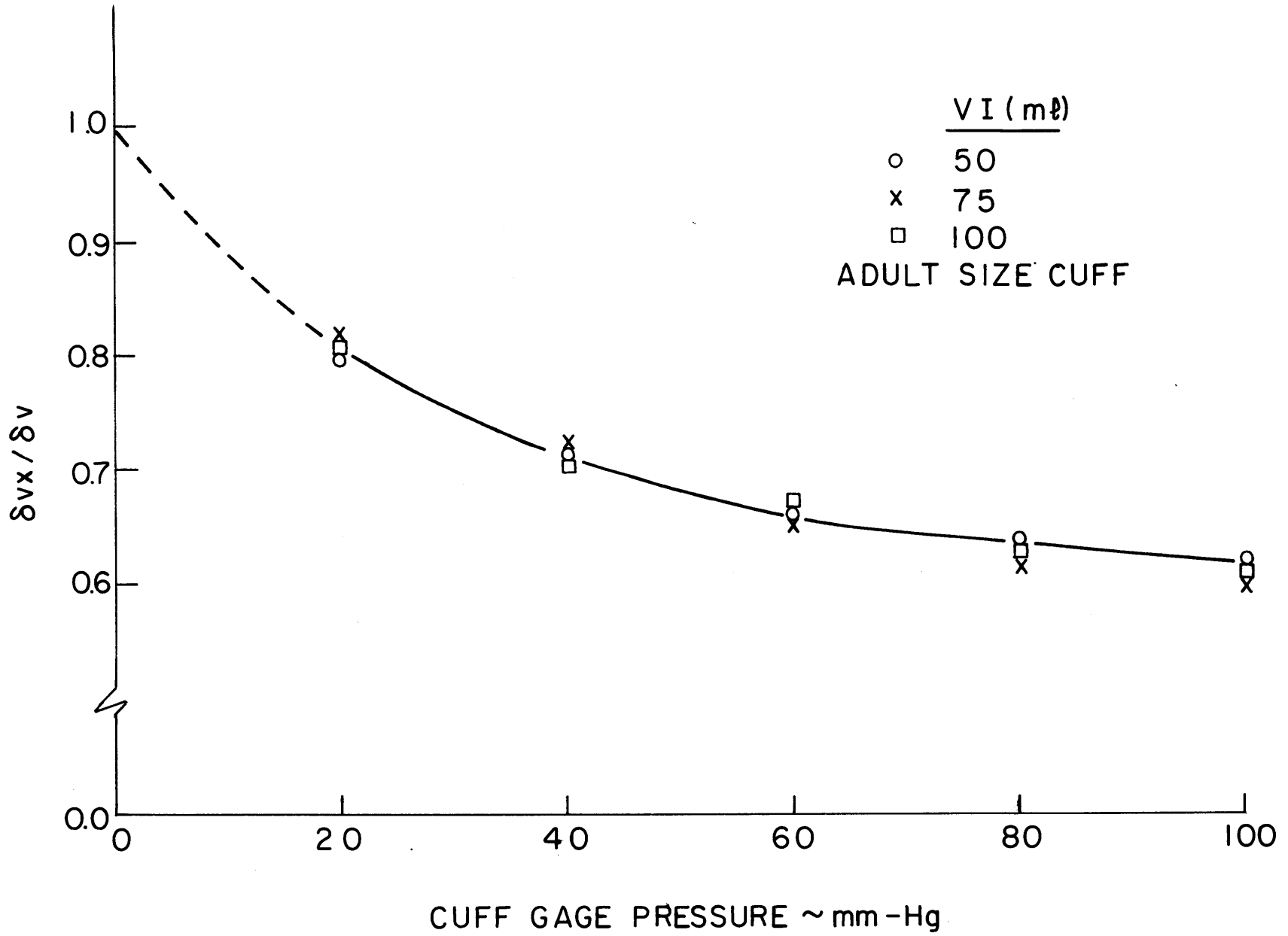

VI (mℓ)
50
75
100
ADULT SIZE CUFF
δvx/δv
1.0
0.9
0.8
0.7
0.6
0.0
0
20
40
60
80
100
CUFF GAGE PRESSURE ~ mm-Hg

Fig. 9

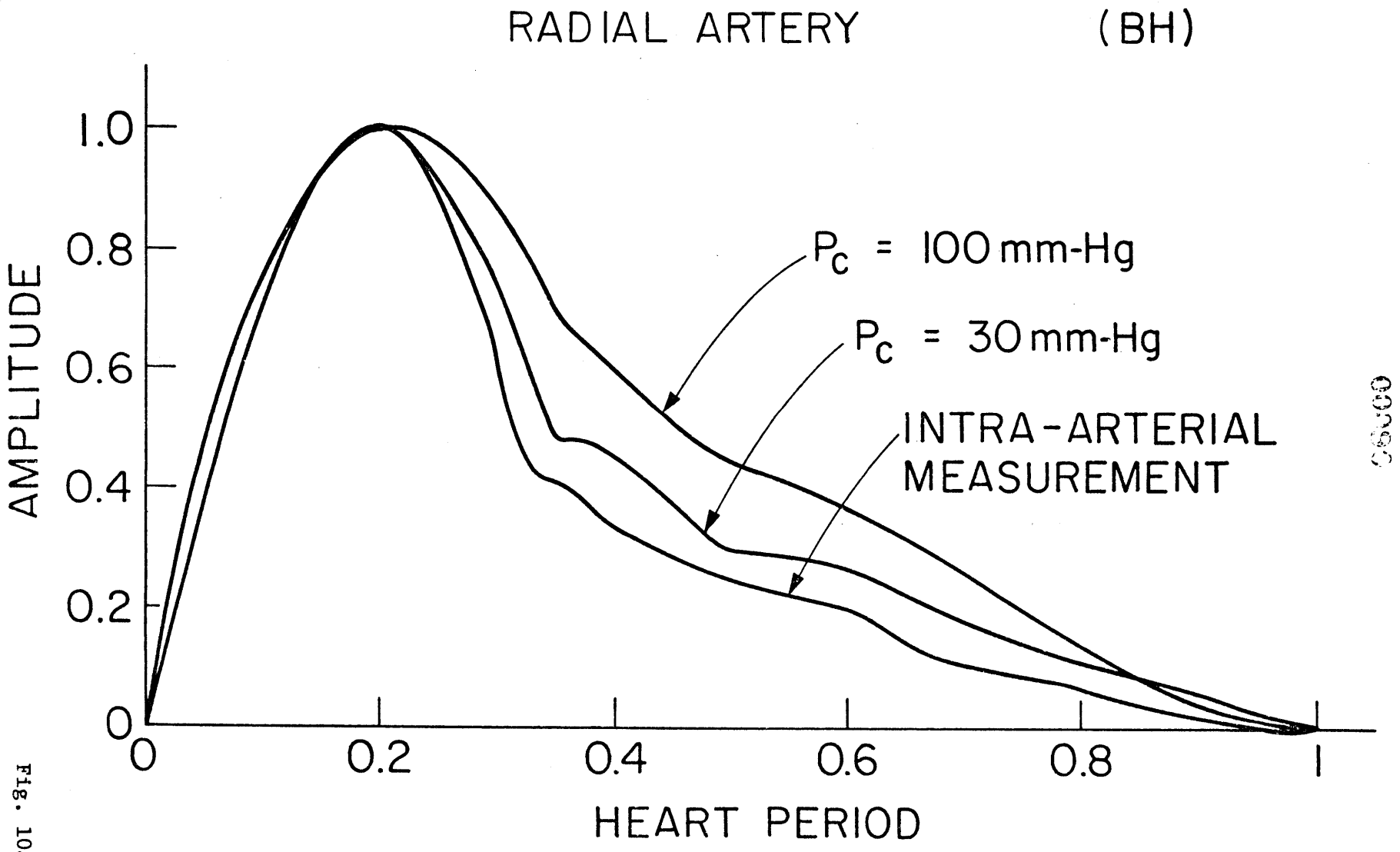

RADIAL ARTERY (BH)
AMPLITUDE
1.0
0.8
0.6
0.4
0.2
0
0
0.2
0.4
0.6
0.8
1
HEART PERIOD
P_c = 100 mm-Hg
P_c = 30 mm-Hg
INTRA-ARTERIAL MEASUREMENT

Fig. 10a

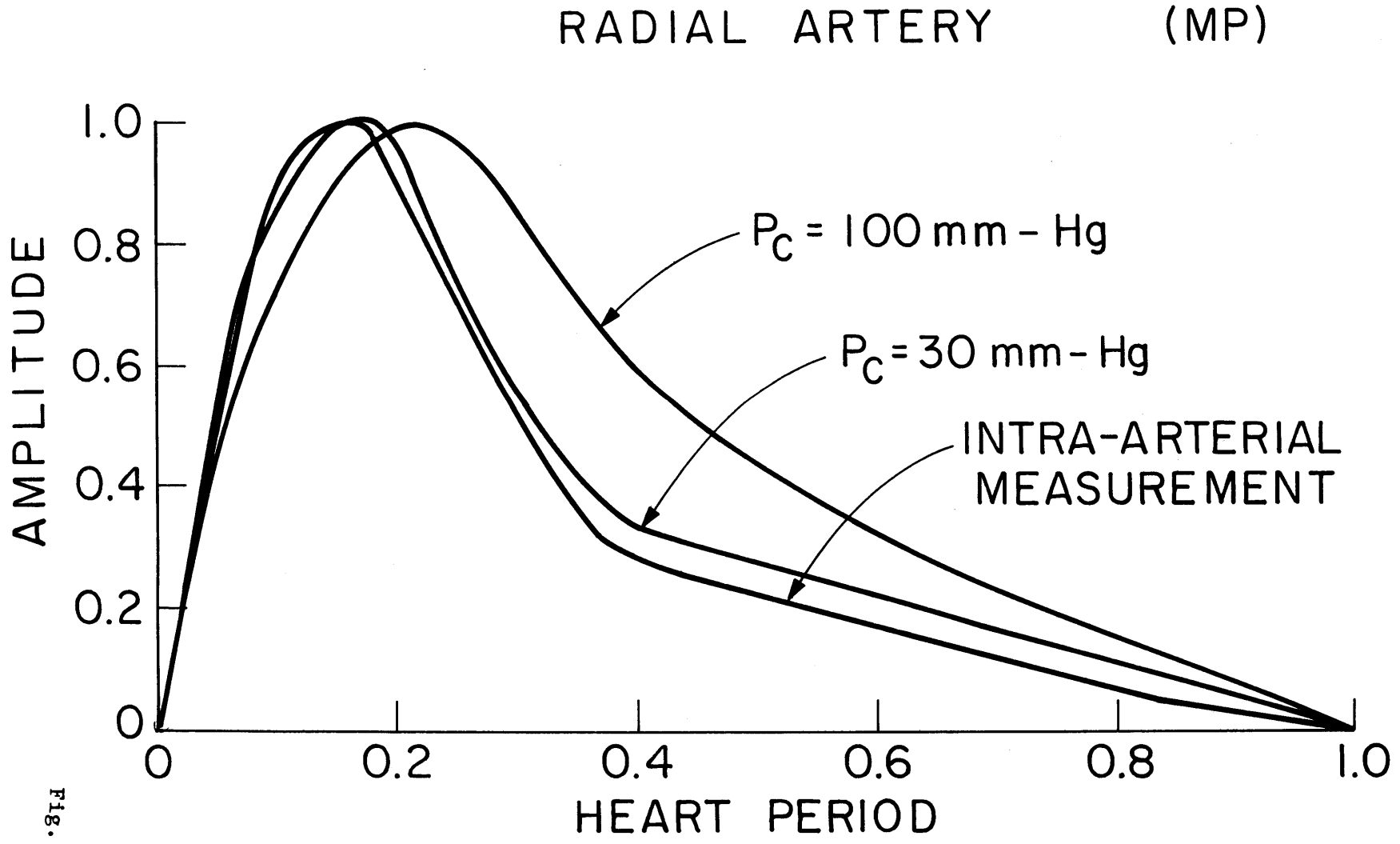

RADIAL ARTERY (MP)
AMPLITUDE
1.0
0.8
0.6
0.4
0.2
0
0
0.2
0.4
0.6
0.8
1.0
HEART PERIOD
P_C = 100 mm - Hg
P_C = 30 mm - Hg
INTRA-ARTERIAL MEASUREMENT

Fig. 10b

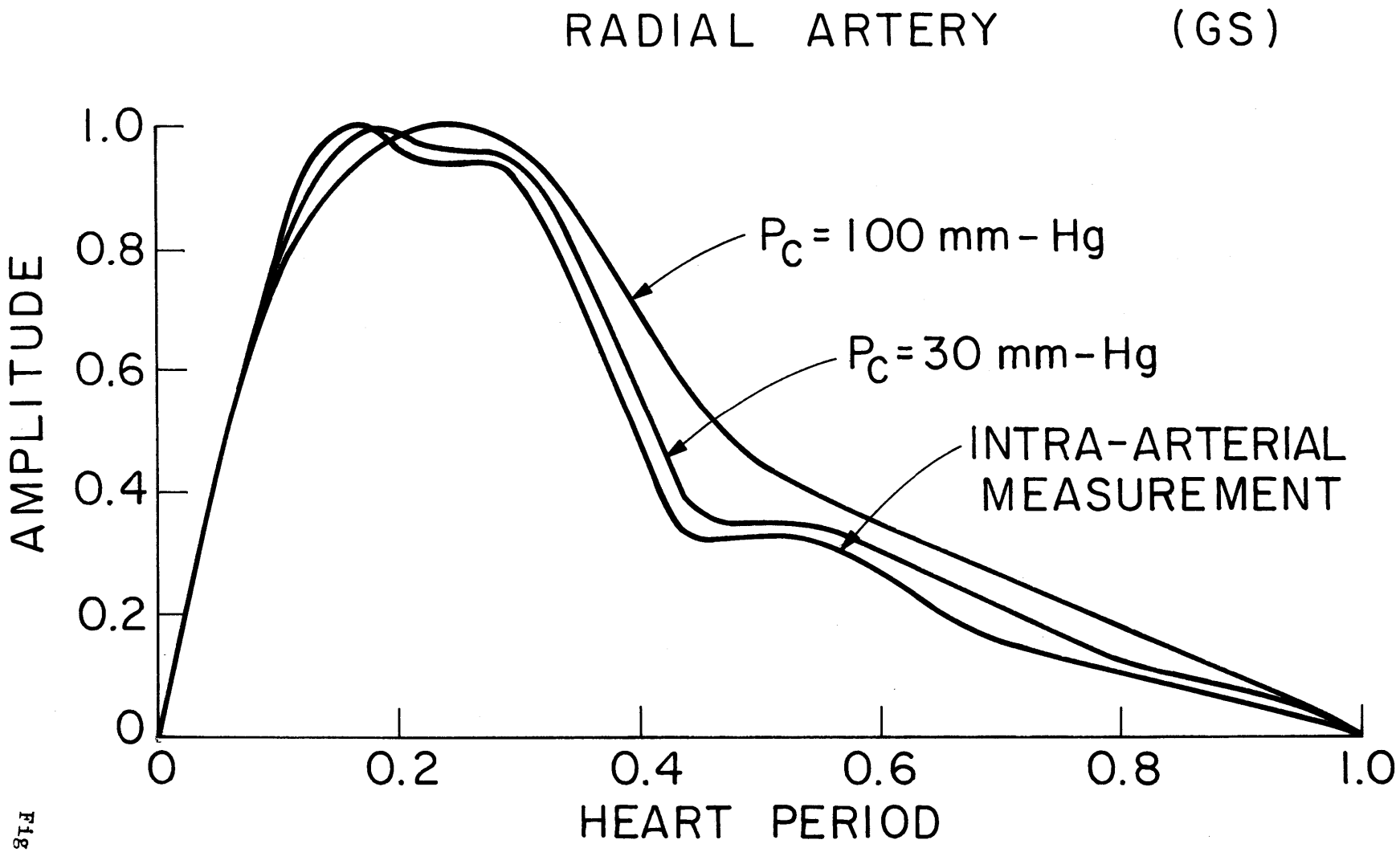

RADIAL ARTERY (GS)
AMPLITUDE
1.0
0.8
0.6
0.4
0.2
0
0
0.2
0.4
0.6
0.8
1.0
HEART PERIOD
P_C = 100 mm-Hg
P_C = 30 mm-Hg
INTRA-ARTERIAL MEASUREMENT

Fig. 10c

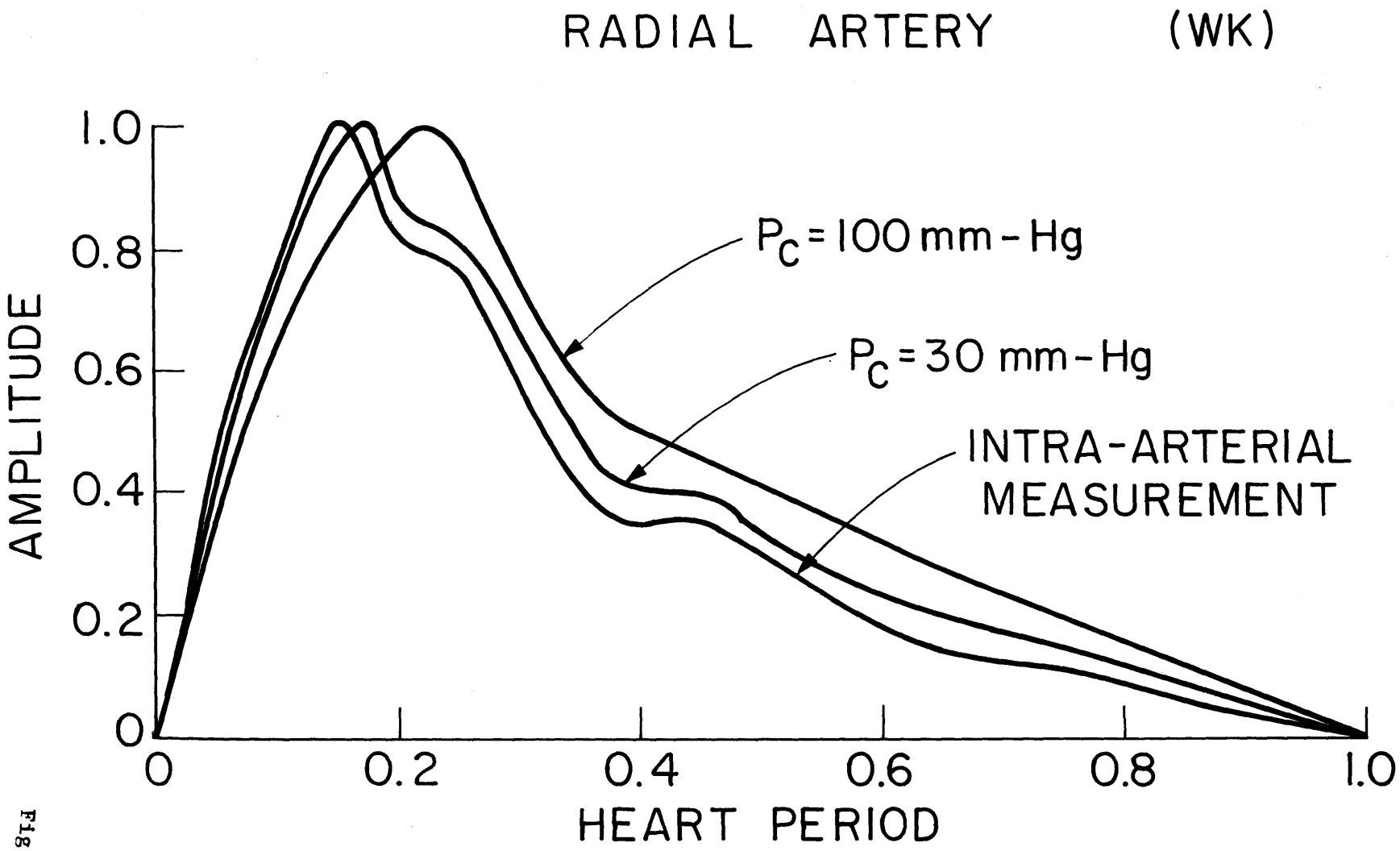

RADIAL ARTERY (WK)
AMPLITUDE
1.0
0.8
0.6
0.4
0.2
0
0
0.2
0.4
0.6
0.8
1.0
HEART PERIOD
P_C = 100 mm-Hg
P_C = 30 mm-Hg
INTRA-ARTERIAL MEASUREMENT

Fig. 10d

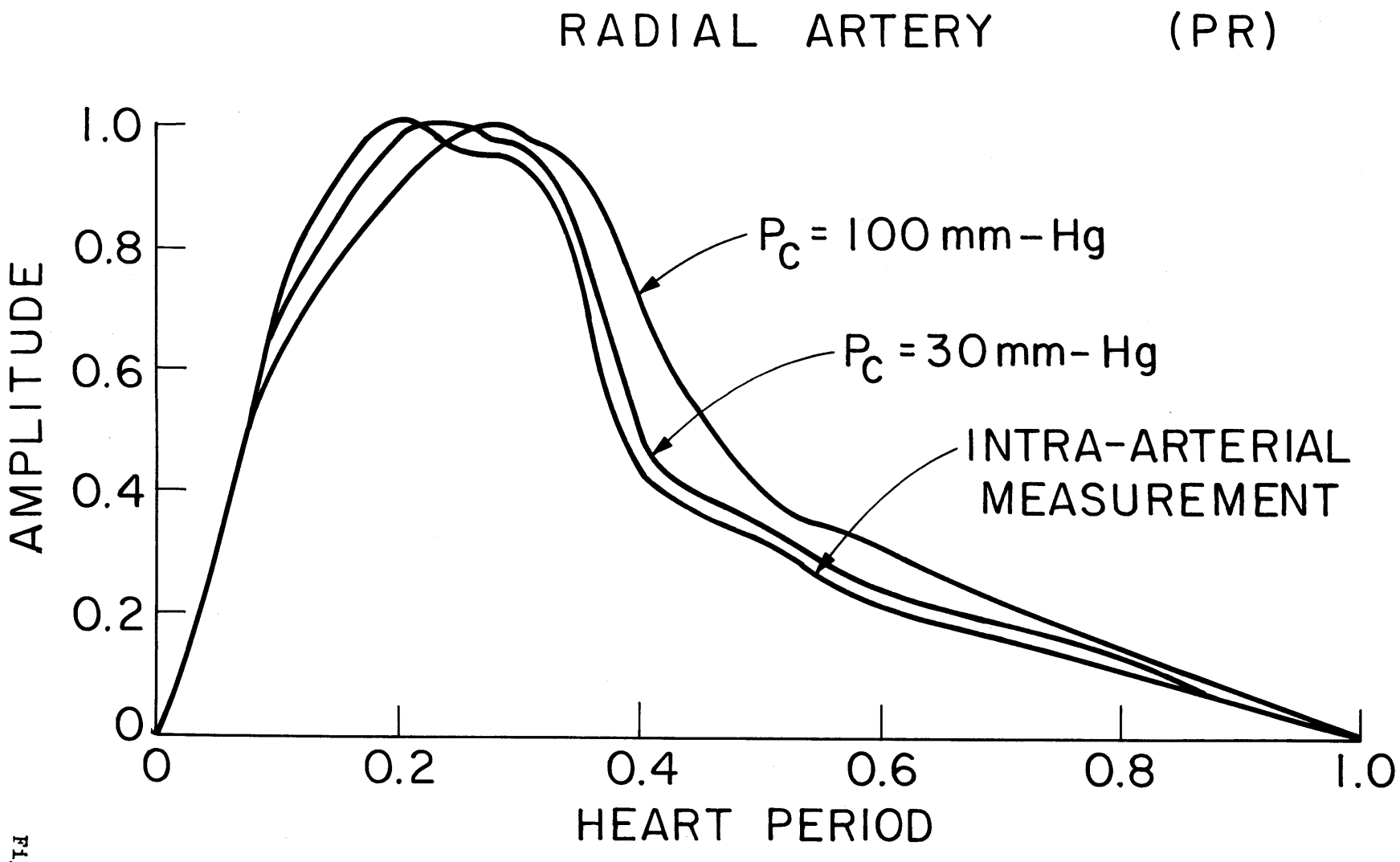

RADIAL ARTERY (PR)
AMPLITUDE
1.0
0.8
0.6
0.4
0.2
0
0
0.2
0.4
0.6
0.8
1.0
HEART PERIOD
P_C = 100 mm-Hg
P_C = 30 mm-Hg
INTRA-ARTERIAL MEASUREMENT

Fig. 10e

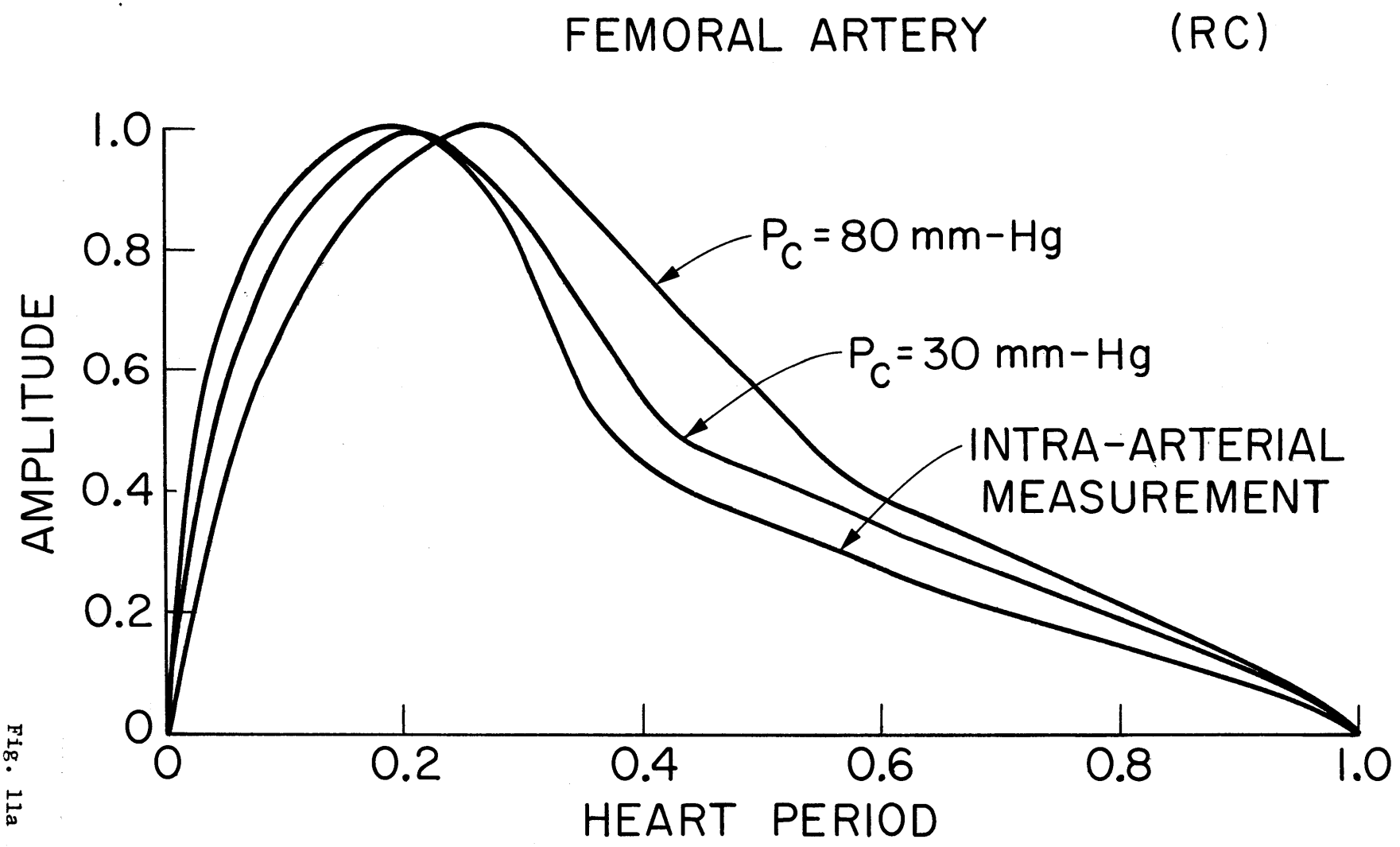

FEMORAL ARTERY (RC)
AMPLITUDE
1.0
0.8
0.6
0.4
0.2
0
0
0.2
0.4
0.6
0.8
1.0
HEART PERIOD
P_C = 80 mm-Hg
P_C = 30 mm-Hg
INTRA-ARTERIAL MEASUREMENT

Fig. 11a

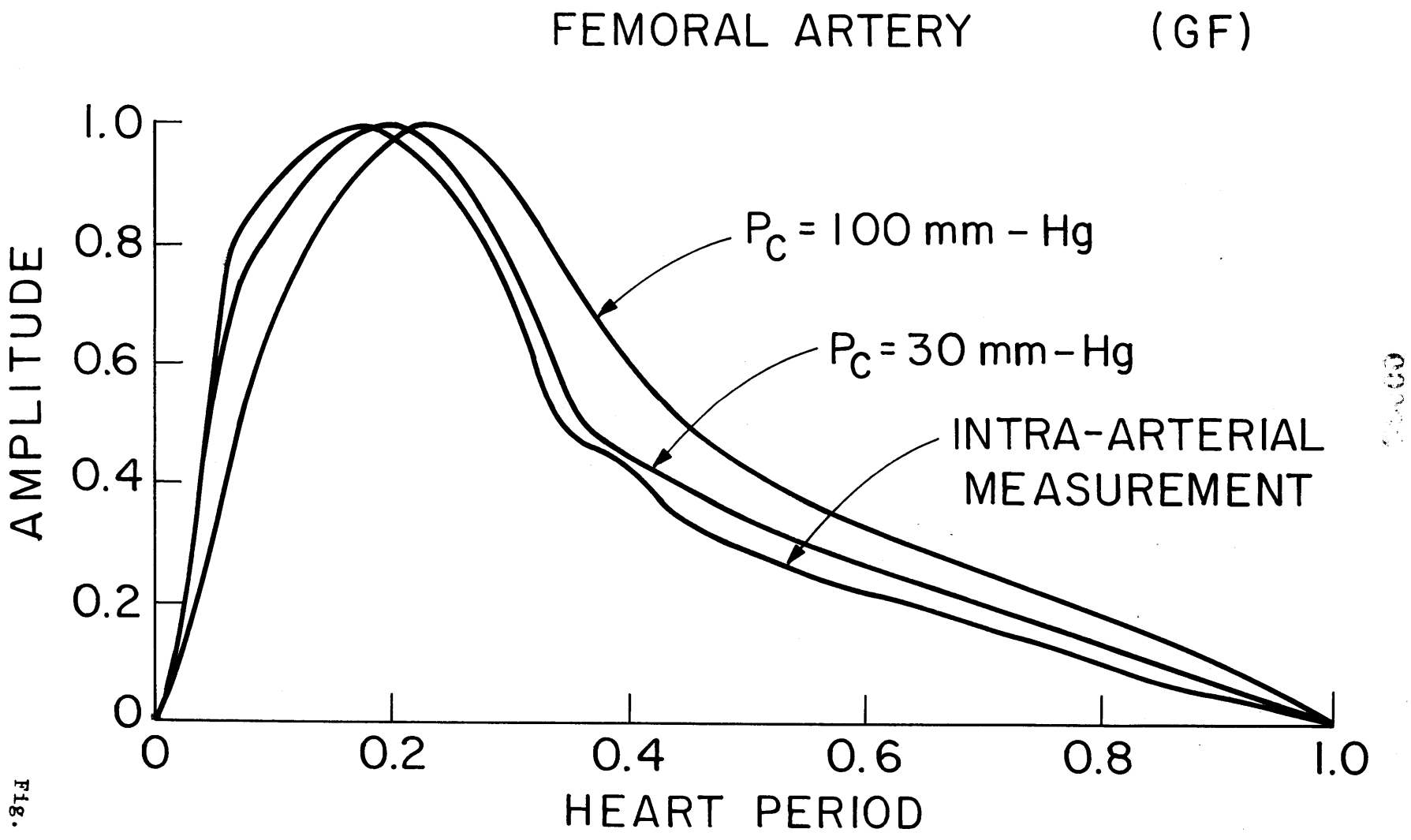

FEMORAL ARTERY (GF)
AMPLITUDE
1.0
0.8
0.6
0.4
0.2
0
0
0.2
0.4
0.6
0.8
1.0
HEART PERIOD
P_C = 100 mm - Hg
P_C = 30 mm - Hg
INTRA-ARTERIAL MEASUREMENT

Fig. 11b

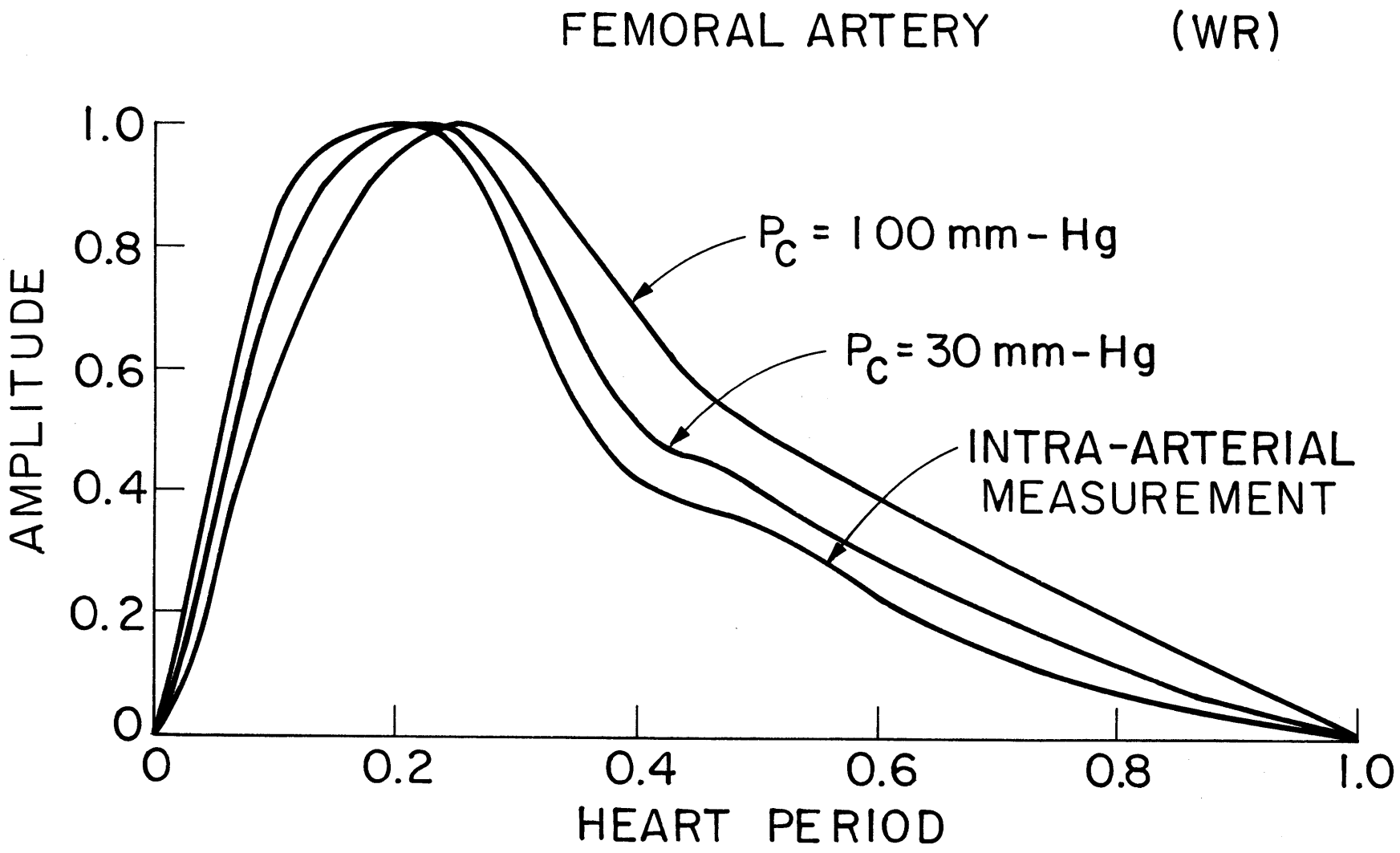

FEMORAL ARTERY (WR)
AMPLITUDE
1.0
0.8
0.6
0.4
0.2
0
0
0.2
0.4
0.6
0.8
1.0
HEART PERIOD
P_c = 100 mm-Hg
P_c = 30 mm-Hg
INTRA-ARTERIAL MEASUREMENT

Fig. 11c

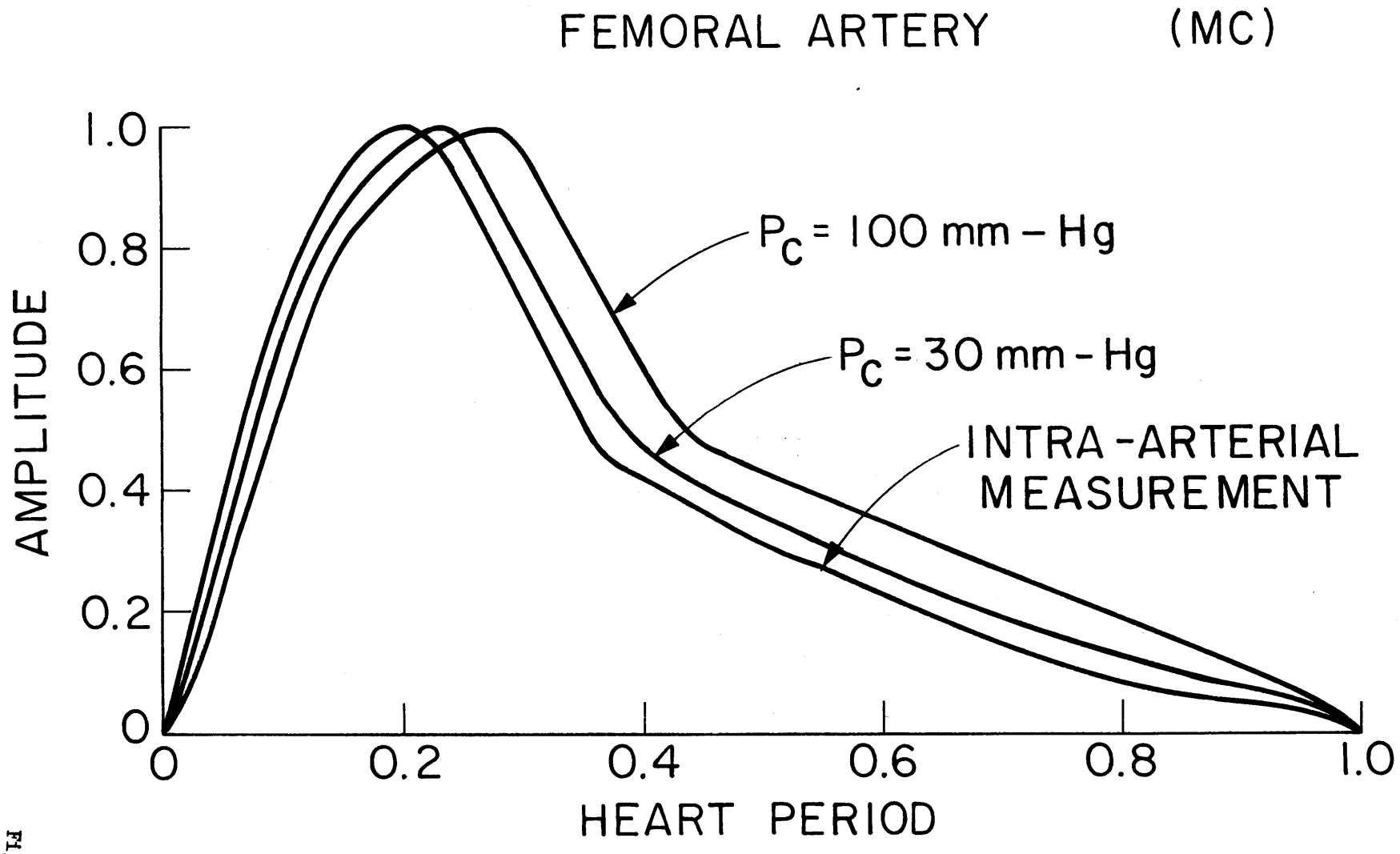

FEMORAL ARTERY (MC)
AMPLITUDE
1.0
0.8
0.6
0.4
0.2
0
0
0.2
0.4
0.6
0.8
1.0
HEART PERIOD
P_c = 100 mm - Hg
P_c = 30 mm - Hg
INTRA-ARTERIAL MEASUREMENT

Fig. 11d

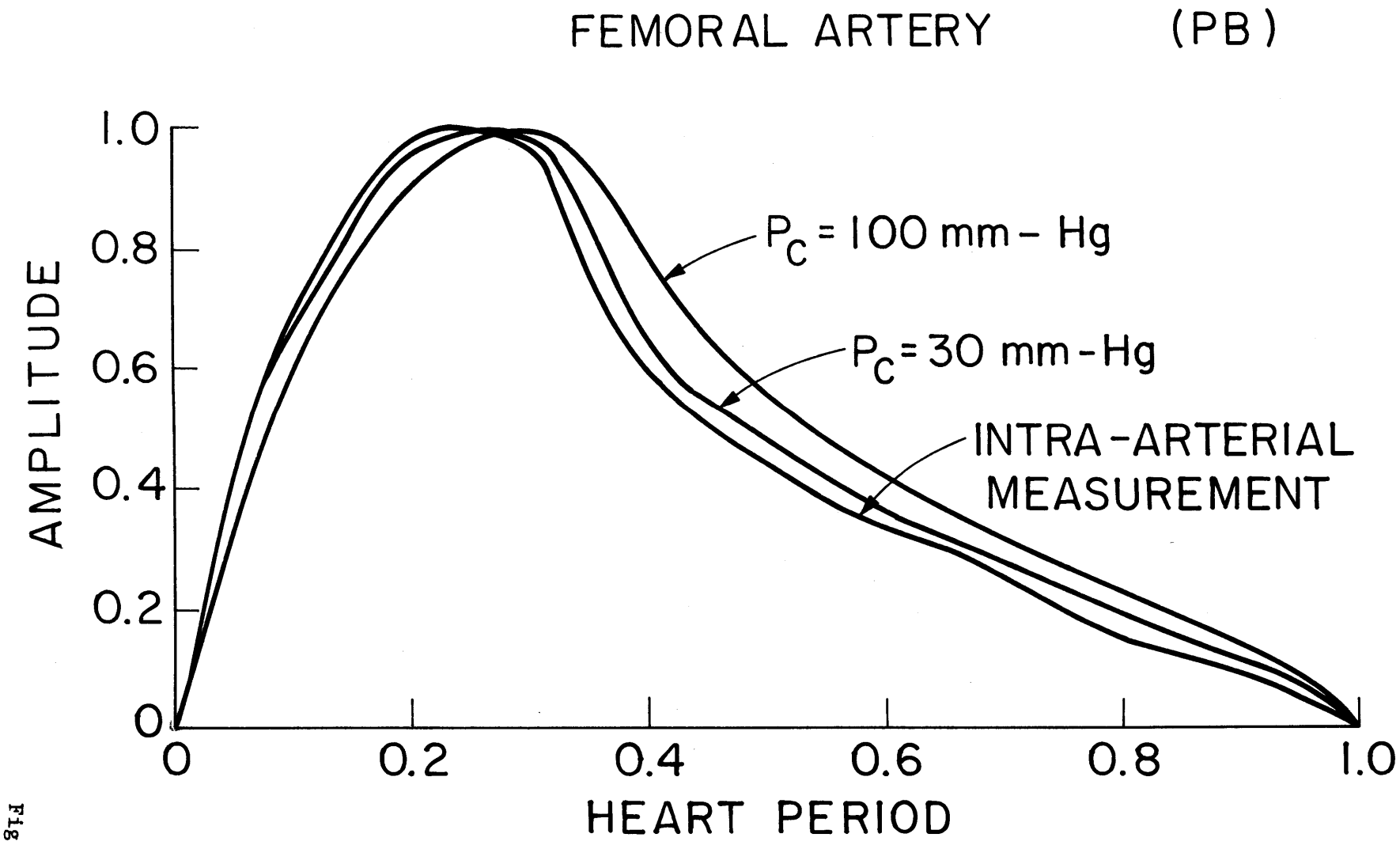

FEMORAL ARTERY (PB)
AMPLITUDE
1.0
0.8
0.6
0.4
0.2
0
0
0.2
0.4
0.6
0.8
1.0
HEART PERIOD
P_C = 100 mm - Hg
P_C = 30 mm - Hg
INTRA-ARTERIAL MEASUREMENT

Fig. 11e

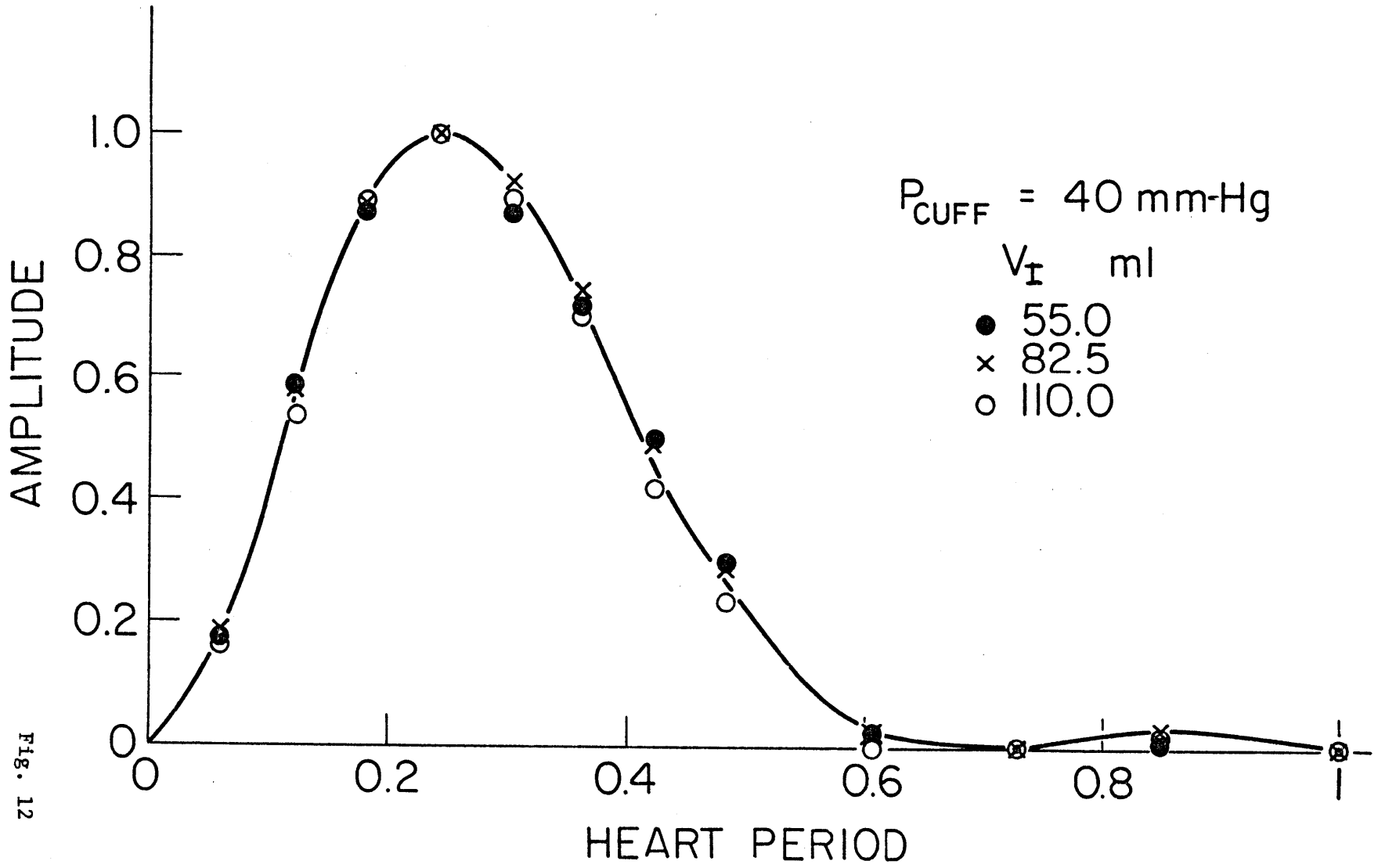

AMPLITUDE
1.0
0.8
0.6
0.4
0.2
0
0
0.2
0.4
0.6
0.8
1
HEART PERIOD
P_{CUFF} = 40 mm-Hg
V_I ml
55.0
82.5
110.0

Fig. 12

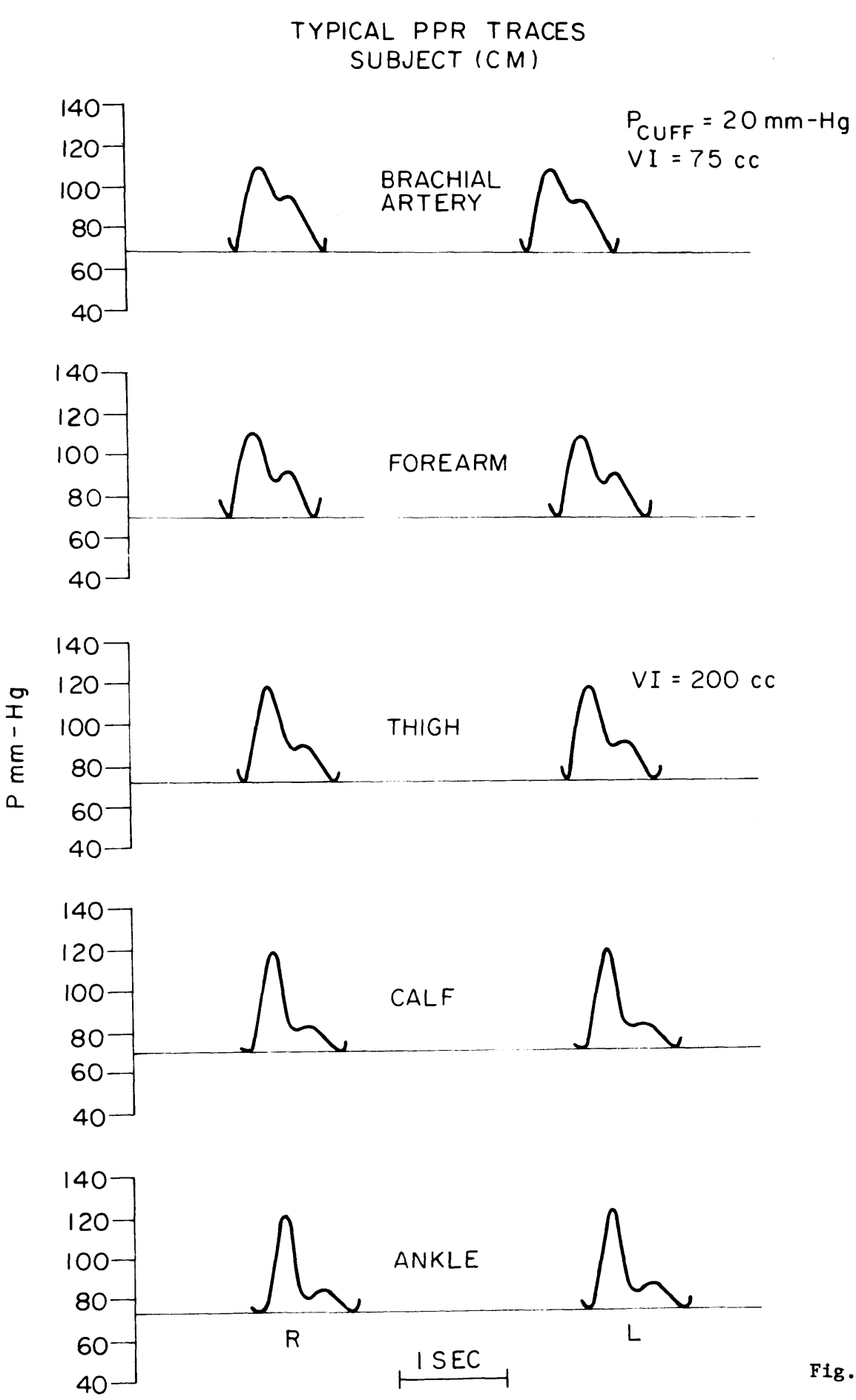
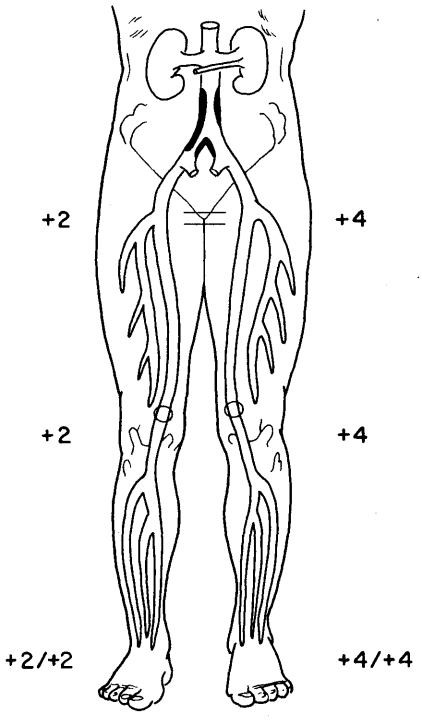

TYPICAL PPR TRACES
SUBJECT (CM)
P_{CUFF} = 20 mm-Hg
VI = 75 cc
BRACHIAL ARTERY
FOREARM
VI = 200 cc
THIGH
CALF
ANKLE
P mm-Hg
140
120
100
80
60
40
R
L
1 SEC

Fig. 13

PRE-OPERATIVE DATA PATIENT YW

ANGIOGRAPHIC FINDINGS



PRESSURE PULSE RECORDINGS

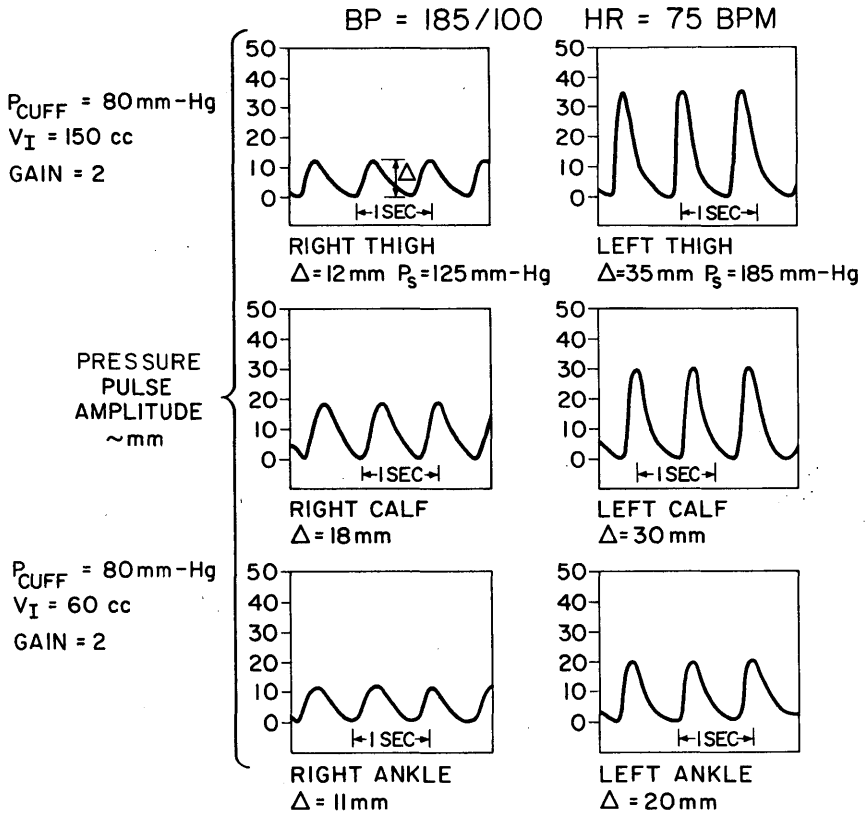


Fig. 14

PRE-OPERATIVE DATA PATIENT YW

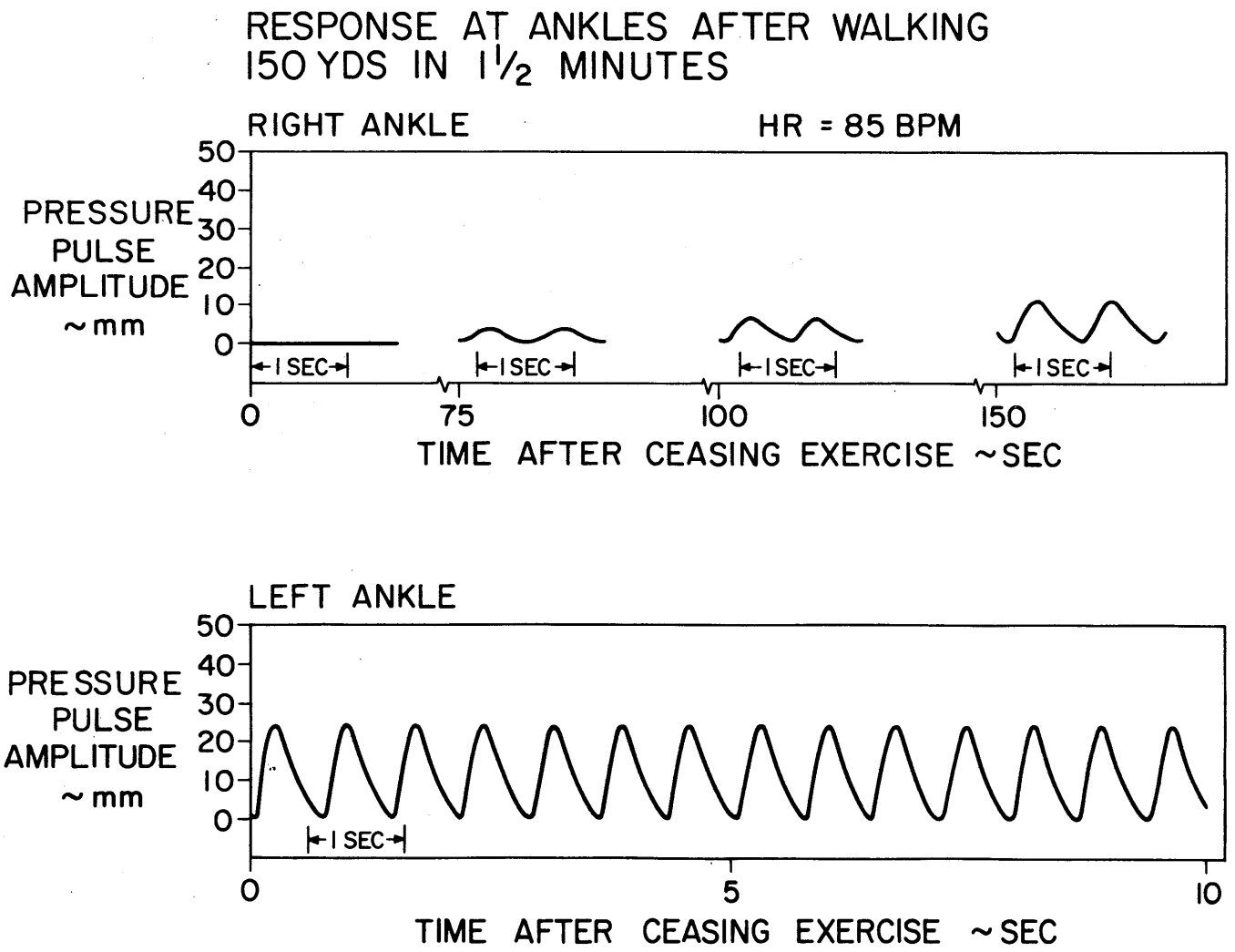
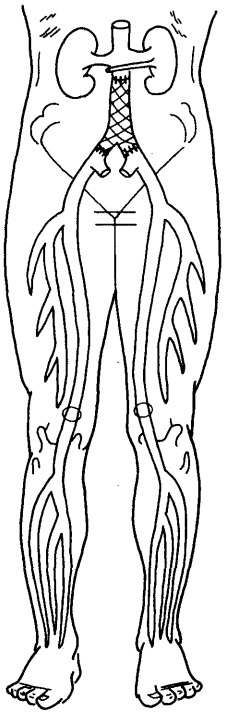


Fig. 15

POST-OPERATIVE DATA PATIENT YW

ANGIOGRAPHIC FINDINGS



PRESSURE PULSE RECORDINGS

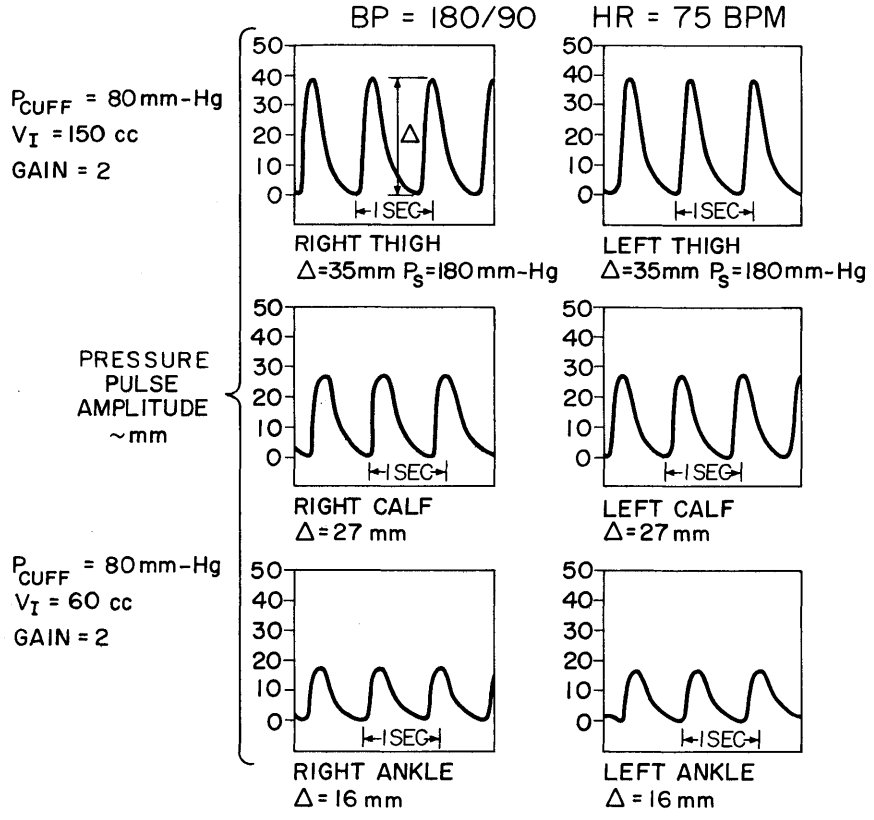


Fig. 16

POST OPERATIVE DATA PATIENT YW

RESPONSE AT ANKLES AFTER WALKING 150 YDS IN 2 MIN.

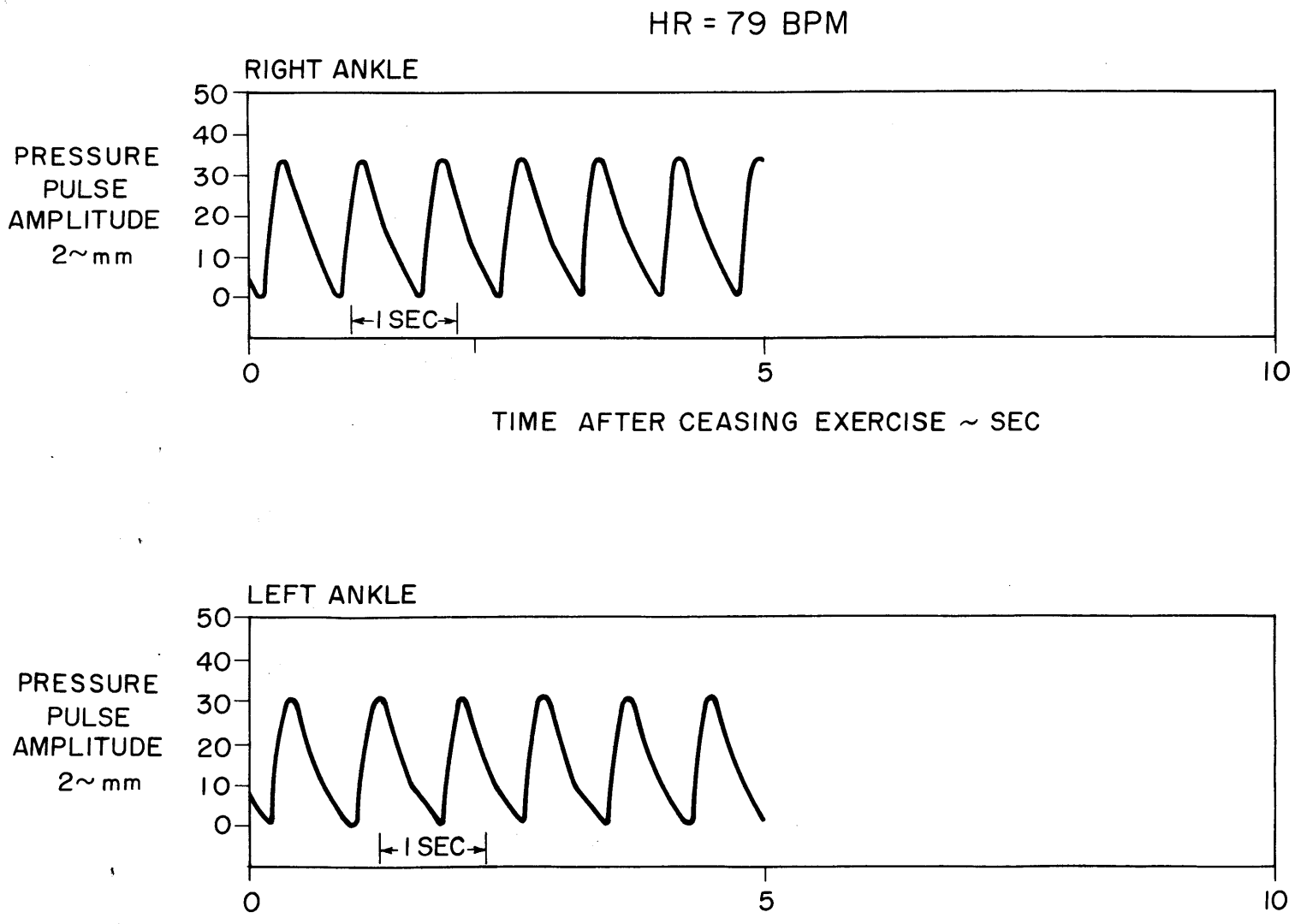
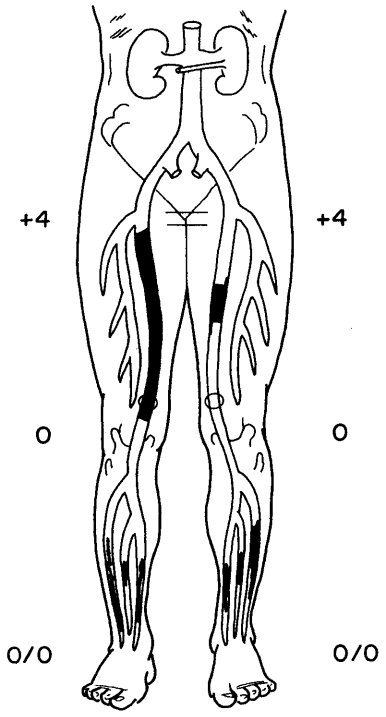


Fig. 17

PRE-OPERATIVE DATA PATIENT KM

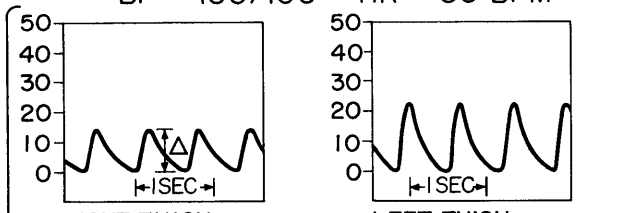
ANGIOGRAPHIC FINDINGS



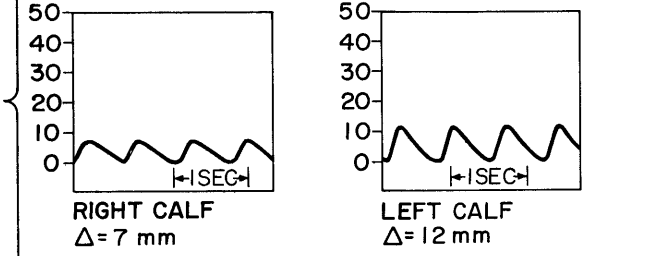
PRESSURE PULSE RECORDINGS

BP = 160/100 HR = 86 BPM

P_{CUFF} = 80mm-Hg
V_I = 400 cc
GAIN = 2



PRESSURE PULSE AMPLITUDE ~mm



P_{CUFF} = 80mm-Hg
V_I = 70 cc
GAIN = 2

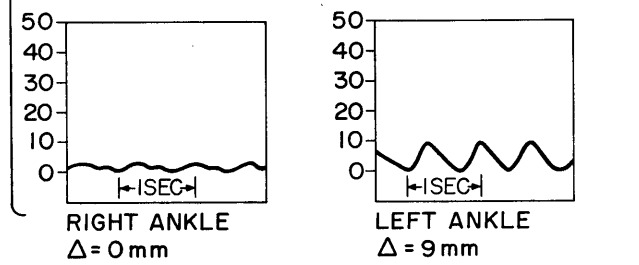
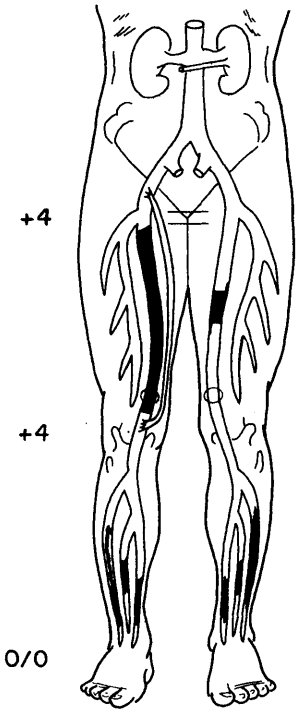


Fig. 18

POST-OPERATIVE DATA PATIENT KM

ANGIOGRAPHIC FINDINGS



PRESSURE PULSE RECORDINGS

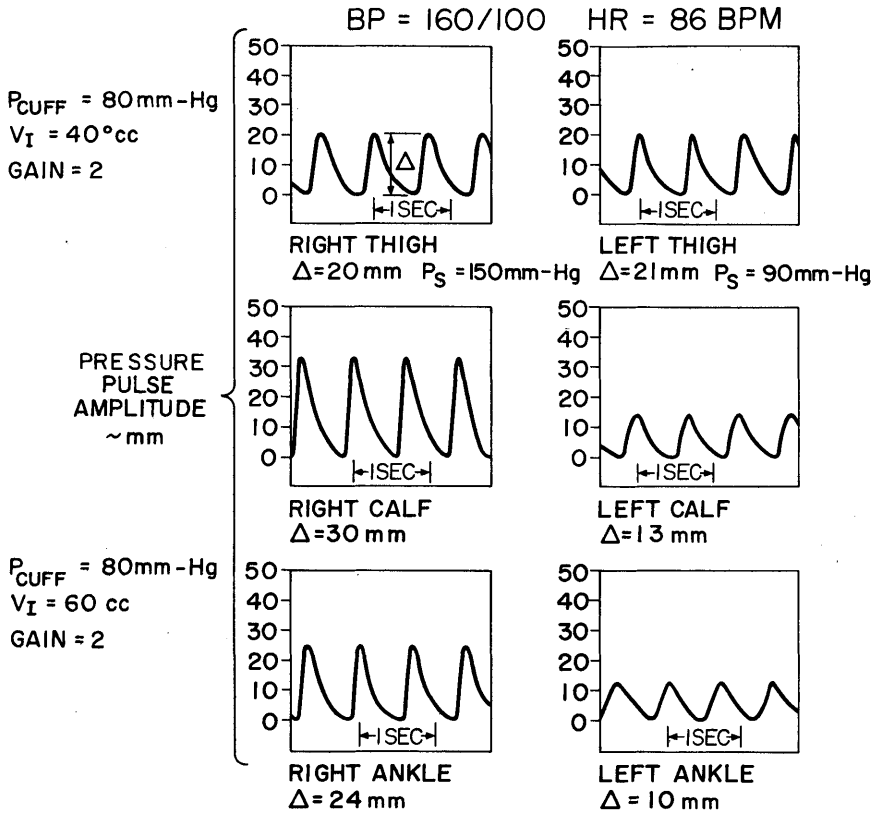


Fig. 19

POST OPERATIVE DATA PATIENT KM

RESPONSE AT ANKLES AFTER WALKING 100 YDS IN 2½ MIN.

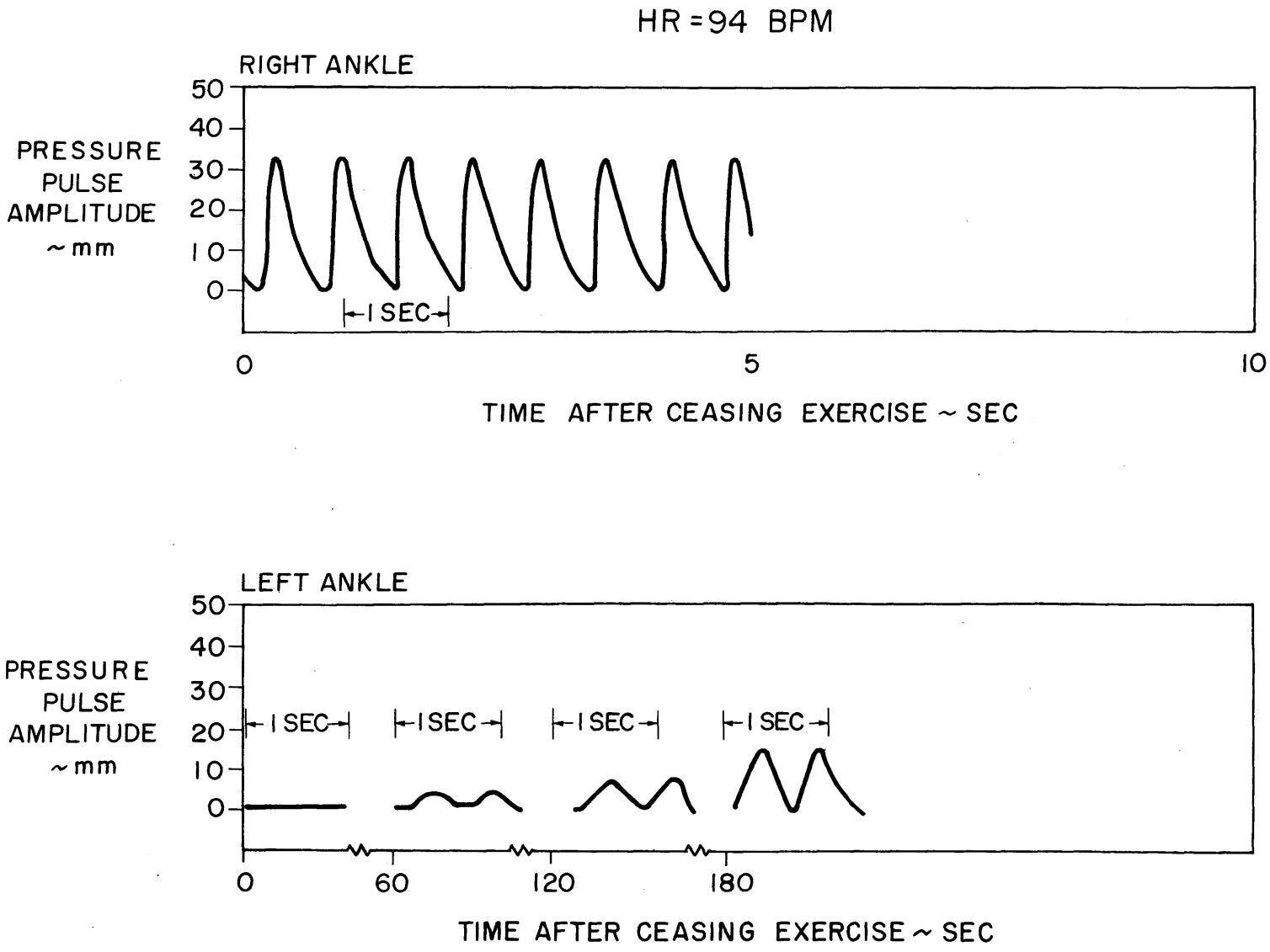
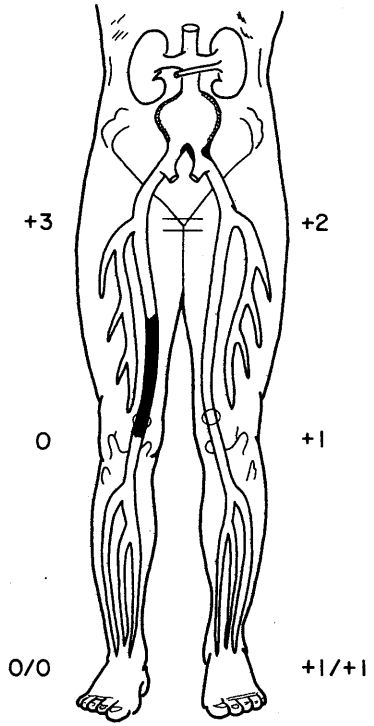


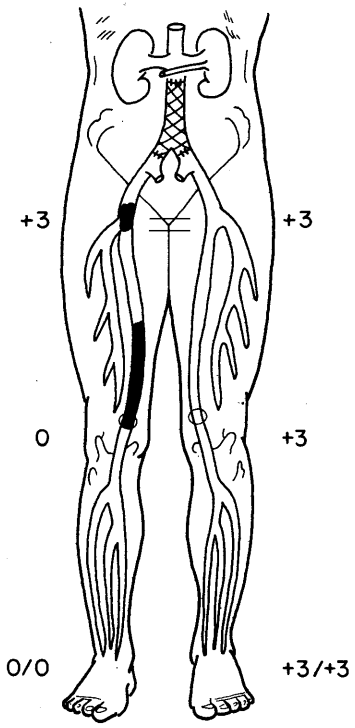
Fig. 20

INTRA-OPERATIVE MONITORING PATIENT TB

PRE-OPERATIVE FINDINGS



CONDITION AT RIGHT ILIAC OPENING



PRESSURE PULSE RECORDINGS

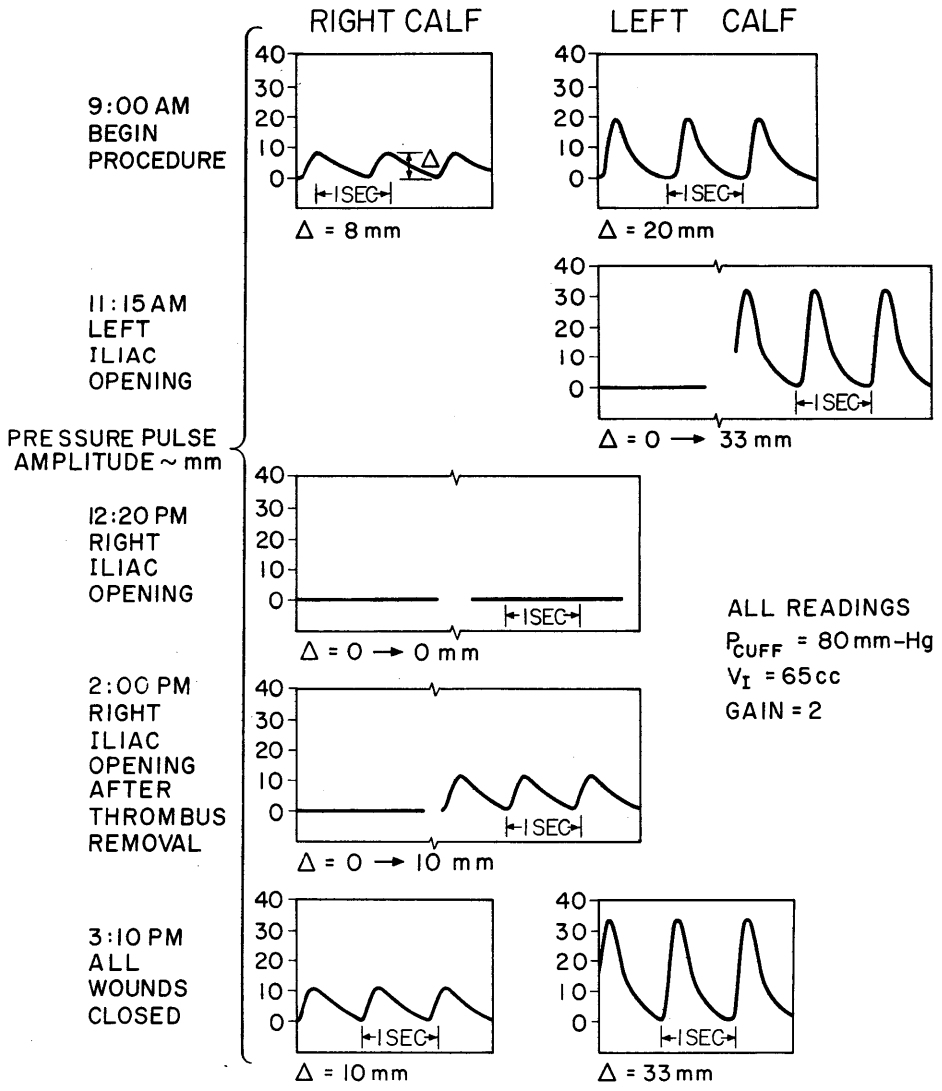


Fig. 21

PATIENT (RS)

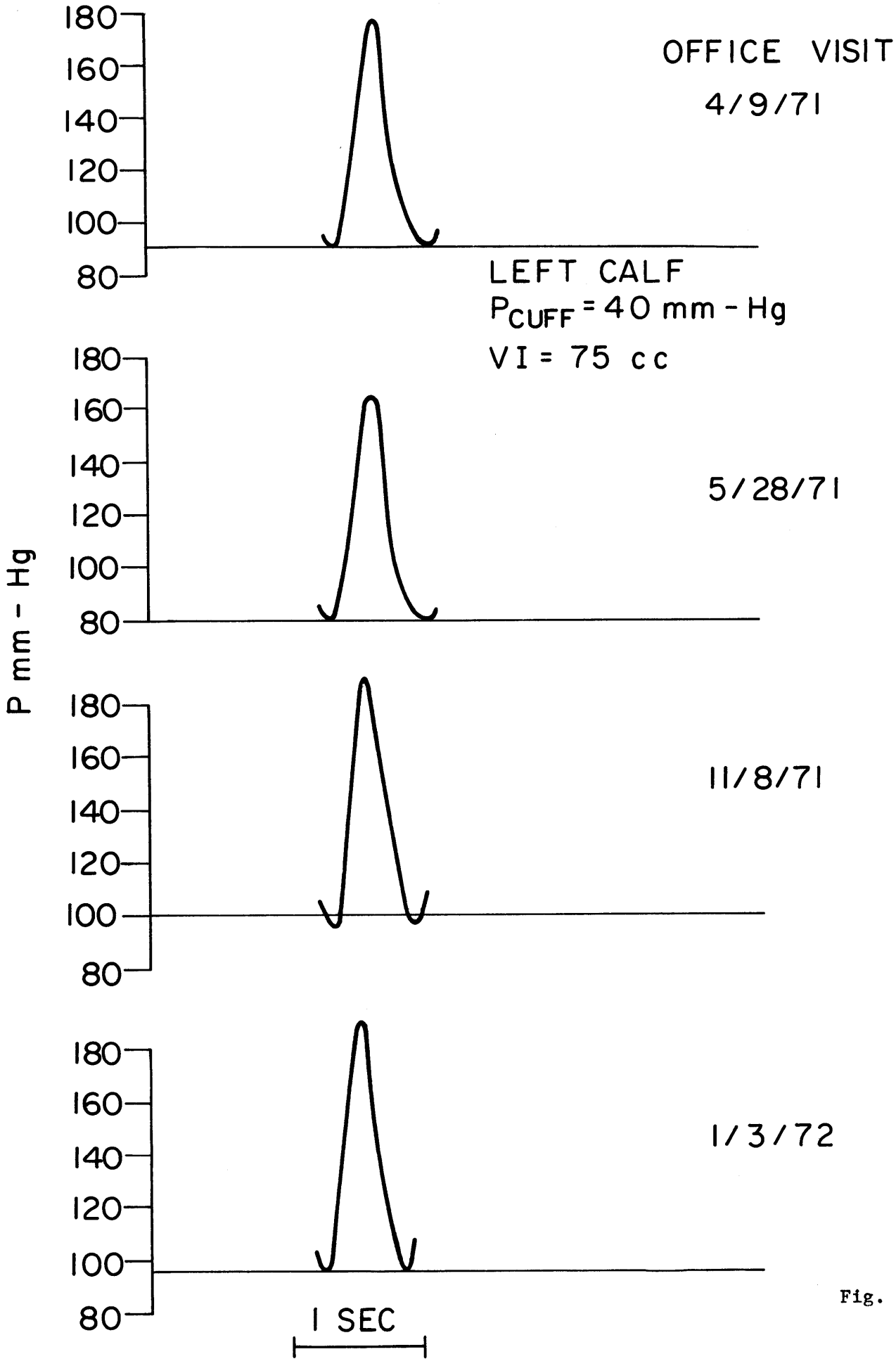


Fig. 22

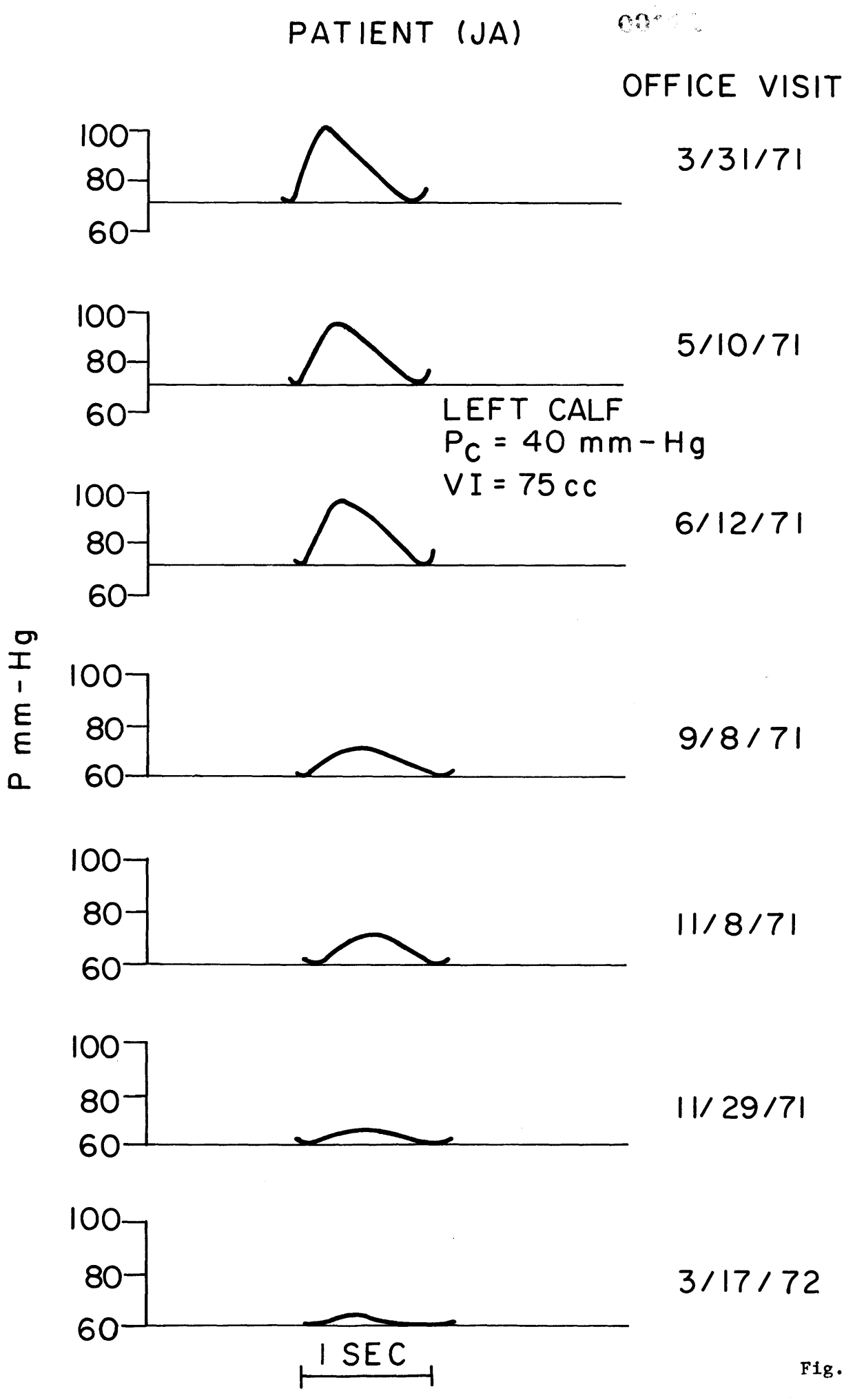

PATIENT (JA)
OFFICE VISIT
100
80
60
3/31/71
100
80
60
5/10/71
LEFT CALF
P_C = 40 mm-Hg
VI = 75 cc
100
80
60
6/12/71
P mm-Hg
100
80
60
9/8/71
100
80
60
11/8/71
100
80
60
11/29/71
100
80
60
3/17/72
1 SEC

Fig. 23

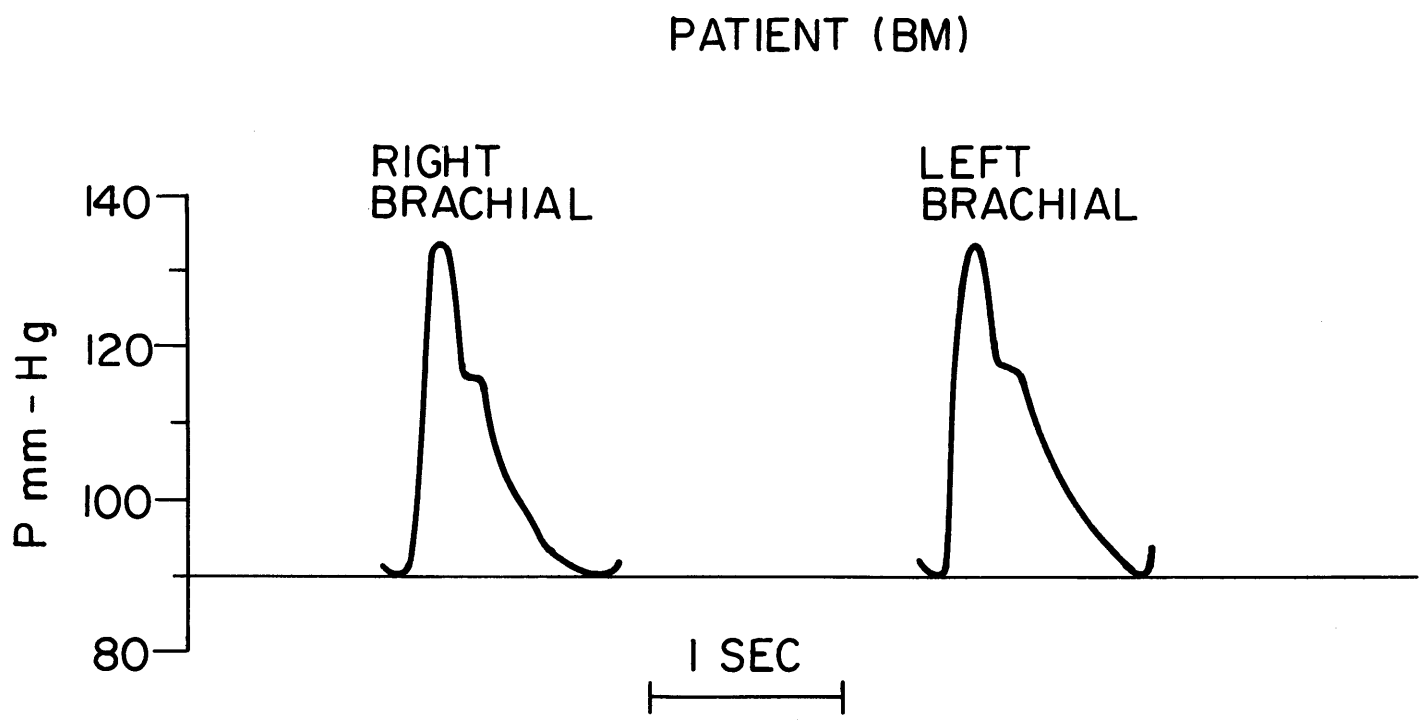

PATIENT (BM)
RIGHT BRACHIAL
LEFT BRACHIAL
140
120
100
80
P mm-Hg
1 SEC
P_{CUFF} = mm-Hg
V I = 60 cc

Fig. 24

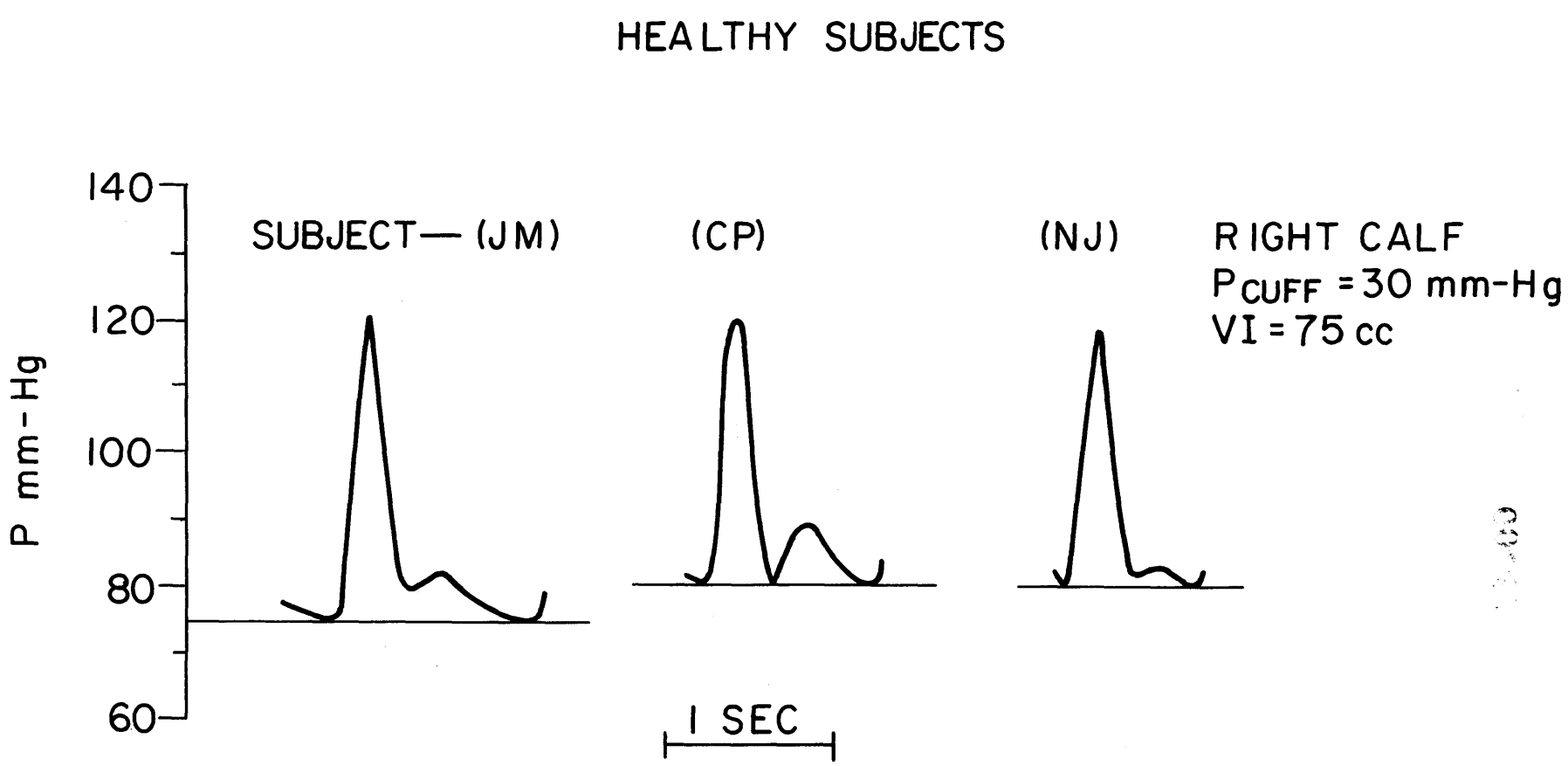

HEALTHY SUBJECTS
140
120
100
80
60
P mm-Hg
SUBJECT— (JM)
(CP)
(NJ)
RIGHT CALF
P_{CUFF} = 30 mm-Hg
VI = 75 cc
1 SEC

Fig. 25

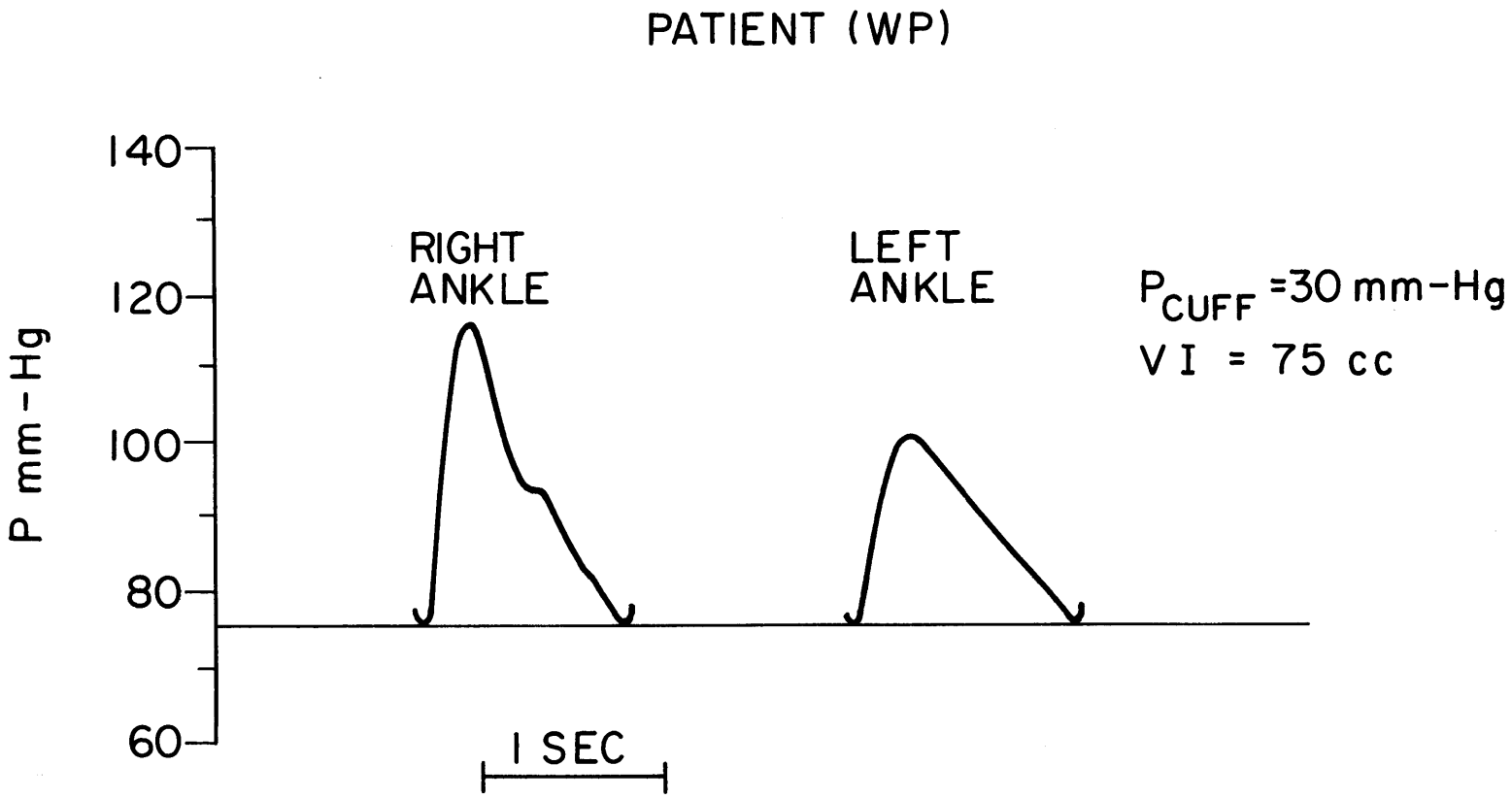

PATIENT (WP)
140
120
100
80
60
P mm-Hg
RIGHT ANKLE
LEFT ANKLE
P_{CUFF} =30 mm-Hg
V I = 75 cc
1 SEC

Fig. 26

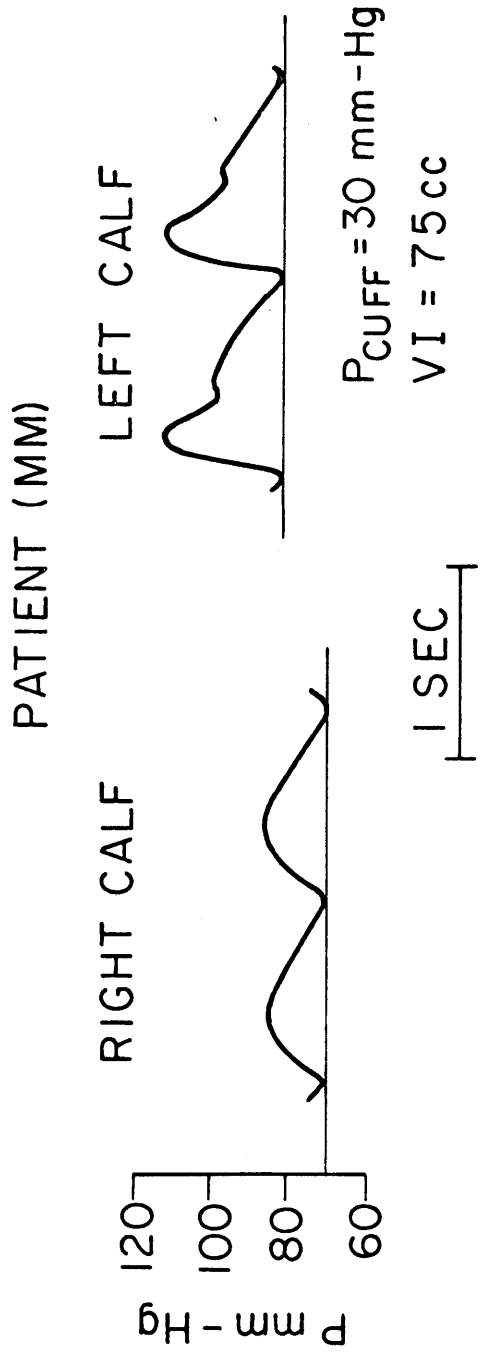

PATIENT (MM)
LEFT CALF
RIGHT CALF
P_{CUFF}=30 mm-Hg
VI = 75cc
1 SEC
P mm-Hg
120
100
80
60

Fig. 27

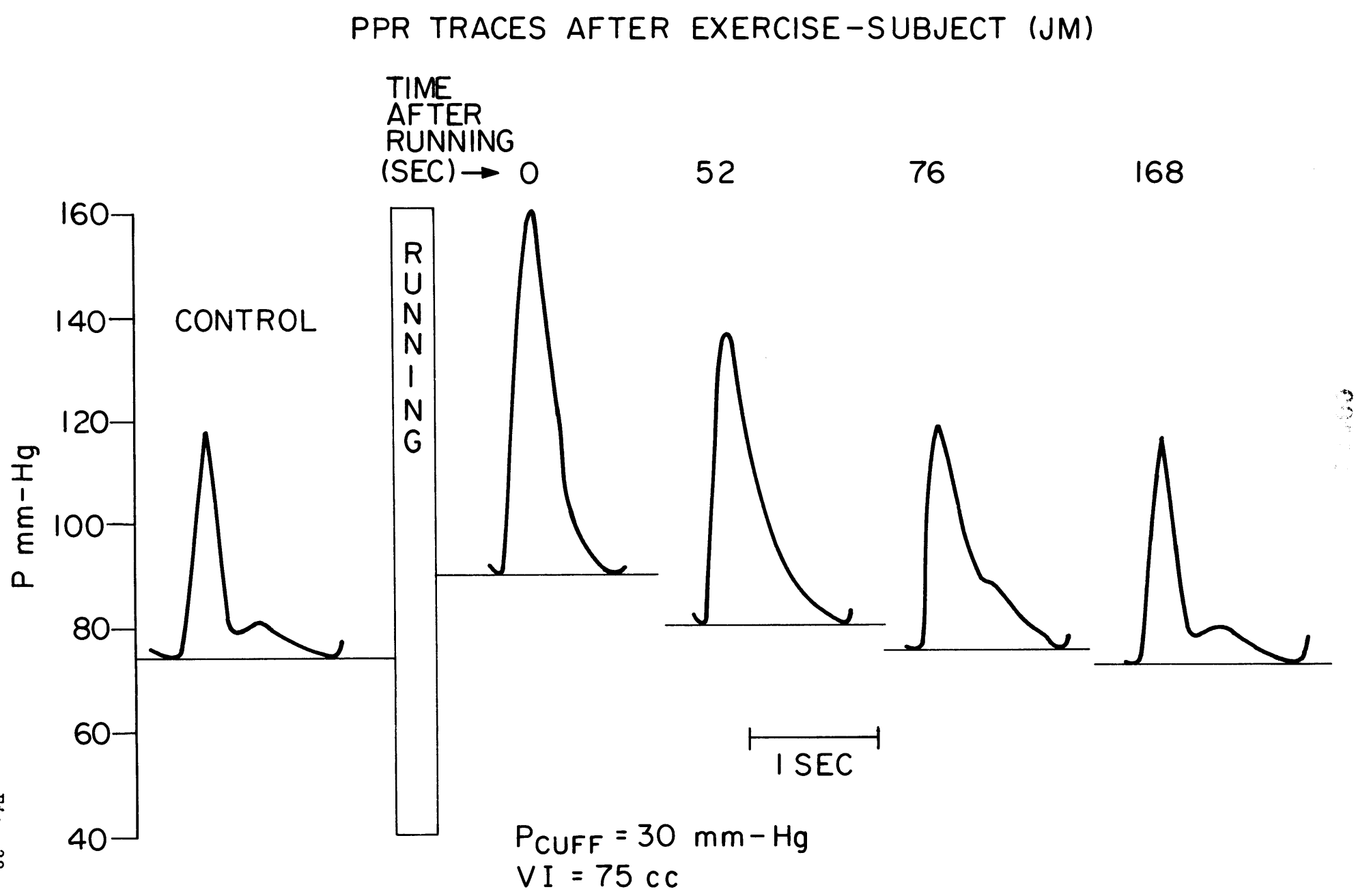
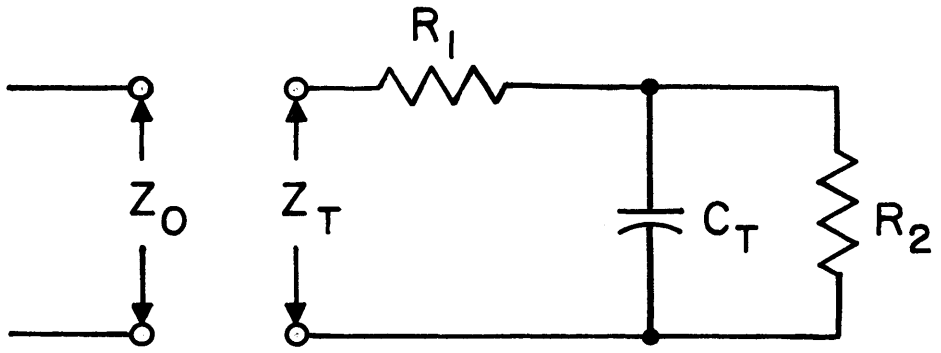

PPR TRACES AFTER EXERCISE-SUBJECT (JM)
TIME AFTER RUNNING (SEC) →
0
52
76
168
160
140
120
100
80
60
40
P mm-Hg
CONTROL
RUNNING
1 SEC
PCUFF = 30 mm-Hg
VI = 75 cc

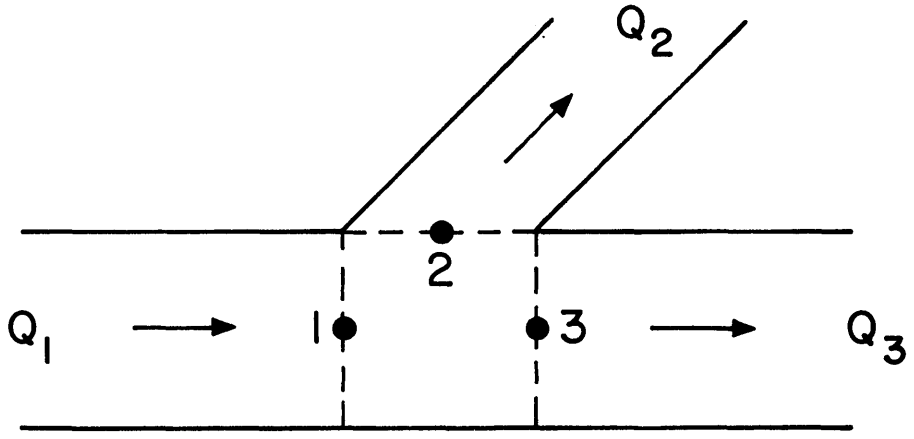
Fig. 28



(a)

$$R_T = R_1 + R_2$$

ELECTRIC ANALOG OF THE DISTAL BOUNDARY CONDITION



(b)

SCHEMATIC OF A BIFURCATION

Fig. 29

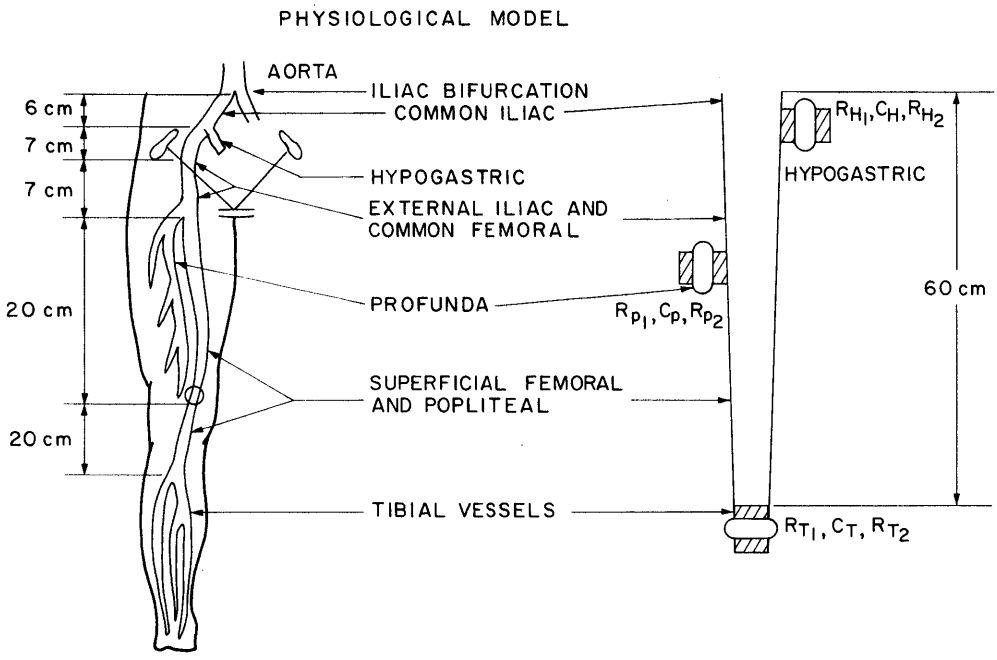

PHYSIOLOGICAL MODEL
AORTA
ILIAC BIFURCATION
COMMON ILIAC
HYPOGASTRIC
EXTERNAL ILIAC AND
COMMON FEMORAL
PROFUNDA
SUPERFICIAL FEMORAL
AND POPLITEAL
TIBIAL VESSELS
6 cm
7 cm
7 cm
20 cm
20 cm
R_{H_1}, C_H, R_{H_2}
HYPOGASTRIC
60 cm
R_{p_1}, C_p, R_{p_2}
R_{T_1}, C_T, R_{T_2}

Fig. 30

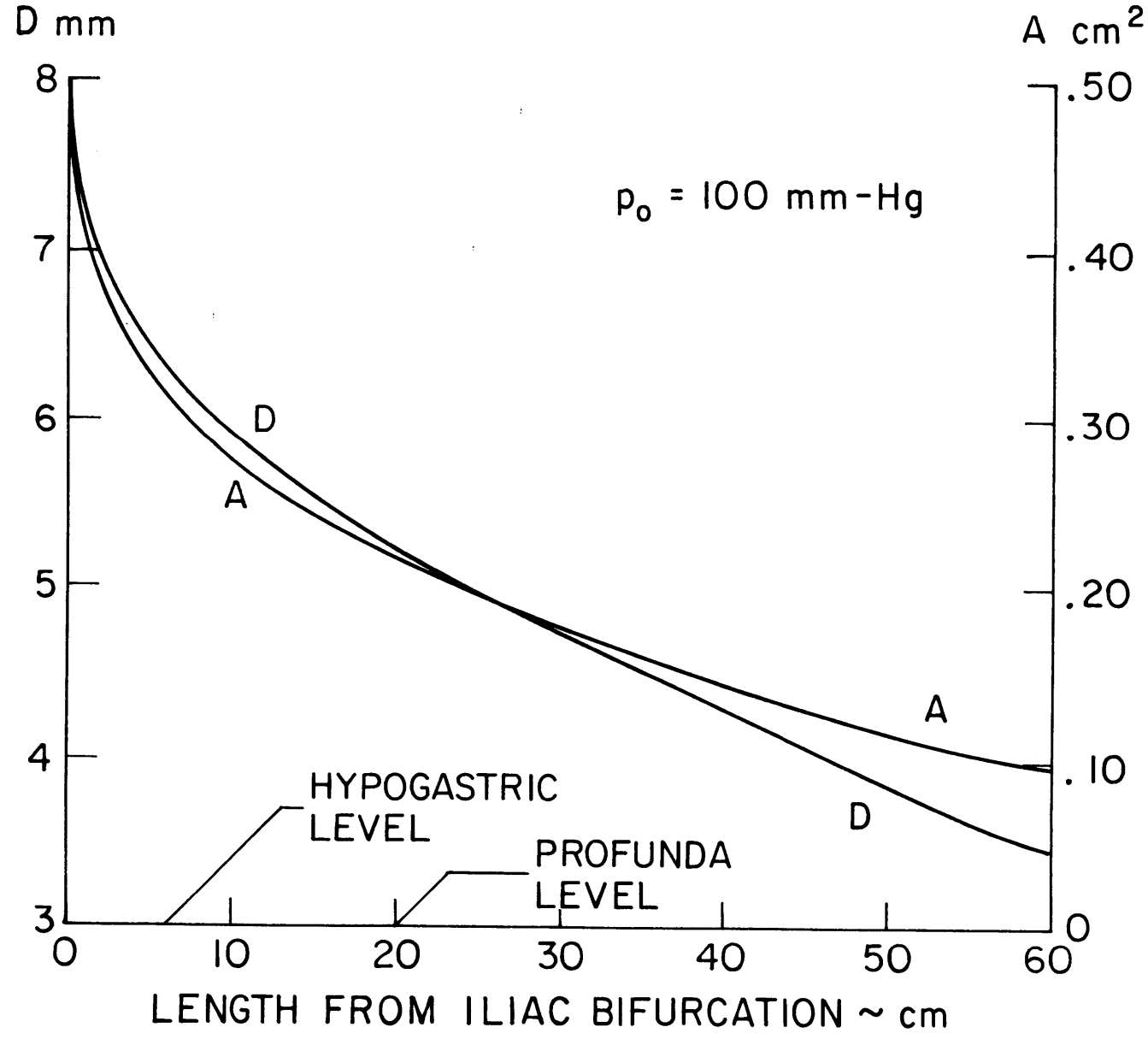

D mm
A cm²
8
7
6
5
4
3
.50
.40
.30
.20
.10
0
p_o = 100 mm-Hg
D
A
A
D
HYPOGASTRIC LEVEL
PROFUNDA LEVEL
0
10
20
30
40
50
60
LENGTH FROM ILIAC BIFURCATION ~ cm

Fig. 31

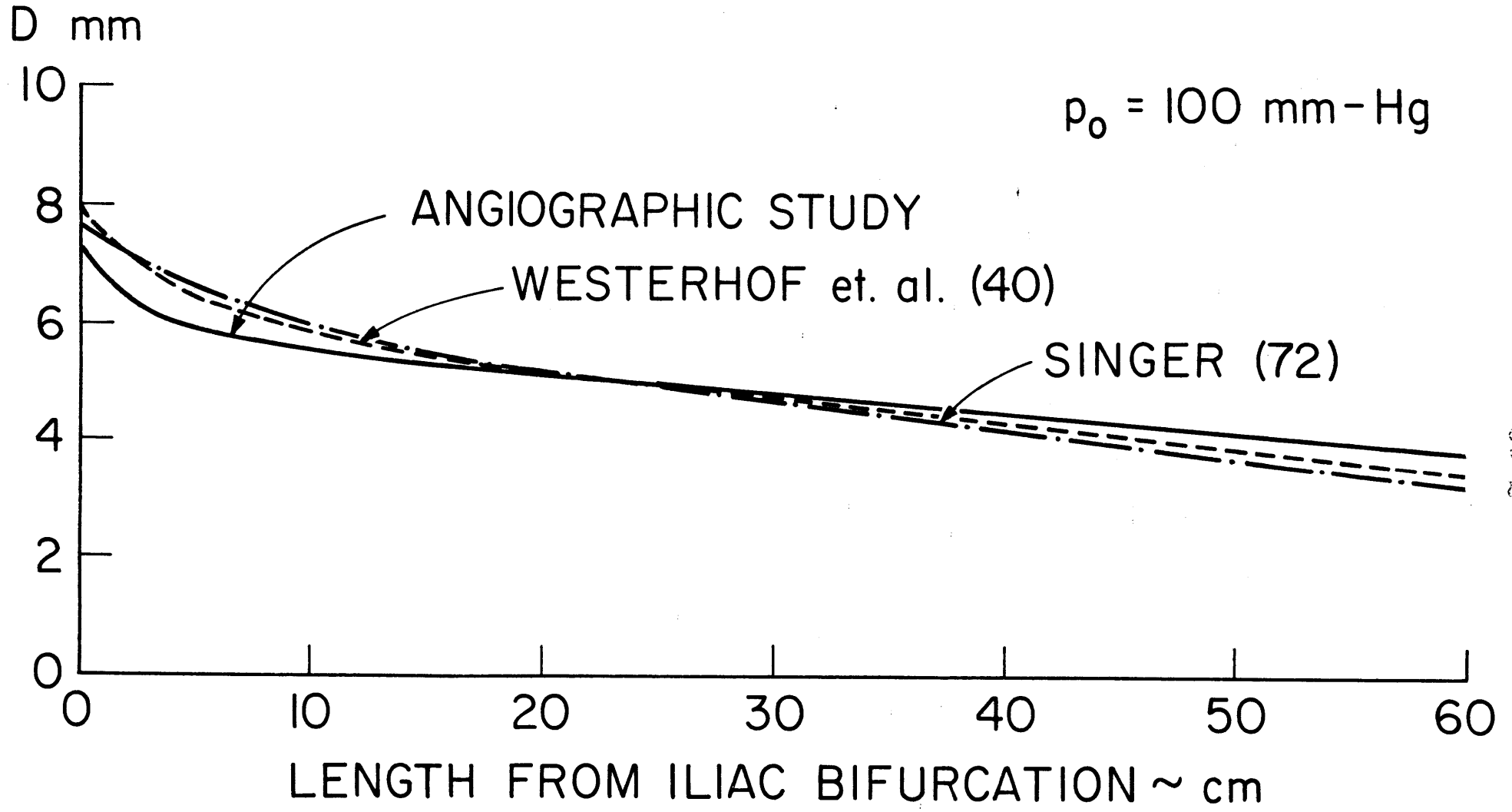

D mm
10
8
6
4
2
0
p_o = 100 mm-Hg
ANGIOGRAPHIC STUDY
WESTERHOF et. al. (40)
SINGER (72)
0
10
20
30
40
50
60
LENGTH FROM ILIAC BIFURCATION ~ cm

Fig. 32

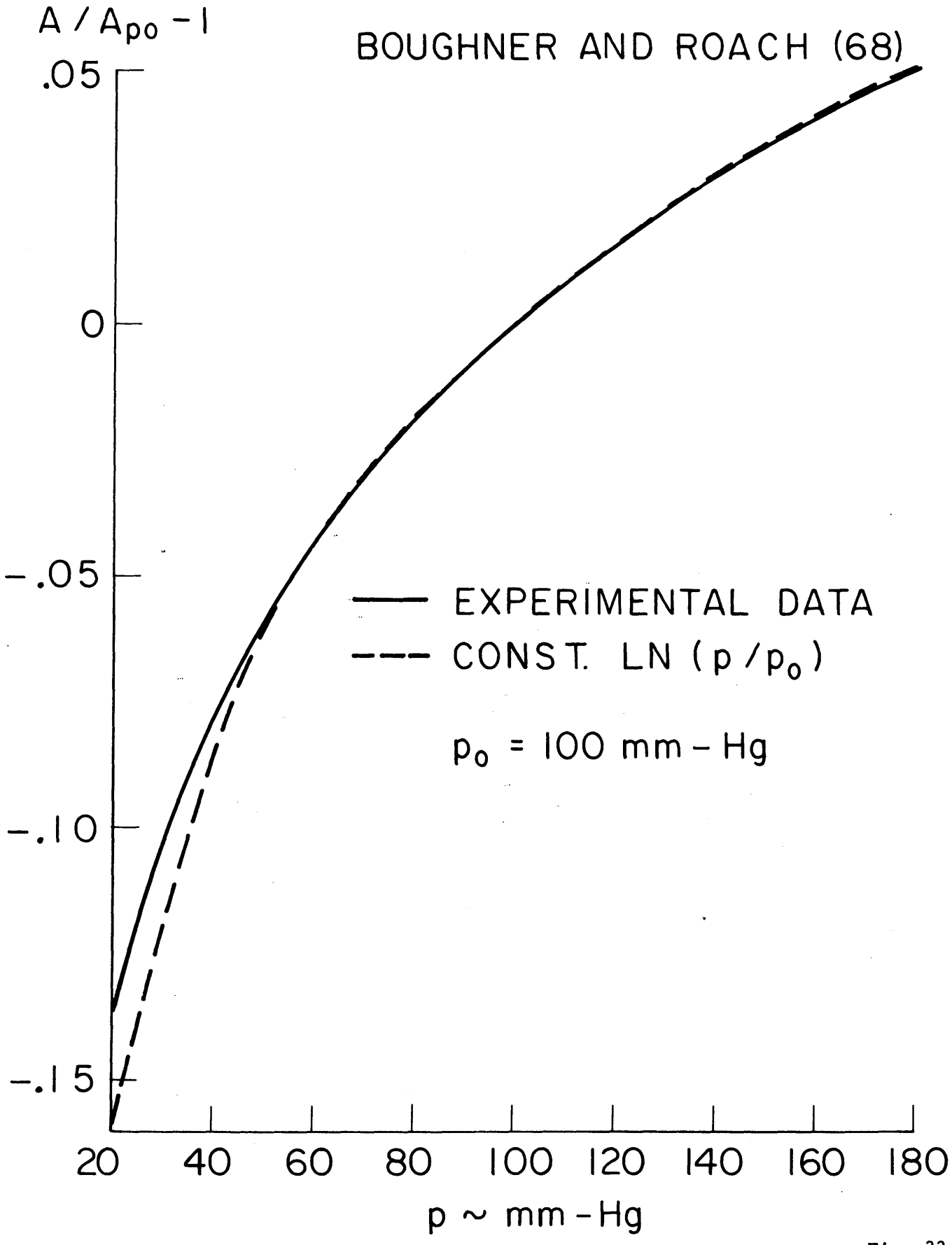

A / Apo - 1
BOUGHNER AND ROACH (68)
.05
0
-.05
-.10
-.15
EXPERIMENTAL DATA
CONST. LN (p / p0)
p0 = 100 mm - Hg
20
40
60
80
100
120
140
160
180
p ~ mm - Hg

Fig. 33

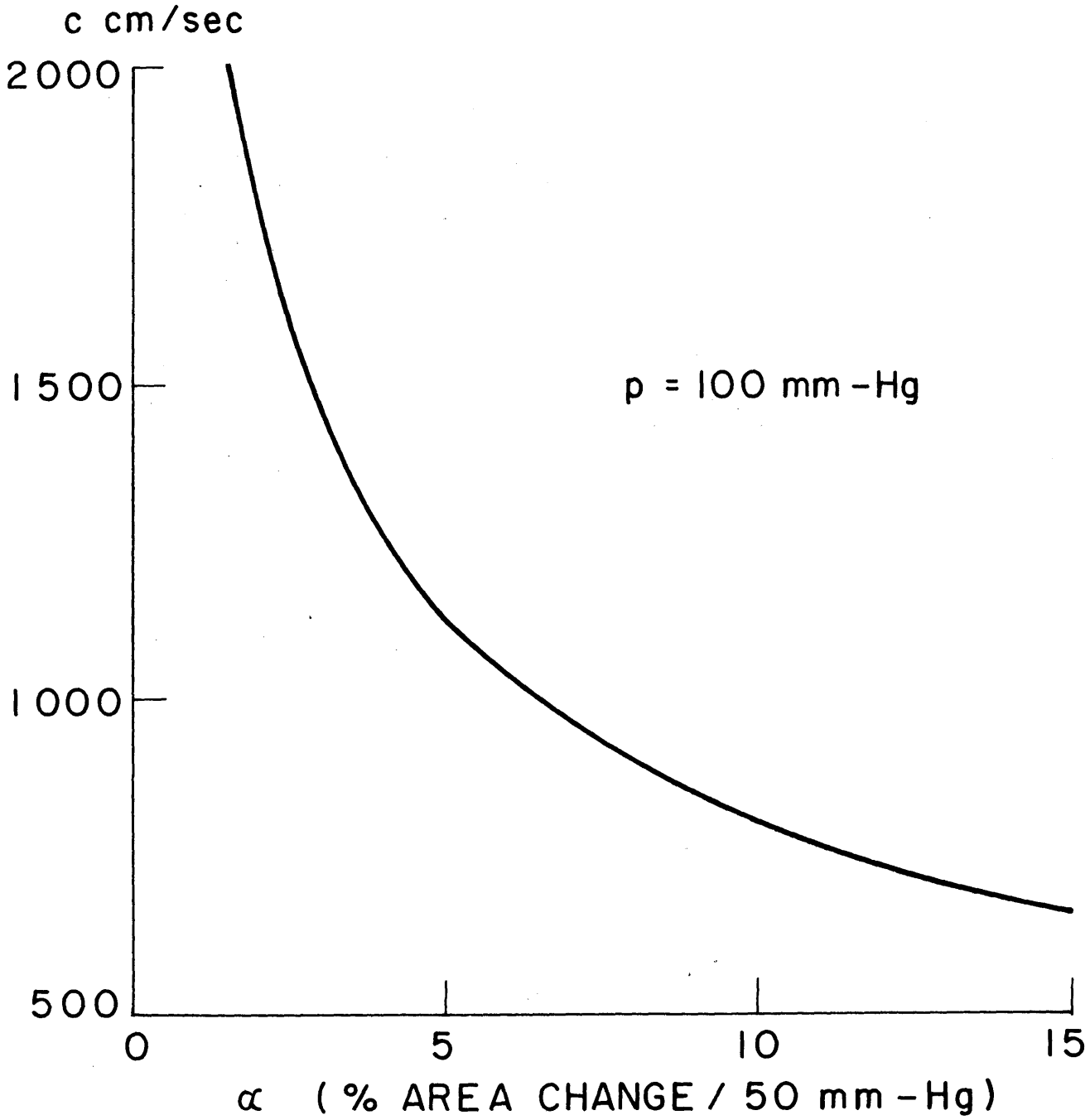

c cm/sec
2000
1500
1000
500
p = 100 mm-Hg
0
5
10
15
α (% AREA CHANGE / 50 mm-Hg)

Fig. 34

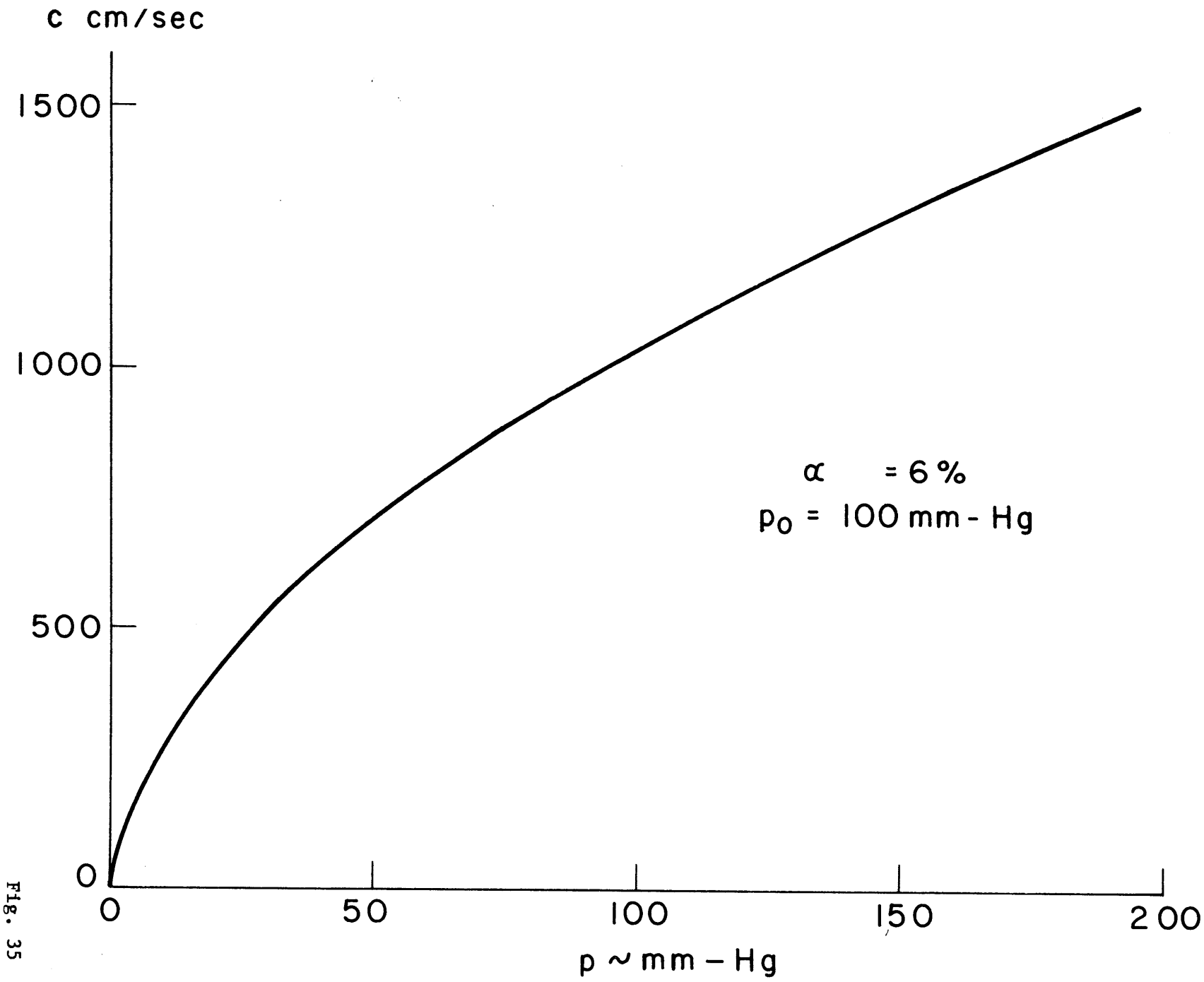


Fig. 35

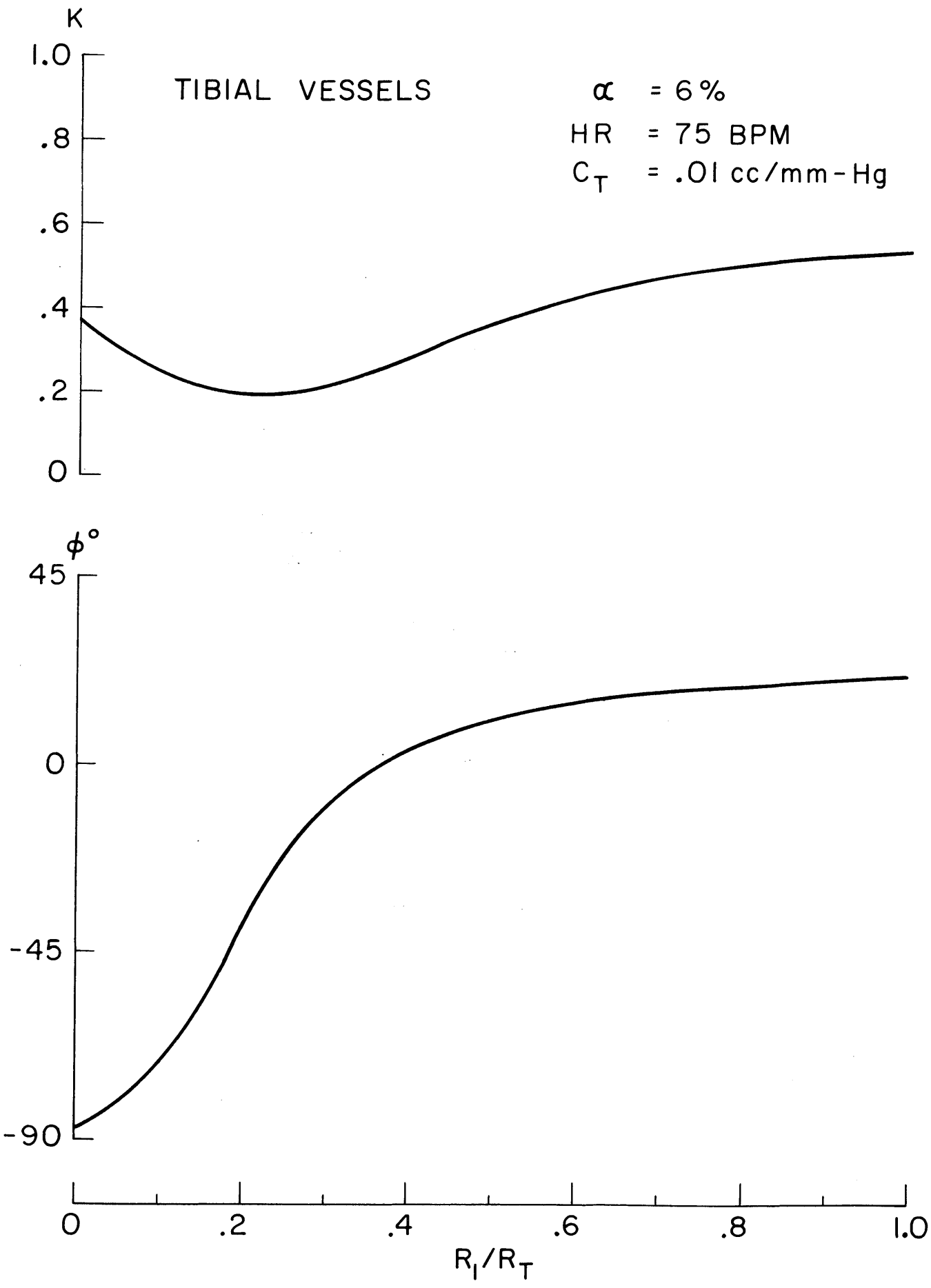

K
1.0
.8
.6
.4
.2
0
TIBIAL VESSELS
α = 6%
HR = 75 BPM
C_T = .01 cc/mm-Hg
φ°
45
0
-45
-90
0
.2
.4
.6
.8
1.0
R_I/R_T

Fig. 36

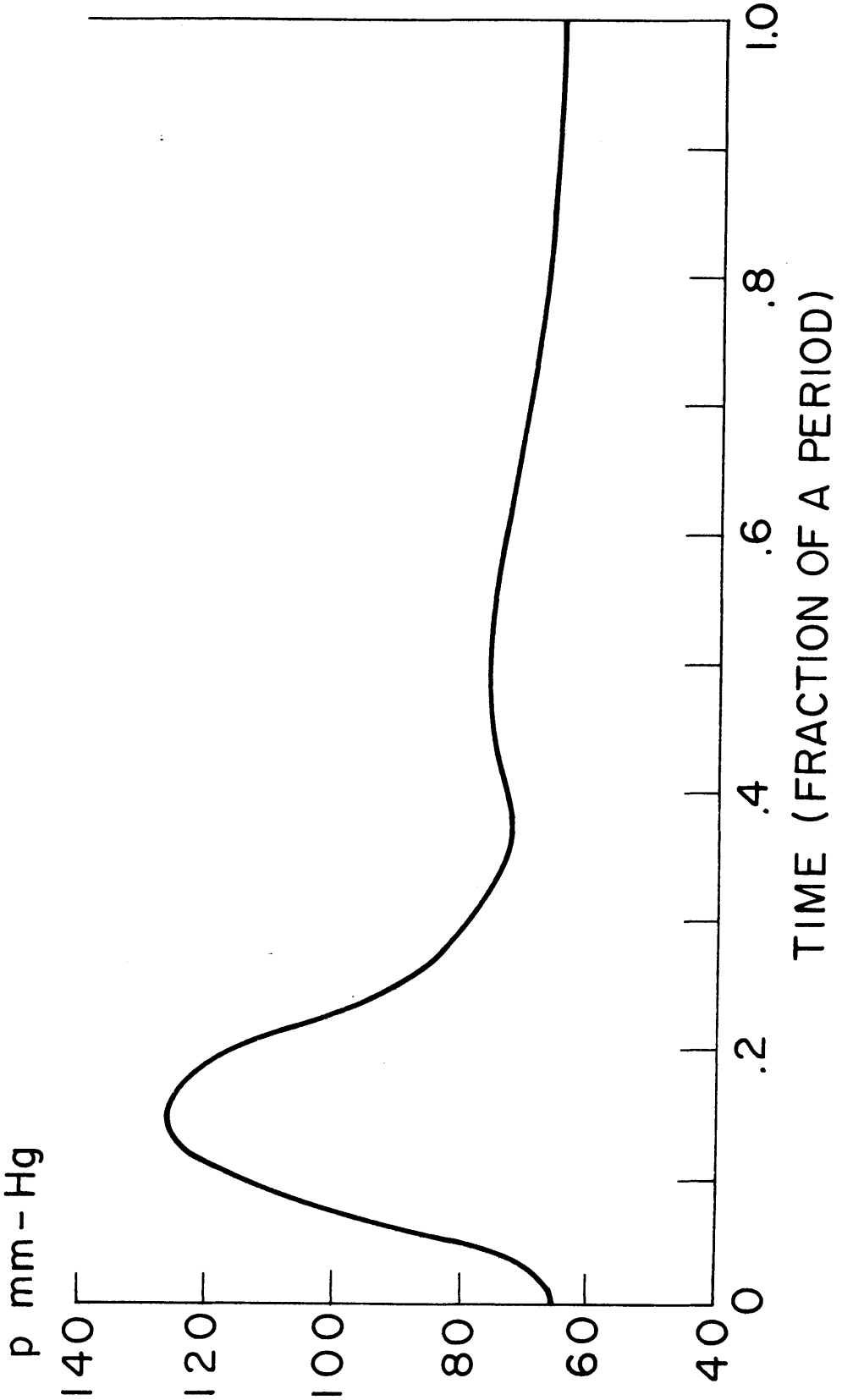
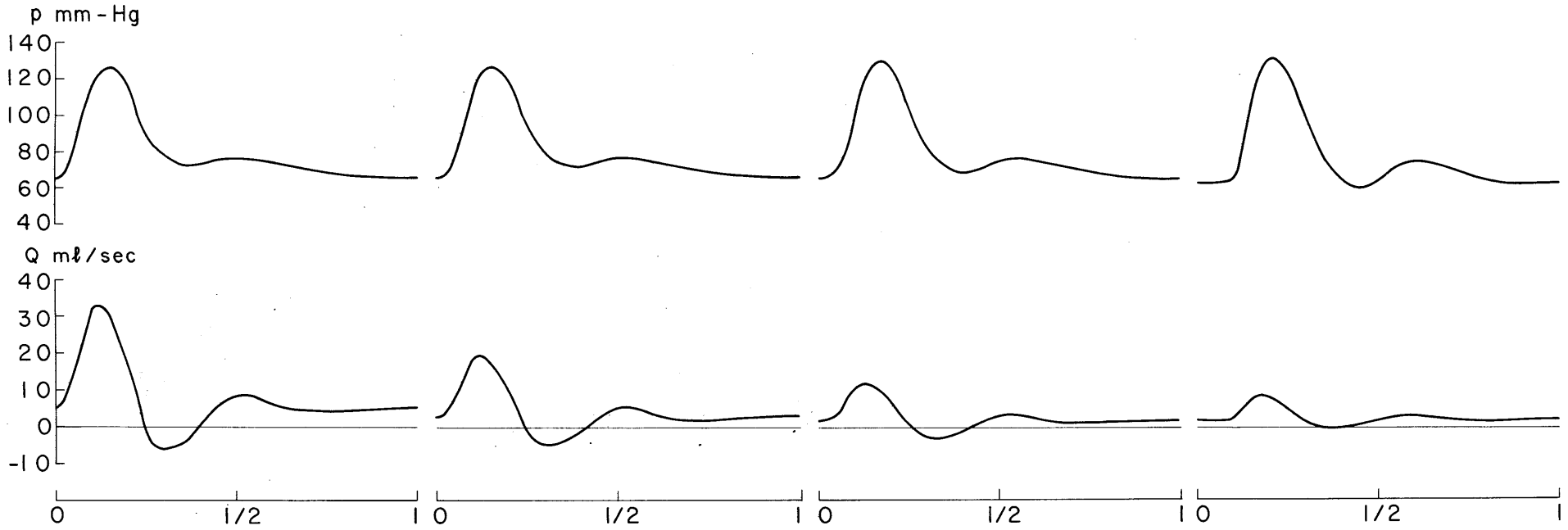


Fig. 37



* LENGTH FROM ILIAC BIFURCATION

Fig. 38

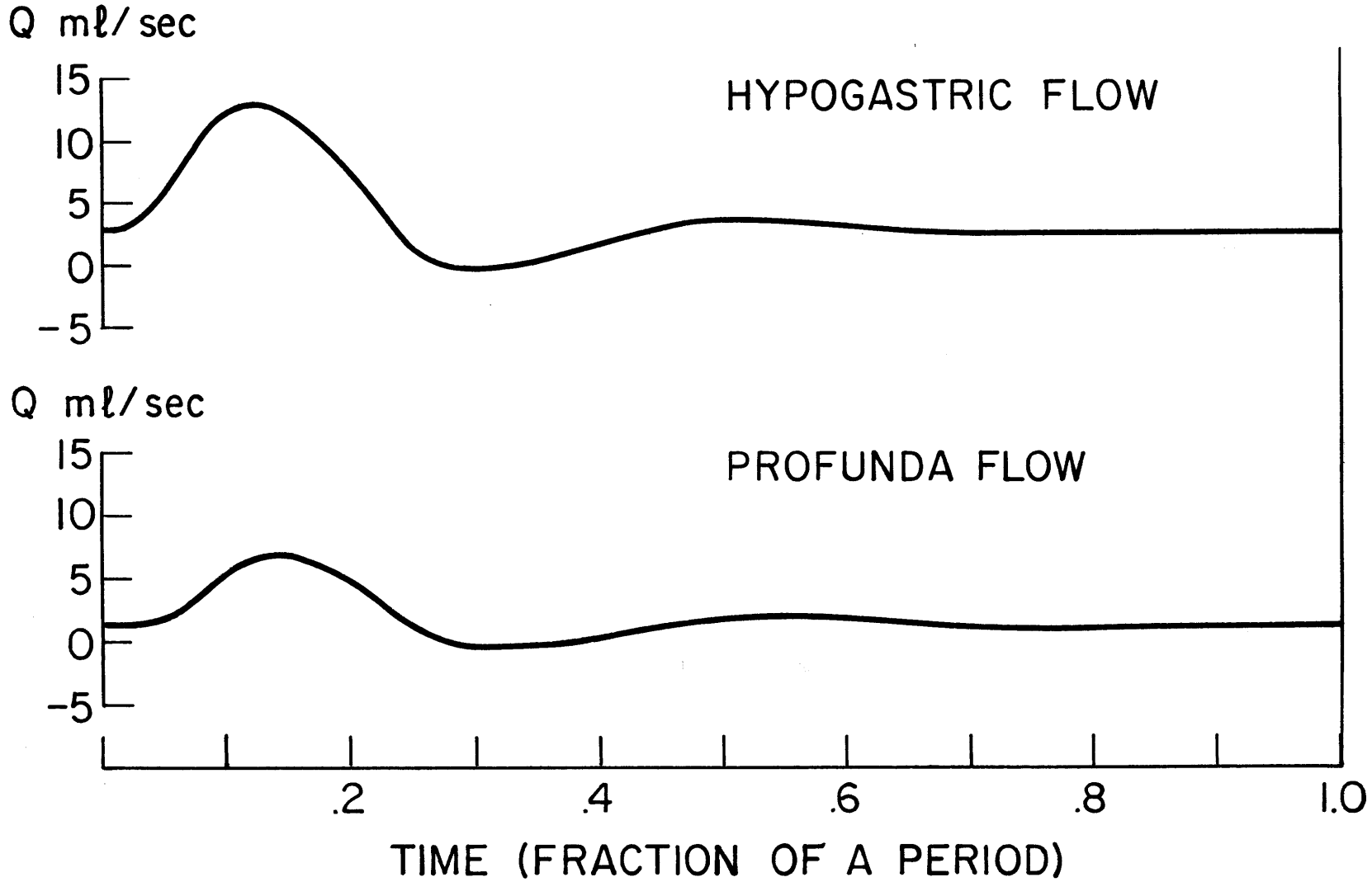

Q mℓ/sec
15
10
5
0
-5
HYPOGASTRIC FLOW
Q mℓ/sec
15
10
5
0
-5
PROFUNDA FLOW
.2
.4
.6
.8
1.0
TIME (FRACTION OF A PERIOD)

Fig. 39

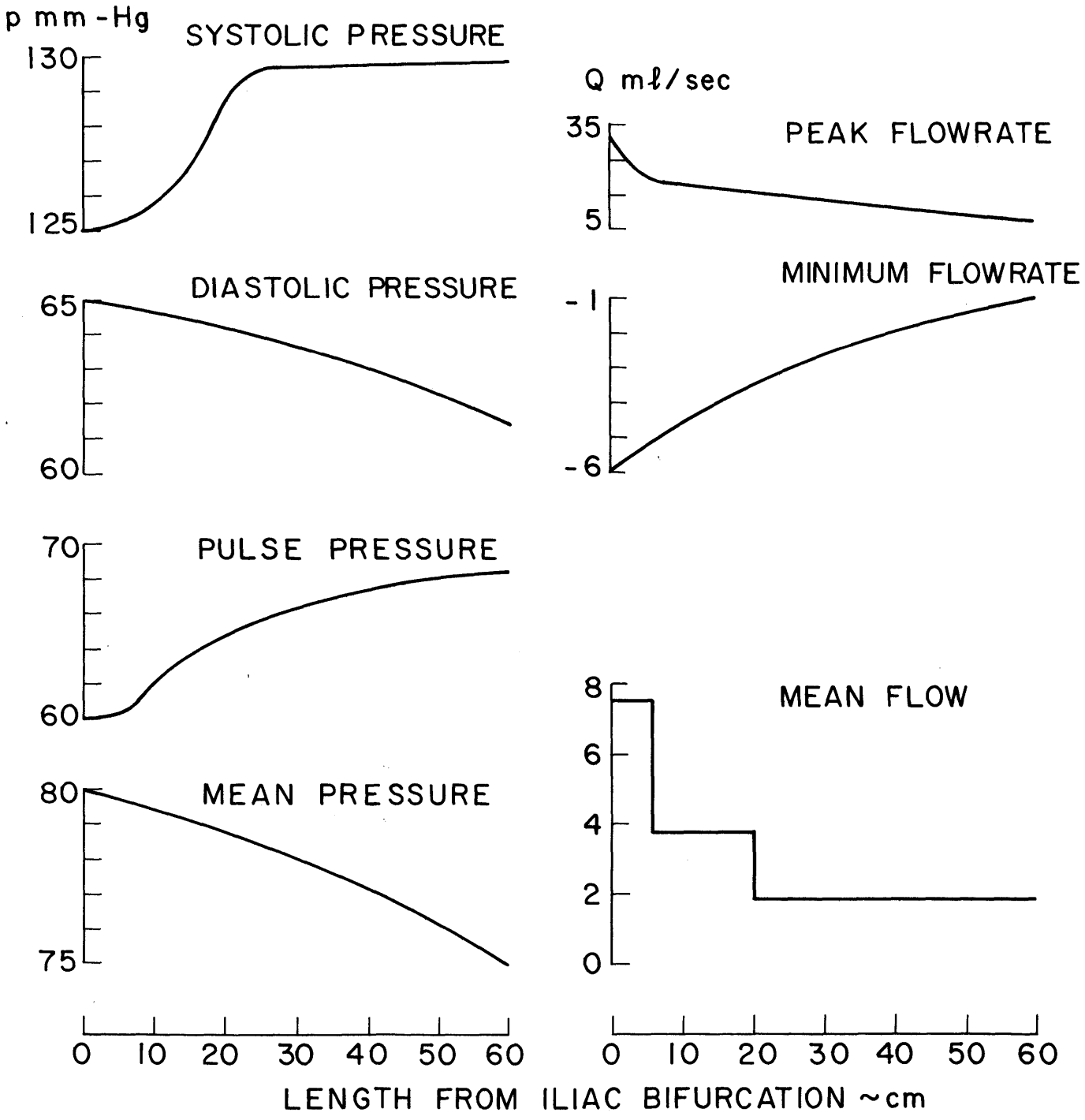

p mm-Hg
SYSTOLIC PRESSURE
130
125
Q mℓ/sec
35
PEAK FLOWRATE
5
DIASTOLIC PRESSURE
65
60
MINIMUM FLOWRATE
-1
-6
70
PULSE PRESSURE
60
8
MEAN FLOW
6
4
2
0
80
MEAN PRESSURE
75
0 10 20 30 40 50 60
0 10 20 30 40 50 60
LENGTH FROM ILIAC BIFURCATION ~cm

Fig. 40

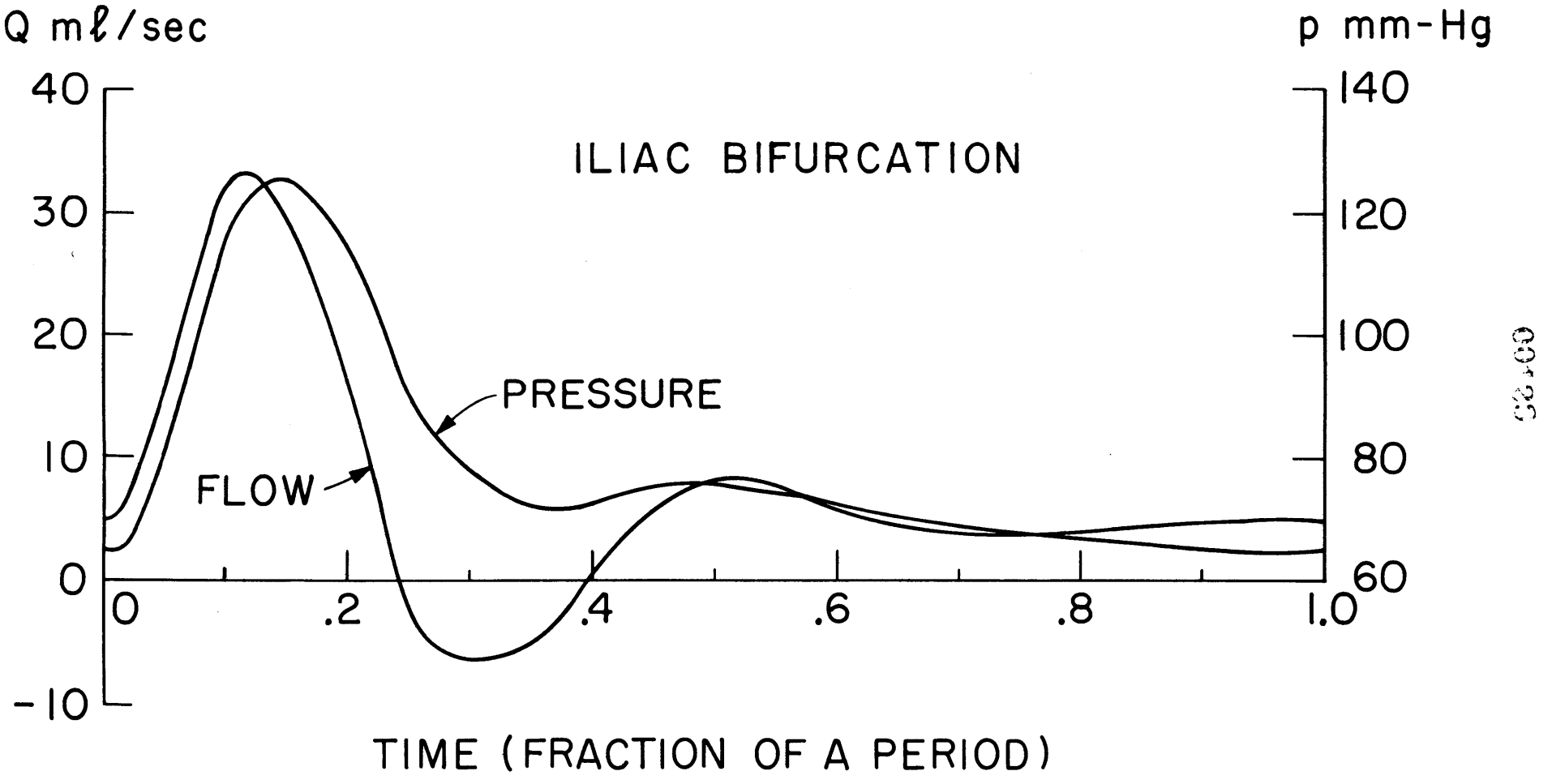

Q mℓ/sec
p mm-Hg
40
30
20
10
0
-10
140
120
100
80
60
ILIAC BIFURCATION
PRESSURE
FLOW
0
.2
.4
.6
.8
1.0
TIME (FRACTION OF A PERIOD)

Fig. 41

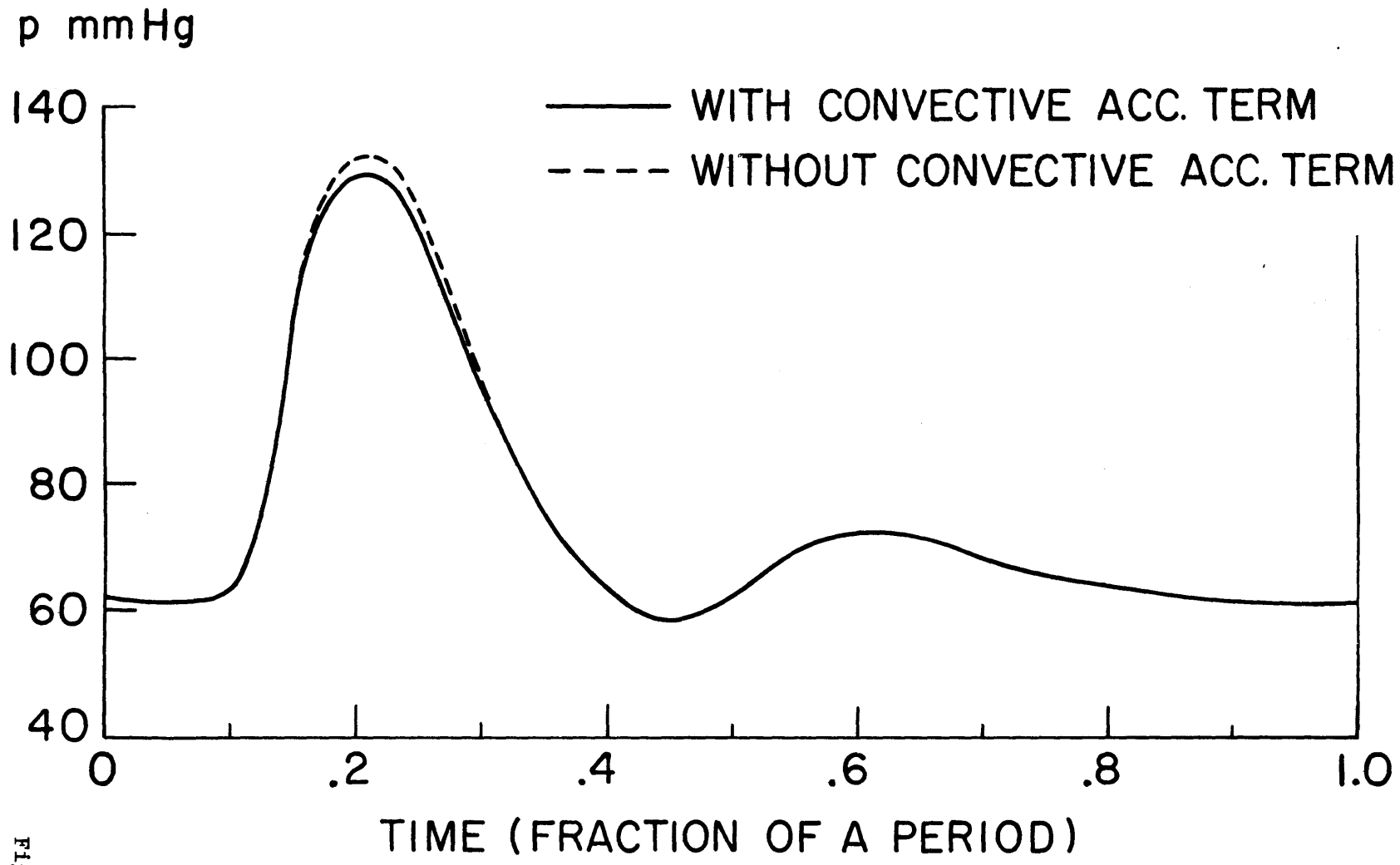

p mmHg
140
120
100
80
60
40
0
.2
.4
.6
.8
1.0
TIME (FRACTION OF A PERIOD)
WITH CONVECTIVE ACC. TERM
WITHOUT CONVECTIVE ACC. TERM

Fig. 42

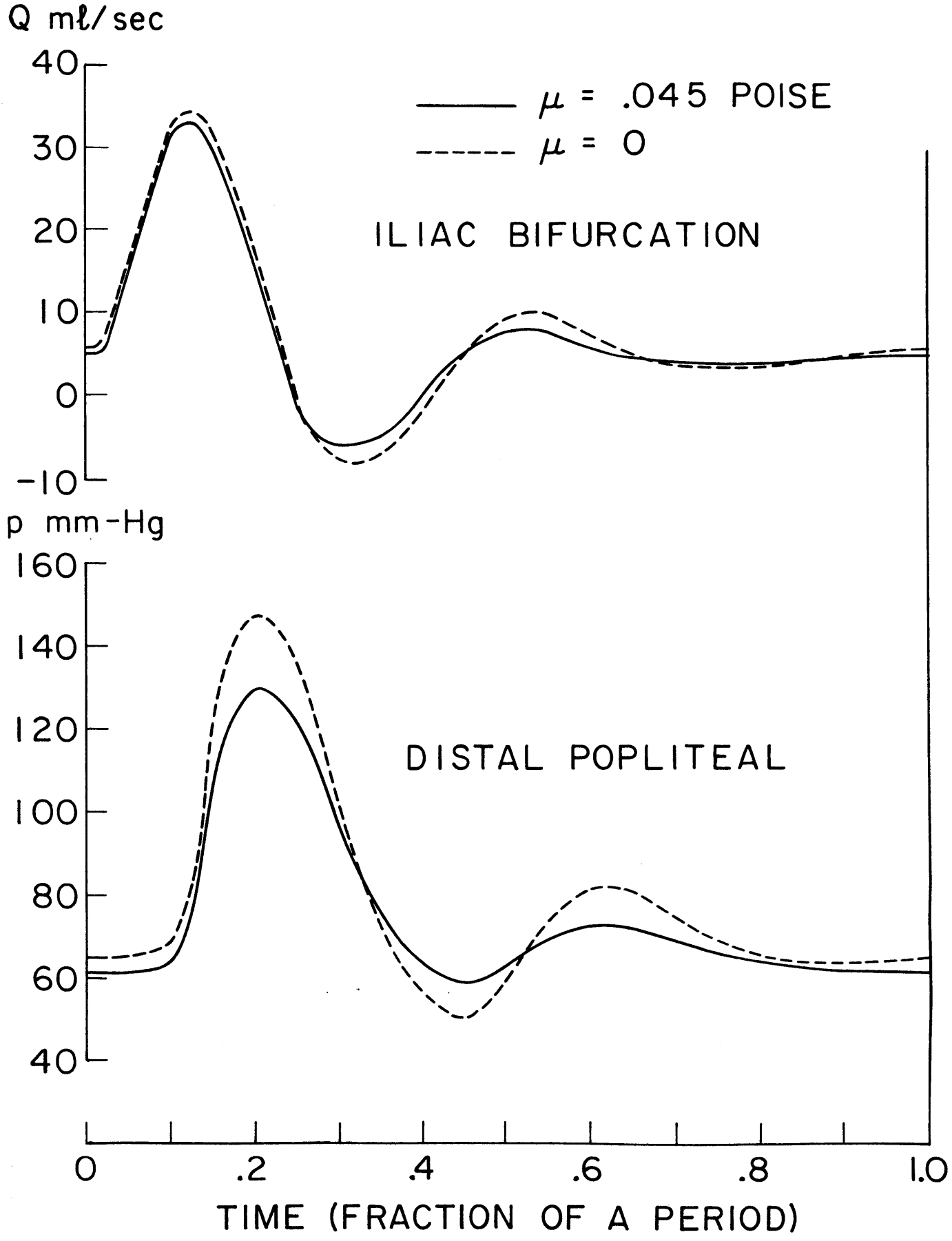

Q ml/sec
40
30
20
10
0
-10
μ = .045 POISE
μ = 0
ILIAC BIFURCATION
p mm-Hg
160
140
120
100
80
60
40
DISTAL POPLITEAL
0
.2
.4
.6
.8
1.0
TIME (FRACTION OF A PERIOD)

Fig. 43

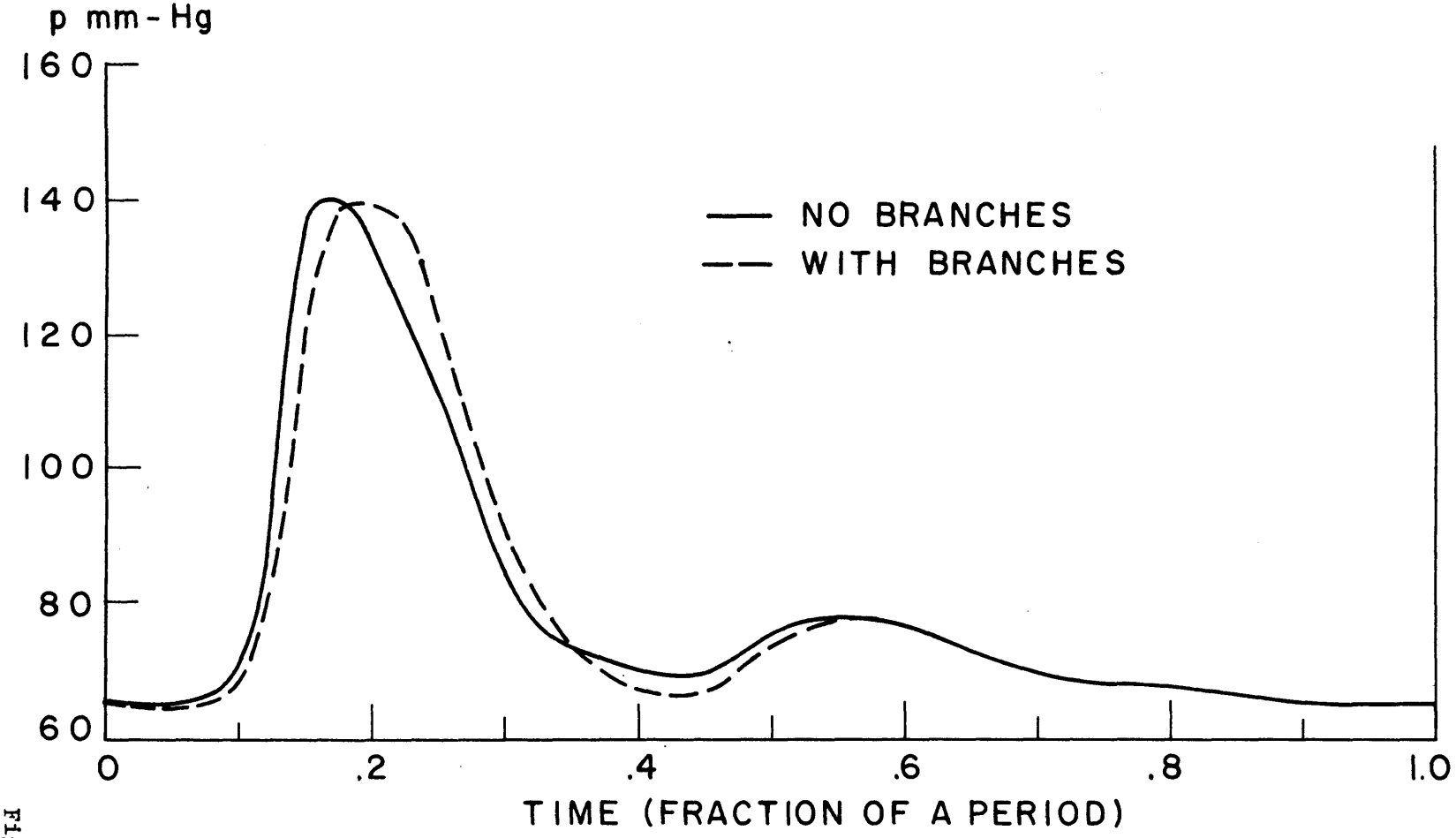

p mm - Hg
160
140
120
100
80
60
0
.2
.4
.6
.8
1.0
TIME (FRACTION OF A PERIOD)
NO BRANCHES
WITH BRANCHES

Fig. 44

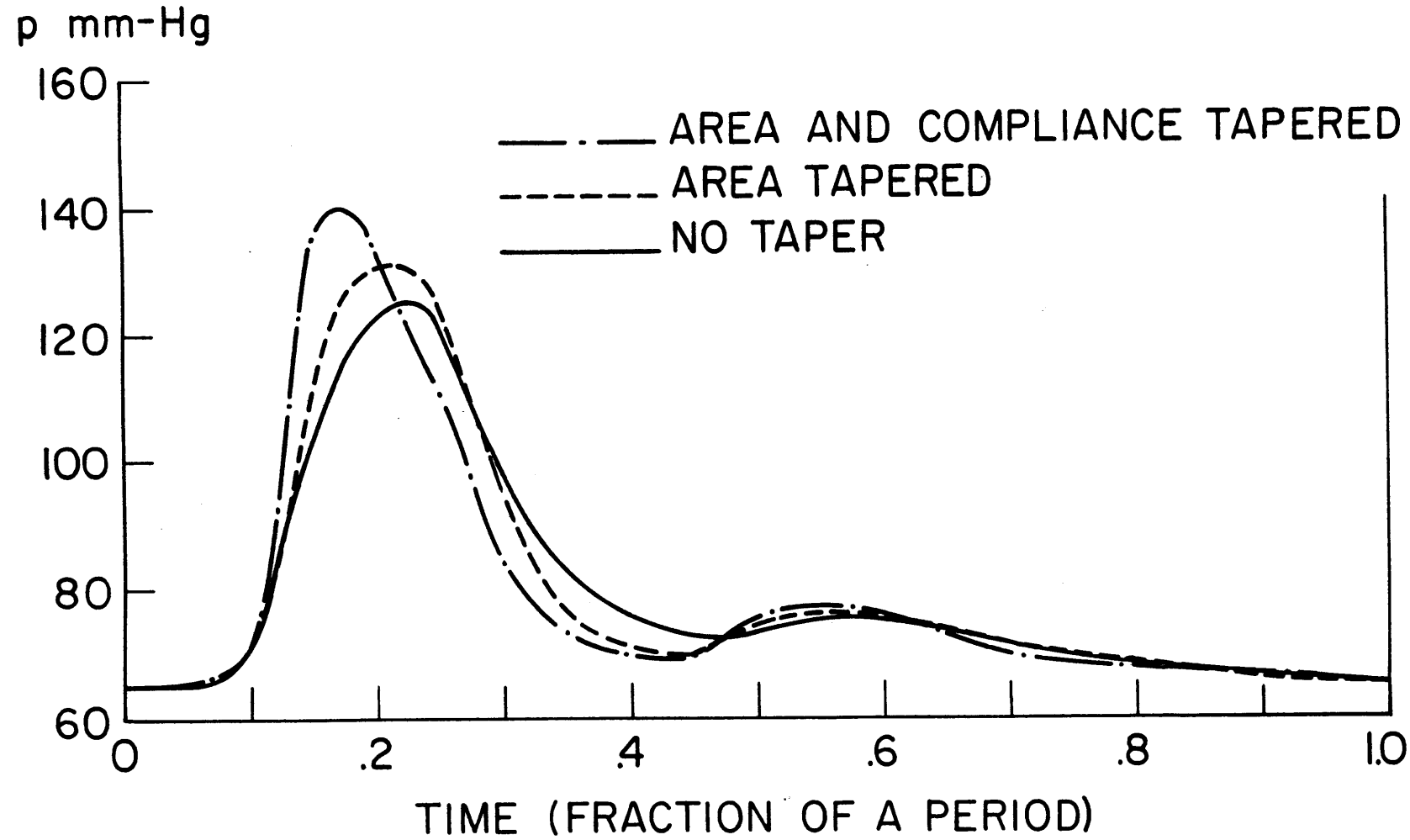

p mm-Hg
160
140
120
100
80
60
0
.2
.4
.6
.8
1.0
AREA AND COMPLIANCE TAPERED
AREA TAPERED
NO TAPER
TIME (FRACTION OF A PERIOD)

Fig. 45

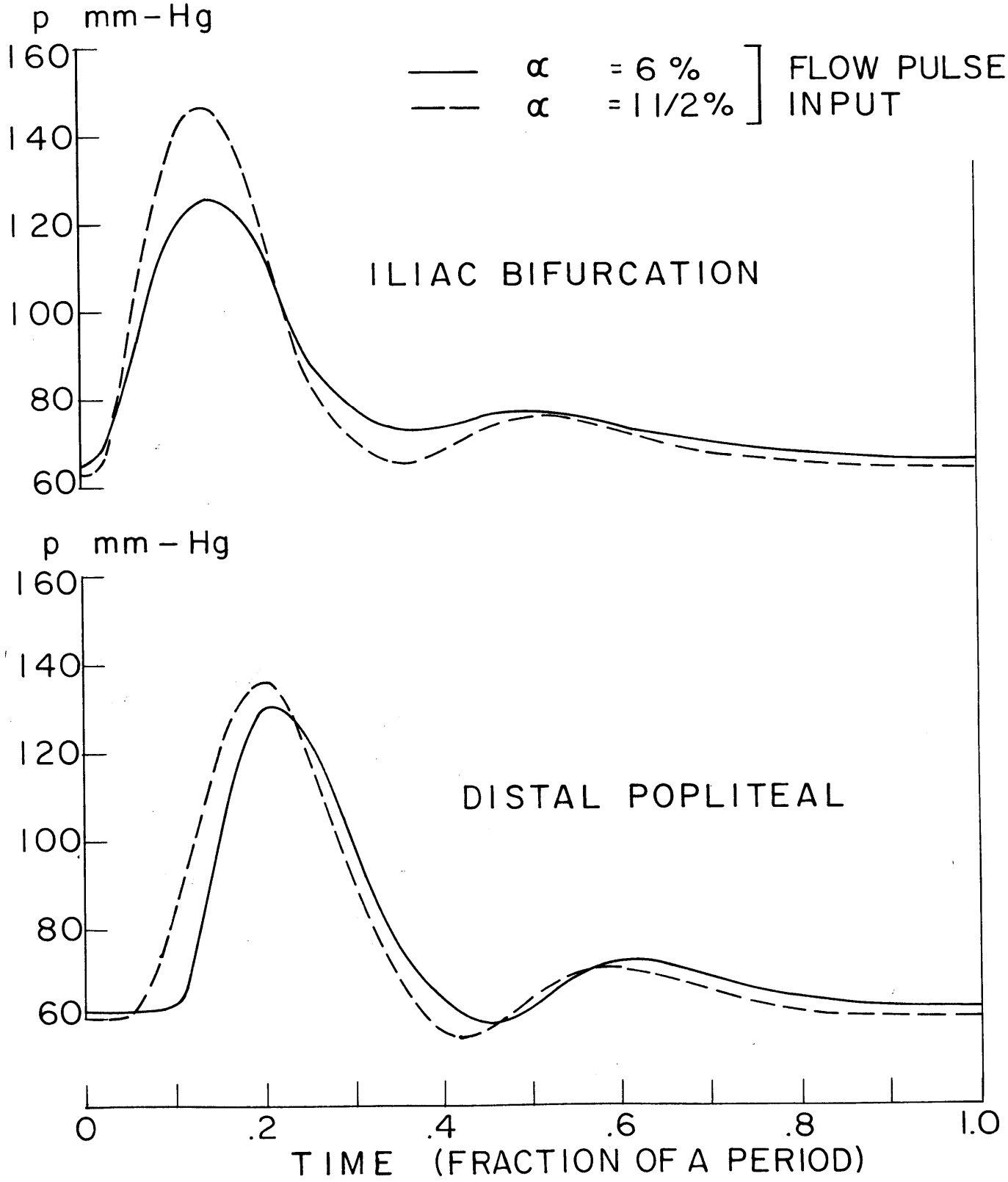

p mm-Hg
160
140
120
100
80
60
α = 6 %
α = 11/2%
FLOW PULSE INPUT
ILIAC BIFURCATION
p mm-Hg
160
140
120
100
80
60
DISTAL POPLITEAL
0
.2
.4
.6
.8
1.0
TIME (FRACTION OF A PERIOD)

Fig. 46

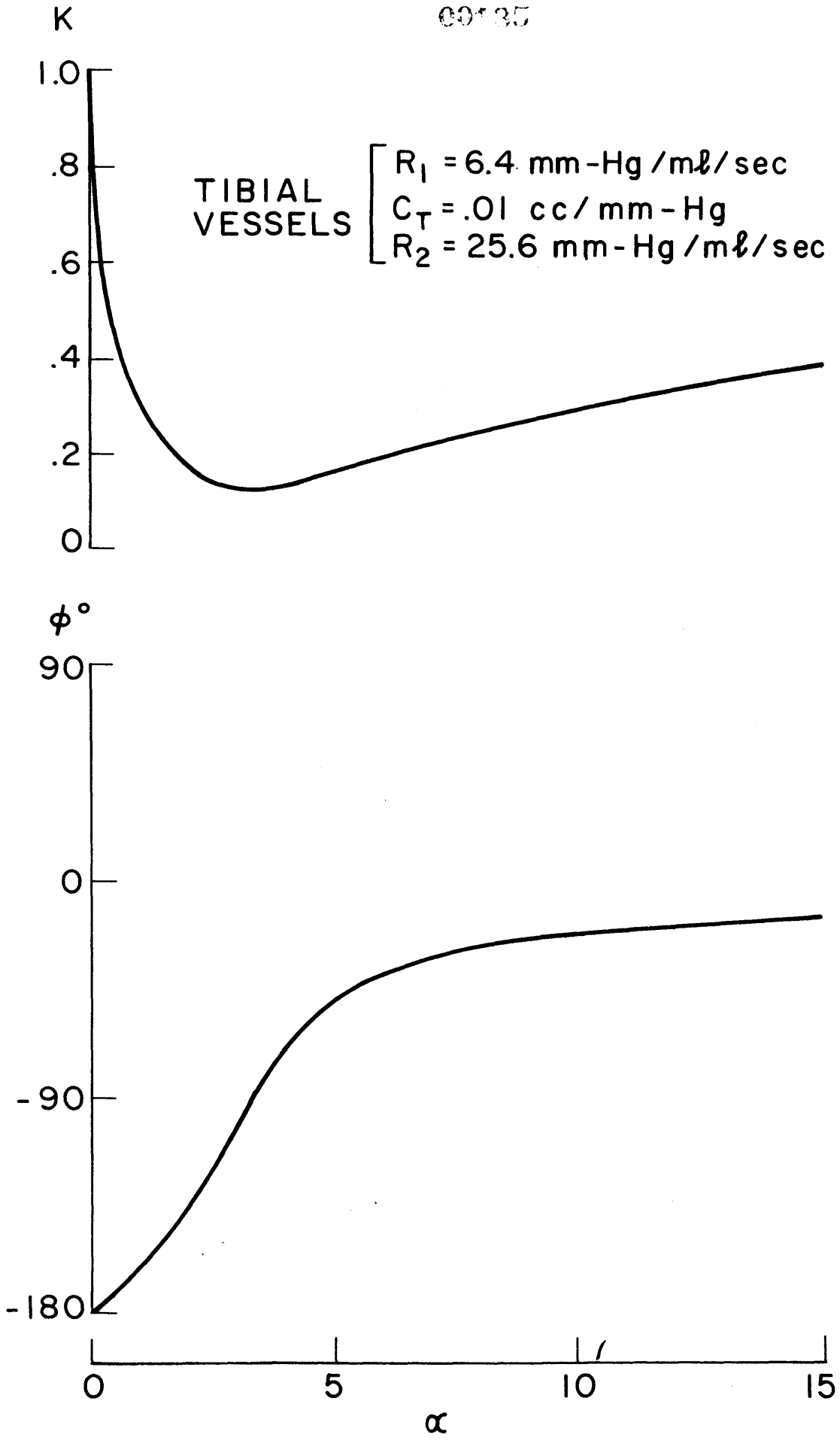

K
1.0
.8
.6
.4
.2
0
TIBIAL VESSELS
R_1 = 6.4 mm-Hg/mℓ/sec
C_T = .01 cc/mm-Hg
R_2 = 25.6 mm-Hg/mℓ/sec
φ°
90
0
-90
-180
0
5
10
15
α

Fig. 47

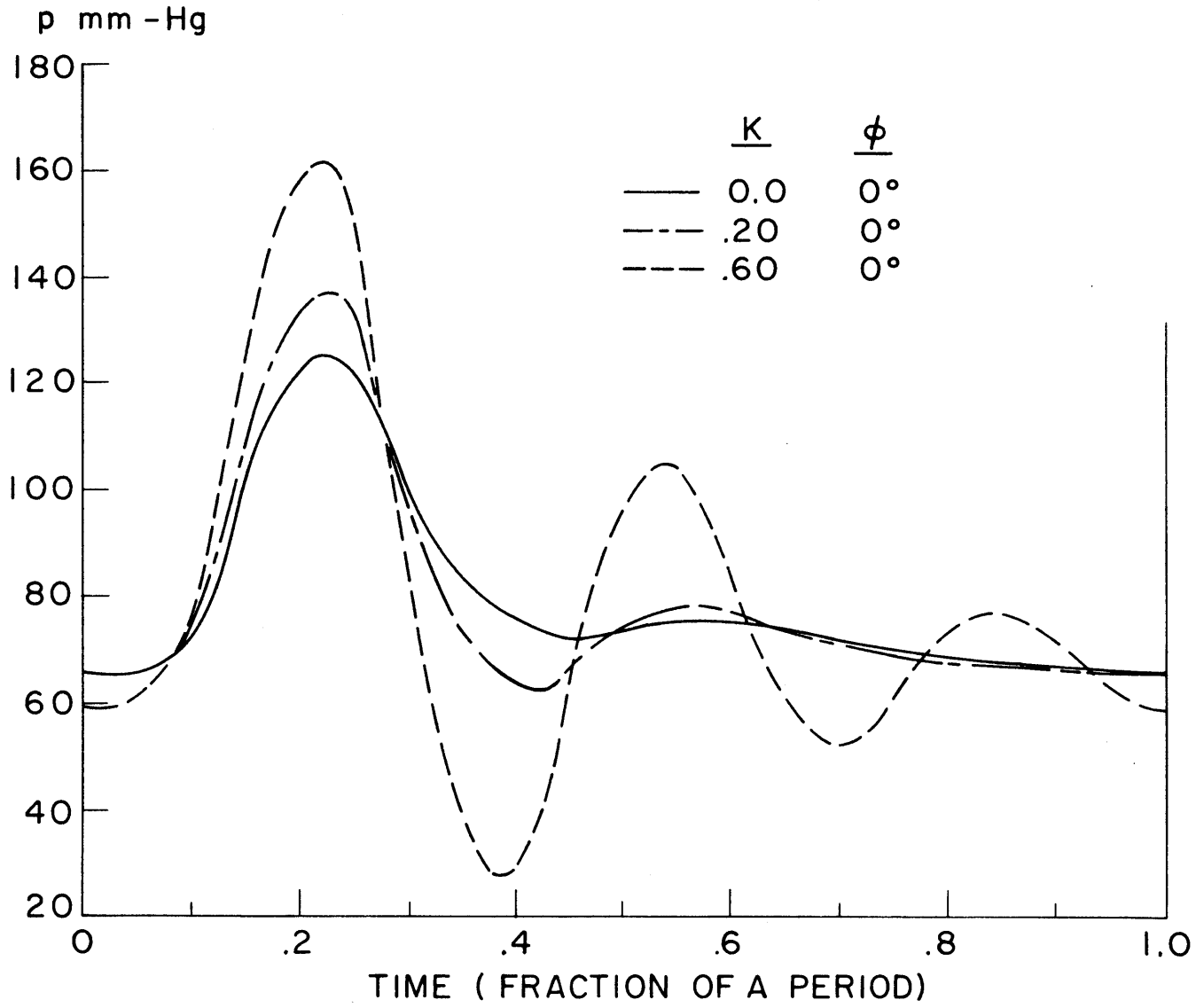

p mm-Hg
180
160
140
120
100
80
60
40
20
0
.2
.4
.6
.8
1.0
TIME (FRACTION OF A PERIOD)
K
φ
0.0 0°
.20 0°
.60 0°

Fig. 48

RESISTANCE APPLIED DISTAL TO PPR RECORDING

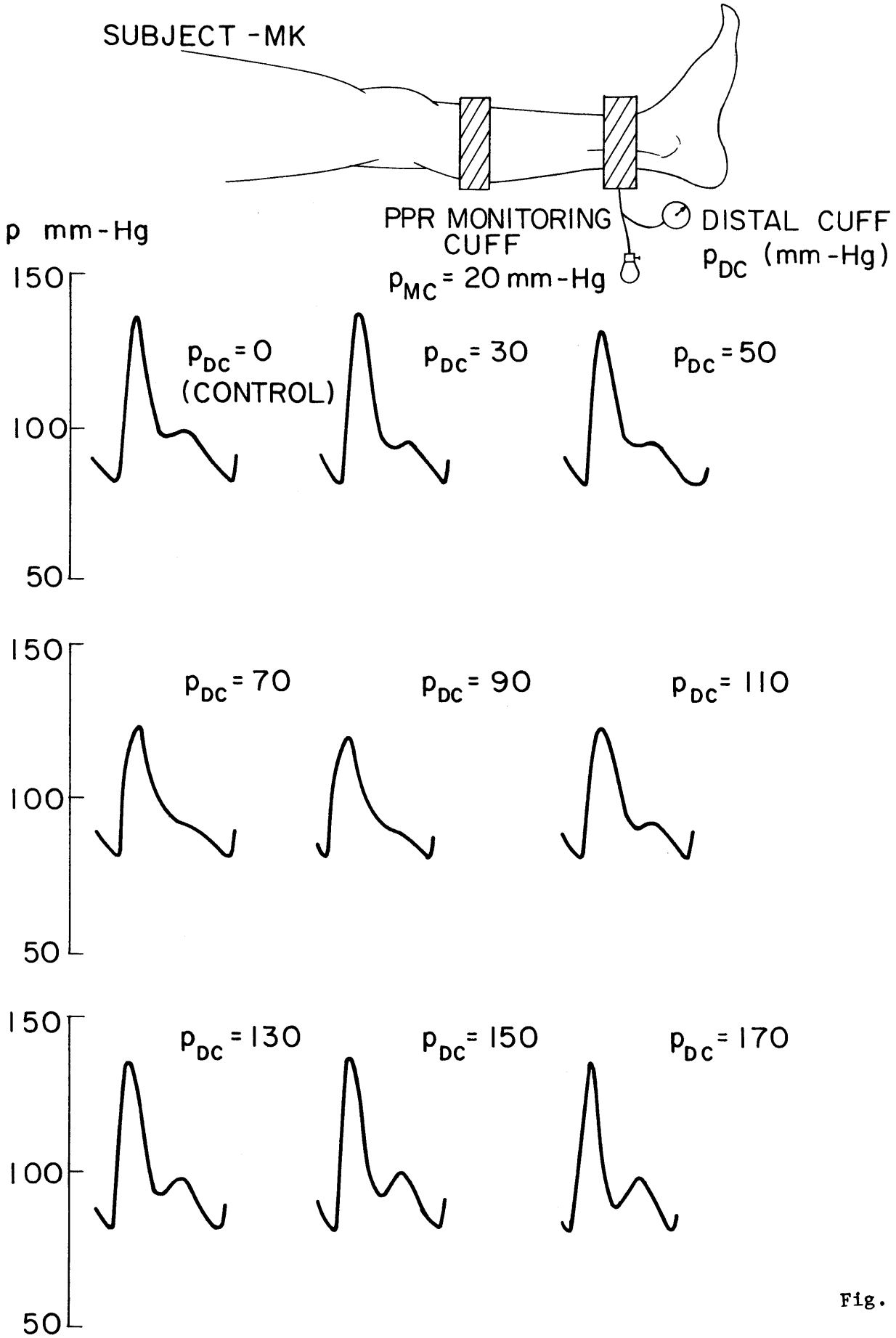


Fig. 49

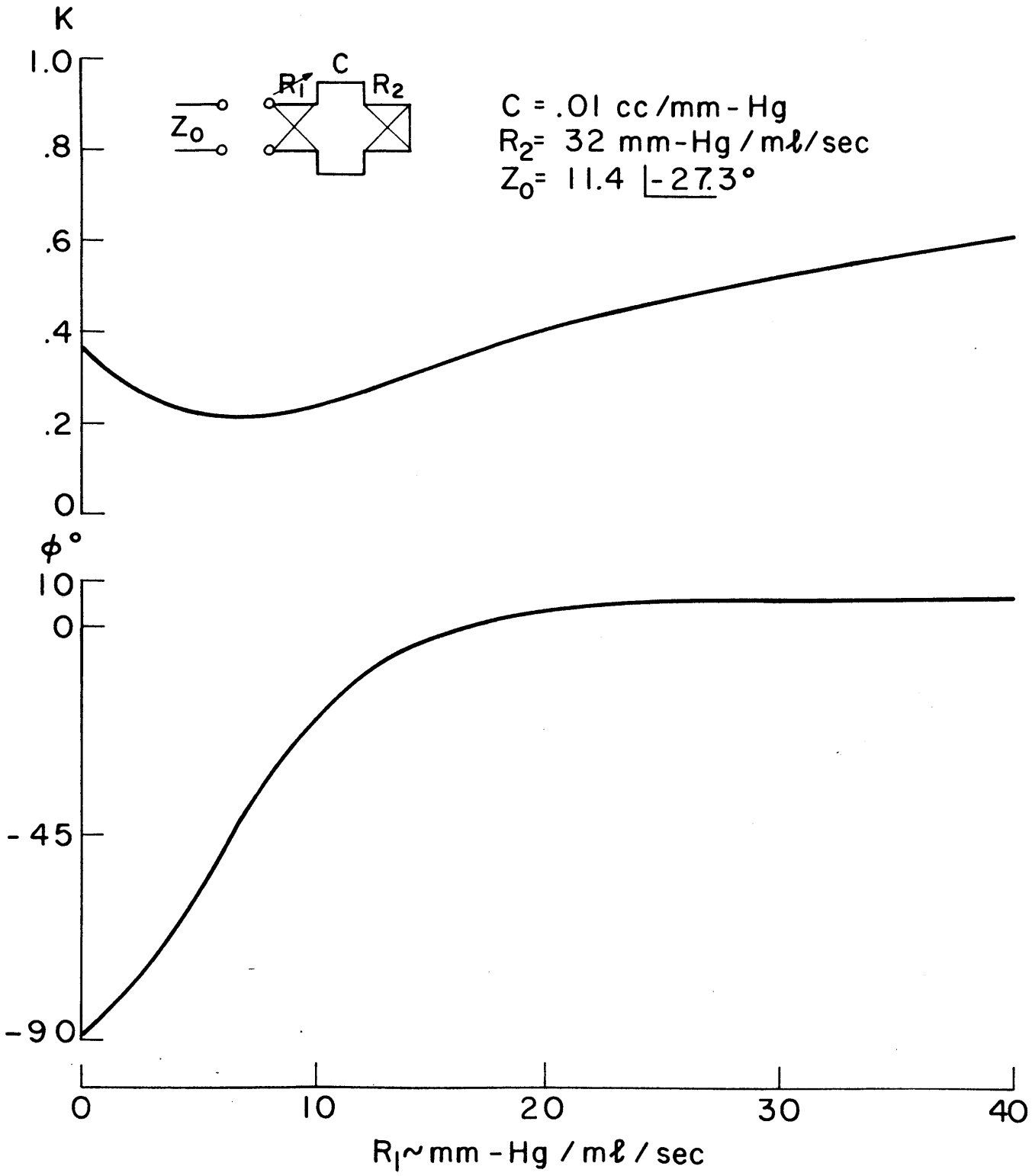

K
1.0
.8
.6
.4
.2
0
Z_0
R_1
C
R_2
C = .01 cc/mm-Hg
R_2= 32 mm-Hg/ml/sec
Z_0= 11.4 ∠-27.3°
φ°
10
0
-45
-90
0
10
20
30
40
R_1~mm-Hg/ml/sec

Fig. 50

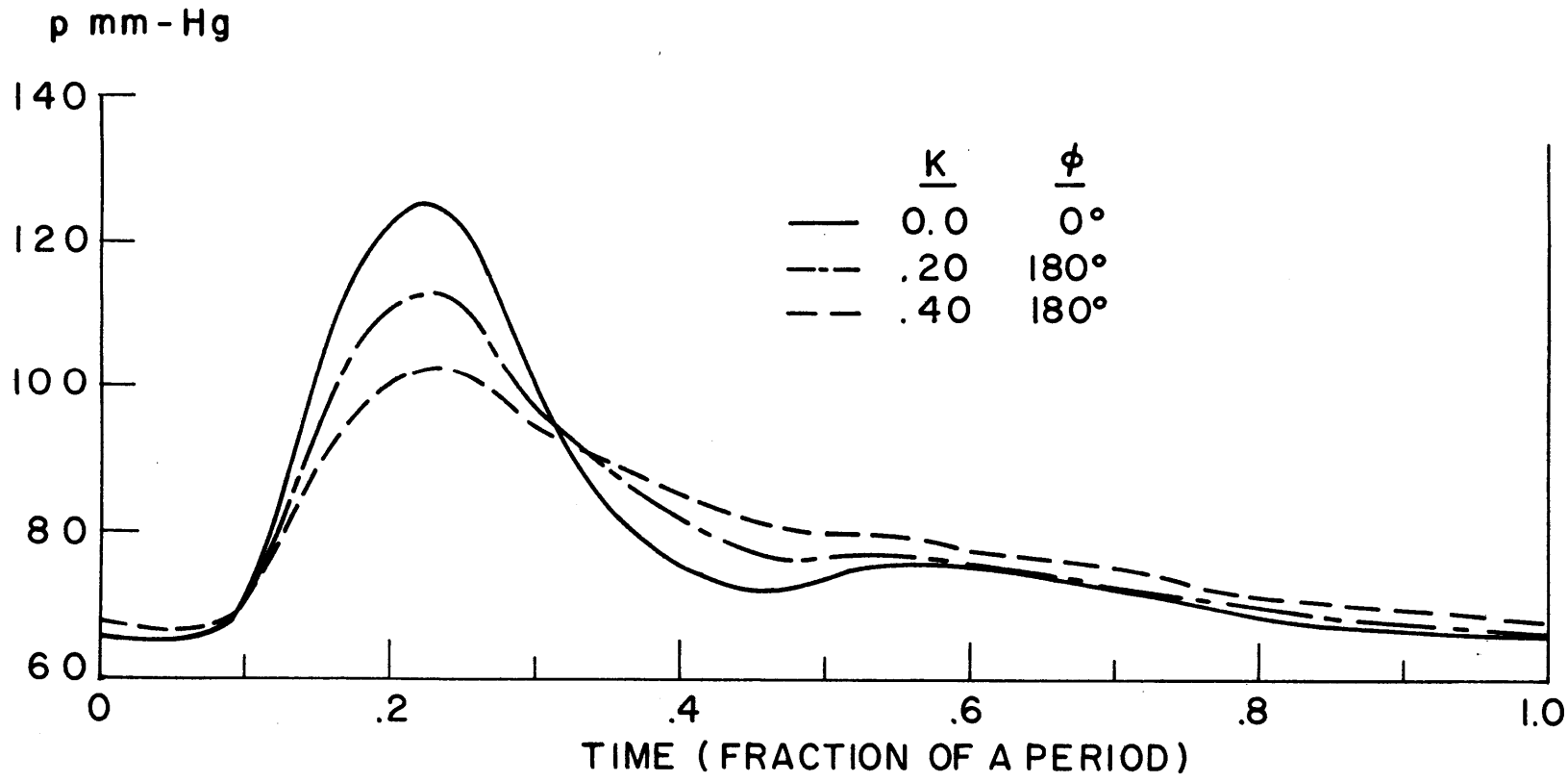

p mm-Hg
140
120
100
80
60
0
.2
.4
.6
.8
1.0
TIME (FRACTION OF A PERIOD)
K
φ
0.0
0°
.20
180°
.40
180°

Fig. 51

PPR RECORDING WITH VASODILATION

SUBJECT - HD

p mm - Hg

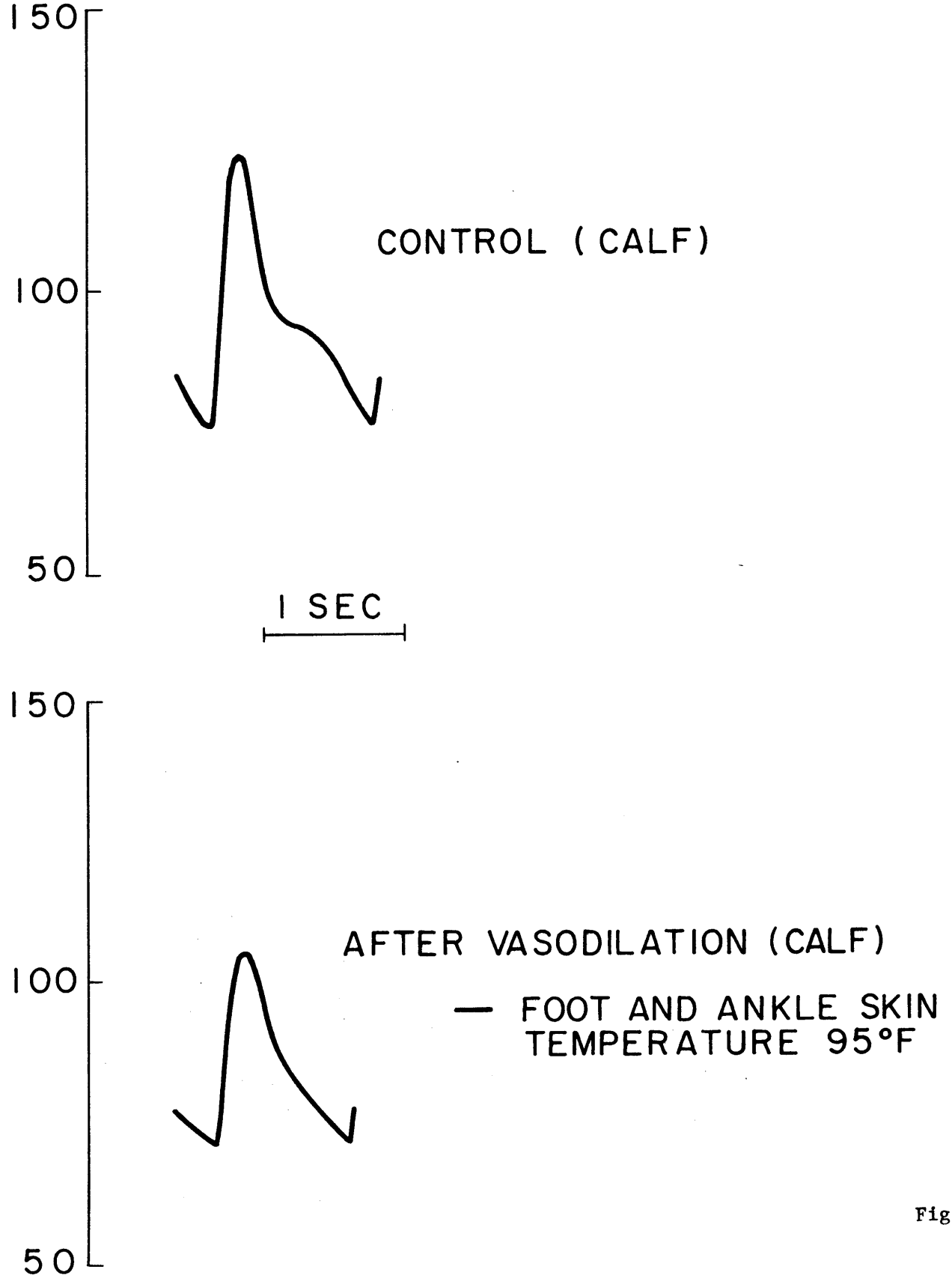


Fig. 52

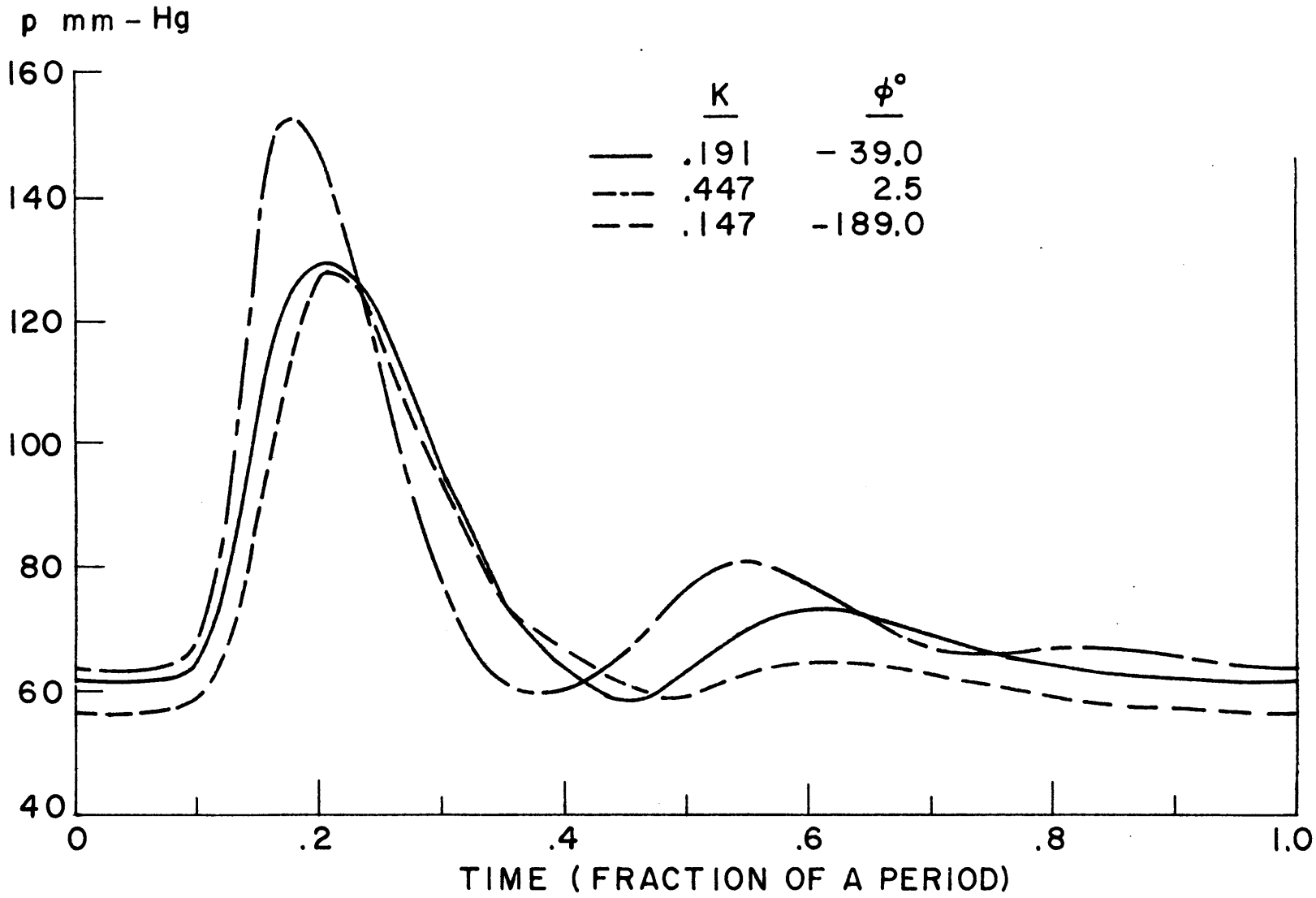

p mm - Hg
160
140
120
100
80
60
40
K
φ°
.191
-39.0
.447
2.5
.147
-189.0
0
.2
.4
.6
.8
1.0
TIME (FRACTION OF A PERIOD)

Fig. 53

OBSTRUCTION MODEL

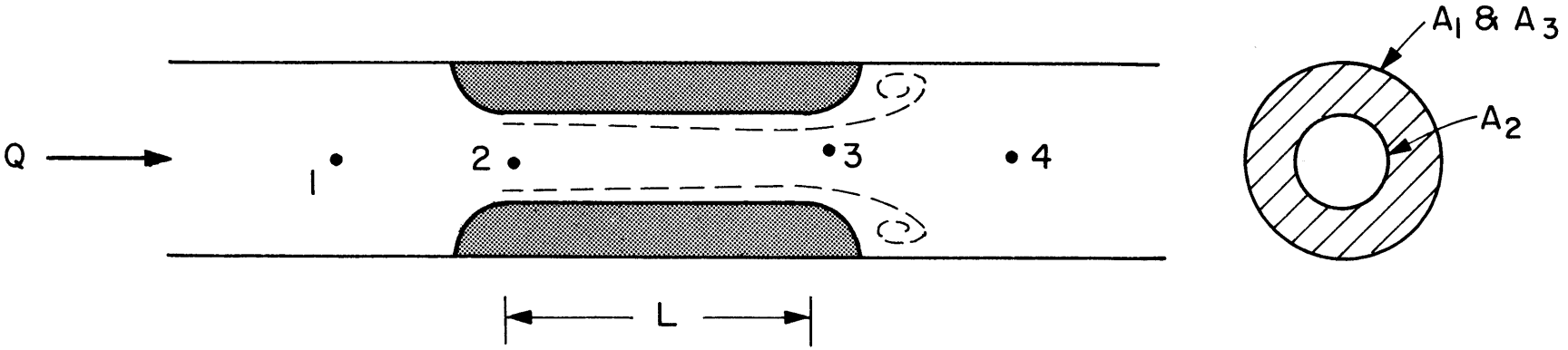


Fig. 54

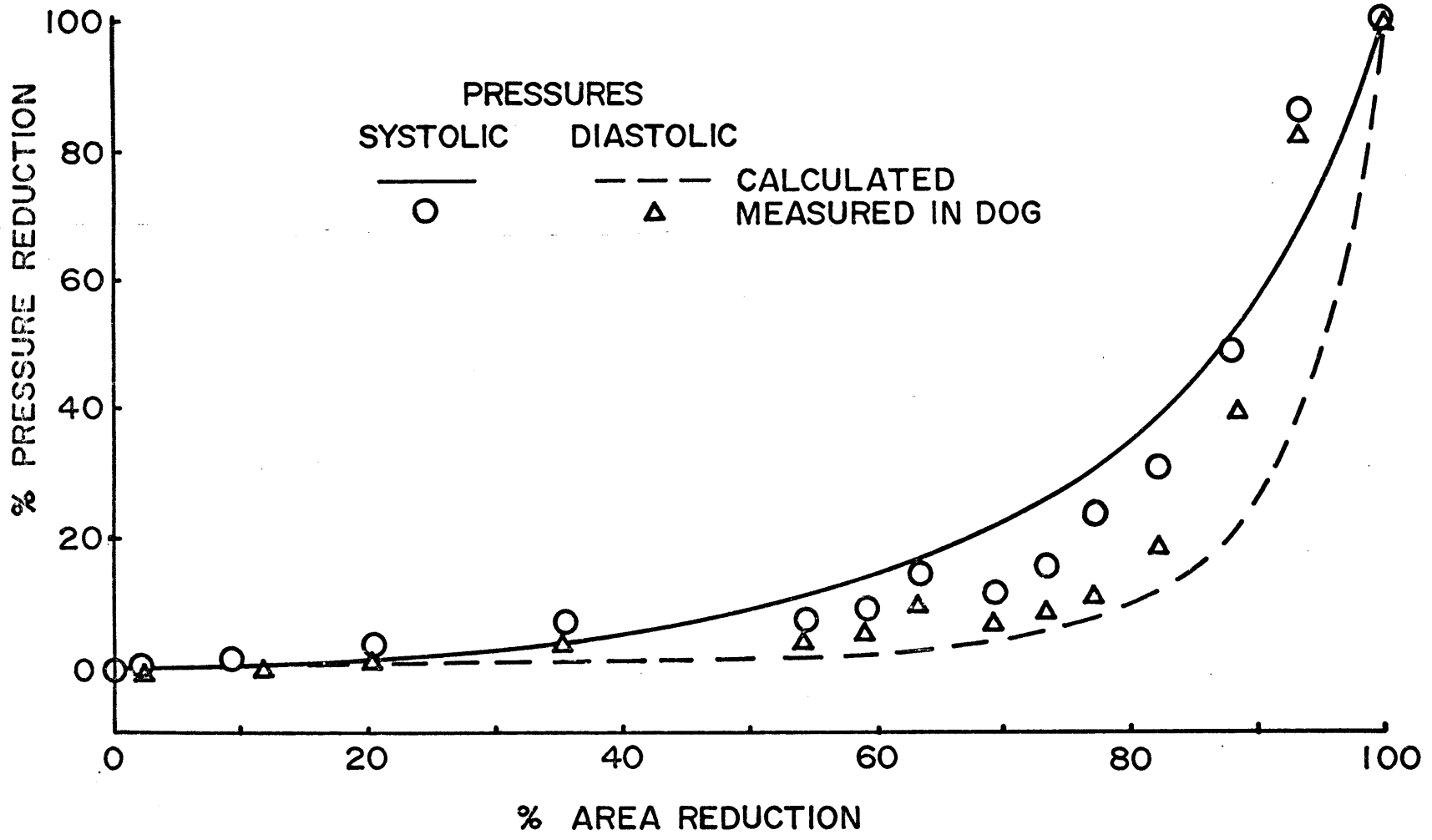

PRESSURES
SYSTOLIC
DIASTOLIC
CALCULATED
MEASURED IN DOG
% PRESSURE REDUCTION
% AREA REDUCTION
0
20
40
60
80
100

Fig. 55

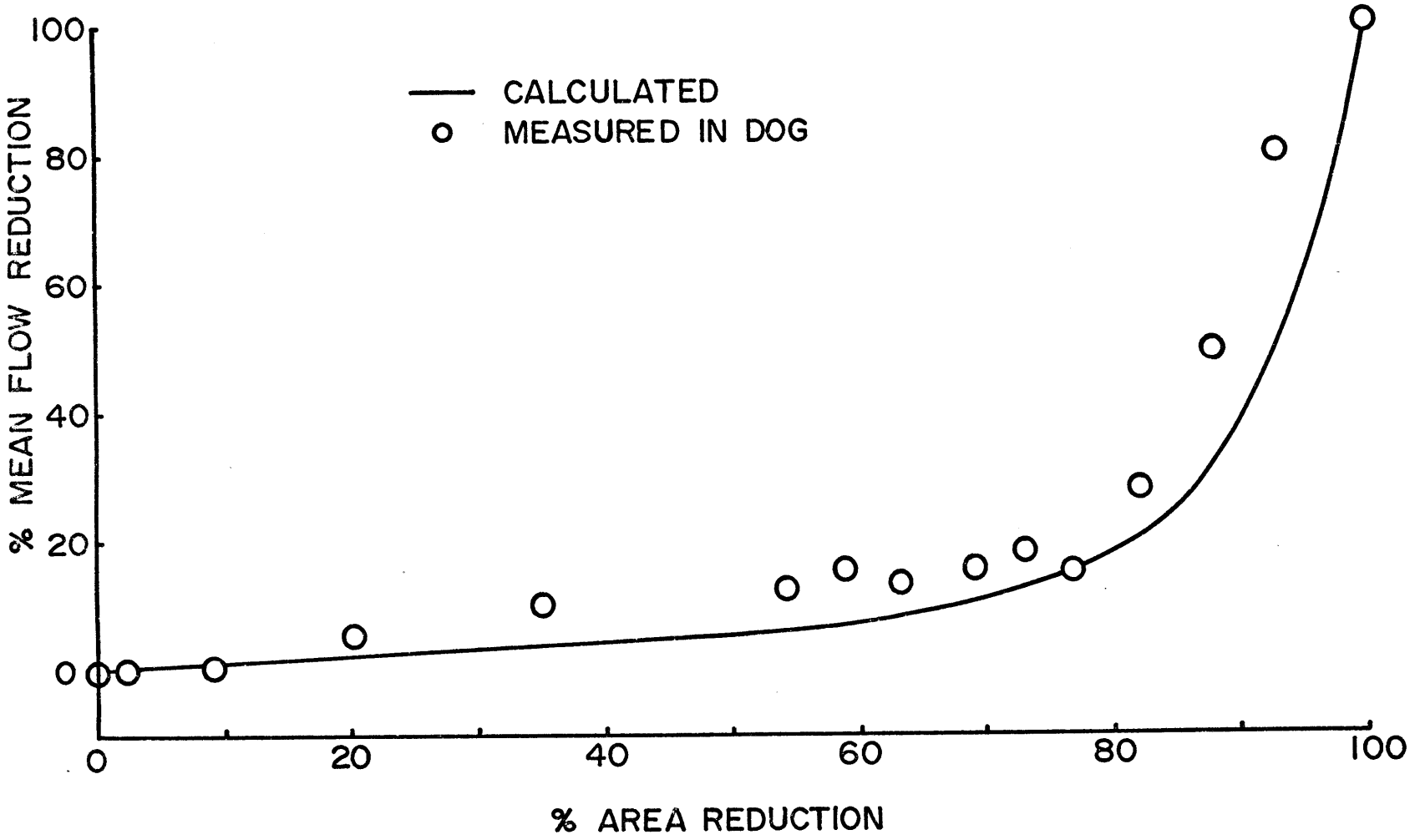

CALCULATED
MEASURED IN DOG
% MEAN FLOW REDUCTION
% AREA REDUCTION
0
20
40
60
80
100

Fig. 56

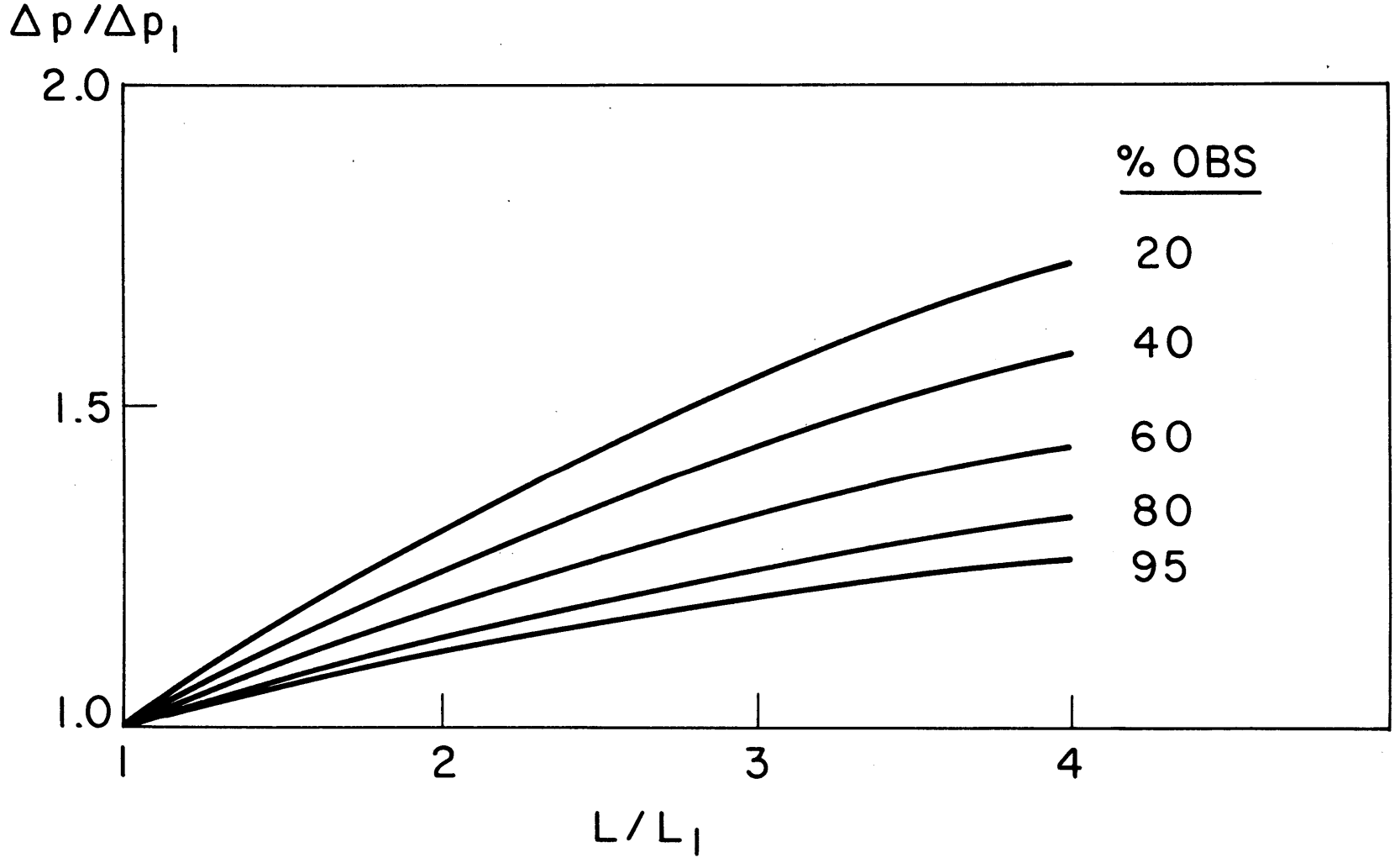


Fig. 57

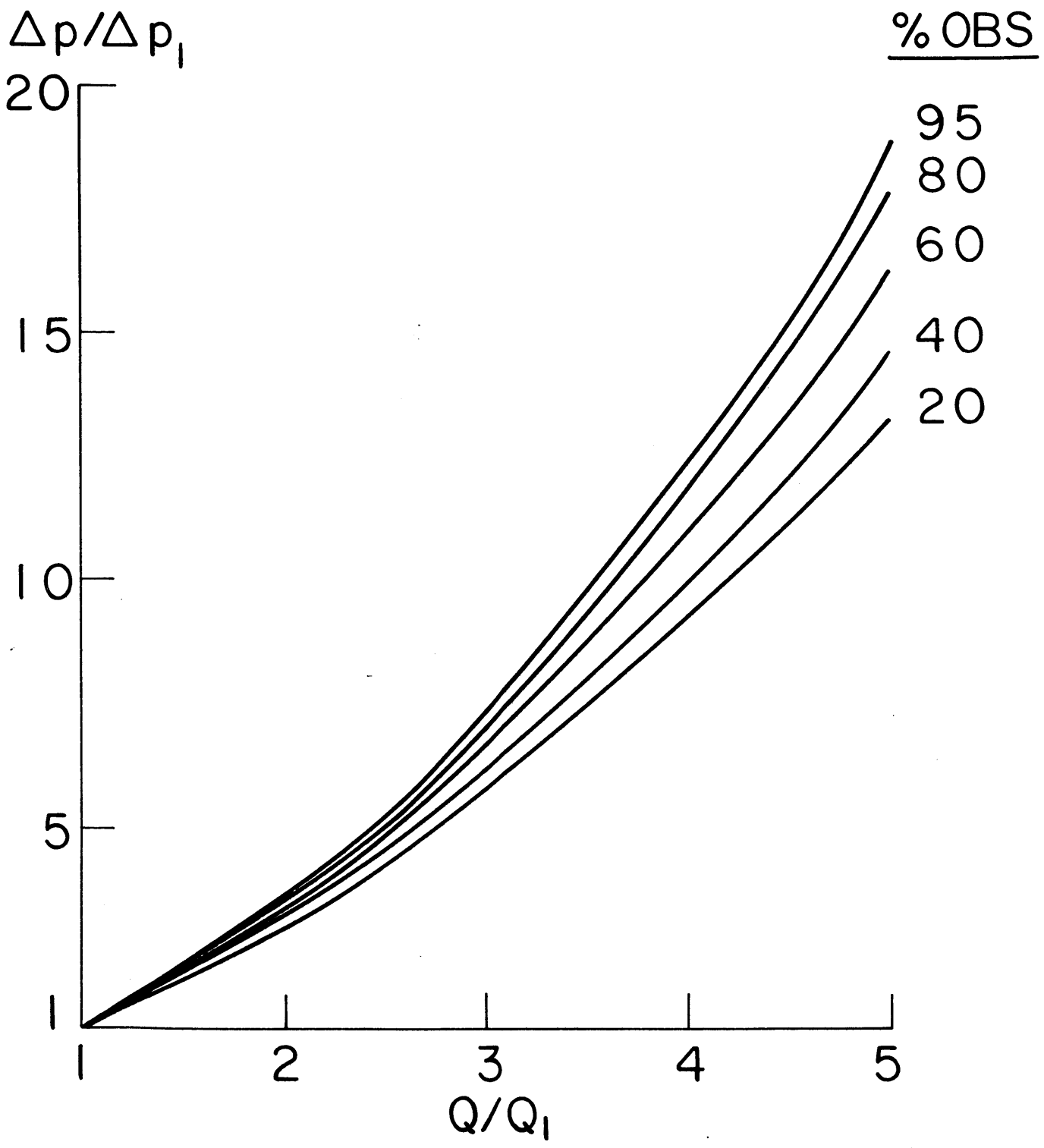


Fig. 58

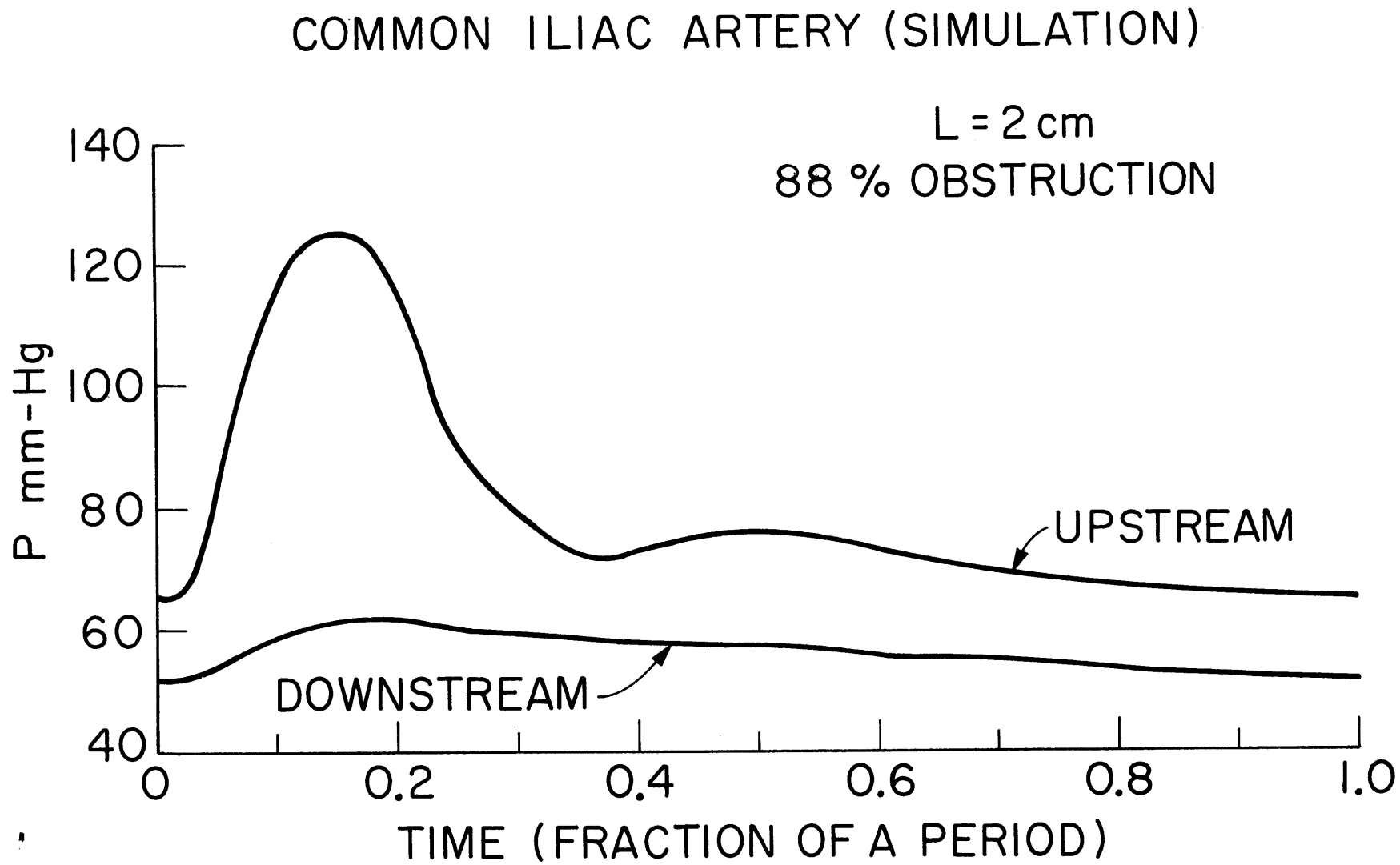

COMMON ILIAC ARTERY (SIMULATION)
L = 2 cm
88 % OBSTRUCTION
140
120
100
80
60
40
P mm-Hg
UPSTREAM
DOWNSTREAM
0
0.2
0.4
0.6
0.8
1.0
TIME (FRACTION OF A PERIOD)

Fig. 59

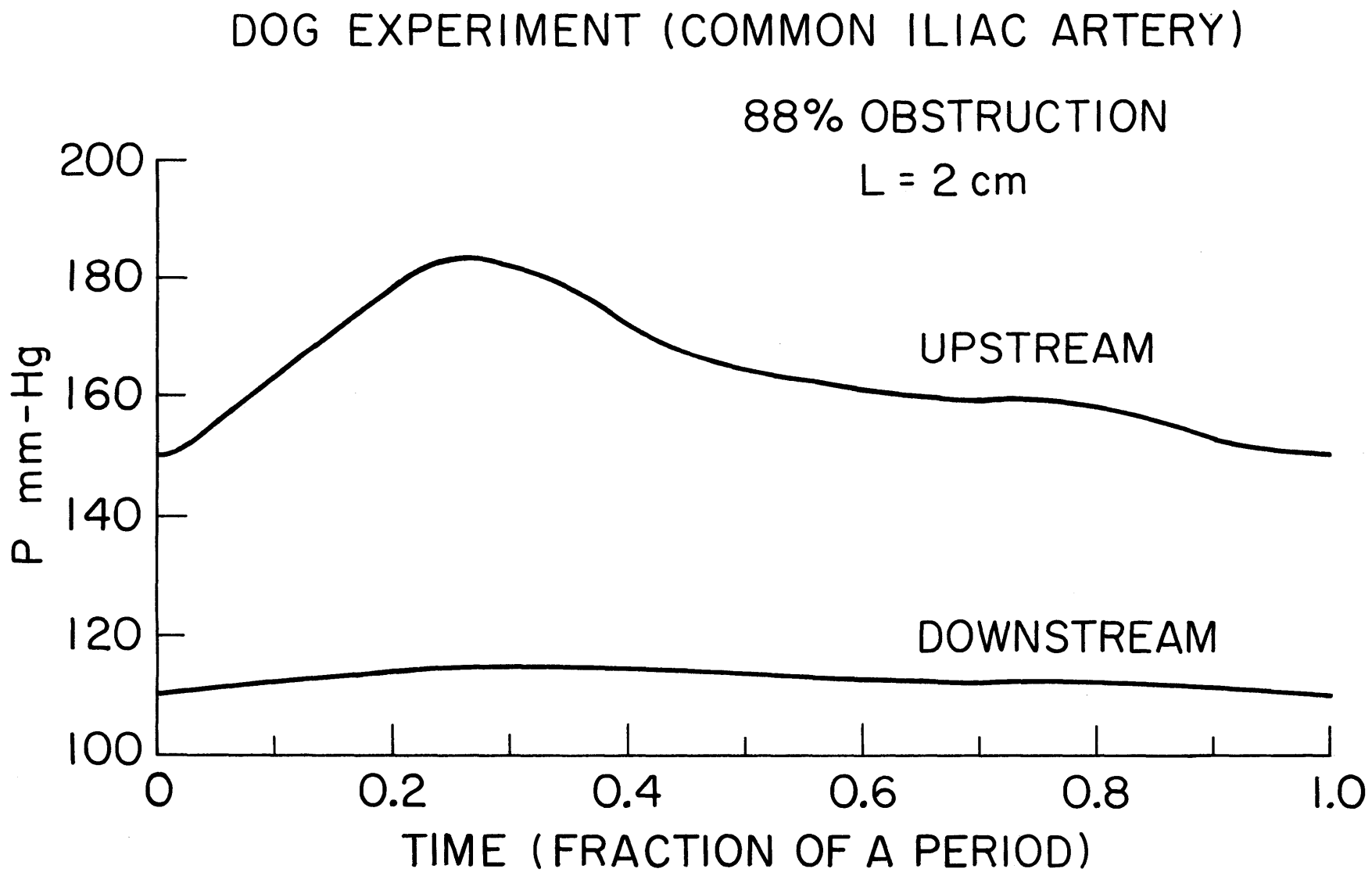

DOG EXPERIMENT (COMMON ILIAC ARTERY)
88% OBSTRUCTION
L = 2 cm
200
180
160
140
120
100
P mm-Hg
UPSTREAM
DOWNSTREAM
0
0.2
0.4
0.6
0.8
1.0
TIME (FRACTION OF A PERIOD)

Fig. 60

APPENDIX A

IBM 360 Computer listing

FORTRAN IV G

	Appendix Page
MAIN PROGRAM	A-1
Subroutines	
PROP	A-11
FUGEN	A-12
QP	A-13
BRANC	A-16

G LEVEL 20 MAIN DATE = 72100 08/43/45

```
C
C       TITLE CARDS
C
C       SIMULATION OF THE ARTERIES OF THE LOWER EXTREMITIES
C
C       JEFF RAINES
C       PH D THESIS WORK
C       FLUIDS LAB - MIT
C       3-239  EXT  7193
C       FALL 1971
C
C       DIMENSION STATEMENTS
C
        DIMENSION P(100),Q(100),CAP(100),CAPM(100),A(100),AX(100),PH(100),
       1          R(100),QL(100),PDUT(100),PQFG(100),AXFG(100),QH(100),
       2          CHAN(16),Y(16)
C
C       PROGRAM INPUT
C
        READ(5,103)CH1U,CH2U,CH3U,CH1D,CH2D,CH3D
        READ(5,103)CP1D,CP2D,CP3D,CP1U,CP2U,CP3U
        READ(5,1033)CFP1,CFP2,CFP3
        READ(5,104)J1,J2,J3,J4,J5
        READ(5,105)MP,MQ
      1 CONTINUE
C
        READ(5,100)NCASE,DT,DX,HR,ACAP
        IF(NCASE)72,72,2
      2 CONTINUE
        READ(5,101)KQP,KOPT,KPRIM,NPERM,NX,NFG,NL,INIT
        READ(5,102)RHY1,RHY2,CHY
        READ(5,102)RPR1,RPR2,CPR
        READ(5,102)RT1,RT2,CT
        TMAX = 60. / HR
        SCFG = NFG / TMAX
        NFGM = NFG + 1
C
C       INITIAL CONDITIONS
C
        T = 0.0
        ROH = 1.06
        XMU = .045
        PO = 100.
        PV = 20.
C
        ISWC = 1
        ISWP = 1
        ISWR = 1
        NPER = 1
        KPRI = KPRIM
        KTOP = NL
C
        IF(INIT)4,4,3
```

```
      3 CONTINUE
        READ(5,106)(PQFG(I), I = 1,NFGM)
        READ(5,106)(Q(I),I = 1,NX)
        READ(5,106)(P(I),I = 1,NX)
        READ(5,106) QHY,QPR,PHY,PPR,PT
        DO 33    I = 1,NX
        POUT(I) = P(I) / 1333.
        QH(I) = Q(I)
     33 CONTINUE
      4 CONTINUE
C
C       OUTPUT CASE PARAMETERS
C
        WRITE(6,200)
        WRITE(6,201)NCASE
        WRITE(6,202)HR,TMAX
        IF(KQP)2003,2003,2004
   2003 WRITE(6,203)
        GO TO 2005
   2004 WRITE(6,204)
   2005 CONTINUE
        WRITE(6,205)ACAP
        WRITE(6,206)MP,MQ
        WRITE(6,207)
        WRITE(6,208)
        WRITE(6,209)
        WRITE(6,210)
        WRITE(6,211)DT,DX,NX,NPERM
        WRITE(6,212)KOPT,KPRIM,NL
        WRITE(6,213)
        WRITE(6,2131)
        WRITE(6,214)INIT,NFG
        WRITE(6,215)SCFG
        WRITE(6,216)J1,J2,J3,J4,J5
        WRITE(6,217)ROH,XMU,PC,PV
        WRITE(6,218)
        WRITE(6,219)
        WRITE(6,220)RHY1,RHY2,CHY,CH1U,CH2U,CH3U
        WRITE(6,221)RPR1,RPR2,CPR,CP1D,CP2D,CP3D
        WRITE(6,222)CFP1,CFP2,CFP3
        WRITE(6,223)RT1,RT2,CT
        PM = 80.
        XL = 60.
        CO = .00595 * ACAP
        RH = RHY1 + RHY2
        RP = RPR1 + RPR2
        RT = RT1 + RT2
        RE = 1. / (1. / RH + 1. / RP + 1. / RT)
        RRH = RHY1 / RHY2
        RRP = RPR1 / RPR2
        RRT = RT1 / RT2
        XMH = RE / RH
        XMP = RE / RP
```

G LEVEL 20 MAIN DATE = 72100 08/43/45

```
      XMT = RE / RT
      BETAH = RE * CHY / TMAX
      BETAP = RE * CPR / TMAX
      BETAT = RE * CT / TMAX
      BETAA = RE * CO / TMAX
      CAM = RE**2 * CO**2 * PM / ROH / XL**2 * 1333.
      VP = 8. * 3.14 * XMU / ROH * XL * RE / PM
C
      WRITE(6,224)
      WRITE(6,225)PM
      WRITE(6,226)XL
      WRITE(6,227)CO
      WRITE(6,228)
      WRITE(6,229)
      WRITE(6,230)BETAA,RE,CAM,VP
      WRITE(6,231)BETAH,RH,RRH,XMH
      WRITE(6,232)BETAP,RP,RRP,XMP
      WRITE(6,233)BETAT,RT,RRT,XMT
      WRITE(6,234)
C
C     DYNAMIC OUTPUT
C
    5 CONTINUE
      CYCTM = T / TMAX
      IF(KPRI - KPRIM)11,6,6
    6 CONTINUE
      IF(KOPT - 1)7,8,7
    7 CONTINUE
C
CC    TAB
C
      IF(KTOP - NL)9,10,10
   10 CONTINUE
      WRITE(6,300)
      WRITE(6,301)J1,J1,J2,J2,J3,J3,J4,J5
      WRITE(6,302)
      KTOP = 3
    9 CONTINUE
      WRITE(6,303)Q(J1),POUT(J1),Q(J2),POUT(J2),Q(J3),POUT(J3),
     1            CHY,QPR,Q(J4),POUT(J5),PT,CYCTM,NPER
      KTOP = KTOP + 1
      KPRI = 0
      IF(KOPT - 1)8,8,11
    8 CONTINUE
C
CC    PLOT
C
      Y(1) = Q(J1)
      Y(2) = P(J1)
      Y(3) = Q(J2)
      Y(4) = P(J2)
      Y(5) = Q(J3)
      Y(6) = P(J3)
```

```
      Y(7) = QHY
      Y(8) = QPR
C
      KPRI = 0
C
   11 CONTINUE
C
C     TIMER / ENDER
C
      KPRI = KPRI + 1
      T = T + DT
      IF(T - TMAX)14,14,12
   12 CONTINUE
      NPER = NPER + 1
      IF(NPER - NPERM)1222,1223,1223
 1223 CONTINUE
      KPRIM = KPRIM
 1222 CONTINUE
      IF(NPER - NPERM)13,13,1
   13 CONTINUE
      T = DT
   14 CONTINUE
C
C     ARTERIAL PROPERTIES
C
      CALL PROP(1  ,3  ,0.00,DX,ISWP,0,0,ACAP,0.00,60.0,AX,AXFG,
     1          P,A,CAPM,CAP,R,QL,ROH,PO,XMU)
      CALL PROP(4  ,5  ,4.00,DX,ISWP,0,0,ACAP,0.00,60.0,AX,AXFG,
     1          P,A,CAPM,CAP,R,QL,ROH,PO,XMU)
      CALL PROP(6  ,7  ,6.00,DX,ISWP,0,0,ACAP,0.00,60.0,AX,AXFG,
     1          P,A,CAPM,CAP,R,QL,ROH,PO,XMU)
      CALL PROP(8  ,13,8.00,DX,ISWP,0,0,ACAP,0.00,60.0,AX,AXFG,
     1          P,A,CAPM,CAP,R,QL,ROH,PO,XMU)
      CALL PROP(14,15,18.0,DX,ISWP,0,0,ACAP,0.00,60.0,AX,AXFG,
     1          P,A,CAPM,CAP,R,QL,ROH,PO,XMU)
      CALL PROP(16,17,20.0,DX,ISWP,0,0,ACAP,0.00,60.0,AX,AXFG,
     1          P,A,CAPM,CAP,R,QL,ROH,PO,XMU)
      CALL PROP(18,27,22.0,DX,ISWP,0,0,ACAP,0.00,60.0,AX,AXFG,
     1          P,A,CAPM,CAP,R,QL,ROH,PO,XMU)
      CALL PROP(28,38,40.0,DX,ISWP,0,0,ACAP,0.00,60.0,AX,AXFG,
     1          P,A,CAPM,CAP,R,QL,ROH,PO,XMU)
      ISWP = 0
C
C     PRESSURE RETENSION
C
      DO 15   I = 1,NX
      PH(I) = P(I)
   15 CONTINUE
C
C     DYNAMIC ANALYZER
C
      IF(KQP)16,16,17
C     IF KQP = 0  :  PRESSURE IS GIVEN
```

```
C       IF KQP = 1   :  FLOW IS GIVEN
     16 CONTINUE
C
CC      PRESSURES WITH PRESSURE GIVEN
C
        CALL FUGEN(POUT(1),T,NFG,PQFG,SCFG)
        P(1) = 1333. * POUT(1)
C
        CALL QP(1,1,MP,2 ,3 ,
       1         P,Q,CAP,A,PH,R,QL,POUT,DT,DX,ROH)
        CALL QP(1,1,MP,5 ,5 ,
       1         P,Q,CAP,A,PH,R,QL,POUT,DT,DX,ROH)
        CALL QP(1,1,MP,7 ,7 ,
       1         P,Q,CAP,A,PH,R,QL,POUT,DT,DX,ROH)
        CALL QP(1,1,MP,9 ,13,
       1         P,Q,CAP,A,PH,R,QL,POUT,DT,DX,ROH)
        CALL QP(1,1,MP,15,15,
       1         P,Q,CAP,A,PH,R,QL,POUT,DT,DX,ROH)
        CALL QP(1,1,MP,17,17,
       1         P,Q,CAP,A,PH,R,QL,POUT,DT,DX,ROH)
        CALL QP(1,1,MP,19,27,
       1         P,Q,CAP,A,PH,R,QL,POUT,DT,DX,ROH)
        CALL QP(1,1,MP,29,38,
       1         P,Q,CAP,A,PH,R,QL,POUT,DT,DX,ROH)
C
        DPHU = SIGN(CH1U*Q(3 )**2,Q(3 ))
       1      + SIGN(CH2U* ABS(Q(3 ))**(1.5),Q(3 ))
       2      + CH3U*SIGN(AMIN1(ABS((Q(3 ) - QH(3 ))/DT) , 1000.) ,
       3        (Q(3 ) - QH(3 )))
        DPHD = SIGN(CH1D*Q(7 )**2,Q(7 ))
       1      + SIGN(CH2D* ABS(Q(7 ))**(1.5),Q(7 ))
       2      + CH3D*SIGN(AMIN1(ABS((Q(7 ) - QH(7 ))/DT) , 1000.) ,
       3        (Q(7 ) - QH(7 )))
        DPPU = SIGN(CP1U*Q(13)**2,Q(13))
       1      + SIGN(CP2U* ABS(Q(13))**(1.5),Q(13))
       2      + CP3U*SIGN(AMIN1(ABS((Q(13) - QH(13))/DT) , 1000.) ,
       3        (Q(13) - QH(13)))
        DPPD = SIGN(CP1D*Q(17)**2,Q(17))
       1      + SIGN(CP2D* ABS(Q(17))**(1.5),Q(17))
       2      + CP3D*SIGN(AMIN1(ABS((Q(17) - QH(17))/DT) , 1000.) ,
       3        (Q(17) - QH(17)))
        DPFP = SIGN(CFP1*Q(27)**2,Q(27))
       1      + SIGN(CFP2* ABS(Q(27))**(1.5),Q(27))
       2      + CFP3*SIGN(AMIN1(ABS((Q(27) - QH(27))/DT) , 1000.) ,
       3        (Q(27) - QH(27)))
C
        P(4 ) = P(3 ) - DPHU * 1333.
        IF(P(4 ) - PV * 1333.)800,800,801
    800 CONTINUE
        P(4 ) = PV * 1333.
    801 CONTINUE
        P(6 ) = P(5 )
        P(8 ) = P(7 ) - DPHD * 1333.
```

G LEVEL 20 MAIN DATE = 72100 08/43/45

```
      IF(P(8 ) - PV * 1333.)802,802,803
  802 CONTINUE
      P(8 ) = PV * 1333.
  803 CONTINUE
      P(14) = P(13) - DPPU * 1333.
      IF(P(14) - PV * 1333.)804,804,805
  804 CONTINUE
      P(14) = PV * 1333.
  805 CONTINUE
      P(16) = P(15)
      P(18) = P(17) - DPPD * 1333.
      IF(P(18) - PV * 1333.)806,806,807
  806 CONTINUE
      P(18) = PV * 1333.
  807 CONTINUE
      P(28) = P(27) - DPFP * 1333.
      IF(P(28) - PV * 1333.)808,808,809
  808 CONTINUE
      P(28) = PV * 1333.
  809 CONTINUE
C
      POUT(4 ) = P(4 ) / 1333.
      POUT(6 ) = P(6 ) / 1333.
      POUT(8 ) = P(8 ) / 1333.
      POUT(14) = P(14) / 1333.
      POUT(16) = P(16) / 1333.
      POUT(18) = P(18) / 1333.
      POUT(28) = P(28) / 1333.
C
CC    FLOWS WITH PRESSURE GIVEN
C
      DO 888   I = 1,NX
      QH(I) = Q(I)
  888 CONTINUE
C
      CALL QP(2,2,MQ,1 ,2 ,
     1        P,Q,CAP,A,PH,R,QL,POUT,DT,DX,ROH)
      CALL QP(2,2,MQ,4 ,4 ,
     1        P,Q,CAP,A,PH,R,QL,POUT,DT,DX,ROH)
      CALL QP(2,2,MQ,6 ,6 ,
     1        P,Q,CAP,A,PH,R,QL,POUT,DT,DX,ROH)
      CALL QP(2,2,MQ,8 ,12,
     1        P,Q,CAP,A,PH,R,QL,POUT,DT,DX,ROH)
      CALL QP(2,2,MQ,14,14,
     1        P,Q,CAP,A,PH,R,QL,POUT,DT,DX,ROH)
      CALL QP(2,2,MQ,16,16,
     1        P,Q,CAP,A,PH,R,QL,POUT,DT,DX,ROH)
      CALL QP(2,2,MQ,18,26,
     1        P,Q,CAP,A,PH,R,QL,POUT,DT,DX,ROH)
      CALL QP(2,2,MQ,28,37,
     1        P,Q,CAP,A,PH,R,QL,POUT,DT,DX,ROH)
C
      CALL BRANC(RHY1,RHY2,CHY,RPR1,RPR2,CPR,RT1,RT2,CT,DT,ISWB,
```

```
     1          PHY,PPR,PT,P(5),P(15),P(38),QHY,QPR,Q(38),
     2          PV,ZHY1,ZPR1,ZT1,ZHYV,ZPRV,ZTV,KQP,PH(5),PH(15))
C
      Q(3 ) = Q(4 )
      Q(5 ) = Q(6 ) + QHY
      Q(7 ) = Q(8 )
      Q(13) = Q(14)
      Q(15) = Q(16) + QPR
      Q(17) = Q(18)
      Q(27) = Q(28)
C
      GO TO 5
C
   17 CONTINUE
C
CC    PRESSURES WITH FLOW GIVEN
C
      CALL QP(1,2,MP,1 ,2 ,
     1        P,Q,CAP,A,PH,R,QL,POUT,DT,DX,ROH)
      CALL QP(1,2,MP,4 ,4 ,
     2        P,Q,CAP,A,PH,R,QL,POUT,DT,DX,ROH)
      CALL QP(1,2,MP,6 ,6 ,
     3        P,Q,CAP,A,PH,R,QL,POUT,DT,DX,ROH)
      CALL QP(1,2,MP,8 ,12,
     4        P,Q,CAP,A,PH,R,QL,POUT,DT,DX,ROH)
      CALL QP(1,2,MP,14,14,
     5        P,Q,CAP,A,PH,R,QL,POUT,DT,DX,ROH)
      CALL QP(1,2,MP,16,16,
     6        P,Q,CAP,A,PH,R,QL,POUT,DT,DX,ROH)
      CALL QP(1,2,MP,18,26,
     7        P,Q,CAP,A,PH,R,QL,POUT,DT,DX,ROH)
      CALL QP(1,2,MP,28,37,
     8        P,Q,CAP,A,PH,R,QL,POUT,DT,DX,ROH)
C
      DPHU = SIGN(CH1U*Q(3 )**2,Q(3 ))
     1     + SIGN(CH2U* ABS(Q(3 ))**(1.5),Q(3 ))
     2     + CH3U*SIGN(AMIN1(ABS((Q(3 ) - QH(3 ))/DT) , 1000.) ,
     3       (Q(3 ) - QH(3 )))
      DPHD = SIGN(CH1D*Q(7 )**2,Q(7 ))
     1     + SIGN(CH2D* ABS(Q(7 ))**(1.5),Q(7 ))
     2     + CH3D*SIGN(AMIN1(ABS((Q(7 ) - QH(7 ))/DT) , 1000.) ,
     3       (Q(7 ) - QH(7 )))
      DPPU = SIGN(CP1U*Q(13)**2,Q(13))
     1     + SIGN(CP2U* ABS(Q(13))**(1.5),Q(13))
     2     + CP3U*SIGN(AMIN1(ABS((Q(13) - QH(13))/DT) , 1000.) ,
     3       (Q(13) - QH(13)))
      DPPD = SIGN(CP1D*Q(17)**2,Q(17))
     1     + SIGN(CP2D* ABS(Q(17))**(1.5),Q(17))
     2     + CP3D*SIGN(AMIN1(ABS((Q(17) - QH(17))/DT) , 1000.) ,
     3       (Q(17) - QH(17)))
      DPFP = SIGN(CFP1*Q(27)**2,Q(27))
     1     + SIGN(CFP2* ABS(Q(27))**(1.5),Q(27))
     2     + CFP3*SIGN(AMIN1(ABS((Q(27) - QH(27))/DT) , 1000.) ,
```

```
     3       (Q(27) - QH(27)))
C
      P(3 ) = P(4 ) + DPHU * 1333.
      P(5 ) = P(6)
      P(7 ) = P(8 ) + DPHD * 1333.
      P(13) = P(14) + DPPU * 1333.
      P(15) = P(16)
      P(17) = P(18) + DPPD * 1333.
      P(27) = P(28) + DPFP * 1333.
C
      POUT(3 ) = P(3 ) / 1333.
      POUT(5 ) = P(5 ) / 1333.
      POUT(7 ) = P(7 ) / 1333.
      POUT(13) = P(13) / 1333.
      POUT(15) = P(15) / 1333.
      POUT(17) = P(17) / 1333.
      POUT(27) = P(27) / 1333.
C
      CALL BRANC(RHY1,RHY2,CHY,RPR1,RPR2,CPR,RT1,RT2,CT,DT,ISWB,
     1           PHY,PPR,PT,P(5),P(15),P(38),QHY,QPR,Q(38),
     2           PV,ZHY1,ZPR1,ZT1,ZHYV,ZPRV,ZTV,KOP,PH(5),PH(15))
      POUT(38) = P(38) / 1333.
C
CC    FLOWS WITH FLOW GIVEN
C
      CALL FUGEN(Q(1),T,NFG,PQFG,SCFG)
C
      CALL QP(2,1,MQ,2 ,3 ,
     1        P,Q,CAP,A,PH,R,QL,POUT,DT,DX,ROH)
      CALL QP(2,1,MQ,5 ,5 ,
     2        P,Q,CAP,A,PH,R,QL,POUT,DT,DX,ROH)
      CALL QP(2,1,MQ,7 ,7 ,
     3        P,Q,CAP,A,PH,R,QL,POUT,DT,DX,ROH)
      CALL QP(2,1,MQ,9 ,13,
     4        P,Q,CAP,A,PH,R,QL,POUT,DT,DX,ROH)
      CALL QP(2,1,MQ,15,15,
     5        P,Q,CAP,A,PH,R,QL,POUT,DT,DX,ROH)
      CALL QP(2,1,MQ,17,17,
     6        P,Q,CAP,A,PH,R,QL,POUT,DT,DX,ROH)
      CALL QP(2,1,MQ,19,27,
     7        P,Q,CAP,A,PH,R,QL,POUT,DT,DX,ROH)
      CALL QP(2,1,MQ,29,38,
     8        P,Q,CAP,A,PH,R,QL,POUT,DT,DX,ROH)
C
      Q(4 ) = Q(3 )
      Q(6 ) = Q(5 ) - QHY
      Q(8 ) = Q(7 )
      Q(14) = Q(13)
      Q(16) = Q(15) - QPR
      Q(18) = Q(17)
      Q(28) = Q(27)
C
      GO TO 5
```

G LEVEL 20 MAIN DATE = 72100 08/43/45

```
C
C      FORMATS
C
  100 FORMAT(I2,8X,4F10.5)
  101 FORMAT(I1,9X,I1,9X,I2,8X,I2,8X,I2,8X,I2,8X,I2,8X,I1)
  102 FORMAT(3F10.5)
  103 FORMAT(6F10.7)
 1033 FORMAT(3F10.6)
  104 FORMAT(5(I2,8X))
  105 FORMAT(I1,9X,I1)
  106 FORMAT(5F10.5)
C
  200 FORMAT('1')
  201 FORMAT(10X,'CASE NO.',27X,I2)
  202 FORMAT(10X,'HEART RATE / TMAX',16X,F4.1,' /',F6.3)
  203 FORMAT(10X,'PRESSURE PULSE INPUT')
  204 FORMAT(10X,'FLOW PULSE INPUT')
  205 FORMAT(10X,'PERCENT AREA CHANGE / 50 MM-HG',3X,F6.2,/)
  206 FORMAT(10X,'MP = ',I1,24X,'MQ = ',I1)
  207 FORMAT(10X,'------',24X,'------')
  208 FORMAT(10X,'MP = 0   NO LEAKAGE',11X,'MQ = 0   NO VISCOUS OR NONLI
     1NEAR TERMS')
  209 FORMAT(10X,'MP = 1   LEAKAGE INCLUDED     MQ = 1   VISCOUS TERM IN
     1CLUDED')
  210 FORMAT(40X,'MQ = 2   VISCOUS AND NONLINEAR TERMS INCLUDED',/)
  211 FORMAT(10X,'DT = ',F6.4,2X,'DX =',F4.1,3X,'NX = ',I3,7X,
     1       'NPERM =  ',I2,/)
  212 FORMAT(10X,'KOPT = ',I1,' ... KOPT = 0   TAB AND PLOT',3X,'KPRIM =
     1 ',I3,5X,'NL = ',I2)
  213 FORMAT(23X,'KOPT = 1   PLOT ONLY')
 2131 FORMAT(23X,'KOPT = 2   TAB ONLY',/)
  214 FORMAT(10X,'INIT = ',I1,' ... INIT = 0   NO FUNCTION GENERATOR OR
     1IC INPUT GIVEN',4X,'NFG = ',I3)
  215 FORMAT(23X,'INIT = 1',3X,'FUNCTION GENERATOR AND IC INPUT GIVEN',
     16X,'SCFG =',F6.2,/)
  216 FORMAT(10X,'J1 = ',I2,4X,'J2 = ',I2,4X,'J3 = ',I2,4X,
     1       'J4 = ',I2,4X,'J5 = ',I2,3X,/)
  217 FORMAT(10X,'ROH =',F5.2,3X,'XMU = ',F5.3,2X,'PO =',F7.2,3X,'PV =',
     1F7.2,/,/)
  218 FORMAT(10X,'ARTERY',12X,'R1',8X,'R2',6X,'COMP',8X,'C1',8X,'C2',
     1       8X,'C3')
  219 FORMAT(10X,'------',12X,'--',8X,'--',6X,'----',8X,'--',8X,'--',
     1       8X,'--',/)
  220 FORMAT(10X,'HYPOGASTRIC   ',F8.3,2X,F8.3,2X,4(F8.5,2X))
  221 FORMAT(10X,'PROFUNDA      ',F8.3,2X,F8.3,2X,4(F8.5,2X))
  222 FORMAT(10X,'FEM / POP',6X,'-------   -------   -------  ',3(F8.5,
     12X))
  223 FORMAT(10X,'TIBIA VESSELS ',F8.3,2X,F8.3,2X,F8.5,3X,'-------',3X,
     1'-------',3X,'-------',/,/)
  224 FORMAT(10X,'NONDIMENSIONAL PARAMETERS',/,/)
  225 FORMAT(10X,'MEAN INPUT PRESSURE          = ',F7.3)
  226 FORMAT(10X,'CHARACTERISTIC LENGTH        = ',F7.3)
  227 FORMAT(10X,'CHARACTERISTIC COMPLIANCE    = ',F7.4,/,/)
```

```
  228 FORMAT(10X,'LOCATION',11X,'BETA',7X,'R',7X,'R1/R2',5X,'RE/R',6X,
     1           'CAM',8X,'VP')
  229 FORMAT(10X,'--------',11X,'----',7X,'-',7X,'-----',5X,'----',6X,
     2           '---',8X,'--',/)
  230 FORMAT(10X,'MAIN ARTERY     ',F7.3,3X,F7.3,3X,'-------',3X,
     3           '-------',3X,F7.3,3X,F7.3)
  231 FORMAT(10X,'HYPOGASTRIC     ',4(F7.3,3X))
  232 FORMAT(10X,'PROFUNDA        ',4(F7.3,3X))
  233 FORMAT(10X,'TIBIA VESSELS   ',4(F7.3,3X),/,/)
  234 FORMAT(10X,'COMMENTS')
C
  300 FORMAT('1')
  301 FORMAT(5X,'Q(',I2,')',3X,'P(',I2,')',4X,'Q(',I2,')',3X,'P(',I2,')'
     1       ,4X,'Q(',I2,')',3X,'P(',I2,')',5X,'QHY',6X,'QPR',5X,'Q(',
     2       I2,')',3X,'P(',I2,')',4X,'PT',5X,'CYCTM',2X,'P')
  302 FORMAT(5X,'-----',3X,'-----',4X,'-----',3X,'-----',4X,'-----',3X,
     1       '-----',5X,'---',6X,'---',5X,'-----',3X,'-----',4X,'--',5X,
     2       '-----',2X,'-',/)
  303 FORMAT(3X,F7.3,1X,F7.2,2X,F7.3,1X,F7.2,2X,F7.3,1X,F7.2,2X,F7.3,
     1       2X,F7.3,2X,F7.3,1X,F7.2,1X,F7.2,1X,F7.4,2X,I1)
C
  400 FORMAT('1')
  401 FORMAT(10X,'POSITION',5X,'FLOWS',5X,'PRESSURES')
  402 FORMAT(10X,'--------',5X,'-----',5X,'---------',/)
  403 FORMAT(13X,I2,6X,F7.3,5X,F7.2)
  404 FORMAT(/)
  405 FORMAT(10X,'QHY = ',F7.3,6X,'QPR = ',F7.3)
  406 FORMAT(10X,'PHY = ',F7.2,6X,'PPR = ',F7.2)
  407 FORMAT(20X,'PT = ',F7.2)
C
   72 CONTINUE
      WRITE(6,400)
      WRITE(6,401)
      WRITE(6,402)
      WRITE(6,403)(I,Q(I),PCUT(I),I = 1,NX)
      WRITE(6,404)
      WRITE(6,405)QHY,QPR
      WRITE(6,406)PHY,PPR
      WRITE(6,407)PT
      STOP
      END
```

G LEVEL 20 PROP DATE = 72100 08/43/45

```
      SUBROUTINE PROP(N1,NF,X1,DX,ISWP,IEFG,NDA,ACAP,QLL,XLL,AX,AXFG,
     1                P,A,CAPM,CAP,R,QL,ROH,PO,XMU)
C
      DIMENSION AX(100),AXFG(100),A(100),CAP(100),CAPM(100),P(100),
     1          R(100),QL(100)
C
      IF(ISWP)1,1,2
    2 CONTINUE
C
      IF(IEFG)3,3,4
    4 CONTINUE
      SC = NDA / 60.
      NDAM = NDA + 1
      READ(2,100)(AXFG(I),I = 1,NDAM)
  100 FORMAT(5F10.5)
      DO 5   N = N1,NF
      X = X1 + DX * (N - N1)
      CALL FUGEN(AX(N),X,NDA,AXFG,SC)
    5 CONTINUE
      GO TO 6
    3 CONTINUE
C     INITIAL DATA OBTAINED BY RAINES - 9/71
      DO 6   N = N1,NF
      X = X1 + DX * (N - N1)
      IF(X - 13.)7,8,8
    7 CONTINUE
      AX(N) = .505 * EXP(- .1925 * SQRT(X))
      GO TO 20
    8 CONTINUE
      AX(N) = .327 * EXP( -.0206 * X)
   20 CONTINUE
      QL(N) = QLL / XLL / PC / 1333.
    6 CONTINUE
C
    1 CONTINUE
C
      DO 9   N = N1,NF
      A(N) = AX(N) * (1. + ACAP * ALOG(P(N) / 1333. / PO) / 51.1)
      CAP(N) = AX(N) * ACAP / 51.1 / P(N)
      CAPM(N) = CAP(N) * 1333.
      R(N) = 8.0 * 3.14 * XMU / A(N)**2
    9 CONTINUE
      RETURN
      END
```

G LEVEL 20 FUGEN DATE = 72100 08/43/45

```
      SUBROUTINE FUGEN(Y,X,NDIV,YFG,SCALE)
C
      DIMENSION YFG(100)
C
      NMAX = NDIV + 1
      I = X*SCALE
      I1 = I + 1
      IF(I1 - NMAX)700,701,701
  701 I1 = NMAX - 1
  700 CONTINUE
      I2 = I1 + 1
      FX1 = I1
      FX2 = I2
      Y = YFG(I1)+ ((YFG(I2) - YFG(I1))/(FX2 - FX1))*(X*SCALE+1.0-FX1)
      RETURN
      END
```

```
G LEVEL  20                    QP                    DATE = 72100          08/43/45

      SUBROUTINE QP(K1,K2,K3,NIN,NOUT,P,Q,CAP,A,PH,R,QL,POUT,DT,DX,ROH)
C
      DIMENSION P(100),Q(100),CAP(100),A(100),PH(100),R(100),QL(100),
     1          POUT(100)
C
      DO 20   N = NIN,NOUT
C
      IF(K1 - 1)1,1,2
    1 CONTINUE
C
C     PRESSURE CALCULATIONS
C
      IF(K2 - 1)3,3,4
    3 CONTINUE
C
C     BACKWARD CALCULATED PRESSURE
C
      IF(K3 - 1)5,6,6
    5 CONTINUE
C
C     DO NOT INCLUDE LEAKAGE IN BACKWARD CALCULATED PRESSURE
C
      P(N) = P(N) - DT/DX/CAP(N)*(Q(N) - Q(N - 1))
      POUT(N) = .00075*P(N)
      GO TO 20
C
    6 CONTINUE
C
C     INCLUDE LEAKAGE IN BACKWARD CALCULATED PRESSURE
C
      P(N) = (P(N) - DT/DX/CAP(N)*(Q(N) - Q(N - 1)))/
     1       (1.0  + DT*QL(N)/CAP(N)                 )
      POUT(N) = .00075*P(N)
      GO TO 20
C
    4 CONTINUE
C
C     FORWARD CALCULATED PRESSURE
C
      IF(K3 - 1)7,8,8
    7 CONTINUE
C
C     DO NOT INCLUDE LEAKAGE IN FORWARD CALCULATED PRESSURE
C
      P(N) = P(N) - DT/DX/CAP(N)*(Q(N + 1) - Q(N))
      POUT(N) = .00075*P(N)
      GO TO 20
C
    8 CONTINUE
C
C     INCLUDE LEAKAGE IN FORWARD CALCULATED PRESSURE
C
      P(N) = (P(N) - DT/DX/CAP(N)*(Q(N + 1) - Q(N)))/
```

```
     1        (1.0  + DT*QL(N)/CAP(N)                    )
      POUT(N) = .0C075*P(N)
      GO TO 20
C
    2 CONTINUE
C
C     FLOW CALCULATIONS
C
      IF(K2 - 1)9,9,10
    9 CONTINUE
C
C     BACKWARD CALCULATED FLOW
C
      IF(K3 - 1)11,12,13
   11 CONTINUE
C
C     NO VISCOUS AND NONLINEAR TERMS IN BACKWARD CALCULATED FLOW
C
      Q(N) = Q(N) - A(N)/RCH*DT/DX*(P(N) - P(N - 1))
      GO TO 20
C
   12 CONTINUE
C
C     VISCOUS TERN INCLUDED IN BACKWARC CALCULATED FLOW
C
      Q(N) = (Q(N) - A(N)/RCH*DT/DX*(P(N) - P(N - 1)))/
     1        (1.0  + P(N)*A(N)*DT/RCH                   )
      GO TO 20
C
   13 CONTINUE
C
C     VISCOUS AND NONLINEAR TERMS INCLUDED IN BACKWARD CALCULATED FLOW
C
      X1 = Q(N) - A(N)/RCH*CT/DX*(P(N) - P(N - 1))
      X2 = - 2.0*DT/DX*Q(N)/A(N)
      X2A = 2.0*DT/DX/A(N)*Q(N)*Q(N - 1)
      X3 = Q(N)/A(N)**2*DT/CX*(A(N) - A(N - 1))
      X4 = - R(N)*A(N)*DT/RCH
C
      Q(N) = (X1 + X2A) / (1.0 - X2 - X3 - X4)
      GO TO 20
C
   10 CONTINUE
C
C     FORWARD CALCULATED FLCW
C
      IF(K3 - 1)15,16,17
   15 CONTINUE
C
C     NO VISCOUS AND NONLINEAR TERMS IN FORWARD CALCULATED FLOW
C
      Q(N) = Q(N) - A(N)/RCH*DT/DX*(P(N + 1) - P(N))
      GO TO 20
```

G LEVEL 20 QP DATE = 72100 08/43/45

```
C
   16 CONTINUE
C
C     VISCOUS TERN INCLUDED IN FORWARD CALCULATED FLOW
C
      Q(N) = (Q(N) - A(N)/RCH*DT/DX*(P(N + 1) - P(N)))/
     1       (1.0  + R(N)*A(N)*DT/ROH                 )
      GO TO 20
C
   17 CONTINUE
C
C     VISCOUS AND NONLINEAR TERMS INCLUDED IN FORWARD CALCULATED FLOW
C
      X1 = Q(N) - A(N)/ROH*DT/DX*(P(N + 1) - P(N))
      DQP = - CAP(N)*(P(N) - PH(N))/DT - QL(N)*P(N)
      X2 = - 2.0*DQP*DT/A(N)
      X3 = Q(N)/A(N)**2*DT/DX*(A(N + 1) - A(N))
      X4 = - R(N)*A(N)*DT/RCH
C
      Q(N) = X1 / (1.0 - X2 - X3 - X4)
C
   20 CONTINUE
C
      RETURN
      END
```

```
G LEVEL  20                    BRANC                DATE = 72100          08/43/45

      SUBROUTINE BRANC(RHY1,RHY2,CHY,RPR1,RPR2,CPR,RT1,RT2,CT,DT,ISWB,
     1                 PHY,PPR,PT,PH,PP,PTB,QHY,QPR,QTB,
     2                 PV,ZHY1,ZPR1,ZT1,ZHYV,ZPRV,ZTV,KQP,PHH,PPH)
C
      IF(ISWB)1,1,2
C
    2 CONTINUE
      ISWB = 0
C
      IF(RHY1)6,6,7
    7 CONTINUE
      ZHY1 = (RHY1 + RHY2) / (RHY1 * RHY2 * CHY)
      ZHYV = PV / (RHY2 * CHY)
    6 CONTINUE
C
      IF(RPR1)8,8,9
    9 CONTINUE
      ZPR1 = (RPR1 + RPR2) / (RPR1 * RPR2 * CPR)
      ZPRV = PV / (RPR2 * CPR)
    8 CONTINUE
C
      ZT1  = (RT1  + RT2 ) / (RT1  * RT2  * CT)
      ZTV  = PV / (RT2  * CT )
C
    1 CONTINUE
C
C     HYPOGASTRIC
C
      IF(RHY1)10,10,11
   11 CONTINUE
      ZHY2 = ZHYV + PH / 1333. / RHY1 / CHY
      PHYH = PHY
      PHY = (PHYH + ZHY2 * DT) / (1. + ZHY1 * DT)
      QHY = (PH / 1333. - PHY) / RHY1
      GO TO 12
   10 CONTINUE
      PHY = PH / 1333.
      QHY = CHY*SIGN(AMIN1(ABS((PH - PHH)/1333./DT),1500.),(PH-PHH))
     1      + (PH/1333. - PV) / RHY2
   12 CONTINUE
C
C     PROFUNDA
C
      IF(RPR1)13,13,14
   14 CONTINUE
      ZPR2 = ZPRV + PP / 1333. / RPR1 / CPR
      PPRH = PPR
      PPR = (PPRH + ZPR2 * DT) / (1. + ZPR1 * DT)
      QPR = (PP / 1333. - PPR) / RPR1
      GO TO 15
   13 CONTINUE
      PPR = PP / 1333.
      QPR = CPR*SIGN(AMIN1(ABS((PP - PPH)/1333./DT),1500.),(PP-PPH))
```

```
     1       + (PP/1333. - PV)/RPR2
  15 CONTINUE
C
C      TIBIA
C
       PTH = PT
       IF(KQP)3,3,4
    3  CONTINUE
       ZT2  = ZTV  + PTB / 1333. / RT1 / CT
       PT = (PTH + ZT2 * DT) / (1. + ZT1 * DT)
       QTB = (PTB / 1333. - PT) / RT1
       GO TO 5
    4  CONTINUE
       PTBM = (QTB*RT2*DT + QTB*RT1*DT + PV*DT + RT1*RT2*QTB*CT
      1        + PTH*CT*RT2) / (DT + RT2*CT)
       PTB = PTBM * 1333.
       PT = PTBM - RT1*QTB
    5  CONTINUE
C
       RETURN
       END
```

APPENDIX B

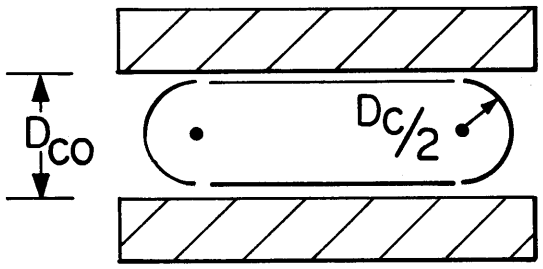
% Area Reduction as a Function of Clamp Opening

B-1,B-2

D_C ~ CLAMP GAP

D_{CO} ~ CLAMP GAP (NO OBSTRUCTION)

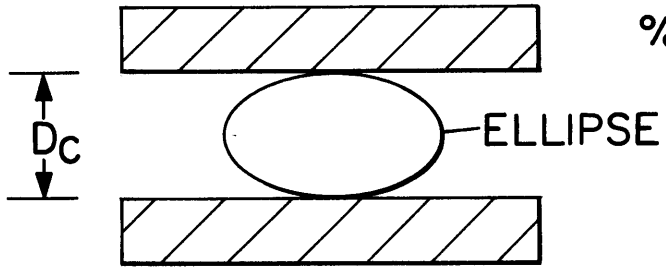
FLATWALL ASSUMPTION



$$\% \text{ OBS} = (1 - D_C/D_{CO})^2 \cdot 100$$

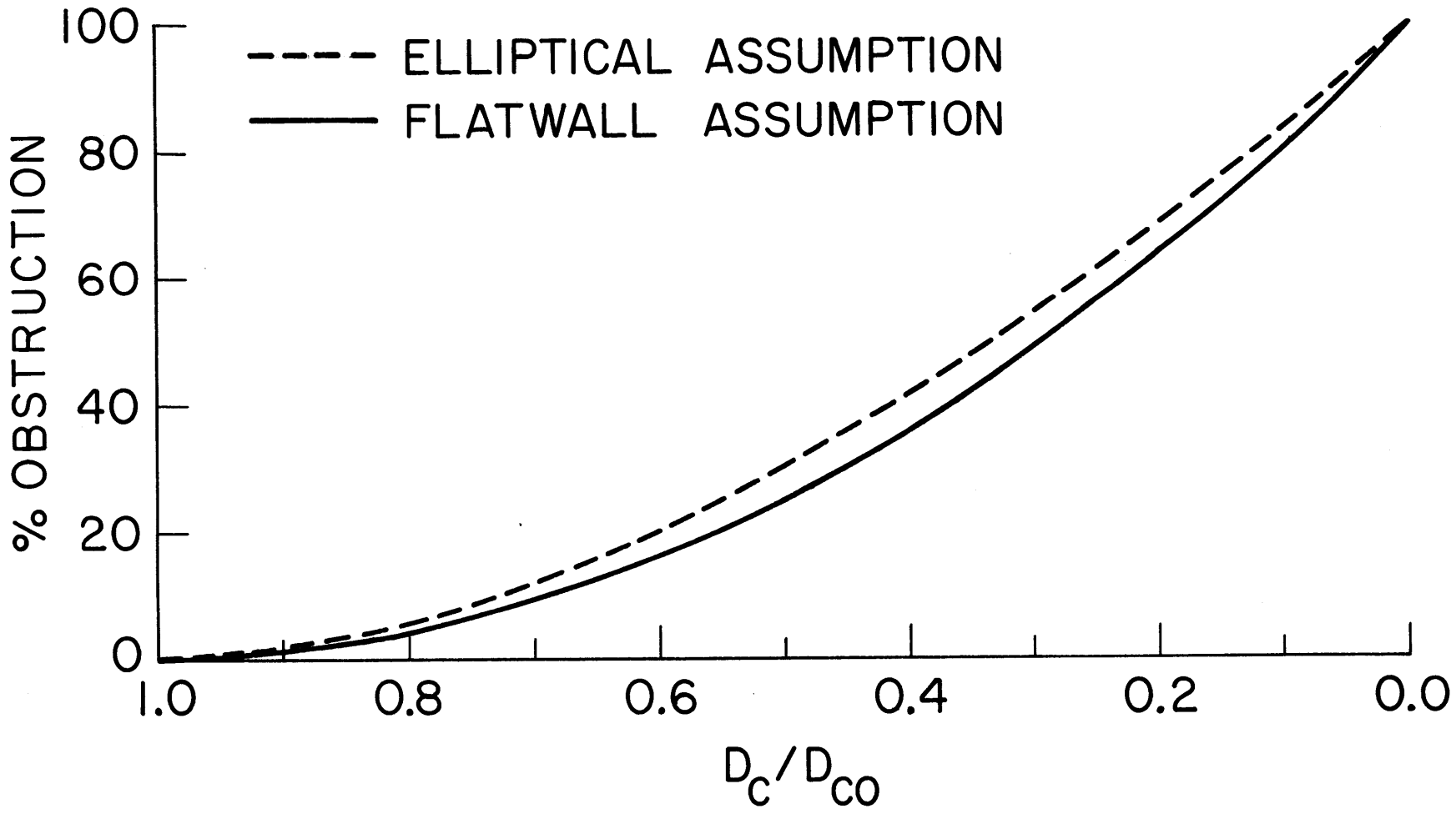
* ARTERY PERIMETER ASSUMED CONSTANT THROUGHOUT CLAMPING

ELLIPTICAL ASSUMPTION



% OBS - CALCULATED WITH ELLIPTICAL INTEGRAL PROGRAM

* ARTERY PERIMETER ASSUMED CONSTANT THROUGHOUT CLAMPING

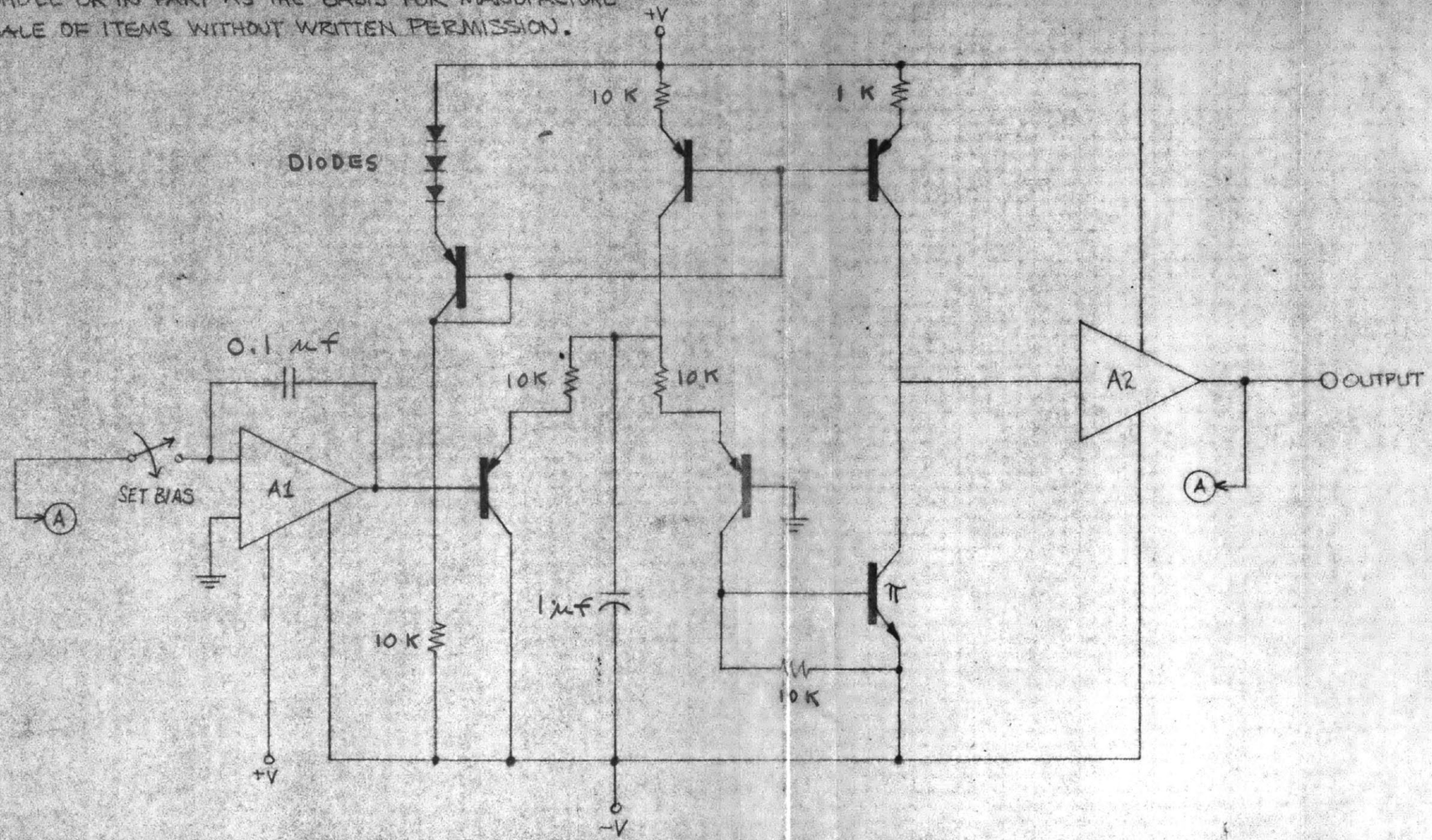

100
80
60
40
20
0
% OBSTRUCTION
ELLIPTICAL ASSUMPTION
FLATWALL ASSUMPTION
1.0
0.8
0.6
0.4
0.2
0.0
D_C/D_{CO}

APPENDIX C

PPR Electrical Drawings and Specifications

THE DRAWING AND SPECIFICATIONS HEREIN ARE FURNISHED BY MEDICAL ENGINEERING CO. ONLY FOR TEST AND MAINTENANCE PURPOSES AND SHALL NOT BE REPRODUCED OR COPIED OR USED IN WHOLE OR IN PART AS THE BASIS FOR MANUFACTURE OR SALE OF ITEMS WITHOUT WRITTEN PERMISSION.

00171



A_1 & A_2 = # T41

V = 15 v (POWER SUPPLY)

TRANSISTORS = # 6N3638

MEDICAL ENGINEERING CO. • MANSFIELD, MASS.		
PPR – ELECTRONICS		
APPROVAL	DATE 4-15-72	PPR02-01

MEDICAL GLOSSARY

A

anastomosis
A communication between two vessels.

aneurysm
A sac formed by the dilatation of the walls on an artery.

angina
(pectoris) A paroxysmal thoracic pain, with a feeling of suffocation, due, most often, to anoxia of the myocardiam.

aorta
The main trunk from which the systemic arterial system proceeds. It arises from the left ventricle of the heart.

arteriole
A minute arterial branch, especially one just proximal to a capillary.

atheroma
Arteriosclerosis with marked degenerative changes (sebaceous cyst).

auscultation
The act of listening to sounds within the body.

B

brachial artery
Artery in the upper arm.

bruit
A sound or murmur heard in auscultation, especially an abnormal one.

C

cannula
A tube for insertion into the body.

capillaries
Minute vessels that connect the arterioles and venules.

carotid artery

The principal artery of the neck.

catheter

A tubular surgical instrument for withdrawing fluids from a location in the body.

claudication

A complex of symptoms characterized by absence of pain or discomfort in a limb when at rest, the commencement of pain, tension, and weakness, after walking is begun, and the disappearance of the symptoms after a period of rest. Ischemic muscle pain.

coarctation

A malformation characterized by deformity of the aortic media, causing narrowing, usually severe, of the lumen of the vessel.

D

diastolic pressure

Systemic pressure (generally the lowest valve) in the cardiac cycle when the ventricles are relaxed.

diuresis

Increased secretion of urine.

E

edema

The presence of abnormally large amounts of fluid in the intercellular tissue spaces of the body.

embolus

A clot or other plug brought by the blood from another vessel and forced into a smaller one so as to obstruct the circulation.

endarterectomy

Excision of the thickened, atheromatous tunica intima of artery.

F

femoral artery

Major artery in the thigh.

H

hematoma

A tumor containing effused blood.

hypertension

Commonly called high blood pressure. An unstable or persistent elevation of blood pressure above the normal range, which may eventually lead to increased heart size and kidney damage.

hypogastric artery

An artery feeding the pelvic and groin area. Also called internal iliac artery.

I

iliac artery

Major artery in the ilium.

inguinal ligament

Ligament in the groin.

in vitro

In a test tube (not in the living body).

in vivo

Within the living body.

ischemia

Deficiency of blood in a part, due to functional constriction or actual obstruction of a blood vessel.

L

lipid

Any one of a group of organic substances which are insoluble in water, but soluble in alcohol, ether, chloroform and other fat solvents. The term embraces fatty acids, neutral fats, steroids, and phosphatides.

lipoproteins

A combination of a lipid and protein, possessing the general properties of proteins. Practically all of the lipids of the plasma are present as lipoprotein complexes.

lumen

The channel within a tube or tubular organ.

lymphedema

Swelling of subcutaneous tissues due to the presence of excessive lymph fluid.

M

metabolism

The sum of all the physical and chemical processes by which living organized substance is produced and maintained, and also the transformation by which energy is made available for the uses of the organism.

myocardium

The muscular wall of the heart. The thickness of the three layers of the heart wall, it lies between the inner layer (endocardium) and the outer layer (epicardium).

N

nausea

An unpleasant sensation, vaguely referred to the epigastrium and abdomen, and often culminating in vomiting.

normotensive

Characterized by normal blood pressure.

P

palpation

The act of feeling with the hand; the application of the fingers with light pressure to the surface of the body for the purpose of determining the consistence of the parts beneath in physical diagnosis.

paramedical

Having some connection with or relation to the science or practice of medicine (not a physician).

pedal

Pertaining to the foot or feet.

peripheral vascular system

Considered all the arteries and veins except in the heart itself.

plaque

Any patch or flat area.

plethysmograph

An instrument for determining and registering variations in the size of an organ, part, or limb and in the amount of blood present or passing through it for recording variations in the size of parts and in the blood supply.

popliteal artery

An artery in the posterior region of the knee.

post-mortem

After death.

profunda femoris

The deep femoral artery located in the thigh.

pulse pressure

The difference between systolic pressure and diastolic pressure.

R

radial artery

An artery located in the forearm.

renal

Pertaining to the kidney.

roentgenogram

A film produced by an X-ray technique.

rubor

Redness, one of the cardinal signs of inflammation.

S

saphenous vein

A large superficial vein in the leg.

stenosis

Narrowing of stricture of a duct or canal.

systolic pressure

Arterial pressure in the systemic circulation at the time the ventricles are fully contracted (the highest pressure level).

T

thoracic outlet syndrome

Positional arterial obstruction caused by the presence of a cervical rib.

thrombectomy

Removal of a thrombus (blood clot) from a blood vessel.

thrombosis

The formation, development or presence of a blood clot.

tibial vessels

Arterial blood vessels running from the lower calf to the foot.

transmural pressure

The difference between arterial pressure and the pressure surrounding the artery (generally atmospheric pressure).

transcutaneous

Through the skin.

V

vasospastic

Spasmodic contraction of the blood vessels.

venous return

Blood flow returning to the heart through the venous system.

REFERENCES

1. Gofman, J. W., Young, W., and Tandy, R., "Ischemic Heart Disease, Atherosclerosis and Longevity", Circulation, 34: pp. 679 (1966).

2. Strandness, D. E., "Peripheral Arterial Disease", Little, Brown and Company (Publishers), Boston, (1969).

3. Blaisdell, F. W., Foster, I., De Weese, J., "Optional Resources for Vascular Surgery", Report of Committee on Vascular Surgery of Inter-Society Commission for Heart Disease Resources, (1971).

4. Gromdin, C. M., Lepage, G., Castonguary, Y. R., Meere, C., and Gromdin, P., "Aortocoronary Bypass Graft: Initial Blood Flow through the Graft, and Early Post-operative Patency", Circulation, 44:814 (1971).

5. Mundth, Eldred E., Buckley, Mortimer, J., Leinback, Robert C., DeSanctis, Roman, W., Sanders, Charles, A., Kantrowitz, Arthur, and Austen, W. Gerald, "Myocardial Revascularization for the Treatment of Cardiogenic Shock Complicating Acute Myocardial Infarction", Surgery, 70, No. 1, pp. 78, (1971).

6. Duncan, W. C., Linton, R. R., and Darling, R. C., "Aortoiliofemoral Atherosclerotic Occlusions Disease: Comparative Results of Endarterectomy and Dacron by pass Grafts", Surgery, 70: pp. 974 (1971).

7. Darling, R. C. Linton, R. R., and Razzuck, M. A., Saphenous vein Types Grafts for Femoropopliteal Occlusive Disease: A Reappraisal, Surgery, 61: pp. 31 (1967).

8. Darling, R. C., "Peripheral Arterial Surgery", New Engl. Journ. of Med., 280; pp. 26-30, 84-91, 141-146, (1969).

9. Lees, R. S., and Wilson, E. D., "The Treatment of Hyperlipidemia", New Engl. J. Med.,284; pp. 186, (1971).

10. Moore, W. S., and Hall, A. D., "Unrecognized Aorto-iliac Stenosis; A Physiological Approach to the Diagnosis", Arch. of Surg., 103, pp. 633 (1971).

11. DeBakey, M. G., Crawford, E. S., Cooley, D. A., Morris, G. C., Aneurysm of Abdominal Aorta: Analysis of Results of Graft Replacement Therapy one to eleven years", Ann. Surg., 160, pp. 622, (1964).

12. Pachon, V., "Oscillometric Sphygmometrique a Grande Semisibilite et a Sensibilite Constante", Compt. Rend. Soc. Biol. Paris, 66: 776, (1909).

13. Winsor, T., "Peripheral Vascular Diseases", Charles C. Thomas (Publisher), Springfield, Ill., (1959).

14. Yao, S. T., et. al., "Transcutaneous Measurement of Blood Flow by Ultrasound", Bio-Med Engineering (British), 5, No. 5., pp. 230, (1970).

15. Kemmerer, W. T., et. al., "Doppler Shifted Ultrasound History and Applications in Clinical Medicine", Minnesota Med., 52, pp. 503, (1969).

16. Allan, J. S., and Terry, H. J., "The Evaluation of an Ultrasonic Flow Detector for the Assessment of Peripheral Vascular Disease", Cardiovascular Res. (British), No. 4., pp. 503, (1969).

17. Strandness, D. E., et. al., "Clinical Applications of a Transcutaneous Ultrasonic Flow Detector", JAMA, 199, No. 5, (1967).

18. Strandness, D. E., et. al., "Application of a Transcutaneous Doppler Flowmeter in Evaluation of Occlusive Arterial Disease", Surg., Gyne., and Obs., pp. 1039, (1966).

19. Strandness, D. E., et. al., "Ultrasonic Flow Detection, a Useful Technique in the Evaluation of Peripheral Vascular Disease", Am. J. Surg., 113, pp. 311, (1967).

20. Strandness, D. E. et. al., "Transcutaneous Directional Flow Detection: A Preliminary Report", Amer. Heart Jour., 78, No. 1, pp. 65, (1969).

21. Strandness, D. E., et al., "The Ultrasonic Velocity Detector for Determining Vascular Patency in Renal Homografts", Transplantation, 8, No. 3, pp. 296, (1969).

22. Sigel, et. al., "A Doppler Ultrasound Method for Distinguishing Laminar from Turbulent Flow", J. Surg. Res., Jan. (1970).

23. Gibbons, Strandness, and Bell, "Improvements in Design of the Mercury Strain Gange Plethysmograph", Surg., Gyne. and Obs., 116, pp. 679, (1963).

24. Strandness, Rodke, and Bell, "Use of a New Simplified Plethysmograph in the Evaluation of Patients with Arteriosclerosis Obliterans", Surg., Gyne, and Obs., 112, pp. 751, (1961).

25. Parks Electronics Lab., Rt. 2, Box 35, Beaverton, Oregon, "Use of Model 270 Plethysmograph".

26. Karvenen, M.T., Telivuo, L.T., and Jarvinen, E.J., "Sphygmomanometer Cuff Size and the Accuracy of Indirect Measurement of Blood Pressure", Amer. J. Cardiology, 13, pp. 688, (1964).

27. Simon, B.R., Kobayashi, A.S., Strandness, D.E., and Wiedorhielm, C.A., "Large Deformation Analysis of the Arterial Cross Section", ASME Preprint 10WA/BMF - 15, (1970).

28. Winsor, T., "The Segmental Plethysmograph", Amer. J. Phy. 180, pp. 1027, (1955).

29. Geddes, L.A., "The Direct and Indirect Measurements of Blood Pressure", Year Book Medical Publishers, Inc., Chicago, (1970).

30. Griffin, L.H., Wray, C.H., Vanghan, B.L. ,and Moretz, W.H., "Detection of Vascular Occlusions During Operations by Segmental Plethysmography and Skin Thermometry", Annals of Surg., pp. 389, March, (1971).

31. Frank, O., Zeitschrift fuer Biologie, 37, 483, (1899).

32. Noordergraaf, A., "Hemodynamics" in Biological Engineering, ed. by H.P. Schwan, McGraw-Hill, New York, (1969).

33. Burton, A.C., "Physiology and Biophysics of the Circulation", Year Book Medical Publishers, Chicago (1965).

34. Winsor, T., Sibley, A.E., Fisher, E.K., Foote, J.L., and Simmons, E., "Peripheral Pulse Contours in Arterial Occlusive Disease", Vascular Diseases, 5, No. 2, pp. 61, (1968).

35. Landes, G., "Physikalische Probleme bei der Untersuchung des menschlichen Kreislaufs", Z. Tech. Physik., 8:192 (1941).

36. Miekisz, S., "Non-linear Theory of Viscous Flow in Elastic Tubes", Phys. Med. Biol., 6:103 (1961).

37. Rockwell, R.L., Biomechanics Laboratory Publication SUDAAR No. 394, Dec. 1969, Stanford Univ., Stanford, Calif.

38. Raines, J.K., Jaffrin, M.Y. and Shapiro, A.H., "A Computer Simulation of the Human Arterial System", Proc. of the Summer Computer Simulation Conf. (SCSC), Boston, (1971).

39. Womersley, J.R., "An Elastic Tube Theory of Pulse Transmission and Oscillatory Flow in Mammalian Arteries", WADC Tech. Rep., 56-614, (1957).

40. Westerhof, N., Bosman, F., De Vries, C.J., and Noordergraaf, A., J. Biomechanics, 2, 121, (1969).

41. Jager, G.N., "Electrical Model of the Human Systemic Arterial Tree", Ph.D. thesis, University of Utrecht, (1965).

42. Jager, B.N., Westerhof, N., and Noordergraaf, A., "Oscillatory Flow Impedance in Electrical Analog of Arterial System", Circulation Res., 16:121 (1965).

43. Noordergraaf, A., "Development of an Analog Computer for the Human Systemic Arterial System", in A. Noordergraaf, G.N. Jager, and N. Westerhof (eds.), "Circulatory Analog Computers", North Holland Publishing Company, Amsterdam (1963).

44. Attinger, E.O., "Pressure-Flow Relations in Canine Arteries: an Analysis of Newly Acquired Experimental Data with Particular References to Womersley's Theory", Ph.D. thesis, University of Pennsylvania, (1965).

45. Westerhof, N., "Analog Studies of Human Systemic Arterial Hemodynamics", Ph.D. thesis, University of Pennsylvania, (1968).

46. Anliker, M., and Rockwell, R.L., "A Nonlinear Model of the Visco-elastic Arterial System", Presented at the 3rd Annual Meeting of the Biomedical Engineering Society, Johns Hopkins Univ., Baltimore, April, (1972).

47. Noordergraaf, A., Verdouw, P.D., Brummelen, A.G., and Wiegel, F.W., "Analog of the Arterial Bed" in Pulsatile Blood Flow, ed. by E.O. Attinger, McGraw-Hill, New York, (1964).

48. Murthy, V.S., McMahon, T.A., Jaffrin, M.Y., and Shapiro, A.H., "The Intraortic Balloon for Left Heart Assistance: an Analytic Model", J. Biomechanics, 4, No. 5, pp. 351, (1971).

49. McDonald, D.A., Blood Flow in Arteries, Edward Arnold (Publishers), Ltd., London, (1960).

50. Taylor, M.G., "Input Impedance and Wave Transmission in a Randomly-branching Assembly of Elastic Tubes", Proc. 18th Annu. Conf. Eng. Med. Biol., Philadelphia, (1965).

51. Cox, R.H., "Determination of the Time Phase Velocity of Arterial Pressure Waves in Vivo", Circulation Res., 29:407, (1971).

52. Magnasson, P.C., Transmission Lines and Wave Propagation, 2nd edition, Allyn and Bacon Inc., Boston, (1970).

53. Attinger, E.O., and Anne, A., "Simulation of the Cardiovascular System", Ann. N.Y. Acad. Sci., 128 (art.3):810, (1966).

54. Attinger, E.O., Anne, A., Mikami, T., and Sugawara, H., "Modelling of Pressure-Flow Relations in Arteries and Veins", Inform. Exchange Group no. 3 Sci. Mem. 41, (1966).

55. Lambert, J.W., "On the Nonlinearities of Fluid Flow in Nonrigid Tubes", J. Franklin Inst., 266:83 (1958).

56. Streeter, V.L., Keitzer, W.F., and Bohr, D.F., "Pulsatile Pressure and Flow through Distensible Vessels", Circulation Res., 13:3 (1963).

57. Fox, P., "The solution of Hyperbolic Partial Differential Equations by Difference Methods", in Mathematical Methods for Digital Computers, ed. by A. Ralston and H.S. Wilb, John Wiley & Sons, New York, (1960).

58. Lax, P.D., "Differential Equations, Difference Equations and Matrix Theory", Communs. Pure Appl. Math., 11, pp. 175 (1958).

59. Crandall, S.H., Engineering Analysis, McGraw-Hill, (1956).

60. Mozersky, D.J., Sumner, D.S. Hokanson, D.E., and Strandness, D.E., "Transcutaneous Measurement of the Elastic Properties of the Human Femoral Artery", Circulation Res., to be published.

61. Wade, O.L., and Bishop, J.M., Cardiac Output and Regional Blood Flow, Blackwell, (1959).

62. Learoyd, B.M., and Taylor, M.G., "Alterations with Age of the Viscoelastic Properties of Human Arterial Walls", : Circulation Res. 18: 278 (1966).

63. Arndt, J.O. and Kober, G., "Die Druck-Durchmesser-Beziehung der intakten A. femoralis des wacken Menschen und ihre Beeinflussunz durch Noradrenalin-Infusionen", Pflugers Arch., 318:130, (1970).

64. Patel, D.J., Greenfield, J.C., Jr., and Fry, D.L., "In Vivo Pressure-Length-Radius-Relationship of Certain Blood Vessels in Man and Dog", in E.O. Attinger (ed.), "Pulsatile Blood Flow", McGraw-Hill Book Company, New York, (1964).

65. Patel, D.J., Austen, W.G., Greenfield, J.C., and Tindall, G.T., "Impedance of Certain Large Bloodvessels in Man", Ann. N.Y. Acad. Sci., 115:1129 (1964).

66. Schultz, R.D., Hokanson, D.E., and Strandness, D.E., "Pressure-Flow and Stress-Strain Measurements of Normal and Diseased Aortoiliac Segments", Surg., Gynecology, and Obstetrics, pp. 1267, June (1967).

67. Lambossy, P., "Apercu historique et critique sur le probleme de la propagation des ondes dans un liquide compressible enferme dans un tube elastique, premiere partie", Helv. Physiol. Acta, 8:209 (1950) deuxieme partie, ibid., 9:145(1951).

68. Boughner, D.R., and Roach, M.R., "Effect of Low Frequency Vibration on the Arterial Wall", Circulation Res., 29:136 (1971).

69. Cachoran, M., Dejdar, R., Roubkova, H., Linhart, J., and Prerovsky, I., "Changes of Some Parameters of Arterial Elasticity in Man during Early Atherosclerosis of the Lower Limbs", Angiology, 20:520 (1969).

70. Zangenek, V.M., and Nassereslami, H., "Das Verbalten der Pulswellengeschwendihert ins Bein in Abhamgigkeit von Lebensalter und Geschlecht", Zeitschrift fur Kreislanfforschung, Band 56, Heft 4, Nov. (1966).

71. Mundth, E.D., Darling, R.C., Moran, J.M., Buckley, M.J., Linton, R.R., and Austen, W.G., "Quantitative Correlation of Distal Arterial Outflow and Patency of Femoropopliteal Reversed Saphenous Vein Grafts with Intraoperative Flow and Pressure Measurements", Surgery, 65, No.1, pp. 197, (1969).

72. Singer, A., "Segmental Distribution of Peripheral Atherosclerosis", Arch. of Surgery, 87:42, (1963).

73. Lee, B.Y., Lapointe, D.G., and Madden, J.L., "Evaluation of Lunbar Sympathectomy by Quantification of Arterial Pulsatile Waveform", Vascular Surgery, 5, No. 2, pp. 61, (1971).

74. Patel, D.J., Greenfield, J.C., Austen, W.G., Morrow, A.G., and Fry, D.L., "Pressure-Flow Relationships in the Ascending Aorta and Femoral Artery of Man", J. Appl. Physiol., 20:459 (1965).

75. Raines, J.K., unpublished data from Catheterization Laboratory, Massachusetts General Hospital.

76. McDonald, D.A., and Attinger, E.O., "The Characteristics of Arterial Pulse Wave Propagation in the Dog", Inform. Exchange Group no. 3 Sci. Mem. 7, (1965).

77. Sabersky, R.H., and Acosta, A.J., Fluid Flow, Macmillan, (1967).

78. Shapiro, A.H., Siegal, R., and Kline, S.J., "Friction Factor in the Laminar Entry Region of a Smooth Tube", Proc. of the 2nd Nat. Cong. of Appl. Mech., pp. 733, (1954).

79. Lam, S., and Li, U., "Principles of Fluid Mechanics", Addison-Wesley Publ., Reading, Mass., (1964).

80. May, A.G., DeWeese, J.A., and Rob, C.G., "Hemodynamic Effects of Arterial Stenosis", Surgery, 53, pp. 513, (1963).

81. Mann, F.G., Herrick, O.F., Essex, H.E., and Baldes, E.J., "The Effect of Blood Flow of Decreasing the Luman of a Blood Vessel", Surgery, 4, pp. 249 (1938).

82. Keitzer, W.F., Fry, W.J., Kraft, R.O., and DeWeese, M.S., "Hemodynamic Mechanism for Pulse Changes Seen in Occlusive Vascular Disease", Surgery, 57, No. 1, pp. 163 (1965).

BIOGRAPHY

The author received a B.S.M.E. from Clemson University in 1965 and a M.M.E. from the University of Florida in 1967. He was a staff member at the Pratt & Whitney Research and Development Center in W. Palm Beach, Florida for three years. In 1968, he joined the research staff at the Massachusetts Institute of Technology working in the areas of computer simulation, fluid mechanics, and biomedical engineering. In 1970 he became a N.I.H. Fellow in the Department of Mechanical Engineering. In addition to numerous industrial and governmental agency reports his publications to date include:

1. Raines, J. K., Jaffrin, M. Y., and Darling, R. C., "Quantitative Electronic Segmental Volume-Time Recorder: A Clinical Tool," presented at the 6th Annual Meeting, Association for the Advancement of Medical Instrumentation (AAMI), Los Angeles, (1971).

2. Raines, J. K., Jaffrin, M. Y., and Shapiro, A. H., "A Computer Simulation of the Human Arterial System," Proc. of the Summer Computer Simulation Conf. (SCSC), Boston, (1971).

3. Raines, J. K., Jaffrin, M. Y., and Rao, S., "Development of a Noninvasive Pressure Pulse Recorder," presented at the 7th Annual Meeting, Association for the Advancement of Medical Instrumentation, Las Vegas, (1972).

4. Raines, J. K., Darling, R. C., Brener, B. J., and Austen, W. G., "Quantitative Segmental Pulse Volume Recorder," to be published in SURGERY, (1972).

5. Raines, J. K., Jaffrin, M. Y., and Rao, S., "A Noninvasive Pressure Pulse Recorder: Development and Rationale," to be published in the JAAMI, (1972).